

UNIVERSITÉ DU QUÉBEC À MONTRÉAL

QUANTIFYING REACTIVE METABOLITE MODIFICATIONS OF TARGET
PROTEINS BY LC-MS

DISSERTATION

PRESENTED

AS PARTIAL FULFILLMENT

OF THE DOCTORATE IN CHEMISTRY

BY

TIMON GEIB

MAY 2020

UNIVERSITÉ DU QUÉBEC À MONTRÉAL

QUANTIFICATION DES MODIFICATIONS DES MÉTABOLITES RÉACTIFS
AUX PROTÉINES CIBLES PAR LC-MS

THÈSE
PRÉSENTÉE
COMME EXIGENCE PARTIELLE
DU DOCTORAT EN CHIMIE

PAR
TIMON GEIB

MAI 2020

UNIVERSITÉ DU QUÉBEC À MONTRÉAL
Service des bibliothèques

Avertissement

La diffusion de cette thèse se fait dans le respect des droits de son auteur, qui a signé le formulaire *Autorisation de reproduire et de diffuser un travail de recherche de cycles supérieurs* (SDU-522 – Rév.10-2015). Cette autorisation stipule que «conformément à l'article 11 du Règlement no 8 des études de cycles supérieurs, [l'auteur] concède à l'Université du Québec à Montréal une licence non exclusive d'utilisation et de publication de la totalité ou d'une partie importante de [son] travail de recherche pour des fins pédagogiques et non commerciales. Plus précisément, [l'auteur] autorise l'Université du Québec à Montréal à reproduire, diffuser, prêter, distribuer ou vendre des copies de [son] travail de recherche à des fins non commerciales sur quelque support que ce soit, y compris l'Internet. Cette licence et cette autorisation n'entraînent pas une renonciation de [la] part [de l'auteur] à [ses] droits moraux ni à [ses] droits de propriété intellectuelle. Sauf entente contraire, [l'auteur] conserve la liberté de diffuser et de commercialiser ou non ce travail dont [il] possède un exemplaire.»

ACKNOWLEDGEMENTS

This Ph.D. study was not possible without the constant support and help of multiple people and organizations, directly and indirectly contributing to my personal life and my research. Firstly, I would like to thank Prof. Lekha Sleno for the continuous support of my studies and research, for her patience, motivation and knowledge. Her guidance helped me in all the time of research and writing of this thesis. Besides my advisor, I would like to thank the rest of my thesis committee, Prof. Joshua Byers, Prof. Mathieu Frenette and Prof. Jeff Smith, for dedicating their time, for their insightful comments and encouragement. I would also like to thank all the past and present members of Prof. Sleno's team, Leanne Ohlund, Dr. André LeBlanc, Dr. Makan Golizeh, Maxime Sansoucy, Biao Ji, Ghazaleh Moghaddam, Vivaldy Prinville, Amal Guesmi, Maggy Lépine, Ons Ousji, Myriam Mireault and Kahina Chabi. I gratefully acknowledge the funding received towards my Ph.D. Financial support was made possible by graduate scholarships from *Fondation Hydro-Québec*, *Groupe de Recherche Axé sur la Structure des Protéines* and *Fonds de recherche du Québec – Nature et technologies*.

A special thanks to my whole family, for their moral support and loving care. I would also like to thank all of my friends who supported me in writing and incited me to strive towards my goal. Especially, I would like to thank my mum for her constant understanding, caring and support from afar during this challenging period. And finally, Lili, who has been by my side throughout this Ph.D., living every single minute of it and without whom, I would not have had the courage to finish this journey.

Ein besonderer Dank geht an meine ganze Familie, für ihre moralische Unterstützung und liebevolle Fürsorge. Ich möchte mich auch bei allen meinen Freunden bedanken, die mich beim Schreiben unterstützt und mich dazu angeregt haben, meine Ziele zu erreichen. Insbesondere möchte ich meiner Mutter danken, für ihr ständiges Verständnis, ihre Fürsorge und ihre Unterstützung aus der Ferne in dieser herausfordernden Zeit. Und zu guter Letzt Lili, die während dieser Promotion immer an meiner Seite stand und jede Minute davon lebte und ohne die ich nicht den Mut gehabt hätte, diese Reise zu beenden.

TABLE OF CONTENTS

LIST OF FIGURES	x
LIST OF TABLES.....	xviii
LIST OF ABBREVIATIONS	xx
LIST OF SYMBOLS AND UNITS.....	xxvii
RÉSUMÉ.....	xxx
ABSTRACT	xxxii
CHAPTER I INTRODUCTION.....	1
1.1 Biotransformation and toxicity.....	2
1.1.1 Xenobiotic metabolism	2
1.1.2 Oxidative stress	12
1.1.3 Reactive metabolite binding to macromolecules.....	15
1.2 Liquid chromatography-mass spectrometry–based technologies.....	22
1.2.1 (Two-dimensional)-liquid chromatography.....	23
1.2.2 Tandem mass spectrometry.....	25
1.2.3 Drug metabolite analysis.....	37
1.2.4 Proteomics techniques	43
1.3 Experimental design and research challenges	50
1.3.1 Sample preparation.....	53
1.3.2 Data processing and treatment	55
1.3.3 Research outline	56
CHAPTER II ABSOLUTE QUANTITATION OF ACETAMINOPHEN- MODIFIED HUMAN SERUM ALBUMIN IN ACUTE LIVER FAILURE PATIENTS BY LIQUID CHROMATOGRAPHY-TANDEM MASS SPECTROMETRY	60

2.1	Abstract	61
2.2	Introduction	62
2.3	Experimental	66
2.3.1	Chemicals.....	66
2.3.2	Patient samples.....	66
2.3.3	Participants.....	67
2.3.4	Modified HSA (surrogate standard and IS) preparation.....	67
2.3.5	Modified peptide stock solutions	68
2.3.6	Serum sample preparation.....	68
2.3.7	Calibration standards and QCs.....	69
2.3.8	Peptide-level calibration standards.....	69
2.3.9	LC-MS/MS analysis	69
2.4	Results.....	72
2.4.1	Method development	72
2.4.2	LC-MRM method validation.....	73
2.4.3	Recovery, matrix effects and comparison of peptide-level to protein-level standards.....	75
2.4.4	APAP hepatotoxicity patient study	77
2.4.5	LC-MRM quantitation of low level samples	81
2.5	Discussion	81
2.6	Acknowledgements.....	84
CHAPTER III LIQUID CHROMATOGRAPHY-TANDEM MASS SPECTROMETRY ANALYSIS OF ACETAMINOPHEN COVALENT BINDING TO GLUTATHIONE S-TRANSFERASES.....		
85		
3.1	Abstract	86
3.2	Introduction	87
3.3	Materials and methods	94
3.3.1	Chemicals and materials	94
3.3.2	GST expression and purification protocols.....	94
3.3.3	Preparation of alkylated GSTs using iodo-APAP or IAM.....	95
3.3.4	NAPQI-GST formation by RLM incubation	95
3.3.5	NAPQI-GST formation by CYP3A4.....	96
3.3.6	Digestion of NAPQI-GST.....	96
3.3.7	High-pH RP peptide fractionation.....	96
3.3.8	LC-MS/MS analysis with DDA	97
3.3.9	LC-MS/MS analysis in MRM mode	98

3.4	Results.....	99
3.4.1	Method development	99
3.4.2	Protein analysis by DDA and detection of NAPQI binding	102
3.4.3	Confirmation of NAPQI binding by MRM strategies	103
3.4.4	Comparison of different strategies	106
3.5	Discussion	110
3.5.1	Performance of different strategies.....	110
3.5.2	Putative NAPQI-cysteine sites in GST.....	112
3.6	Data availability.....	115
3.7	Author contributions.....	116
3.8	Funding	116
3.9	Supplementary material	116
CHAPTER IV IDENTIFICATION OF 4-HYDROXYNONENAL-MODIFIED PROTEINS IN HUMAN OSTEOARTHRITIC CHONDROCYTES		118
4.1	Abstract	119
4.2	Introduction	120
4.3	Materials and methods	122
4.3.1	Chemicals and materials	122
4.3.2	Cartilage samples.....	122
4.3.3	Chondrocyte culture conditions.....	123
4.3.4	Protein extraction and HNE treatment.....	123
4.3.5	Protein quantitation and western blot analysis.....	124
4.3.6	Immunoprecipitation and HDAC activity.....	124
4.3.7	Protein digestion and peptide standard sample preparation.....	124
4.3.8	LC-MS/MS analysis and data processing	125
4.4	Results.....	126
4.4.1	HNE induces modification of nuclear proteins.....	127
4.4.2	HNE inhibits HDAC activity by HNE-HDAC adduct formation.....	128
4.4.3	Effect of HNE on histone acetylation status	129
4.4.4	LC-MS/MS analysis of HNE-modified proteins.....	131
4.4.5	Enrichment analysis of proteins related to OA disease and HNE binding	132
4.4.6	HNE-peptide adduct confirmation with <i>in vitro</i> modified peptides.....	133
4.5	Discussion	134
4.5.1	HNE-nuclear protein adducts.....	134

4.5.2	Other HNE-modified proteins.....	137
4.5.3	Target proteins linked to OA pathogenesis.....	139
4.6	Conclusion.....	141
4.7	Acknowledgements.....	142

CHAPTER V INVESTIGATION OF CLOZAPINE AND OLANZAPINE
REACTIVE METABOLITE FORMATION AND PROTEIN BINDING BY
LIQUID CHROMATOGRAPHY-TANDEM MASS SPECTROMETRY 143

5.1	Abstract.....	144
5.2	Introduction.....	145
5.3	Experimental procedures.....	147
5.3.1	Chemicals and materials.....	147
5.3.2	Purified protein preparation.....	148
5.3.3	<i>In vitro</i> metabolism and GSH trapping.....	148
5.3.4	Peptide and protein binding protocol.....	149
5.3.5	Metabolite and standard peptide analysis.....	149
5.3.6	Bottom-up proteomics analysis.....	150
5.4	Results and discussion.....	152
5.4.1	Metabolites and GSH adducts identification.....	152
5.4.1.1	Oxidative metabolism.....	158
5.4.1.2	Reactive metabolite and GSH adduct formation.....	158
5.4.2	Standard peptide adducts.....	160
5.4.3	Protein adducts.....	160
5.4.3.1	Binding to purified human proteins.....	165
5.4.3.2	Binding to microsomal rat proteins.....	166
5.4.4	Potential link between reactive metabolite-protein adducts and toxicity	166
5.4.5	Comparison of untargeted DDA and targeted MS/MS of modified peptides from protein digests.....	168
5.4.6	Effects of CLZ and OLZ modifications on proteomic analysis.....	169
5.5	Conclusion.....	170
5.6	Associated content.....	171
5.6.1	Supporting information.....	171
5.7	Author information.....	172
5.7.1	Funding.....	172
5.7.2	Notes.....	172

5.8 Acknowledgment.....	172
CHAPTER VI SUMMARY AND CONCLUSIONS.....	173
6.1 Summary of findings	174
6.1.1 Identification of drug reactive metabolism and protein binding.....	175
6.1.2 Identification of HNE protein binding.....	177
6.1.3 Quantification of APAP-related binding to hSA.....	178
6.2 Limitations and perspectives	179
6.2.1 Sample preparation workflow applicability.....	180
6.2.2 Limitations in reactive metabolite-GSH and GST adduct identification....	183
6.2.3 Challenges in HNE-chondrocyte protein analysis.....	184
6.2.4 Limitations in APAP-protein quantitation.....	185
6.2.5 Perspectives and improvements	187
APPENDIX A FIGURES OF APAP-PEPTIDE CHROMATOGRAMS, MS AND MS/MS SPECTRA, AND PEPTIDE DISTRIBUTION IN CONCATENATED FRACTIONS.....	192
APPENDIX B METHODS OF HNE-CHONDROCYTE PROTEIN QUANTITATION, WESTERN BLOT, AND MS/MS SPECTRA AND ENRICHMENT ANALYSIS RESULTS	205
Protein quantitation and western blot analysis	205
Immunoprecipitation and HDAC activity assay.....	206
Supporting tables	208
Supporting figures	214
APPENDIX C ADDITIONAL PROTEIN EXPRESSION PROTOCOL, GSH ADDUCT SPECTRA, MODIFIED PEPTIDE SPECTRA, CHROMATOGRAMS AND FOUND DIAGNOSTIC FRAGMENT IONS, AND CHARGE DISTRIBUTION OF MODIFIED STANDARD PEPTIDES	222
Purified hMGST1 preparation.....	223
Offline LC peptide purification	224
LC-MS/MS.....	224
Supporting figures	226
Supporting tables	240

REFERENCES 248

LIST OF FIGURES

Figure	Page
1.1 General metabolism pathway of xenobiotics, such as drugs or environmental compounds. Phase I and phase II metabolism introduces polar functional groups and conjugations to the parent compound, respectively, to increase hydrophilicity and to facilitate clearance into bile or urine. Besides stable metabolites, some intermediates can be unstable and reactive, and subsequently bind to glutathione for excretion, or to biomolecules. These pathways can equally apply to endogenously formed compounds.	3
1.2 Catalytic reaction cycle of CYP enzymes. The cycle starts with heme iron in low-spin state and displacement of weakly bound water by the substrate (RH), which results in a high-spin state iron. Further reduction and incorporation of O ₂ leads to a ferric-peroxo intermediate and subsequent protonation leads to a hydroperoxo compound (also known as compound 0). Upon further protonation and dehydration an oxoferryl porphyrin radical cation (compound I) is formed. Compound I then abstracts a hydrogen from the substrate, forming a substrate radical (R [•]). Subsequently, hydroxyl “rebounds” to the substrate radical and forms the hydroxylated substrate product (ROH). The resting state is achieved by water returning to the distal coordination position of the iron.	6
1.3 Structure of the cofactor NADPH.	7
1.4 Structure of the antioxidant tripeptide GSH, consisting of a glutamate residue γ -linked to cysteine followed by a regular peptide bond between cysteine and glycine.	8
1.5 Exemplary mercapturic acid pathway starting with a R-SG conjugate and resulting in the mercapturic acid conjugate.	12

1.6	A brief overview of the LPO process of a PUFA, starting with the attack from a pro-oxidant resulting in the formation of a lipid radical. Subsequently, the lipid radical reacts with molecular oxygen forming a lipid peroxy radical which either propagates or terminates the reaction. Propagation by-products can be malondialdehyde or HNE.	14
1.7	A brief overview of common reactive metabolite/intermediate substructures formed through transformation of exemplary parent drugs/compounds. Irreversible binding sites (<i>e.g.</i> , from Michael addition) of nucleophiles are marked with a red asterisk (*) (APAP, acetaminophen; CLZ, clozapine; HNE, 4-hydroxynonenal; OLZ, olanzapine; PhIP, 2-amino-1-methyl-6-phenylimidazo[4,5- <i>b</i>]pyridine).	16
1.8	Michael addition of a thiol to an unsaturated aldehyde forming a carbanionic transition state and, subsequently after protonation, the enolic product (keto–enol tautomerization is possible, depending on structure). ..	17
1.9	Relative amounts of Aroclor 1254-induced RLM phase I and II enzymes. Data was based on unpublished label-free quantitation of microsomal peptic and tryptic digests ($n = 6$; error bars representing standard deviation, SD).	20
1.10	Comparison of reactive metabolite formation of APAP and its regioisomer AMAP (based on (Kenna, 2013)).	22
1.11	Number of LC-MS–related publications over the course of time. Bar graph based on a simple PubMed search of the acronym LC-MS (taken from (National Center for Biotechnology Information, 2020)).	23
1.12	Schematic of possible ESI models. A high voltage (several kV) is applied between the ESI emitter and the MS orifice to create an aerosol of multiply charged droplets. These droplets shrink through solvent evaporation (through heat) and Coulombic explosion. Possible ion formation models are 1) ion evaporation of a small ion or an unfolded protein from the droplet, or 2) formation of a residual ion after the droplet charge exceeds the Rayleigh limit and the droplet explosively dissociates.	27
1.13	Schematic of a linear quadrupole mass analyzer (adapted from (March and Todd, 2015)).	29

- 1.14 Structure of the antioxidant tripeptide GSH, consisting of a glutamate residue γ -linked to cysteine followed by a regular peptide bond between cysteine and glycine..... 30
- 1.15 General scheme of hyphenated MS/MS platforms. LC-MS/MS systems usually operate under atmospheric pressure at the sample inlet. Fragmentation can occur at different positions of the MS/MS system, depending on the utilized technique. In this example, a discrete fragmentation cell is separated between two mass analyzers, as in the case of the very popular triple quadrupole platform. 32
- 1.16 Representative MS analysis scheme of (A) two MRM experiments (transitions) and (B) a DDA survey scan with subsequent ion selection, based on ion intensity, and fragmentation analysis of selected ion. In MRM acquisitions, pre-selected precursor and product ion pairs are monitored through fixed ion isolation in Q_1 and Q_3 , respectively. DDA is presented here in a QqTOF setup using a reflectron TOF as second mass analyzer. During the DDA survey scan, Q_1 and q_2 are set to be both non-mass filtering (RF-only mode). Mass analysis occurs only through reflectron TOF measurement. 34
- 1.17 (A) Representation of a chromatographic peak (<10 s total peak width) acquired using four different cycle times. (B) Visualization of a cycle time of 1 s (C) with representative MRM analysis using eight transitions or DDA with top 15 ions..... 36
- 1.18 Simplified QqQ analysis schematic representation of (A) product ion scan, (B) precursor ion scan and (C) neutral loss scan experiments. In a product ion scan, Q_1 is set at a fixed m/z of a pre-selected precursor with subsequent acquisition (scanning) of its product ions. The precursor ion scan utilizes a similar concept where the product ion m/z is fixed in Q_3 and possible precursors are scanned in Q_1 . The resulting mass spectrum consist of all precursor m/z values yielding the pre-defined product ion. Neutral loss scanning methods utilize Q_1 and Q_3 in synchronous scanning mode with a pre-defined mass difference (Q_1-Q_3), corresponding the mass of the pre-selected neutral loss (*e.g.*, water loss of 18 u or ammonia loss of 17 u)..... 38
- 1.19 Isotope pattern of $[M+H]^+$ adducts of (A) clozapine ($C_{18}H_{19}ClN_4$) and (B) its GSH adduct ($CLZ-2H+GSH, C_{28}H_{34}ClN_7O_6S$)..... 40

- 1.20 Peptide fragmentation scheme showing peptide bond cleavage leading to different product ions. Either the peptide amide bond (a and x-ions), the amino alkyl bond (b and y-ions) or the alkyl carbonyl bond (c and z-ions) are cleaved during dissociation. Fragmentation products with the charge remaining on the N-terminal side are termed a, b or c-ions, and x, y or z-ions with the charge on the C-terminal side (Biemann, 1990). The subscript number besides the letter refers to the number of amino acid residues within the peptide fragment ion..... 48
- 1.21 Overview of common stable and reactive metabolites of (A) APAP, (B) CLZ and (C) OLZ. The majority of APAP metabolism consist of direct glucuronidation (Gluc) and sulfation, aside from bioactivation to NAPQI, to a lesser extent (5–15%). Main stable metabolites of CLZ are a result of demethylation (desmethylclozapine, DCLZ) and *N*-oxidation (clozapine *N*-oxide, CLZ-NO). The well-known reactive metabolite of CLZ corresponds to CLZox. OLZ undergoes similar phase I metabolism (forming desmethylolanzapine, DOLZ; olanzapine *N*-oxide, OLZ-NO; and 2-hydroxymethyl-olanzapine, 2-OH-OLZ) as well as bioactivation to OLZox. Reactive metabolites NAPQI, CLZox and OLZox are normally conjugated to GSH for detoxification and excretion from the body, a reaction mostly mediated by GSTs during phase II metabolism. GSH can also directly conjugate to reactive metabolites without the need for enzymatic catalysis via GSTs (Li, 2009). 52
- 1.22 General workflow scheme to study *in vitro* reactive metabolite formation and binding of xenobiotics using LC-MS/MS. 53
- 1.23 NADPH regenerating cycle using glucose 6-phosphate and NADP⁺ in the CYP-mediated oxidation. 54
- 1.24 Comparison of cysteine binding through (A) the bioactivation of APAP to NAPQI, and the chemically labeling using the custom-made alkylating agents (B) iodo-APAP (*N*-(4-hydroxyphenyl)-2-iodoacetamide) and (C) d₄-iodo-APAP (*N*-(4-hydroxy[2,3,5,6-d₄]phenyl)-2-iodoacetamide). 58
- 2.1 (A) Metabolism pathway of APAP, showing sulfation and glucuronidation as the main metabolic pathways and oxidation by CYPs to form NAPQI with subsequent conjugation to GSH. Conjugation of cysteine-containing proteins is also shown as an alternative pathway. (B) Representative alkylation reaction of serum albumin with custom-designed iodo-APAP

and d ₄ -iodo-APAP to yield surrogate calibration standard and IS, respectively.....	64
2.2 High-resolution MS/MS spectrum of iodo-APAP-LQQCPFEDHVKL (theoretical [M+3H] ³⁺ precursor at <i>m/z</i> 535.9292) showing three chosen product ions (bold) y ₈ , PFEDH and (y ₁₀ -H ₂ O) ²⁺ at <i>m/z</i> 984.4, 626.1 and 673.9 at CE = 30 V (±10 V), respectively, and NAPQI-Cys related diagnostic ions (underlined).....	73
2.3 MRM chromatograms of double blank sample (A), lowest standard (0.11 nmol/mL, B), mid-range standard (5.41 nmol/mL, C), and a representative patient sample (3.91 nmol/mL, D). MRM transitions were <i>m/z</i> 535.9 → 984.4 (dark) for analyte and surrogate standard, and <i>m/z</i> 537.2 → 984.4 (light) for IS.	76
2.4 Linear agreement (dashed line) between LC-MRM and LC-HRMS/MS results of standards, QCs and patient samples.	79
2.5 (A) Extracted MS/MS chromatogram of a patient sample (3.91 nmol/mL, 60 min gradient), for product ion at <i>m/z</i> 984.5149 (±0.01 u, CE = 28 V). High-resolution MS/MS spectra of NAPQI-LQQCPFEDHVKL (theoretical [M+3H] ³⁺ precursor at <i>m/z</i> 535.9292) showing product ions (in bold) and NAPQI-Cys related diagnostic ions (underlined) of isomer 1 (B) and isomer 2 (C).....	80
3.1 Simplified scheme of APAP metabolism, leading to the formation of NAPQI with subsequent GSH conjugation. Hepatotoxicity of NAPQI is linked to protein binding to cysteine sites.....	88
3.2 Representative workflow of <i>in vitro</i> NAPQI binding to recombinant GSTs followed by reductive alkylation and digestion (trypsin or pepsin), SPE with optional LC fractionation, and LC-MS/MS analysis (A). NAPQI generation was achieved by activation of APAP with either RLM or CYP3A4 Supersomes. MRM methods were based on isomeric iodo-APAP-GST standard, digested and first analyzed by DDA to investigate ionization and fragmentation properties of iodo-APAP-peptides (B). Then, MRM transitions were built and optimized for each peptide individually. Cysteine alkylation reagent iodo-APAP yields positional isomer label to NAPQI-modified cysteine (C).....	92

3.3	Proposed structures of diagnostic fragment ions.....	103
3.4	Overlaid high-resolution extracted ion chromatograms (± 0.01 u) of detected modified peptide precursors (A). Confirmation was based on high-resolution accurate mass TOFMS (B) and triggered (DDA) MS/MS (C) analyses, including diagnostic NAPQI-cysteine fragment ions.....	105
3.5	Comparison of LC-DDA and LC-MRM results, used to identify NAPQI-modified GSTP1 peptide IHEVLAPGC ¹⁷⁰ L (underlined) from <i>in vitro</i> incubation with CYP3A4 (Supersomes). DDA analysis of the target peptide (theoretical $[M+2H]^{2+}$ at m/z 600.8077) eluting at 23.4 min (A) did not yield MS/MS acquisition (B). Fragmentation was triggered by an interfering ion at m/z 601.3123, which resulted in a MS1 isolation window (red rectangle) not incorporating target peptide. MRM analysis (C) confirmed presence of IHEVLAPGC*L ²⁺ by comparing to iodo-APAP-GST (D).....	108
4.1	Immunoreactive HNE-protein adduct profile of OA chondrocytes without and with 10 μ M HNE treatment (A). Immunoprecipitation of HNE-H2A and HNE-H2B adducts and western blot analysis of total histone H2A and H2B in nuclear extracts from human OA chondrocytes treated with HNE (0, 5 and 10 μ M) (B).....	128
4.2	Total HDAC activity in HNE-treated OA human chondrocytes at different concentrations of HNE (0–20 μ M; *, p -value ≤ 0.05 ; **, p -value ≤ 0.01) (A). Immunoprecipitation followed by western blot analysis of HNE-HDAC2 adduct formation in nuclear protein extracts, monitored at different doses of HNE (0–20 μ M) for 24 h (B). Histones H2A and H2B acetylation levels in HNE-treated human OA chondrocytes. Levels of acetylated histone H2A (K5) (C) and H2B (K20) (D) were analyzed in nuclear extract of human OA chondrocytes by western blot analysis at different levels of HNE (0–20 μ M) treatment.....	130
4.3	Proposed diagnostic fragment ion structures at m/z 139.1118 and 266.1863, resulting from HNE and the HNE-histidine adduct (H*), respectively.....	131
4.4	Scatter plot of significantly enriched GO terms (FDR ≤ 0.05 , against reference of all proteins identified in all samples) of HNE-modified proteins unique to OA-related samples (total chondrocyte extracts).....	133

5.1	Extracted ion chromatograms of $[M+2H]^{2+}$ of GSH adducts in incubations of (A) CLZ, (B) OLZ, (C) CLZ-NO and (D) DCLZ with RLM. Retention times in parentheses. Metabolite IDs can be found in Tables S1–2.	154
5.2	(A) MS/MS spectrum of $[M+H]^+$ of the ‘CLZ–2H+GSH’ adduct (at 10.3 min) and (B) proposed fragmentation scheme.	155
5.3	(A) MS/MS spectrum of $[M+H]^+$ of the ‘OLZ–2H+GSH’ adduct (at 2.9 min) and (B) proposed fragmentation scheme.	156
5.4	General workflow for modified peptide manual identification using DDA and targeted MS/MS data. First, DDA runs were analyzed for potential peptide ions (+2 to +4) in MS1 (A) and further verified through mass accuracy (B). Then, potential peptides with missing or poor MS2 data were selected for targeted MS/MS analyses (triggered DDA MS/MS of an unrelated feature at m/z 423.5936 highlighted as red square). Candidates for manual peptide sequencing were based on MS2 extracted ion chromatograms with co-eluting diagnostic fragment ions (C, targeted MS/MS of activated $[M+4H]^{4+}$).	161
5.5	Peptide precursor ion charge distribution (+2 to +4) of CAM-peptides, and corresponding (A) CLZ and (B) OLZ reactive metabolite-peptide adducts from digests of hGSTA1, hGSTM2, hGSTP1, hMGST1 and hSA, and rat proteins. (OLZ–2H)-hGSTM2 CAM-peptide (*) was found singly and doubly charged only.....	164
5.6	Selection of stable metabolites and GSH adducts found in (A) CLZ, CLZ-NO and DCLZ, and (B) OLZ incubations (parents underlined). Adduct ‘+O+GSH’ were presumed to be derived from a novel intermediate.....	157
6.1	Categorization of thesis research on <i>in vitro</i> reactive metabolite formation of APAP, CLZ and OLZ, and investigation of OA-related <i>in vivo</i> protein binding of reactive HNE. <i>In vivo</i> quantitation was possible by monitoring APAP-hSA in ALF patient serum. Reactive metabolite sources were CYP oxidations or LPO.....	174
6.2	A nucleosome consisting of a segment of DNA (grey) wound around an octamer of histones of four variants (H2A, H2B, H3 and H4). With the addition of histone H1, nucleosomes coil into a 30 nm helical structure, the chromatin. PTMs can alter the electric charge of the core histones	

which either repels or attracts molecules and transcription factors (taken from (McCarthy and Nugent, 2013)).	178
6.3 Chemical structures of (A) mixed-mode strong cation-exchange (MCX), (B) mixed-mode strong anion-exchange (MAX) and (C) hydrophilic-lipophilic balance (HLB) SPE polymer resins.	182
6.4 Exemplary principle of DIA MS/MS analysis on a QqTOF platform. All or a selection of precursor ions are sequentially fragmented by isolating multiple precursor ions at once through Q ₁ windows of multiple mass units. Generally, these isolation windows are sequentially scanned in each acquisition cycle and normally overlap (~1 u) to allow homogenous precursor sampling. Resulting MS/MS are normally composite MS/MS of multiple precursors.	189

LIST OF TABLES

Table	Page
1.1 Selection of common human CYPs, selected substrates, inhibitors, inducers and expression sites (APAP, acetaminophen; CLZ, clozapine; OLZ, olanzapine).....	5
1.2 Selection of common human GSTs and their known substrates, inhibitors, inducers and top expression sites (APAP, acetaminophen; CLZ, clozapine; HNE, 4-hydroxynonenal).....	10
1.3 Brief overview of liver fraction inducers and known induced rat enzymes	19
1.4 Overview of (electrospray) MS-compatible solvents and additives.....	25
1.5 Overview of commercially available MS platforms.....	26
1.6 Selection of common phase II conjugate-related characteristic product ions and neutral losses.....	41
1.7 Common phase I and phase II transformations and corresponding exact mass shift ^a	42
1.8 Common proteases in MS-based bottom-up proteomics.....	47
1.9 Brief overview of reactive metabolite-derived modifications of amino acids in protein described in the literature.....	56
2.1 Comparison of results from LC-MRM, LC-HRMS/MS, LC-HRMS (using MS1 for quantitation).....	75

2.2	Accuracy, within-run %CV ($n = 6$ for standards, $n = 9$ for QCs) and total %CV ($n = 12$ for standards, $n = 18$ for QCs) data, obtained from LC-MRM and LC-HRMS/MS evaluation runs	77
2.3	Calculated range, mean, median and SD of NAPQI-HSA concentrations of two patient cohorts.....	79
3.1	Overview of studied human GST enzymes ^a	93
3.2	Coverage of iodo-APAP-cysteine sites in DDA HRMS/MS	101
3.3	NAPQI-GST peptides confirmed by DDA and MRM methods ^a	104
3.4	NAPQI-cysteine diagnostic fragment ions (MS2) detected in HRMS/MS experiments	106
3.5	Comparison of NAPQI-peptide to the IAM-modified (CAM) version found with >95% confidence in the same DDA experiments.....	109
4.1	Overview of histones (H1–4), histone deacetylase (HDAC) and collagen (COL) sequence coverage from LC-MS/MS analyses of OA disease and healthy control samples.....	136
5.1	Found peptides from screened protein targets and RLM proteins modified by CLZ or OLZ reactive metabolites.....	163
6.1	Brief overview of possible improvements and their theoretical benefits	187

LIST OF ABBREVIATIONS

2D	two-dimensional
2-OH-OLZ	2-hydroxymethyl-olanzapine
ABC	ammonium bicarbonate buffer
AC	alternating current
ACN	acetonitrile
ADH	alcohol dehydrogenase
ADME	absorption, distribution, metabolism, and excretion
ALDH	aldehyde dehydrogenase
ALF	acute liver failure
ALI	acute liver injury
AMAP	3-acetamidophenol
APAP	acetaminophen
BH	Benjamini-Hochberg
C18	18-carbon-long hydrocarbon
CAM	carbamidomethylated

CE	collision energy
CES	carboxylesterase
CID	collision-induced dissociation
CLZ	clozapine
CLZ-NO	clozapine <i>N</i> -oxide
CLZox	clozapine nitrenium ion
COL2	type II collagen
COL6A3	collagen alpha-3(VI) chain
COX	cyclooxygenase
CV	coefficient of variation
CYP	cytochrome P450
DC	direct current
DCLZ	desmethylclozapine
DDA	data-dependent acquisition
DDM	<i>n</i> -dodecyl- β -D-maltopyranoside
DDX21	protein nucleolar RNA helicase 2
DIA	data-independent acquisition
DMEM	Dulbecco's modified Eagle's medium
DMPK	drug metabolism and pharmacokinetics

DNA	deoxyribonucleic acid
DOLZ	desmethyloanzapine
DTT	dithiothreitol
ECD	electron capture dissociation
EDTA	ethylenediaminetetraacetic acid
EIF4A1	eukaryotic translation initiation factor 4A1
ELISA	enzyme-linked immunosorbent assay
ESI	electrospray ionization
ETD	electron transfer dissociation
FBS	fetal bovine serum
FDR	false discovery rate
FMO	flavin-dependent monooxygenases
FRQNT	<i>Fonds de recherche du Québec – Nature et technologies</i>
FRQS	<i>Fonds de recherche du Québec – Santé</i>
FTICR	Fourier-transform ion cyclotron resonance
FWHM	full width at half maximum
G6PDH	glucose-6-phosphate dehydrogenase
GAPDH	glyceraldehyde-3-phosphate dehydrogenase
GC	gas chromatography

GO	gene ontology
GRASP	<i>Groupe de Recherche Axé sur la Structure des Protéines</i>
GSH	glutathione
GST	glutathione <i>S</i> -transferase
HCD	higher-energy collisional dissociation
HDAC2	histone deacetylase 2
HEPES	4-(2-hydroxyethyl)-1-piperazineethanesulfonic acid
HLB	hydrophilic-lipophilic balance
HNE	4-hydroxynonenal
HRMS	high-resolution mass spectrometry
hSA/HSA	human serum albumin
HSP90	heat shock protein 90
IADR	idiosyncratic adverse drug reaction
IAM	iodoacetamide
iNOS	inducible nitric oxide synthase
IS	internal standard
LC	liquid chromatography
LIT	linear ion trap
LLOQ	lower limit of quantitation

LPO	lipid peroxidation
MALDI	matrix-assisted laser desorption ionization
MAPEG	membrane-associated proteins in eicosanoid and glutathione metabolism
MAX	mixed-mode, strong anion-exchange
MCX	mixed-mode, strong cation-exchange
MeOH	methanol
MGST	microsomal glutathione <i>S</i> -transferase
MMP-13	matrix metalloproteinase 13
MRM	multiple reaction monitoring
MS	mass spectrometry
MS/MS	tandem mass spectrometry
MS ⁿ	multistage mass spectrometry
MT	methyltransferase
NADPH	nicotinamide adenine dinucleotide phosphate
NAPQI	<i>N</i> -acetyl <i>p</i> -benzoquinone imine
NAT	<i>N</i> -acetyltransferase
NP-40	nonyl phenoxy polyethoxy ethanol
NSERC	Natural Sciences and Engineering Research Council of Canada

OA	osteoarthritis
OLZ	olanzapine
OLZ-NO	olanzapine <i>N</i> -oxide
OLZ _{ox}	olanzapine nitrenium ion
PDGFR- β	platelet-derived growth factor receptor beta
PhIP	2-amino-1-methyl-6-phenylimidazo[4,5- <i>b</i>]pyridine
PMF	peptide mass fingerprinting
POR	cytochrome P450 oxidoreductase
PSM	peptide-spectrum matching
PTM	post-translational modification
PUFA	polyunsaturated fatty acid
Q/q	quadrupole
QC	quality control
QqLIT	quadrupole-linear ion trap
QqQ	triple quadrupoles
QqTOF	quadrupole–time-of-flight
RF	radio frequency
RLM	rat liver microsome
ROS	reactive oxygen species

RP	reversed-phase
rSA/RSA	rat serum albumin
SCX	strong cation exchange
SD	standard deviation
SDS-PAGE	sodium dodecyl sulfate–polyacrylamide gel electrophoresis
SMC	smooth muscle cell
SPE	solid-phase extraction
SULT	sulfotransferase
TBS	Tris-buffered saline
TOF	time-of-flight
TOF/TOF	tandem time-of-flight
TPCK	L-(tosylamido-2-phenyl) ethyl chloromethyl ketone
UGT	UDP-glucuronosyltransferase

LIST OF SYMBOLS AND UNITS

%	percentage
°C	degree Celsius
a	quadrupole parameter
A	area
Å	angstrom
cc	cubic centimeter
cps	counts per second
Da	dalton
e	elementary charge
E_{el}	potential energy
E_{kin}	kinetic energy
g	gram or g-force
h	hour
L	liter
l	length

M	molarity
m	meter
<i>m</i>	mass
<i>m/z</i>	mass-to-charge ratio
<i>m_a</i>	exact mass
<i>m_i</i>	accurate mass
min	minute
mol	mole
<i>n</i>	number of analytical replicates
OD ₆₀₀	optical density at a wavelength of 600 nm
Pa	pascal
pH	power of hydrogen
pI	isoelectric point
ppm	part per million
psi	pound-force per square inch
<i>p</i> -value	calculated probability
<i>q</i>	quadrupole parameter
<i>r</i>	radius
<i>R</i>	resolution

R^2	coefficient of determination
rpm	revolutions per minute
RT	retention time
s	second
S/N	signal-to-noise ratio
t	time
U	voltage
u	unified atomic mass unit
U	enzyme unit
V	volt
V	voltage
v/v	volume concentration
w/w	weight concentration
w/v	weight by volume
z	charge
z/m	charge-to-mass ratio
Δm	mass difference
Φ_0	potential
ω	angular frequency

RÉSUMÉ

Les métabolites chimiquement réactifs peuvent provenir du stress oxydatif ou de l'administration des médicaments. Ces électrophiles peuvent réagir avec des protéines et d'autres macromolécules, affectant leurs fonctions biologiques et pouvant entraîner des effets toxiques. L'identification de ces biomolécules cibles modifiées est une étape cruciale dans la compréhension complète de leurs effets néfastes et leur toxicité.

Ces types d'analyses présentent souvent des défis en raison des faibles quantités de cibles modifiées, de la grande variété de leurs propriétés physicochimiques dans des échantillons complexes ainsi que des obstacles technologiques. Une technique efficace pour l'analyse des métabolites réactifs des protéines modifiées est la chromatographie liquide couplée à la spectrométrie de masse en tandem (LC-MS/MS), qui combine la séparation d'échantillons complexes par LC, une analyse de masse spectrale et une élucidation structurale par MS/MS.

L'objectif de cette thèse était de développer et d'utiliser différentes stratégies LC-MS/MS pour étudier la formation de métabolites réactifs, leur réactivité et leurs liaisons covalentes aux protéines dans différents tissus, présumé jouer un rôle important dans les effets indésirables et la toxicité. Afin d'obtenir de meilleurs résultats, la préparation des échantillons, l'acquisition et l'analyse des données ont été optimisées. D'abord, la formation de métabolites réactifs des médicaments tels que l'acétaminophène, la clozapine et l'olanzapine a été étudiée dans des microsomes hépatiques. Ensuite, les liaisons covalentes à d'importantes enzymes telles que les glutathion *S*-transférases, ont été étudiées *in vitro*. De plus, la toxicité hépatique liée à l'acétaminophène a été suivie chez les patients atteints d'insuffisance hépatique aiguë en quantifiant la quantité d'albumine sérique humaine modifiée. Enfin, la liaison de 4-hydroxynonénal aux histones et à d'autres protéines dans le cartilage des patients souffrant d'arthrose a également été étudiée.

Mots-clés : métabolites réactifs, LC-MS/MS, insuffisance hépatique aiguë, arthrose, acétaminophène, clozapine, olanzapine, 4-hydroxynonénal, histone, albumine sérique humaine, glutathion *S*-transférase

ABSTRACT

Chemically reactive metabolites can be derived from oxidative stress or from drug administration. These electrophilic species can react with proteins and other macromolecules, affecting their biological function, and potentially resulting in toxic effects or tissue injury. Identifying these modified biomolecule targets is one important step in the complete understanding of related adverse effects and toxicity.

These types of analyses are often challenging due to low quantities of modified targets, a large variety of targets with different physicochemical properties in complex biological samples and technological hurdles. One effective technique for the analysis of reactive metabolite-modified proteins is liquid chromatography-tandem mass spectrometry (LC-MS/MS), which combines the separation of complex samples by LC, and comprehensive mass spectral analysis and structural elucidation by MS/MS.

The goal of this thesis was to develop and utilize different LC-MS/MS strategies to study the formation of reactive metabolites, their reactivity and the resulting covalent binding to proteins in different tissues, presumed to play an important role in adverse effects and toxicity. In order to yield the best results, sample preparation, data acquisition and data analysis were carefully optimized. The reactive metabolite formation of the drugs acetaminophen, clozapine and olanzapine was studied in liver microsomes. Then, covalent protein binding of their reactive metabolites to important glutathione *S*-transferase enzymes was investigated *in vitro*. In addition, acetaminophen-related liver toxicity was monitored in acute liver failure patients by quantifying the amount of circulating, modified human serum albumin. Furthermore, the endogenous reactive metabolite, 4-hydroxynonenal, was studied with regards to binding to histones and other proteins in cartilage of osteoarthritis patients.

Keywords: reactive metabolites, LC-MS/MS, acute liver failure, osteoarthritis, acetaminophen, clozapine, olanzapine, 4-hydroxynonenal, histone, human serum albumin, glutathione *S*-transferase

CHAPTER I

INTRODUCTION

Throughout all living organisms, nutrients, drugs, toxins and other chemical compounds undergo chemical alterations known as the process of biotransformation. Even though these biotransformations are vital for normal cellular functions, certain unwanted species may be formed, leading to toxicity and oxidative burden. This can have an important effect on cellular survival and can lead to pathogenesis or life-threatening adverse effects.

In order to study complex biotransformation reactions, such as xenobiotic metabolism and oxidative processes, several very important technical developments and achievements have been made. Especially in analytical chemistry and biochemistry, instrumental development and advancements in sample treatment have led to an increasing body of in-depth, high-quality research to better understand diverse cellular processes. In the context of proteomics, these techniques include recombinant protein expression, selective protein extraction, affinity binding assays, protein digestion, peptide extraction, (multidimensional) liquid chromatography (LC) and hybrid mass spectrometry (MS) platforms. All these methodologies have contributed to a vast amount of data leading to constant development of novel bioinformatics tools to increase data mining efficiency.

This introductory chapter will cover a brief overview of the concept of reactive metabolites formed through xenobiotic metabolism or oxidative stress. Furthermore,

analytical tools, integral for this research, are also presented. Finally, research design and inherent challenges are discussed to conclude this chapter.

1.1 Biotransformation and toxicity

Biotransformation in the form of metabolism is an essential function in living organisms, altering lipophilic compounds to water-soluble clearance products. In general, these reactions can be grouped into phase I and phase II reactions. Phase I metabolism combines (non-synthetic) oxidative, reductive or hydrolytic reactions, which introduce or reveal a polar functional group. Conjugation reactions are grouped into phase II metabolism, adding a mostly polar endogenous molecule to the compound, such as a glucuronic acid or sulfate group. Finally, phase I and II metabolites are excreted via passive or active transport, facilitated by specific drug transporter enzymes. The process of biotransformation, although essential for clearance of xenobiotics, is also highly connected to the toxicity associated with many chemicals, forming toxic intermediates. These products, from phase I and II metabolism, may be stable toxic products, unstable reactive electrophiles, radicals or reactive oxygen species (ROS). The detailed study of these complex biotransformation reactions and the resulting products is crucial to many fields of research and drug safety assessments.

1.1.1 Xenobiotic metabolism

The underlying purpose of xenobiotic metabolism is to allow for the clearance of endogenous or exogenous molecules from the body, which cannot be processed as foods or energy sources or would ultimately be harmful if they are not removed from the body in a timely manner (Benedetti *et al.*, 2009). In general, lipophilic chemicals,

such as drugs, which need to permeate the cell's lipid-bilayer, are converted to hydrophilic metabolites to facilitate excretion into bile or urine (see Figure 1.1). Most metabolism occurs in the liver; however metabolic activities are well distributed throughout the whole body. Drug metabolism (including in the liver) following administration can limit bioavailability and lead to clearance before reaching the bloodstream. This circumstance is specifically referred to as first-pass metabolism (Pond and Tozer, 1984). In general, drug metabolites can be either pharmacologically active or inactive (Mittal *et al.*, 2015), regardless of the activity of the parent compound. The concept of an inactive parent compound (prodrug), with the formation of an active metabolite, is increasingly used in modern medicines (Rautio *et al.*, 2018).

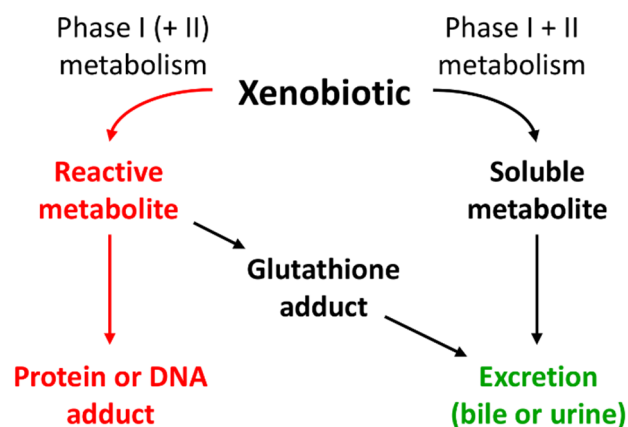


Figure 1.1 General metabolism pathway of xenobiotics, such as drugs or environmental compounds. Phase I and phase II metabolism introduces polar functional groups and conjugations to the parent compound, respectively, to increase hydrophilicity and to facilitate clearance into bile or urine. Besides stable metabolites, some intermediates can be unstable and reactive, and subsequently bind to glutathione for excretion, or to biomolecules. These pathways can equally apply to endogenously formed compounds.

Abundantly expressed in hepatocytes as major phase I enzymes, the cytochromes P450 (CYPs), are mainly found in the smooth endoplasmic reticulum and

mitochondria of the cell (Mittal *et al.*, 2015). They are heme-thiolate proteins, named after their wavelength absorption maximum at 450 nm, resulting from reduced heme bound to carbon monoxide (Guengerich, 2008). Human CYP genes comprise of more than 115 genes and pseudogenes, starting from *CYP1A1* as far as *CYP51P3* (Almazroo *et al.*, 2017). CYP3A4 is the most abundant among total hepatic CYP in human (22.1% of 3A4 in total CYP protein), followed by CYP2E1 (15.3%) and CYP2C9 (14.6%) (Achour *et al.*, 2014). An overview of important human CYP enzymes and their substrates, inducers and inhibitors can be found in Table 1.1; information was taken from databases (Stelzer *et al.*, 2016; Wishart *et al.*, 2006). Even though the amino acid sequence homology can range greatly between different isoforms, all CYPs follow the same oxidation mechanism of a one-electron radical abstraction/recombination (Guengerich, 2008; Wen and Nelson, 2011) (see Figure 1.2). Among CYP-mediated transformations, such as epoxidation, (*N,O,S*)-dealkylation, *S*-oxidation, dehalogenation, heteroatom oxidation and oxidative desulfuration (Croom, 2012), hydroxylation is the primary CYP-catalyzed reaction (Zanger and Schwab, 2013). With nicotinamide adenine dinucleotide phosphate (NADPH, Figure 1.3)-cytochrome P450 oxidoreductase (POR) and/or cytochrome *b*₅-mediated electron transfer, this leads to the incorporation of hydroxyl groups into the parent compound (see Equation 1.1; with RH as the parent compound and ROH as the oxidized metabolite):



Table 1.1 Selection of common human CYPs, selected substrates, inhibitors, inducers and expression sites (APAP, acetaminophen; CLZ, clozapine; OLZ, olanzapine)

CYP	Substrate	Inhibitor	Inducer	Expression
1A2	APAP, CLZ, diclofenac, dihydralazine, ethinylestradiol, paroxetine, tamoxifen, OLZ and zolpidem	Amiodarone, CLZ, dihydralazine and isoniazid	Insulin and nicotine	Liver and kidney
2B6	Diclofenac, halothane and tamoxifen	Raloxifene and tamoxifen	Dexamethasone	Liver
2C9	CLZ, diclofenac, ethinylestradiol, halothane and tamoxifen	Amiodarone, amodiaquine, isoniazid, OLZ, sulfamethoxazole, tamoxifen and tienilic acid	Rifampicin and secobarbital	Liver, liver secretome and lung
2C19	Amiodarone, CLZ, diclofenac and tamoxifen	Amiodarone, CLZ, ethinylestradiol, isoniazid and OLZ	Dexamethasone	Liver
2D6	APAP, amiodarone, CLZ, OLZ and tamoxifen	Amiodarone, amodiaquine, CLZ, isoniazid, OLZ and tamoxifen	Dexamethasone	Liver
2E1	APAP, halothane, isoniazid and tamoxifen	Diclofenac and isoniazid	Dexamethasone and isoniazid	Liver and lung
3A4	APAP, amiodarone, CLZ, dexamethasone, diclofenac, ethinylestradiol, halothane and tamoxifen	APAP, amiodarone, CLZ, dexamethasone, diclofenac, isoniazid and OLZ	APAP, CLZ, dexamethasone and tamoxifen	Liver

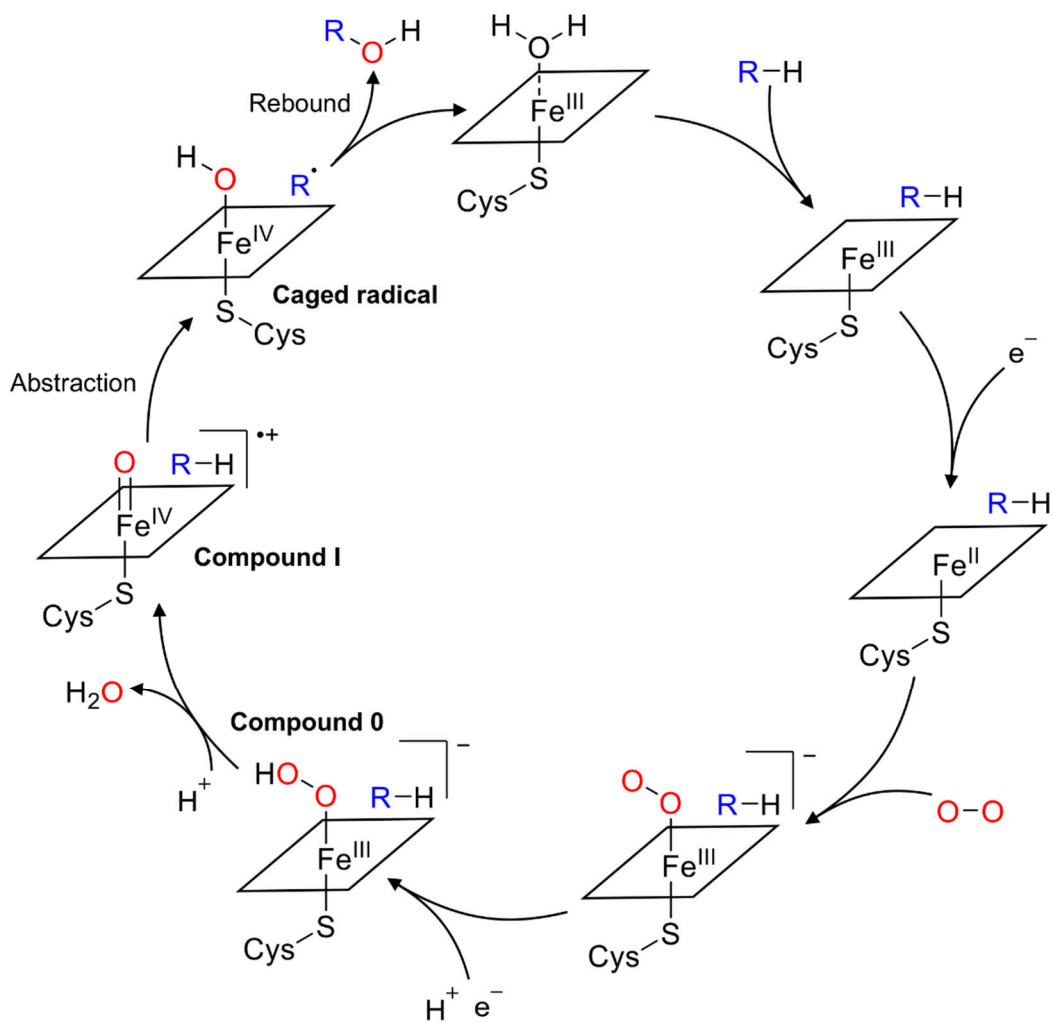


Figure 1.2 Catalytic reaction cycle of CYP enzymes. The cycle starts with heme iron in low-spin state and displacement of weakly bound water by the substrate (RH), which results in a high-spin state iron. Further reduction and incorporation of O₂ leads to a ferric-peroxo intermediate and subsequent protonation leads to a hydroperoxo compound (also known as compound 0). Upon further protonation and dehydration an oxoferryl porphyrin radical cation (compound I) is formed. Compound I then abstracts a hydrogen from the substrate, forming a substrate radical (R[·]). Subsequently, hydroxyl "rebounds" to the substrate radical and forms the hydroxylated substrate product (ROH). The resting state is achieved by water returning to the distal coordination position of the iron.

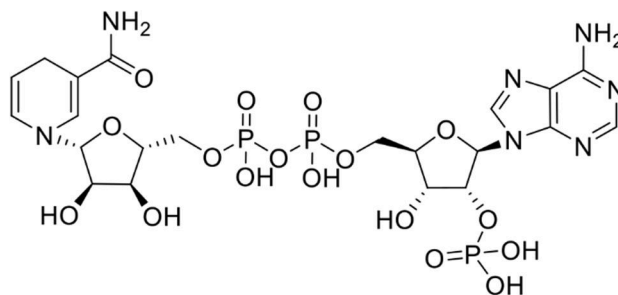


Figure 1.3 Structure of the cofactor NADPH.

Other important phase I enzymes are flavin-containing monooxygenase (FMOs), monoamine oxidase, (carboxyl-) esterases (CESs), peroxidases, epoxide hydrolases (EPHXs), (alcohol/aldehyde) dehydrogenases (ADHs/ALDHs) and amidases (Croom, 2012). Unlike CYPs, FMOs catalyze solely oxygenation reactions of soft nucleophilic groups (nitrogen, sulfur, phosphorus or selenium) requiring an oxygen, NADPH as a cofactor and a flavin adenine dinucleotide prosthetic group (Kulkarni, 1984). FMOs are more substrate-specific and are less susceptible to induction or inhibition effects (Kulkarni, 1984). In addition, electron transfer of FMO-catalyzed reactions happens directly from NADPH and does not require NADPH reductases (Croom, 2012). Aside from increasing research interest as phase I enzymes, FMOs have gained recent attention as potent biocatalysts in chemical industries (Huijbers *et al.*, 2014).

Aside from non-synthetic metabolism, the contribution and importance of conjugating enzymes are increasingly becoming research focus (Terada and Hira, 2015). During phase II clearance, xenobiotics or their phase I metabolites are conjugated to a mostly hydrophilic, endogenous compound via several different transferase enzymes. Most common phase II transferases are UDP-glucuronosyltransferases (UGTs), sulfotransferases (SULTs), *N*-acetyltransferases (NATs) and methyltransferases (MTs) (Jancova *et al.*, 2010). Most phase II enzymes

are mainly located in the cytosol, with the exception of UGTs, which are mainly found as membrane-associated proteins in microsomal compartments (fragments of endoplasmic reticulum and ribosomes). One specific set of transferases, namely glutathione *S*-transferases (GSTs) (Sheehan *et al.*, 2001), are important catalysts for glutathione (GSH, see Figure 1.4) conjugation¹ to highly electrophilic substrates (see Equation 1.2; where RX represents an electrophilic compound, X⁻ an anion and R-SG the conjugate):

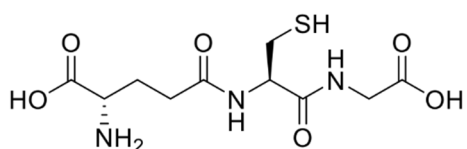


Figure 1.4 Structure of the antioxidant tripeptide GSH, consisting of a glutamate residue γ -linked to cysteine followed by a regular peptide bond between cysteine and glycine.

GSTs are ubiquitously present in almost all species. They are highly distributed throughout the human body, and are mostly expressed in liver, kidney, brain, heart, lung and gut. They are crucial for electrophilic substrate detoxification, and protection from endogenously produced free radicals and from oxidative stress. They consist of two superfamilies, one being soluble GSTs, distributed widely in the cytosol, as well as in the mitochondria. In some cases, soluble GSTs are also considered as two separate

¹ It should be noted that GSH conjugations can also be non-enzymatic. However, GST catalysis increases the reactivity of GSH significantly for electrophilic substrates.

superfamilies, namely cytosolic and mitochondrial proteins. These soluble GSTs are further separated into eight classes: alpha, delta, kappa, mu, omega, pi, theta and zeta (A, D, K, M, O, P, T and Z, respectively). Located in the endoplasmic reticulum and outer mitochondrial membrane, the second GST superfamily is referred to as microsomal transferases or membrane-associated proteins in eicosanoid and GSH metabolism (MAPEG) (Jakobsson *et al.*, 2008). There are six members in the MAPEG superfamily, including microsomal GST (MGST) 1, 2 and 3. Cytosolic GSTs are known to dimerize (Sheehan *et al.*, 2001), whereas MAPEG proteins have shown to form dimers (Lam *et al.*, 1997; Nicholson *et al.*, 1993) and trimers (Hebert *et al.*, 1997). MGST1 is an example of one that is known to trimerize (Hebert *et al.*, 1995). A brief overview of GSTs can be found Table 1.2; information was taken from (Arakawa *et al.*, 2012; Bag *et al.*, 2013; Balogh and Atkins, 2011; Barańczyk-Kuźma *et al.*, 2004; Boerma *et al.*, 2011; Buchard *et al.*, 2012; Committee on Herbal Medicinal Products, 2013; Czerwinski *et al.*, 1996; Kap *et al.*, 2014; Kusama *et al.*, 2006; Kweekel *et al.*, 2009; Mans *et al.*, 1992; Mukanganyama *et al.*, 1997; Münzel *et al.*, 2014; Nobuoka *et al.*, 2004; Parker *et al.*, 2008; Peters *et al.*, 2000; Ralat and Colman, 2006; Sawers *et al.*, 2014; Stelzer *et al.*, 2016; Stocco *et al.*, 2014; Stoehlmacher *et al.*, 2002; van Iersel *et al.*, 1997; Zhai *et al.*, 2016).

Table 1.2 Selection of common human GSTs and their known substrates, inhibitors, inducers and top expression sites (APAP, acetaminophen; CLZ, clozapine; HNE, 4-hydroxynonenal)

GST	Substrate	Inhibitor	Inducer	Expression
GSTA1	Azathioprine and busulfan	Curcumin	N/A	Liver secretome, liver and nasal epithelium
GSTA4	HNE	N/A	N/A	Esophagus, spleen and liver
GSTM1	APAP, azathioprine, busulfan, carboplatin, cisplatin, isosorbide mononitrate and oxaliplatin	Curcumin and chloroquine	N/A	Liver secretome, liver and adipocyte
GSTM2	N/A	N/A	N/A	Cardia, oral epithelium and rectum (and liver)
GSTP1	APAP, busulfan, carboplatin, chlorambucil, cisplatin, etoposide and oxaliplatin	α -tocopherol acetate / succinate, clomipramine, CLZ, curcumin, etacrynic acid and vitamin E	N/A	Amniocyte, oral epithelium and spleen (and liver)
GSTT1	APAP	N/A	N/A	Cardia, liver secretome and stomach
MGST1	N/A	N/A	N/A	Nasal epithelium, liver and nasopharynx

Besides important biological functions as phase II enzymes, GSTs are also very commonly used in protein pull-down assays. For this purpose, the coding sequence of a GSTM 26 kDa isozyme (UniProt: P08515) from *Schistosoma japonicum* (Smith and Johnson, 1988) is cloned into the expression vector of the protein of interest yielding a fusion protein after expression in bacteria, yeast or cell lines. Subsequently, the fusion protein can be selectively purified through the high binding affinity to GSH. This can be used to facilitate purification using GSH-agarose (Datta *et al.*, 2015). This represents a viable alternative to polyhistidine-tag (His-tag) purification using nickel-nitrilotriacetic acid resin or biotin using streptavidin affinity ligands but can also be easily applied to targeted expression and subsequent purification of any other GST.

GSH conjugation, through GSTs, is one of the first steps leading to mercapturic acid (*N*-acetylcysteine *S*-conjugate) formation. The hepatic GSH conjugates are transported out of the cell (phase III) for further metabolism by γ -glutamyl transferase and dipeptidases, which catalyze the successive removal of glutamate and glycine, respectively. These enzymes are predominantly found at the surface of epithelial tissues (outer surfaces of organs and blood vessels). The resulting cysteine conjugates are reabsorbed, then acetylated by intracellular NATs forming mercapturic acids (see Figure 1.5). These metabolites are then released into the circulation and delivered to the kidneys for final elimination. Involving the liver as major site of GSH conjugation and the kidneys as primary sites for GSH to cysteine conjugate conversion, the mercapturic acid pathway is generally considered to be an inter-organ process (Hinchman and Ballatori, 1994).

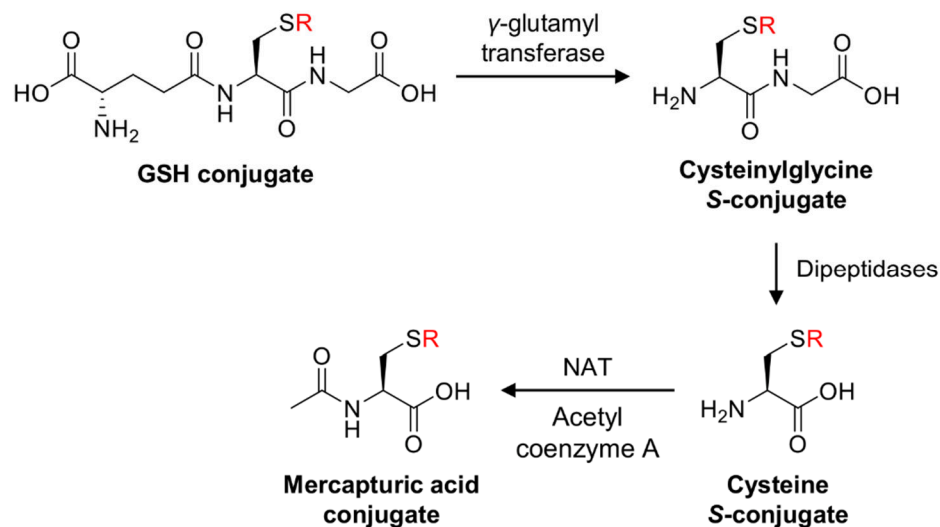


Figure 1.5 Exemplary mercapturic acid pathway starting with a R-SG conjugate and resulting in the mercapturic acid conjugate.

1.1.2 Oxidative stress

Besides phase I and phase II metabolism, another important factor in (aerobic) cellular life is the dependence on molecular oxygen. Oxidation-reduction (redox) homeostasis, like pH control, is essential and related processes are involved in many fundamental functions (Sies *et al.*, 2017). However, imbalances between pro-oxidants and antioxidants cause disturbances in redox state and related toxic effects, known as oxidative stress. As by-products derived from oxidative stress, ROS present reactive molecules and free radicals, able to react with many compounds. They are predominantly formed during mitochondrial electron transport and are associated to destructive processes, but also to important cell signaling cascades (Hancock *et al.*, 2001). Common ROS are superoxide, hydrogen peroxide, hydroxyl radical, peroxy radical, alkoxy radical and singlet oxygen. Endogenous ROS production is located in the mitochondria, plasma membrane, endoplasmic reticulum and peroxisomes (Moldovan and Moldovan, 2004), and are either enzymatically controlled or formed

via autooxidation of several precursors, including catecholamines and hydroquinone (Ayala *et al.*, 2014). Cells have evolved a complex system of response mechanism to ROS. However, cases of increased levels of ROS can lead to toxic effects (Betteridge, 2000).

High amounts of ROS are considered to be mostly detrimental for health and are involved in extensive tissue damage. This damage includes the degradation of lipids, in the form of lipid peroxidation (LPO) (Ayala *et al.*, 2014) (see Figure 1.6). Polyunsaturated fatty acids (PUFAs) are the preferential targets of LPO. Commonly in cells, LPO is initiated by iron and to some extent copper. Cellular iron is mostly ligated by heme, bound in iron–sulfur clusters or stored in the protein ferritin. However, a small amount of iron is loosely ligated and thus able to participate in redox reactions (Breuer *et al.*, 2008), including Fenton/Haber–Weiss chemistry which can yield hydroxyl radicals. This step initiates subsequent steps of LPO propagation and termination, ultimately leading to the formation of multiple degradation products (see Figure 1.6). Malondialdehyde and 4-hydroxynonenal (HNE) are very common LPO by-products. The latter is especially linked to peroxidation of ω -3 and ω -6 PUFAs in the biomembrane (Riahi *et al.*, 2010).

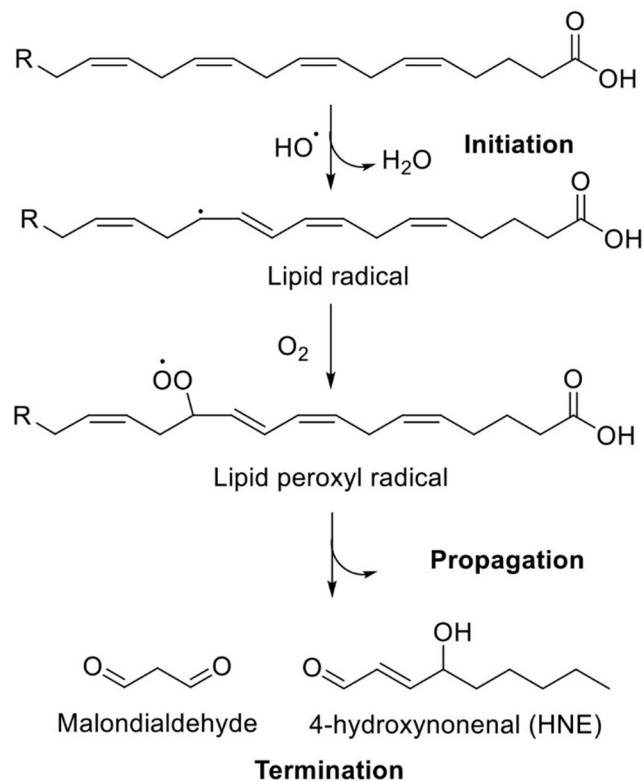


Figure 1.6 A brief overview of the LPO process of a PUFA, starting with the attack from a pro-oxidant resulting in the formation of a lipid radical. Subsequently, the lipid radical reacts with molecular oxygen forming a lipid peroxy radical which either propagates or terminates the reaction. Propagation by-products can be malondialdehyde or HNE.

The LPO product HNE is perceived to be one of the most toxic α,β -unsaturated aldehydes due to its highly reactive nature (Guillén and Goicoechea, 2008). It has been reported that HNE is able to covalently bind to a variety of biomolecules, such as proteins, lipids and nucleic acids (Poli *et al.*, 2008; Schaur, 2003). Being putatively involved in many signaling pathways (Lee *et al.*, 2008a), HNE is also believed to be highly cytotoxic. Studies have shown toxicity in the low micromolar range (Benedetti *et al.*, 1984). Thus, detoxification through phase I and phase II metabolism generally

occurs to protect cell functions from high amounts of HNE. An important detoxification pathway is the GSH conjugation through the GSTA4 dimer (GSTA4-4) (Balogh and Atkins, 2011), which results in removal of the α,β -unsaturation and formation of the HNE-GSH adduct or its lactone form. Furthermore, ALDH2 was found to play a protective role against HNE toxicity as well (Chen *et al.*, 2008). The formation of HNE-GSH conjugates, for instance, can be used to monitor HNE formation and LPO effects in different disease states by quantifying HNE-mercapturic acid conjugates in urine (Kuiper *et al.*, 2010).

1.1.3 Reactive metabolite binding to macromolecules

Unstable or reactive metabolites, such as HNE as well as many xenobiotic metabolites, play a pivotal role in the pathogenesis of idiosyncratic adverse drug reactions (IADRs) and tissue degenerative processes. Initially reported by the Millers in the late 1940s, the concept of reactive metabolite formation was first linked to biomolecule binding and chemical carcinogenicity (Miller and Miller, 1947, 1952). They stated that *N,N*-dimethyl-4-aminoazobenzene was found to be a carcinogen in rat livers through metabolic activation to a reactive intermediate. After an increasing body of research, these electrophilic intermediates are known to react with nucleophilic groups in biological macromolecules, including proteins (Kevin Park *et al.*, 1987). A brief overview of common substructures of reactive metabolites can be found in Figure 1.7. Reactions often occur as Michael-type additions between the nucleophilic center in the biomolecule and the reactive metabolite, the Michael acceptor (see Figure 1.8) (Schwöbel *et al.*, 2010). Reversible Schiff base reactions are observed as well, but are less prevalent and, based on their reversibility, difficult to detect (Doorn and Petersen, 2002). Information of each reactive metabolite structure, as seen in Figure 1.7, was taken from (Bolton, 2014; Jaladanki *et al.*, 2017; Klopčič and Dolenc, 2019; Murata and Kawanishi, 2011; Mutlib *et al.*, 2002; Peterson, 2013; Rademacher *et al.*, 2012;

Scott Obach and Kalgutkar, 2010; Walton *et al.*, 1997; Wei and Yin, 2015; Wiciński and Węclewicz, 2018).

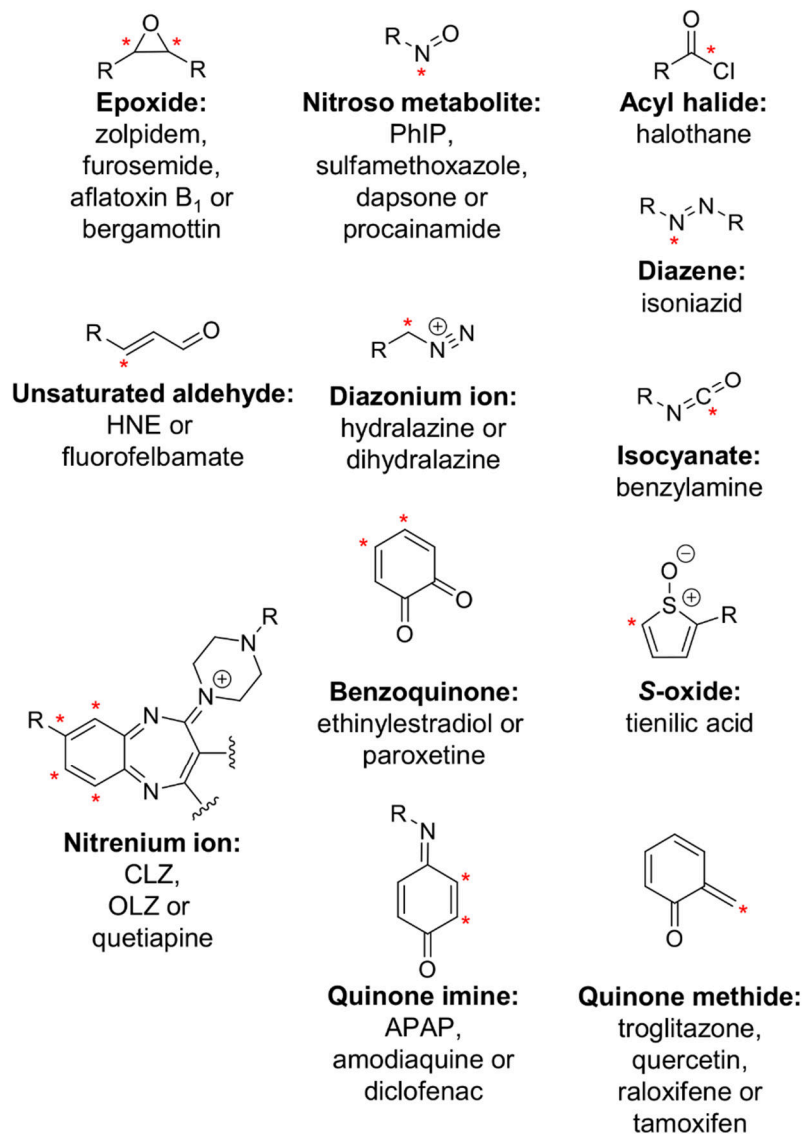


Figure 1.7 A brief overview of common reactive metabolite/intermediate substructures formed through transformation of exemplary parent drugs/compounds. Irreversible binding sites (*e.g.*, from Michael addition) of nucleophiles are marked with a red asterisk (*) (APAP, acetaminophen; CLZ, clozapine; HNE, 4-hydroxynonenal; OLZ, olanzapine; PhIP, 2-amino-1-methyl-6-phenylimidazo[4,5-*b*]pyridine).

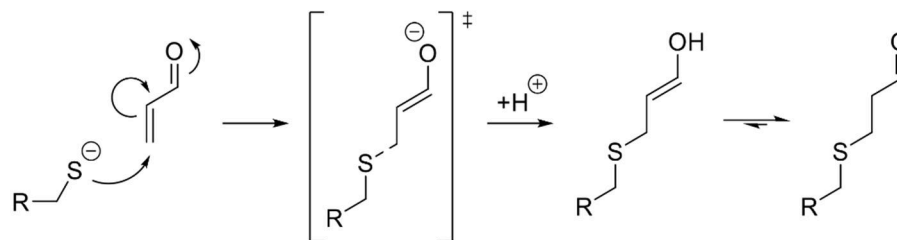


Figure 1.8 Michael addition of a thiol to an unsaturated aldehyde forming a carbanionic transition state and, subsequently after protonation, the enolic product (keto–enol tautomerization is possible, depending on structure).

In current theories, reactive metabolite-macromolecule adducts are directly or indirectly linked to the onset of toxicity (Park *et al.*, 2005; Utrecht and Naisbitt, 2013). High reactivity combined with low circulation makes the identification and quantitation of these adducts *in vivo* complicated, up to impossible (Guengerich, 2005). The bioactivation to reactive metabolites that can interfere with cellular functions, specifically in liver, offers many challenges. Moreover, there is evidence for drug metabolism by keratinocytes or immune cells, leading to organ-specific reactions, such as in skin cells (Baron *et al.*, 2001; Oesch *et al.*, 2007; Saeki *et al.*, 2002) or in neutrophils (Utrecht, 1992). For instance, covalent protein adducts were found in normal human epidermal keratinocytes treated with sulfamethoxazole, proving metabolic activity of skins cells and possible bioactivation of topical medications (Reilly *et al.*, 2000). Reactive metabolites can lead to the irreversible loss of function or activity (Attia, 2010), through their intrinsic reactivity towards GSH and protein thiols, resulting in irreversible adduct formation, and potential protein inhibition and immunological reactions. Several drugs are known to form reactive (and toxic) intermediates, including acetaminophen (APAP), halothane, hydralazine and tienilic acid (Kalgutkar *et al.*, 2012). Furthermore, there are many compounds generally toxic across species (*e.g.*, APAP, isoniazid, tetracycline and cyclosporine A) (Pan *et al.*, 2019). In order to design sufficient *in vitro* metabolite risk assessments, especially in

liver tissue, liver microsomal or S9 fractions are often used as model metabolism systems (Ames *et al.*, 1973; Levin *et al.*, 1984). Metabolites generated from human liver fractions have been found to be mostly identical to metabolites in Aroclor 1254 (polychlorinated biphenyl mixture)-induced rat liver systems (Obach and Dobo, 2008). Thus, induced rat liver fractions are currently a common tool for *in vitro* studies, since it enables the formation of increased amounts of metabolites of interest (Obach and Dobo, 2008). There are several enzyme-inducing reagents available with different effects on protein induction (Borlak and Thum, 2001; Ejiri *et al.*, 2005; Martignoni *et al.*, 2004; Poloyac *et al.*, 2004; Silkworth *et al.*, 2005). A brief overview of these inducers and induced enzymes can be found in Table 1.3, and a comparison of relative amounts of phase I and II enzymes in Aroclor 1254-induced rat liver microsomes (RLM) can be found in Figure 1.9. However, constant development and improvement of reliable analytical methods is in high demand, since IADRs are representing a large challenge in the health care sector and drug development industries. Even though being dose-dependent in susceptible individuals and more frequent in the context of overdoses, IADRs can also occur at doses within the usual therapeutic range (Cameron and Ramsay, 1984), which presents many challenges even after drug approval. In addition, patients which are rechallenged with the same drug after experiencing IADRs are likely to encounter the same IADRs in a shorter period of time (Utrecht, 2007). Thus, correct prediction of IADRs remains highly complicated. Even parent compounds with very similar structure and ability to form reactive intermediates can be very differently cytotoxic. For instance, the antipsychotics clozapine (CLZ) and olanzapine (OLZ) are structurally similar and both are able to form a reactive nitrenium ion. However, CLZ demonstrates high levels of cytotoxicity and is known to form IADRs in about 1% of patients (Pirmohamed and Park, 1997), whereas OLZ is considerably safer (Gardner *et al.*, 1998b).

Table 1.3 Brief overview of liver fraction inducers and known induced rat enzymes

Inducer	Induced rat enzymes
Aroclor 1254	CYP1A1, 1A2, 2B1, 2B2, 3A1 and 4A1; and GSTA2
Dexamethasone	CYP1A2, 2B1 and 3A1
Isoniazid	CYP2E1
Phenobarbital	CYP2B1 and 3A1
β -naphthoflavone	CYP1A1, 1A2 and 2B1

Besides idiosyncratic drug-induced liver injury and acute liver failure (*e.g.*, from APAP), other forms of IADRs have been observed as well. For instance, IADR in the form of agranulocytosis has been reported with a number of drugs. Agranulocytosis is believed to be caused by the oxidation/activation of drugs through myeloperoxidase-derived hypochlorous acid in neutrophils (white blood cells) (Hampton *et al.*, 1998; Uetrecht, 1992). The condition can lead to mature neutrophil destruction and to severe leukopenia and increased susceptibility to infections. As with drug-induced hepatotoxicity, proposed mechanisms of drug-related agranulocytosis include direct toxicity and immunological reactions (Claas, 1989; Tesfa *et al.*, 2009). Neutropenia, the severe outcome of agranulocytosis, is defined as an absolute neutrophil count $<1,500$ cells/ μ L. Drugs like CLZ, amodiaquine, carbamazepine, diclofenac, dipyron, levamisole, prophylthiouracil, spironolactone, sulfamethoxazole-trimethoprim, ticlopidine and vancomycin have been associated with neutropenia (Andersohn *et al.*, 2007).

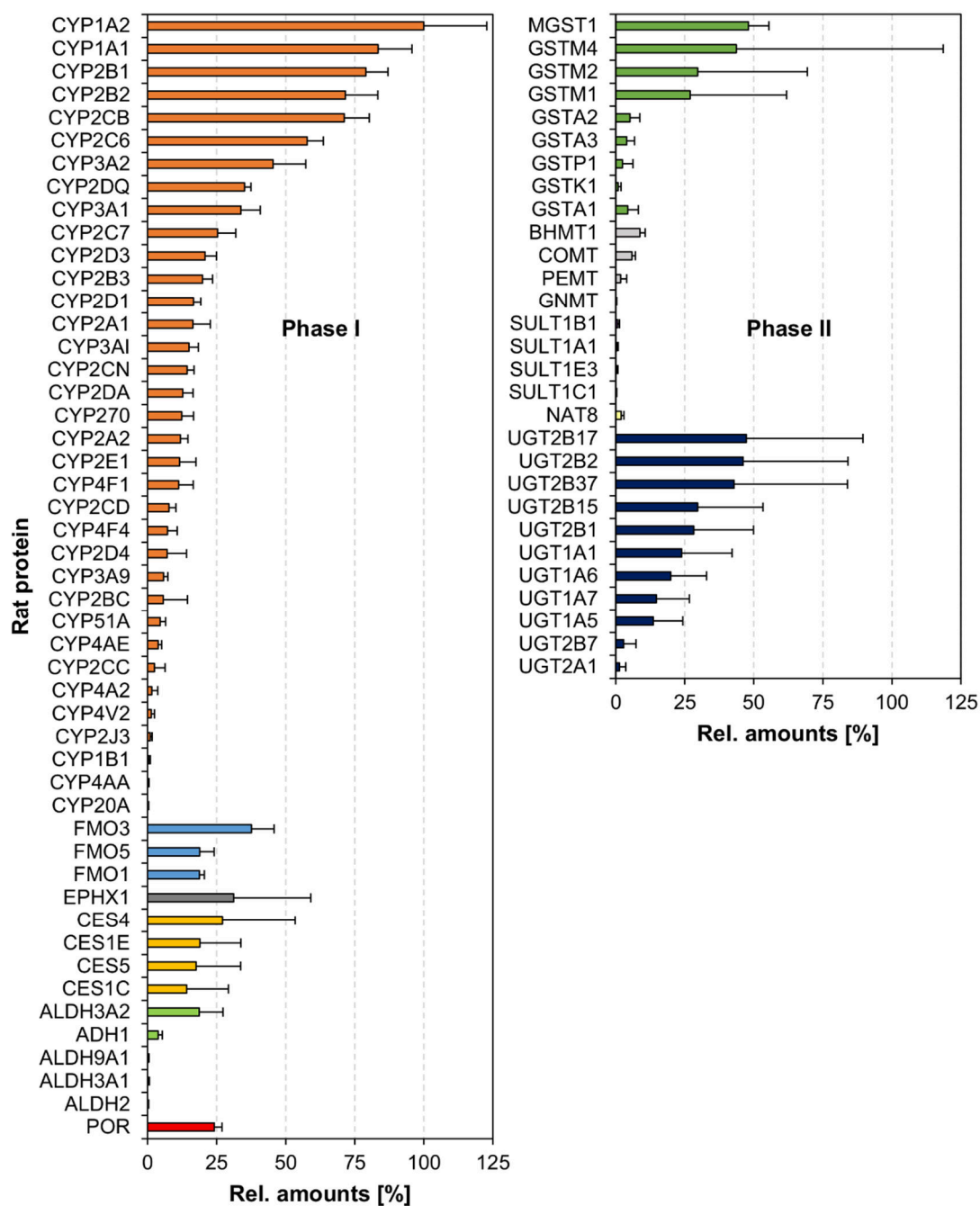


Figure 1.9 Relative amounts of Aroclor 1254-induced RLM phase I and II enzymes. Data was based on unpublished label-free quantitation of microsomal peptic and tryptic digests ($n = 6$; error bars representing standard deviation, SD).

While the precise mechanism of reactive metabolite toxicity remains unknown, some studies have linked damaging effects to conformational changes of modified biomolecules (Nerland *et al.*, 2001; Oakley *et al.*, 1997a). Other findings suggest that some IADRs are potentially immune-related (Utrecht and Naisbitt, 2013). A possible mechanism is the hapten hypothesis (Landsteiner and Jacobs, 1935; Langman and Cohn, 2000). The mechanism describes that upon modification of a native protein with the hapten, here the reactive metabolite, antibody production is induced. These antibodies then bind to the reactive metabolite-protein complex and might initiate a severe immune response against the modified protein. Utrecht and co-workers have introduced other hypotheses as well (Utrecht, 2007), including the danger hypothesis (Matzinger, 1994; Pirmohamed *et al.*, 2002; Séguin and Utrecht, 2003), in which reactive metabolites cause cell damage and the subsequent release of danger signals and the upregulation of costimulatory factors. This might initiate an immune response. Nevertheless, mechanism remain mostly hypothetical and highly complex, while research progress has been slow (Utrecht, 2008). Furthermore, the exact subcellular location of reactive metabolite formation and covalent protein binding has been shown to be important as well. Comparing the covalent binding of APAP to its less or non-toxic² regioisomer, 3-acetamidophenol (AMAP) (Kenna, 2013) (Figure 1.10), equal levels of protein binding was observed for both compounds at equimolar drug concentrations. However, subcellular fractionation pinpointed at increased levels of covalent binding to mitochondrial proteins for APAP and not AMAP (Tirmenstein and Nelson, 1989). This highlighted the importance of quantitative assessments of reactive metabolite binding in order to interpret underlying toxicity correctly. This makes detailed evaluation of metabolite-protein binding very important, especially careful

² To date, the exact toxicity of AMAP is not fully elucidated (Hadi *et al.*, 2013a; Kenna, 2013).

identification and quantitation of low abundant adducts, demanding sensitive and accurate analytical tools.

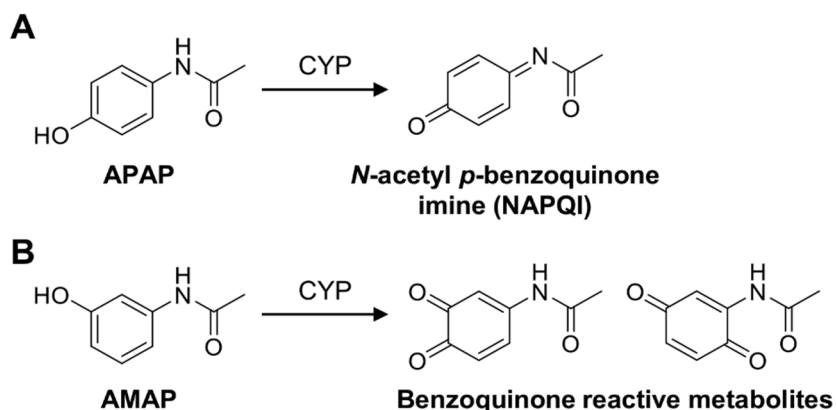


Figure 1.10 Comparison of reactive metabolite formation of APAP and its regioisomer AMAP (based on (Kenna, 2013)).

1.2 Liquid chromatography-mass spectrometry-based technologies

Following the commercialization of gas chromatography-mass spectrometry (GC-MS) systems in the 1970s, hyphenation of LC and MS was considered the next logical step. With the introduction of atmospheric pressure ionization techniques in the 1980s, it was finally possible to robustly hyphenate LC systems to MS platforms, allowing for separation of soluble, nonvolatile compounds in solution with subsequent detection and analysis of their ions in the gas phase. This allowed for reliable analysis of complex sample mixtures, including isomeric species with identical masses, which would pose an important challenge in MS alone. Since then, LC-MS has been applied to many fields of research and routine analysis (see Figure 1.11), including clinical biochemistry, quality control in food processing, environmental analysis and many industrial sectors, especially the pharmaceutical industry.

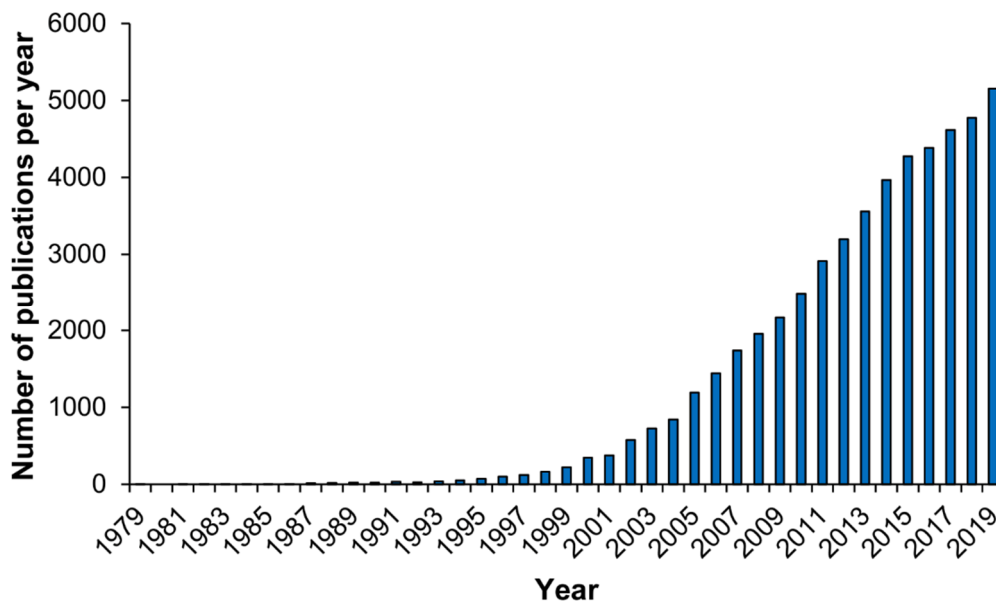


Figure 1.11 Number of LC-MS-related publications over the course of time. Bar graph based on a simple PubMed search of the acronym LC-MS (taken from (National Center for Biotechnology Information, 2020)).

1.2.1 (Two-dimensional)-liquid chromatography

Generally in LC applications, three main aspects play significant roles in achieving adequate separation of a mixture of analytes/compounds: 1) the physicochemical properties of the analyte, 2) the stationary phase chemistry and 3) the mobile phase composition. In reversed-phase (RP) LC, a nonpolar stationary phase (*e.g.*, 18-carbon-long hydrocarbon attached to the surface of silica, C18) is used in combination with a polar solvent as mobile phase. These solvents are often a combination of water and water-miscible organic solvents (*e.g.*, acetonitrile or methanol). Briefly, separation of a mixture of compounds is achieved as they interact differently with the stationary phase (immobilized onto particles in a column) and the mobile phase, while a constant or gradual flow of mobile phase is applied. This flow

can either be isocratic, with constant mobile phase composition, or gradually changing in composition (in gradient mode). Hydrophobic molecules tend to adsorb to the hydrophobic stationary phase, whereas hydrophilic molecules will pass through (elute off) the column earlier. Chemical alterations of the stationary phase, mobile phase composition and additives, as well as changes in gradients can have an influence on selectivity, retention and peak resolution (Poole and Lenca, 2017). However, a relatively trivial technique to improve separation of highly complex samples is multidimensional LC, especially two-dimensional (2D)-LC. This application combines two independent, orthogonal separation techniques in series. Consecutive chromatography can be achieved in an online or offline setup, in which, respectively, either both LC systems are directly coupled or a second dimension of LC is applied to pre-fractionated samples (Wu *et al.*, 2012). 2D-LC is most effective if two orthogonal separation techniques are employed using different stationary phases, such as RPLC combined with strong cation exchange (SCX) chromatography, which separates ions and polar molecules on the basis of their affinity to an ion-exchange resin (Nägele *et al.*, 2004). However, orthogonality can also be achieved by altering the properties of the mobile phase or its additives, while the stationary phase remains the same. Especially, changes in pH alter the charge state of solubilized ions (*e.g.*, peptides). As a result, orthogonal RPLC separation using high-pH (pH ~9 to 10) mobile phases in the first dimension combined with low-pH (pH ~2 to 3) elution in the second dimension (online to MS) is possible, and has become more popular recently (Batth *et al.*, 2014; Yang *et al.*, 2012). This allows for orthogonal LC using identical stationary phase and mobile phases (except additives) (Yang *et al.*, 2012). This is especially interesting in the hyphenation of LC and (electrospray) MS, where only a limited selection of volatile additives and solvents are suitable (see Table 1.4). This can have a positive effect on sample throughput, recovery and reproducibility, due to less sample preparative steps needed, such as multiple solid-phase extractions (SPEs) to remove incompatible additives prior to MS.

Table 1.4 Overview of (electrospray) MS-compatible solvents and additives

Solvent or additive	Use	General guidelines
Water	Solvent	None
Acetonitrile (ACN)	Solvent	None
Methanol (MeOH)	Solvent	None
Ethanol	Solvent	None
(Iso)propanol	Solvent	None
Ammonium hydroxide	Additive	None
Formic acid	Additive	None
Acetic acid	Additive	None
Ammonium formate	Additive	≤10 mM
Ammonium acetate	Additive	≤10 mM
Dichloromethane	Solvent	≤5%
Dimethylformamide	Solvent	≤5%
Dimethyl sulfoxide	Solvent	≤5%
Trifluoroacetic acid	Additive	≤0.5%
Sulfolane	Additive	≤1%

1.2.2 Tandem mass spectrometry

In general, MS allows for the mass-to-charge (m/z) analysis of gaseous ions. Since its first practical implementation in 1912 by J. J. Thomson (Thomson, 1913), many mass analyzers, for the separation of these gaseous ions, have been established, including magnetic sectors, ion traps, Fourier-transform ion cyclotron resonance (FTICR) MS, quadrupoles and time-of-flight (TOF) platforms (see overview in Table 1.5).

Table 1.5 Overview of commercially available MS platforms

MS platform	<i>m/z</i> limits	Mass resolution	Mass accuracy (ppm)	Ion transmission
Quadrupole	10–4,000	Unit	100	Continuous
Sector	<20,000	5,000	<10	Continuous
Ion trap				
Linear ion trap	50–4,000	2,000	100	Pulsed
Quadrupole ion trap	<3,000	1,000	100	Pulsed
Orbitrap	<50,000	<500,000	<5	Pulsed
FTICR	<30,000	1,000,000	<1	Pulsed
TOF				
Linear TOF	Unlimited	10,000	<10	Pulsed
Reflectron TOF	<10,000	>50,000	<10	Pulsed

MS is highly dependent on ionization effects. This includes the ability to form molecular ions (M^+) through high-energetic ionization techniques or protonated molecules or salt (*e.g.*, sodium or potassium) adducts ($[M+nH]^{n+}$, $[M+nNa]^{n+}$ and $[M+nK]^{n+}$) via soft ionization techniques. Ion suppression, specifically in electrospray ionization (ESI)-based MS, can be caused by changes in the spray droplet properties via the presence of non-volatile or less volatile chemicals (King *et al.*, 2000) including salts, ion-pairing agents, or detergents and surfactants. These compounds change effects in droplet formation, droplet evaporation or hinder ion evaporation out of the droplet (see Figure 1.12). In addition, ion evaporation was observed to be competitive between different ions in the same droplet, leading to potential signal depletion for specific analytes co-eluting with interfering compounds (Annesley, 2003; Furey *et al.*, 2013). Ion suppression continues to be a noticeable challenge in ESI-MS assays and needs to be constantly addressed in method development and optimization.

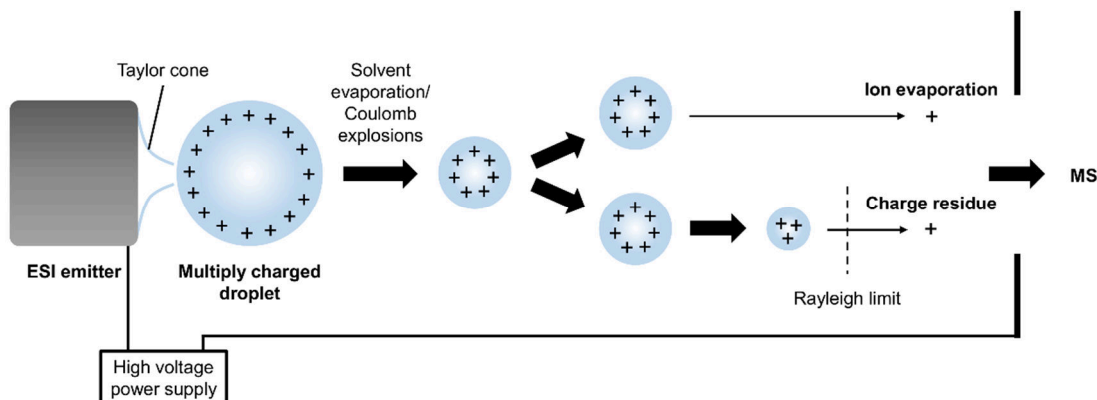


Figure 1.12 Schematic of possible ESI models. A high voltage (several kV) is applied between the ESI emitter and the MS orifice to create an aerosol of multiply charged droplets. These droplets shrink through solvent evaporation (through heat) and Coulombic explosion. Possible ion formation models are 1) ion evaporation of a small ion or an unfolded protein from the droplet, or 2) formation of a residual ion after the droplet charge exceeds the Rayleigh limit and the droplet explosively dissociates.

As stand-alone MS systems, quadrupole (often abbreviated as Q) and TOF are highly available in many different commercial systems. With high ion transmission and ion scan capabilities, low-cost production and robust setup, quadrupoles are a versatile tool in MS laboratories. In general, a quadrupole analyzer consists of four parallel metal rods, fixed in a square configuration (see Figure 1.13). Gaseous ions enter the quadrupole with a trajectory parallel to the rods (z-axis in Figure 1.13) and are attracted by an opposite charge on the rods. This charge is possible by applying a direct current (DC) and an alternating current (AC) to pairs of opposite rods. With inhomogeneous periodic changes in the potential Φ_0 (consisting of a DC voltage U and a radio frequency (RF) voltage V , see Equation 1.3), attractive forces are interchanging with repulsive forces, leading to a displacement of ions from their trajectory on the z-axis, following the rules of the Mathieu equation (see Equation 1.4) (Gross, 2004).

$$\Phi_0 = U + V\cos(\omega t) \quad (1.3)$$

$$\begin{aligned} \frac{d^2x}{d\left(\frac{\omega t}{2}\right)^2} + (a_x + 2q_x\cos(\omega t))x &= 0 \\ \frac{d^2y}{d\left(\frac{\omega t}{2}\right)^2} + (a_y + 2q_y\cos(\omega t))y &= 0 \end{aligned} \quad (1.4)$$

Parameters a and q are dependent on a specific range of m/z values (see Equation 1.5) (Gross, 2004):

$$a_x = -a_y = \frac{4eU}{m_i r_0^2 \omega^2} \quad \text{and} \quad q_x = -q_y = \frac{2eU}{m_i r_0^2 \omega^2} \quad (1.5)$$

Thus, ions oscillating within a $2r_0$ distance between electrode rods traverse the quadrupole without hitting the rods. This can be implemented in filtering out these specific ions using specific magnitude of RF voltage V and ratio of U/V . The final mass resolution of linear quadrupoles is limited by the U/V ratio and mechanical accuracy of the rods ($\pm 10 \mu\text{m}$). Higher resolution can only be achieved by reducing ion transmission. As a result, linear quadrupoles operate most often at unit resolution (resolution of integer masses only) and often fail to resolve ions with similar integer masses (also referred to as isobaric ions) (Gross, 2004).

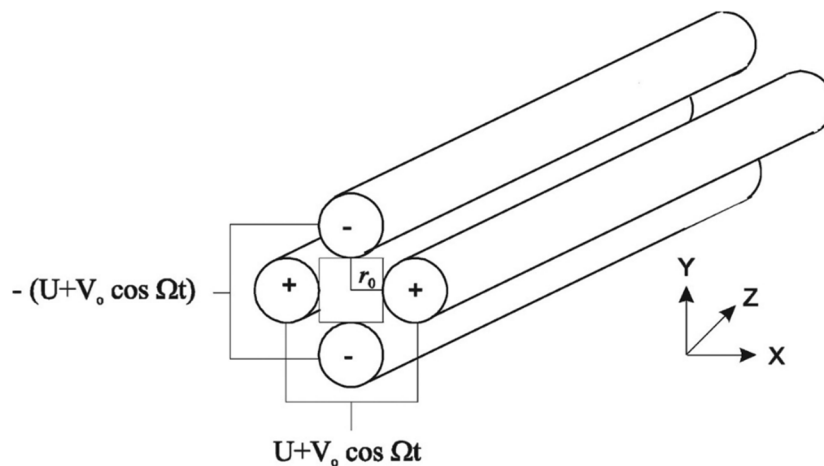


Figure 1.13 Schematic of a linear quadrupole mass analyzer (adapted from (March and Todd, 2015)).

In TOF-based MS, a very simple principle is applied. Ions are accelerated into a field-free drift tube of a pre-defined length (l). If a mixture of ions is accelerated simultaneously, larger and less charged ions (larger m/z values) travel through the drift tube for a longer amount of time (t) than smaller and more highly charged ions (smaller m/z values). The energy (E_{el}) from accelerating the ions through applying a voltage U , is equal to the product of the charge of the ion (z), the electron charge e and U . Since ions are accelerated in high vacuum, the potential energy, E_{el} , is completely converted into kinetic energy (E_{kin}) of an ion with the mass m_i (see Equation 1.6) (Gross, 2004):

$$E_{el} = ezU = \frac{m_i v^2}{2} = E_{kin} \quad (1.6)$$

The velocity of the ion in Equation 1.6 is v and is proportional to the square root of the charge-to-mass ratio (z/m) of the ion (see Equation 1.7) (Gross, 2004).

$$v = l/t = \sqrt{\frac{2ezU}{m_i}} \quad (1.7)$$

This allows for very accurate determination of m/z values based on simple travel time measurements (in field-free vacuum). Theoretically, TOF combines high resolving power with an unlimited ion transmission capability. However, accurate measurements are only possible if ion acceleration is simultaneous for all ions and if all ions are in the same location. Effects of time, spatial and kinetic energy dispersion reduce the mass resolution of linear TOF analyzers drastically. Developed by B. A. Mamyrin (Mamyrin, 2001), the reflectron (or reflector) TOF analyzer was introduced to correct inaccuracies from different kinetic energy dispersion effects. This technique employs an ion mirror (reflectron) that applies a retarding electric field to ions passing through it (see Figure 1.14). When ions penetrate that electric field, they travel until they lose their kinetic energies and are repelled. Ions with higher kinetic energies enter the reflectron deeper, whereas lower energetic ions are repelled faster. This corrects kinetic energy dispersions of ions with identical m/z values and therefore increases the TOF mass resolving power (Gross, 2004).

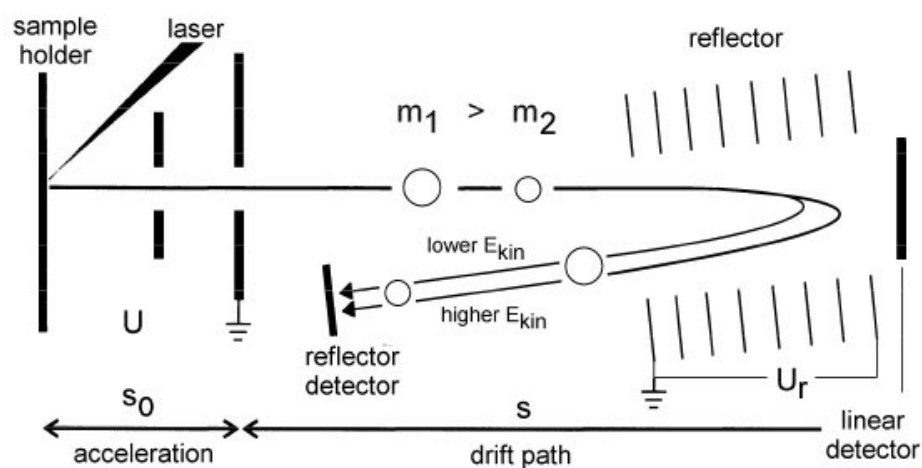


Figure 1.14 Reflectron TOF schematic using a laser ionization technique, subsequent ion acceleration and a reflectron at the opposite side of the drift path. A second detector to allow linear TOF acquisition is possible as well (adapted from (Gross, 2004)).

Although most MS techniques are being continuously developed and improved, individual advantages and disadvantages have consequently led to the hyphenation of two or more MS techniques to increase performance. This concept is generally referred to as tandem MS (MS/MS) and has become reasonably standard on commercial systems. Using multiple MS filters in tandem makes it possible to include diverse fragmentation techniques, allowing for more structural information to be obtained. A general scheme of MS/MS systems with a fragmentation cell can be found in Figure 1.15. Overall, this made MS/MS a powerful technique for analysis of unknown compounds, especially combined with LC, which provides separation of complex samples and additional information through retention time. However, applicable hyphenation of LC-MS/MS requires sufficient mass acquisition speed, to allow mass and fragmentation analysis on the separation time scale. In addition to analytical speed, m/z acquisition range, mass resolution and mass accuracy are important key elements in choosing a MS platform for a given experiment. The instrument's mass resolution (R , see Equation 1.8) is determined by the peak width (Δm) at half maximum (FWHM) of a mass signal (m), whereas the difference of the measured (accurate) mass (m_i) to the theoretical (exact) mass (m_a) is defined as the mass accuracy (Gross, 2004). The relative mass accuracy, the difference between the measured and exact m/z divided by the exact m/z , is usually reported in parts per million (ppm, see Equation 1.9).

$$R_{FWHM} = \frac{m}{\Delta m} \quad (1.8)$$

$$(\text{Relative}) \text{ mass accuracy} = \frac{m_i - m_a}{m_a} \times 10^6 \quad (1.9)$$

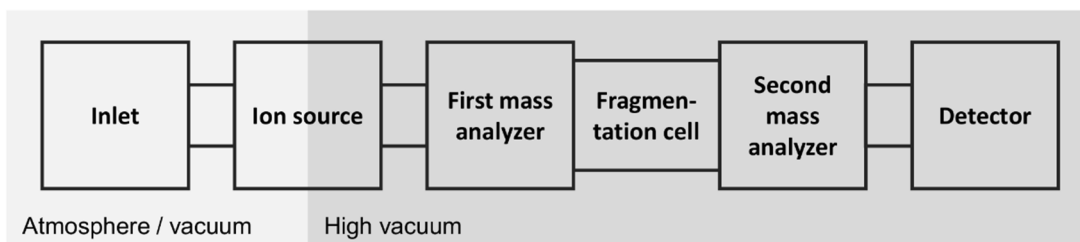


Figure 1.15 General scheme of hyphenated MS/MS platforms. LC-MS/MS systems usually operate under atmospheric pressure at the sample inlet. Fragmentation can occur at different positions of the MS/MS system, depending on the utilized technique. In this example, a discrete fragmentation cell is separated between two mass analyzers, as in the case of the very popular triple quadrupole platform.

Two common MS/MS setups are triple quadrupoles (QqQ) and quadrupole–time-of-flight systems (QqTOF). Both instruments use a low-resolution quadrupole mass analyzer at the first stage, which can function as a continuous or static mass filter (Q_1), followed by an RF-only quadrupole serving as the fragmentation (collision) cell, and either a second quadrupole mass analyzer or a higher resolution TOF analyzer. For QqQ platforms, the most common acquisition mode is multiple reaction monitoring (MRM, also known as selected reaction monitoring) (Lange *et al.*, 2008; Picotti and Aebersold, 2012), whereas QqTOF systems are mostly used for discovery workflows in data-dependent acquisition (DDA) mode (Mann *et al.*, 2001). Both these platforms use collision-induced dissociation (CID) for precursor ion fragmentation in most cases (see Figure 1.16). Typically, CID is possible by accelerating ions through a collision cell filled with an inert gas (nitrogen or argon) at a pressure of 0.1–0.3 Pa (Gross, 2004). This enables selective fragmentation in low-resolution MRM, or structural elucidation or confirmation in high-resolution MS/MS product ion scans. Acquisition using DDA mode rely mostly on a survey scan (no fragmentation, MS1) in which the acquisition software selects, in an automated fashion (based on pre-defined settings and m/z inclusion/exclusion lists), ions for subsequent fragmentation analysis (MS2). This

automated selection can be list-, isotope pattern-, mass defect- or intensity-dependent. It is often restricted to the most abundant precursor ions, often referred to as DDA with top N ion selection (N being the maximum number of ions selected in each acquisition cycle). Many other MS/MS or analysis modes are possible on commercially available platforms. Other common modes include, selected ion, precursor ion and neutral loss scans (on QqQ) (Hopfgartner *et al.*, 2004), data-independent acquisition (DIA) on QqTOF or hybrid Orbitrap platforms (Ludwig *et al.*, 2018), or multiple steps of fragmentation in ion traps (tandem-in-time or MSⁿ) (Cody *et al.*, 1982). Additional ion fragmentation techniques include electron capture or transfer dissociation (ECD/ETD) of multiply charged ions (Riley and Coon, 2018; Zubarev, 2004), surface-induced dissociation (Wysocki *et al.*, 2008), infrared multiphoton dissociation (Brodbeck and Wilson, 2009), or ultraviolet photodissociation (Ly and Julian, 2009), among others.

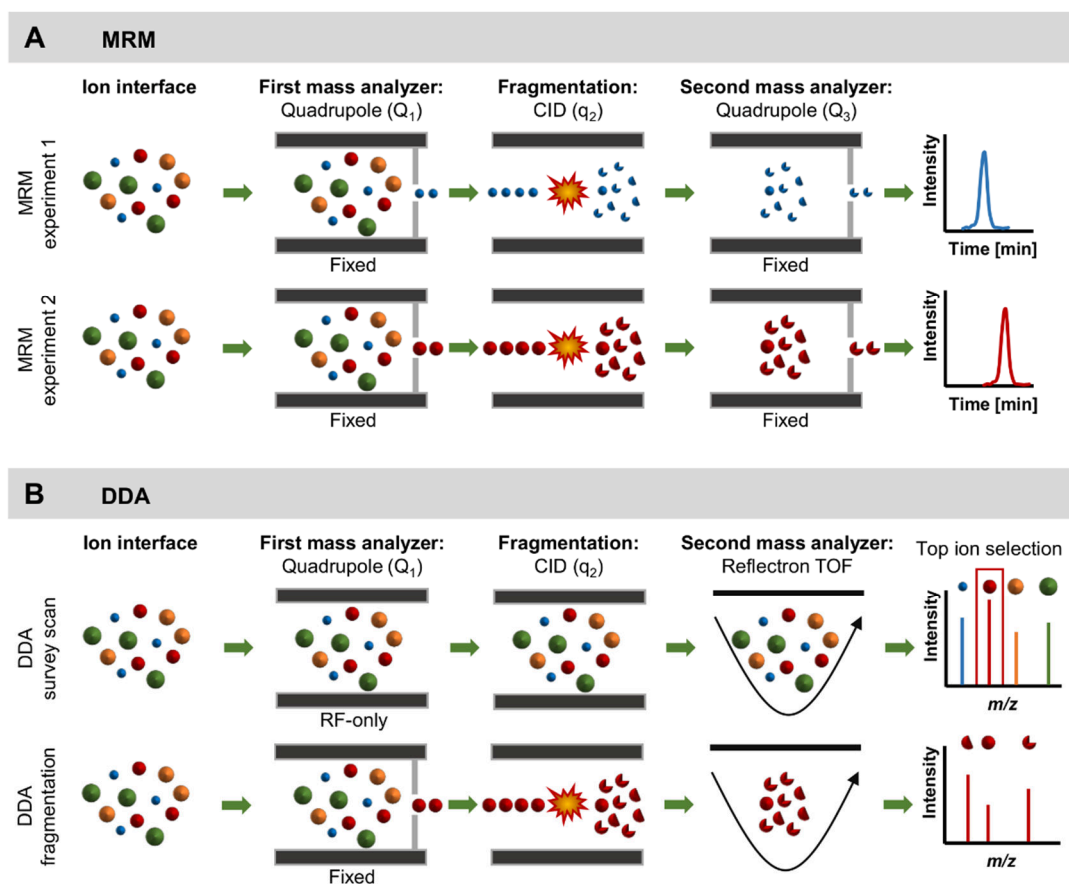


Figure 1.16 Representative MS analysis scheme of (A) two MRM experiments (transitions) and (B) a DDA survey scan with subsequent ion selection, based on ion intensity, and fragmentation analysis of selected ion. In MRM acquisitions, pre-selected precursor and product ion pairs are monitored through fixed ion isolation in Q_1 and Q_3 , respectively. DDA is presented here in a QqTOF setup using a reflectron TOF as second mass analyzer. During the DDA survey scan, Q_1 and q_2 are set to be both non-mass filtering (RF-only mode). Mass analysis occurs only through reflectron TOF measurement.

In order to analyze highly complex samples with appropriate sensitivity, mass accuracy and under reproducible conditions, several analytical standards have been established. To facilitate the hyphenation of LC and MS, scanning cycles and acquisition modes were especially optimized. Thus, to allow for accurate determination of the area under chromatographic peaks, approximately 10–20 data points are needed for each LC peak (see Figure 1.17A). Accurate peak area measurements are especially important in quantitative studies, where peak intensities are less reliable. This limits the number of MS experiments possible during an acquisition cycle, which is referred to as the cycle time (see Figure 1.17B). As an effect, the maximum number of MS experiments depends on the sensitivity of the detector and analytical speed of the mass analyzer. The actual time each individual MS experiment collects data and accumulates detector signal is known as the dwell or accumulation time. A representative experimental setup can be found in Figure 1.17C, where an MRM experiment with eight individual transitions is equally distributed within 1 s of total cycle time. In addition, a top 15 ions DDA method is represented with a MS1 precursor scan of 250 ms, to ensure high sensitivity for precursor ion selection, and 15 individual MS/MS experiments of each 50 ms accumulation time. These 15 fragmentation experiments in general require less accumulation time, due to the reduced spectral complexity and increased selectivity of a Q₁ pre-filtered MS2 acquisition (see Figure 1.16B). However, Q₁ selectivity is limited by its unit resolution (Jemal and Ouyang, 2000). This can lead to co-selection (co-isolation) of multiple precursors, and cause interferences in MRM transitions (Qi *et al.*, 2015a) or overlapping (composite) MS/MS spectra in HRMS fragmentation spectra (Chalkley *et al.*, 2014). As an effect, quantitative MRM or DDA studies could be negatively impacted by co-isolated precursors. This makes a well optimized LC separation indispensable.

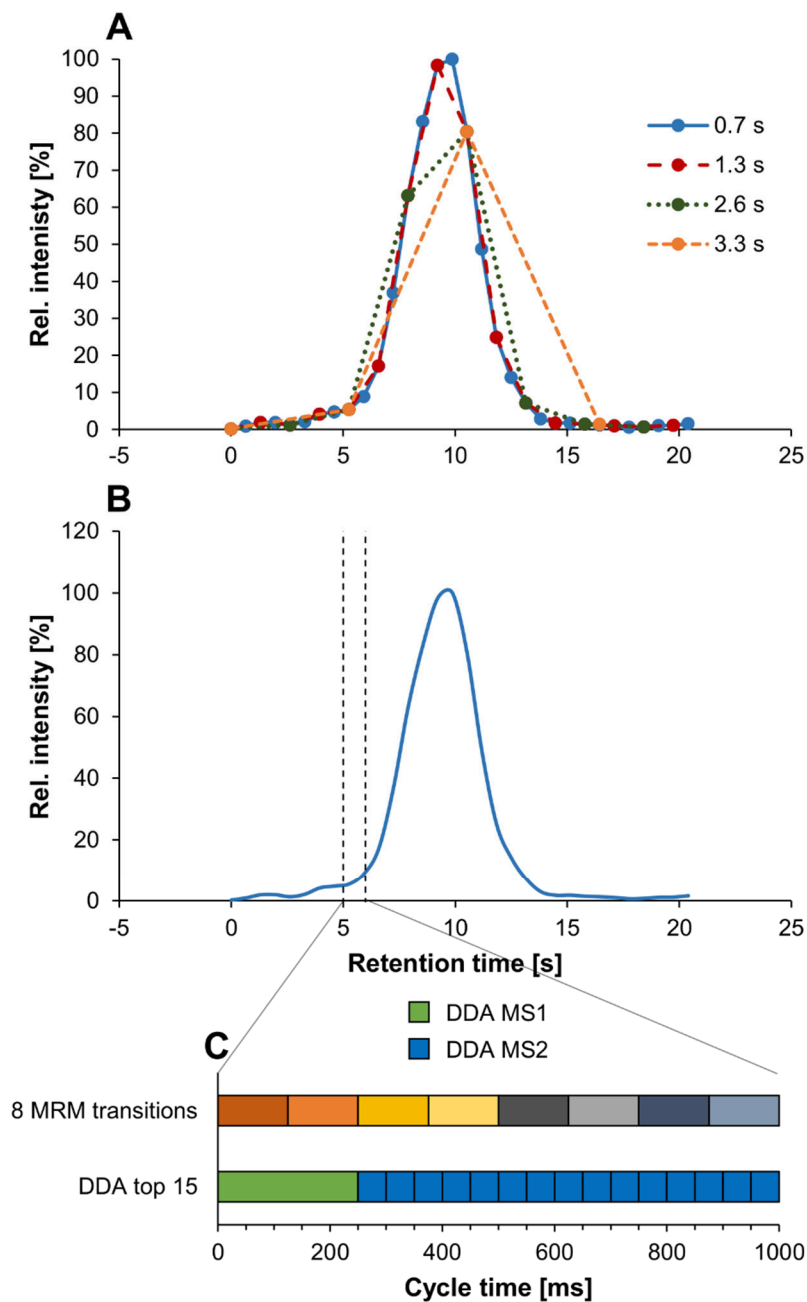


Figure 1.17 (A) Representation of a chromatographic peak (<10 s total peak width) acquired using four different cycle times. (B) Visualization of a cycle time of 1 s (C) with representative MRM analysis using eight transitions or DDA with top 15 ions.

1.2.3 Drug metabolite analysis

Drug metabolism studies are crucial for determining drug efficacy and toxicity within the pharmaceutical industry. The industrial discipline of DMPK (drug metabolism and pharmacokinetics), correct understanding of ADME (absorption, distribution, metabolism, and excretion), and identification of toxic and reactive metabolites are critical aspects during drug development and beyond. These studies profit from constant improvements in analytical technologies, which facilitate drug metabolite identification in various biological matrices. Reactive metabolite screening and biotransformation studies were established as an integral part in drug candidate selection with increased success rates (Caldwell *et al.*, 2009).

In earlier times of drug metabolite analyses, QqQ (and later quadrupole-linear ion trap, QqLIT) platforms were the preferred tool in MS-based studies. Precursor ion and neutral loss scans (see Figure 1.18) allowed the pharmaceutical scientist to screen for metabolites, without knowing their exact structures or chemical formula. These scanning techniques employ pre-existing knowledge of specific, anticipated fragmentation of metabolites and conjugate classes (Clarke *et al.*, 2001). Combining the high sensitivity of QqQ systems with the great versatility of precursor ion scans, neutral loss scans or MRM acquisitions, these techniques are widely accepted as standards in profiling of stable metabolites and conjugation products. Adding to the overall performance of quadrupole-based technologies, QqLIT platforms offer additional experiments (such as enhanced product ion scans, enhanced resolution scans, enhanced multiply charged scan and MS³). These systems are built on a QqQ framework, where Q₃ can be either used as a regular quadrupole or as a LIT with increased sensitivity, varying resolution and the potential to accumulate ions over time. Thus, researchers were able to combine higher resolution fragmentation analysis with the high sensitivity of regular QqQ (Hopfgartner *et al.*, 2003; Mauriala *et al.*, 2005; Xia *et al.*, 2003; Yao *et al.*, 2008).

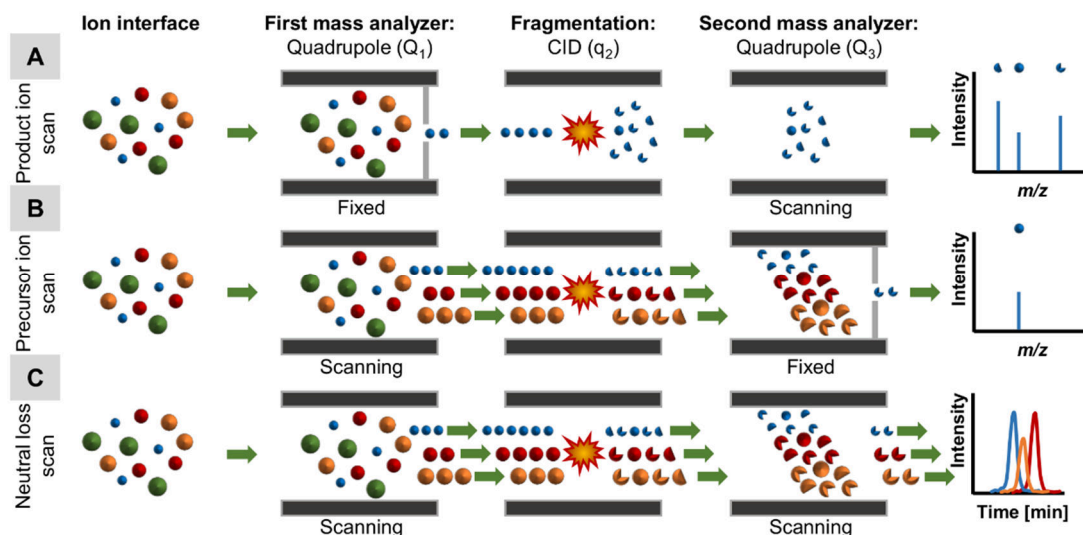


Figure 1.18 Simplified QqQ analysis schematic representation of (A) product ion scan, (B) precursor ion scan and (C) neutral loss scan experiments. In a product ion scan, Q₁ is set at a fixed m/z of a pre-selected precursor with subsequent acquisition (scanning) of its product ions. The precursor ion scan utilizes a similar concept where the product ion m/z is fixed in Q₃ and possible precursors are scanned in Q₁. The resulting mass spectrum consist of all precursor m/z values yielding the pre-defined product ion. Neutral loss scanning methods utilize Q₁ and Q₃ in synchronous scanning mode with a pre-defined mass difference (Q₁–Q₃), corresponding the mass of the pre-selected neutral loss (e.g., water loss of 18 u or ammonia loss of 17 u).

HRMS instruments, including QqTOF, Orbitrap and FTICR MS, were rarely used in earlier developments of drug metabolite identification studies. High instrument and maintenance costs, compared to QqQ and QqLIT systems, and missing true precursor ion and neutral loss scans slowed down the implementation of HRMS techniques. However, with the increasing performance and analytical speed of HRMS and ion traps (Peterman *et al.*, 2006), these platforms became increasingly attractive. For instance, novel isotope pattern-dependent MS/MS acquisition modes introduced another useful tool to detect metabolites of drug precursors with distinct isotope pattern

(*e.g.*, the ^{35}Cl -to- ^{37}Cl ratio of $\sim 3:1$, see example in Figure 1.19) (Du *et al.*, 2013; Ruan and Zhu, 2010). This allows for HRMS/MS of potentially unknown or unpredicted metabolites, and opening up the possibility for structural interpretation. Consequently, other DDA acquisitions, such as intensity based DDA, have been increasingly and effectively used for metabolite screening, especially GSH trapped reactive metabolites (Ma *et al.*, 2008a, 2008b). With the detailed study of GSH adducts and specific characterization of their fragmentation behavior (Baillie and Davis, 1993; Haroldsen *et al.*, 1988; Pearson *et al.*, 1990), useful GSH-dependent characteristics have been identified. Fragmentation of GSH occurs preferentially at the peptide backbone of GSH. For instance, the neutral loss of pyroglutamate ($\text{C}_5\text{H}_7\text{NO}_3$) is very common in CID-based fragmentation of GSH adducts (Baillie and Davis, 1993). This neutral loss of 129.0426 u is thus commonly used in QqQ neutral loss scans or post-acquisition filtering of HRMS/MS data. Other GSH-related fragment ions or neutral losses (see complete overview in Table 1.6) include the neutral loss of 307.0838 u (loss of $\text{C}_{10}\text{H}_{17}\text{N}_3\text{O}_6\text{S}$) in positive ion mode (Levsen *et al.*, 2005; Yan and Caldwell, 2004) and the product ion at m/z 272.0888 ($\text{C}_{10}\text{H}_{14}\text{N}_3\text{O}_6$) in negative mode (Dieckhaus *et al.*, 2005). However, some GSH adducts have higher signals as multiply charged ions in positive ion electrospray MS, thus altering the fragmentation behavior of the GSH adduct and potentially interfering with precursor ion or neutral loss acquisition, or post-analysis data filtering (Dieckhaus *et al.*, 2005). Another noteworthy acquisition strategy, the mass defect-based DDA, was specifically developed for HRMS instruments to yield MS/MS acquisition of drug metabolites in complex biological matrices (Liu *et al.*, 2011). Mass defects (non-integral portion of m/z values) of metabolites normally range (mass defect change) within 70 mu of the mass defect of the parent drug (Zhang *et al.*, 2003). This allows for pre-defined m/z limits for a more targeted DDA approach, avoiding fragmentation analysis of unnecessary or unrelated features.

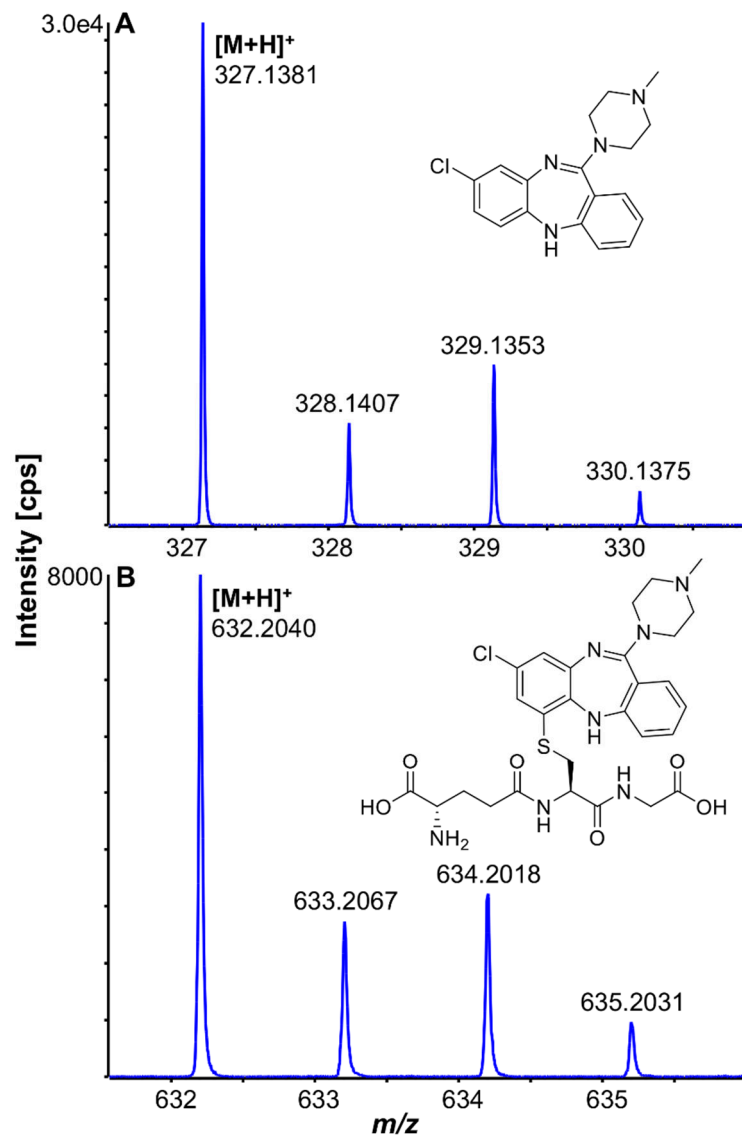


Figure 1.19 Isotope pattern of [M+H]⁺ adducts of (A) clozapine (C₁₈H₁₉ClN₄) and (B) its GSH adduct (CLZ-2H+GSH, C₂₈H₃₄ClN₇O₆S).

Table 1.6 Selection of common phase II conjugate-related characteristic product ions and neutral losses

Conjugate	Neutral loss (u)	Neutral chemical formula	Product ion (<i>m/z</i>)	
			[M+H] ⁺	[M-H] ⁻
GSH	307.0838	C ₁₀ H ₁₇ N ₃ O ₆ S	308.0910	306.0765
	305.0681	C ₁₀ H ₁₅ N ₃ O ₆ S		
	275.1122	C ₁₀ H ₁₇ N ₃ O ₆		
	273.0961	C ₁₀ H ₁₅ N ₃ O ₆	274.1033	272.0888
		C ₁₀ H ₁₃ N ₃ O ₅		254.0782
	146.0691	C ₅ H ₁₀ N ₂ O ₃		
		C ₅ H ₈ N ₂ O ₃	145.0608	
	129.0426	C ₅ H ₇ NO ₃	130.0499	
	75.0320	C ₂ H ₅ NO ₂	76.0393	
	Mercapturic acid	163.0303	C ₅ H ₉ NO ₃ S	
129.0426		C ₅ H ₇ NO ₃	130.0499	
Glucuronide		C ₆ H ₈ O ₇		191.0197
	176.0321	C ₆ H ₈ O ₆		175.0248
		C ₅ H ₆ O ₃		113.0244
		C ₄ H ₆ O ₂		85.0295
Sulfate	79.9568	SO ₃		
	63.9619	SO ₂		

HRMS-based DDA techniques normally collect a large amount of data, making efficient data mining technologies necessary to extract metabolism-related information. These strategies include isotope-pattern-dependent data mining (Zhu *et al.*, 2009a), neutral loss and product ion filtering (Ruan *et al.*, 2008). Another targeted data-mining technique is relying on extracted ion chromatograms, where structurally anticipated metabolites and conjugates are directly searched based on their corresponding shift in

(MS1) mass (see Table 1.7 for common metabolite mass shifts) and retention time. In addition, untargeted data-mining technologies involve several background subtraction algorithms (Zhang *et al.*, 2008; Zhang and Yang, 2008; Zhu *et al.*, 2009b), control sample comparisons and approaches derived from metabolomics studies. A great advantage of untargeted strategies is that unbiased detection of metabolites and conjugates is possible, without pre-existing knowledge of potential metabolism or well understood behavior during metabolism itself or sample treatment/analysis.

Table 1.7 Common phase I and phase II transformations and corresponding exact mass shift^a

Phase	Metabolism	Neutral mass shift (u)	Description	Mass defect change (mu)
I	Deacetylation	-42.0106	-C ₂ H ₂ O	-10.6
I	Dehydration	-18.0106	-H ₂ O	-10.6
I	Demethylation	-14.0157	-CH ₂	-15.7
I	Dehydrogenation	-2.0157	-2H	-15.7
I	Hydrogenation	+2.0157	+2H	+15.7
I	Oxidation	+15.9949	+O	-5.1
I	Internal hydrolysis	+18.0106	+H ₂ O	+10.6
II	Methylation	+14.0157	+CH ₂	+15.7
II	Acetylation	+42.0106	+C ₂ H ₂ O	+10.6
II	Glycine conjugation	+57.0215	+C ₂ H ₃ NO	+21.5
II	Sulfation	+79.9568	+SO ₃	-43.2
II	Mercapturic acid	+161.0147	+C ₅ H ₇ NO ₃ S	+14.7
II	Glucuronidation	+176.0321	+C ₆ H ₈ O ₆	+32.1
II	GSH conjugation	+305.0682	+C ₁₀ H ₁₅ N ₃ O ₆ S	+68.2

^aMass shifts of conjugations are based on hydrogen substitution. Halide substitution is also possible and mass shifts change accordingly.

1.2.4 Proteomics techniques

Proteins are essential cellular building blocks and represent the functional information of genes in the form of enzymatic catalysis, signaling and molecular interactions. The study of proteins, often referred to as proteomics, is essential as a third “omics”-discipline of biochemical sciences (Yarmush and Jayaraman, 2002). Proteomics encompasses the identification, modification, quantitation and localization of proteins in different cell types and matrices. One widely established technique to study proteins is known as the western blot. This technique was initially described by H. Towbin and co-workers in the 1970s (Towbin *et al.*, 1979) and named³ by W. N. Burnette (Burnette, 1981). In brief, denaturated proteins are separated by gel electrophoresis and then transferred (blotted) onto nitrocellulose or polyvinylidene difluoride membrane. Using a (primary) target protein-specific antibody and subsequently a (secondary) antibody, the proteins of interest are visualized and detected. Usually, the secondary antibody is complexed with an enzyme that produces a detectable signal after addition of a specific substrate. Through separate marker solutions, western blot enables size estimation of proteins (Mahmood and Yang, 2012). Several factors play a pivotal role in western blot analyses: 1) the primary antibody specificity and affinity, and 2) the target protein concentration in the desired sample. Low analyte amounts or low specificity/affinity can have detrimental effects on detection. In addition, post-translational modifications (PTMs) and protein–protein interactions can alter the size of a given target protein. In addition, western blot results are mostly of qualitative nature. Quantitative western blot analysis is often only

³ Western blot, like the RNA northern blot, is not capitalized and is a play on the DNA Southern blot technique, named after E. Southern.

available as relative (or semi) quantitation, comparing equally treated and analyzed samples against a control set.

Another protein immunoassay is known as enzyme-linked immunosorbent assay (ELISA). E. Engvall and P. Perlmann, and B. K. Van Weemen and A. H. W. M. Schuurs developed the diagnostic assay in the 1970s (Engvall and Perlmann, 1972; Van Weemen and Schuurs, 1971). The antigen, here the target protein, is immobilized in a direct or indirect manner, the latter using a specific capture antibody. Then, a primary antibody is added which binds to the antigen protein. This primary antibody can be labeled with an enzyme that, similar to western blotting, creates a detectable signal after a substrate is added. This procedure is known as direct ELISA, whereas indirect ELISA utilizes a secondary (detection) antibody which is complexed with the enzyme. Detectable signals are directly linked to the antigen concentration, enabling quantitation of target proteins/antigens in a cost-effective manner (Shah and Maghsoudlou, 2016). For instance, ELISA is commercially used in at-home and point-of-care testing, including modern pregnancy tests in which the hormone human chorionic gonadotropin is detected via a sandwich ELISA technique (Vaitukaitis, 2004). However, ELISA shares the same advantages and disadvantage with western blot techniques and immunoassays in general. All immunoassay techniques are dependent on specific and effective antibodies against the proteins of interest.

High-throughput and advanced proteomics techniques, in which the proteins are analyzed without the necessity for antibodies, are either MS-based or are relying on nuclear magnetic resonance spectroscopy. MS-based techniques combine high sensitivity with selectivity (Dunn *et al.*, 2011; Emwas, 2015). Nevertheless, MS analysis of proteins and peptides remained challenging until relatively recently, based on their polar, non-volatile and thermally unstable nature. Requiring soft ionization techniques that transfer proteins and peptides into the gas phase without degradation, two important developments paved the way for MS-based proteomics. These

techniques are known as matrix-assisted laser desorption ionization (MALDI) (Karas and Hillenkamp, 1988; Tanaka *et al.*, 1988) and ESI (Fenn *et al.*, 1989). With MS being capable of proteomics analyses, three specific applications were established: 1) analysis of protein expression, 2) analysis of protein–protein interactions and 3) identification of modification sites. In general, MS-based techniques are considered highly exhaustive and versatile tools to answer questions in the multidisciplinary research field of proteomics (Yates *et al.*, 2009).

MS strategies in proteomics encompass the analysis of enzymatically/chemically digested proteins up to intact protein–protein interaction complex analyses. The analysis of proteolytically digested proteins is known as bottom-up or shotgun proteomics, whereas intact protein MS is referred to as top-down or native proteomics. Complex peptide or protein samples are effectively separated by different types of (multidimensional) LC strategies prior to MS analysis, each with advantages for specific study needs. These can be based on RP, ion exchange (*e.g.*, SCX) or isoelectric point separations. Especially in bottom-up proteomics the “break-then-sort” idea has been broadly distributed. The “break-then-sort” approach is referring to initial protein digestion with one or multiple proteases (see overview of common proteases in Table 1.8) (Giansanti *et al.*, 2016) and subsequent peptide fractionation prior to LC-MS/MS analysis (Michalski *et al.*, 2011). In contrast, the “sort-then-break” approach is known in bottom-up proteomics, where proteins are separated and fractionated by LC (*e.g.*, size-exclusion chromatography) first, then digested, and peptides finally analyzed by LC-MS/MS (Han *et al.*, 2008). MS/MS analysis of bottom-up proteomics samples is commonly used in DDA mode to cover a large range of peptides with a vast concentration range and different physicochemical properties and m/z values. In order to achieve reproducible analyses of proteins, robust and optimized digestion protocols are highly important. Independent of the used protease, two steps are important to facilitate accurate peptide identification. The first step requires thiol reducing agents, such as dithiothreitol (DTT) or tris(2-carboxyethyl)phosphine, which reversibly reduce

intrachain disulfide bonds between cysteine residues. To prevent reformation of these bonds, reagents are added to irreversibly alkylate free cysteines. This process prohibits intrachain bonds and reduces protein stability and folding. Common alkylating agents are iodoacetamide (IAM), iodoacetic acid and *N*-ethylmaleimide. Ultimately, this preparation step aids in the reproducible proteolysis of protein sequences to facilitate high throughput sequencing (Jiang *et al.*, 2013; Rebecchi *et al.*, 2011).

Efficient peptide identification (sequencing), and ultimately protein identification, requires sufficient collection of MS/MS spectra of each individual peptide feature. Peptide fragmentation follows very reproducible fragmentation rules which depend on the dissociation technique. Backbone bond cleavage during fragmentation (see Figure 1.20) yields the most abundant product ions in peptide MS/MS. Especially in CID-based QqTOF and Orbitrap MS/MS, a, b and y-ions are commonly observed and used to effectively identify predicted or unpredicted peptide sequences (the latter known as *de novo* sequencing) (Ahmadi and Winter, 2019; Griss, 2016). Depending on precursor charge state, fragments are often singly charged, less often doubly or triply charged. In addition to CID-derived a, b and y-ions, neutral water loss is common with ions containing serine, threonine, aspartic acid and glutamic acid. Peptide ions consisting of asparagine, glutamine, lysine and arginine can undergo neutral ammonia loss. Internal fragments are also possible, which include a double backbone bond cleavage.

Table 1.8 Common proteases in MS-based bottom-up proteomics

Protease family	Protease	Cleavage	Note
Aspartic protease	Pepsin	Proximity of F, L, W and Y	Specificity is pH dependent (optimal pH: 1.5–2.5)
Cysteine protease	ArgC	C-terminal of R	Cleavage at K also possible
Serine protease	Chymotrypsin	C-terminal of F, L, M, W and Y	
	GluC	C-terminal of E	Cleavage at D also possible
	LysC	C-terminal of K	
	Trypsin	C-terminal of K and R	No cleavage if P on C-terminal side
Metalloproteinase	AspN	N-terminal of D	Cleavage at E also possible

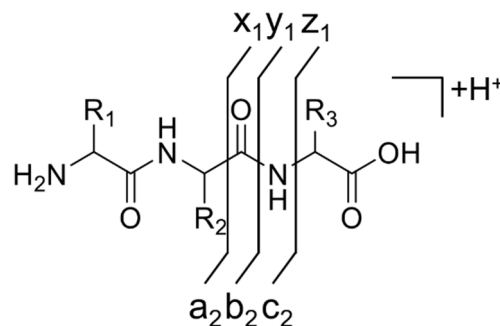


Figure 1.20 Peptide fragmentation scheme showing peptide bond cleavage leading to different product ions. Either the peptide amide bond (a and x-ions), the amino alkyl bond (b and y-ions) or the alkyl carbonyl bond (c and z-ions) are cleaved during dissociation. Fragmentation products with the charge remaining on the N-terminal side are termed a, b or c-ions, and x, y or z-ions with the charge on the C-terminal side (Biemann, 1990). The subscript number besides the letter refers to the number of amino acid residues within the peptide fragment ion.

The above fragmentation rules are commonly used in modern sequencing algorithms. In order to correctly assign peptide sequences and protein identities, peptide MS/MS spectra are matched to a database of previously identified protein sequences or sequences derived from genomic sequencing. Peptide-spectrum matching (PSM) is a well-established computational tool to identify most peptide MS/MS spectra in a proteomics experiment. In PSM analyses, protein sequences from various databases (*e.g.*, UniProtKB/Swiss-Prot) are theoretically digested (based on protease cleavage specificity, see Table 1.8) and peptide MS/MS spectra are predicted. These predicted spectra are compared to acquired MS/MS spectra and matches are sorted based on matching confidence. *De novo* sequencing approaches rely on correct identification of the peptide sequence through its acquired MS/MS spectra. Sequences are then compared to protein sequences in a database (Griss, 2016). For confident identification, both approaches equally require MS/MS spectra with sufficient spectral

quality and low complexity (ideally no composite MS/MS), and peptide fragmentation yield. In addition, PSM and *de novo* sequencing can be used to identify PTMs on protein sequences (Heazlewood, 2011). In general, PTMs of a specific residue increase the exact mass of the modified amino acid. This can be often implemented in sequencing algorithms and, combined with empirical values of modification probability, this can be used to efficiently detect protein modifications which are normally only a fraction of the unmodified protein. However, ion dissociation and fragmentation techniques can have a direct effect on the stability of the PTM itself, thus the ability to detect these PTMs. For instance, analysis of ubiquitination is believed to be difficult using CID-based methods, including higher-energy collisional dissociation (HCD) in Orbitrap MS systems. HCD fragmentation is equivalent to CID-type dissociation in QqQ and QqTOF systems (Olsen *et al.*, 2007). CID in Orbitrap MS systems is referred to the ion trap (low-energy) resonant-excitation CID. HCD is not equivalent to “high-energy” CID in tandem magnetic sector mass spectrometers and in tandem TOF-MS (TOF/TOF) (Pittenauer and Allmaier, 2009), but instead allows for multiple collision events of the precursor as in a traditional quadrupole-type collision cell (de Graaf *et al.*, 2011). However, strategies using ECD/ETD have proven to be complementary to CID, allowing for identification of, for instance, novel ubiquitination sites through analyzing c and z+1-ions⁴ (Sobott *et al.*, 2009). Other less stable modifications include non-covalent binding. For instance, cyclodextrin inclusion complexes, which can be analyzed via ECD (Qi *et al.*, 2015b). Nonetheless, many protein modifications remain stable in MS and MS/MS acquisitions, such as acetylation

⁴ It should be noted that electron-based peptide fragmentation methods generally yield c and z'-ions (z-ion radicals). In Biemann nomenclature, these radicals are named z+1-ions. If the z'-ion abstracts an additional hydrogen it is named z+2. In some literature z'-ions are confusedly termed z-ions; z'-ions with abstracted hydrogen z+1-ions.

(Larsen *et al.*, 2006) or other irreversible covalent modifications (*e.g.*, from reactive metabolite binding reactions).

1.3 Experimental design and research challenges

Regarding reactive metabolite formation and related biomolecule binding, there are still important scientific questions to be answered and improvements needed, to increase compound risk assessments (Thompson *et al.*, 2016). Protein binding presents a major challenge in drug research and development. Covalent protein adducts, from endogenous and exogenous sources, play a key role in the onset of multiple health issues, cancers and immune responses (Baillie, 2009; Barrera *et al.*, 2015; Loeb and Harris, 2008; Sharma *et al.*, 2013). The detection of these protein adducts, and their modification sites is often not straightforward, even with modern methodologies. Challenges can be the low abundance of protein modifications, namely the site occupancy of the occupied amino acid, the instability of the reactive metabolite-amino acid adduct, and the low target protein quantities in the analyzed sample. A common approach in most types of investigations is to perform shotgun proteomics using DDA on a QqTOF or Orbitrap MS platform (Gan *et al.*, 2016; Sabbioni and Turesky, 2017; Tailor *et al.*, 2016). Even though successful applications have shown the analytical potential of these types of studies, challenges remain even with constant improvements in mass spectrometer and search algorithms. In DDA-based methods, using intensity selection, roughly 16% of actually detectable peptides are identified and with very low level reproducibility (Michalski *et al.*, 2011). Thus, improvements in sample preparation and MS-based strategies are needed to lower the limit of detection for very low abundant modified peptide features, but also to increase the sampling capabilities of highly complex samples.

In this research thesis, the *in vitro* metabolism of the antipyretic and analgesic APAP and two antipsychotics, CLZ and OLZ, were studied in detail. These three drugs have been well studied in previous research (see Figure 1.21 for a brief overview of known metabolism), however, many questions regarding reactive metabolism, and the exact outcome and effects of related protein binding still need to be assessed. In addition, these three compounds are highly different in their adverse effects and toxicity. APAP is the most commonly used painkiller in Western societies, but also one of the major cause of acute liver failure (ALF) (Fagan and Wannan, 1996; James *et al.*, 2013; Lee, 2004; Sivilotti *et al.*, 2005). Its hepatotoxicity is linked to the formation of a reactive metabolite, *N*-acetyl *p*-benzoquinone imine (NAPQI), which is known to form covalent adducts with cysteine residues in GSH and proteins (Dahlin *et al.*, 1984; Gibson *et al.*, 1996; Jollow *et al.*, 1973). The antipsychotics CLZ and OLZ are used in the treatment of schizophrenia and psychosis. Based on its increased likeliness to induce agranulocytosis and neutropenia, CLZ is used as a third-line medication in treatment-resistant cases (Baldessarini and Frankenburg, 1991; Curto *et al.*, 2015; Kane *et al.*, 1988). In direct comparison, OLZ is considered less dangerous, not leading to reported white blood cell depletion or other adverse effects (Fulton and Goa, 1997). Thus, it is used as a first-line medication for schizophrenia (Murray, 2006; Schwenger *et al.*, 2011), even being less effective than CLZ (Fulton and Goa, 1997). In addition, OLZ is also used in the treatment of mood disorders (Luan *et al.*, 2017; Samara *et al.*, 2017), anorexia nervosa (Attia *et al.*, 2019) and chemotherapy-induced nausea (Navari *et al.*, 2016; Sutherland *et al.*, 2018). With apparent differences in efficacy and likelihood of IADRs, CLZ and OLZ remain interesting targets for reactive metabolite studies, since both are structurally similar, forming a similar nitrenium ion metabolite (CLZox and OLZox, respectively; see Figure 1.21) with different toxicity-related outcomes.

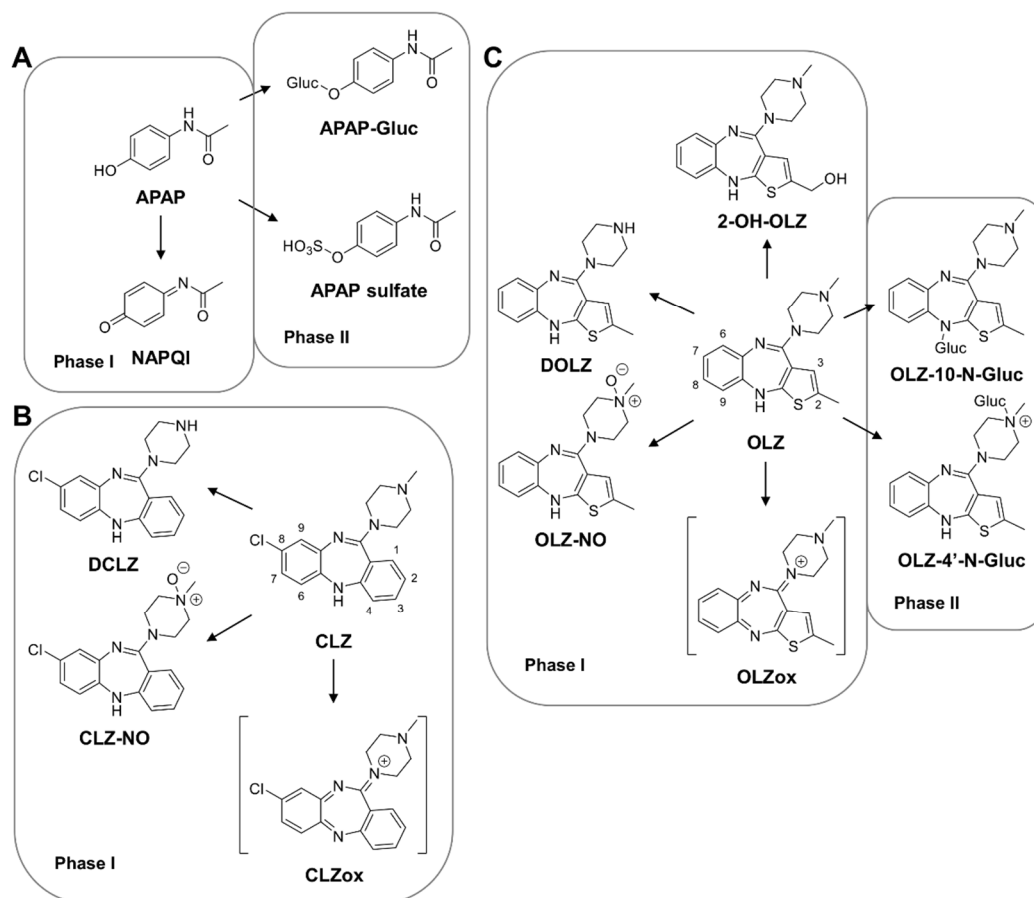


Figure 1.21 Overview of common stable and reactive metabolites of (A) APAP, (B) CLZ and (C) OLZ. The majority of APAP metabolism consist of direct glucuronidation (Gluc) and sulfation, aside from bioactivation to NAPQI, to a lesser extent (5–15%). Main stable metabolites of CLZ are a result of demethylation (desmethylclozapine, DCLZ) and *N*-oxidation (clozapine *N*-oxide, CLZ-NO). The well-known reactive metabolite of CLZ corresponds to CLZox. OLZ undergoes similar phase I metabolism (forming desmethylolanzapine, DOLZ; olanzapine *N*-oxide, OLZ-NO; and 2-hydroxymethyl-olanzapine, 2-OH-OLZ) as well as bioactivation to OLZox. Reactive metabolites NAPQI, CLZox and OLZox are normally conjugated to GSH for detoxification and excretion from the body, a reaction mostly mediated by GSTs during phase II metabolism. GSH can also directly conjugate to reactive metabolites without the need for enzymatic catalysis via GSTs (Li, 2009).

Two approaches regarding the formation of reactive metabolites and their subsequent binding reactions are discussed: 1) a small molecule analysis approach to investigate the (reactive) metabolism of the compound or drug of interest *in vitro*, and 2) several bottom-up proteomics strategies to allow for detection of low abundant covalent modifications on specific protein targets or proteins from the incubation system itself (*e.g.*, microsomal proteins) (see Figure 1.22).

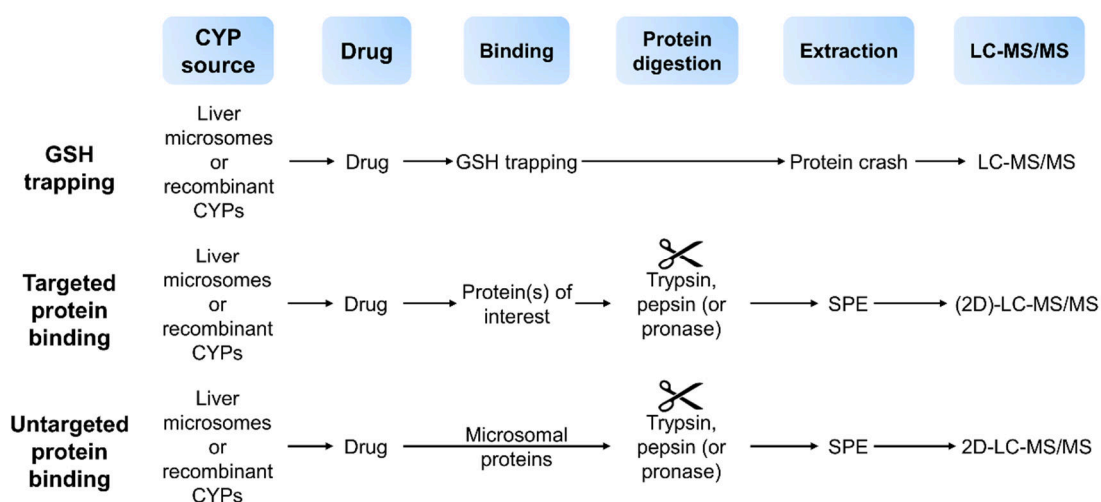


Figure 1.22 General workflow scheme to study *in vitro* reactive metabolite formation and binding of xenobiotics using LC-MS/MS.

1.3.1 Sample preparation

In this research, *in vitro* incubations incorporated the following: 1) the compound of interest, 2) a CYP protein source (always including oxidoreductase and/or cytochrome *b₅*), 3) the cofactor NADPH, and 4) the addition of a reactive metabolite trapping reagent (*e.g.*, small molecules or proteins). NADPH can be used directly or can be supplied by using a NADPH regenerating system (using NADP⁺ as a substrate). This system consists of magnesium chloride, glucose 6-phosphate and glucose-6-phosphate dehydrogenase (G6PDH) (see Figure 1.23). In order to focus on

reactive metabolite binding to either small molecule trapping agents, like GSH or *N*-acetylcysteine, or to large molecules such as proteins, subsequent sample preparation steps need to be selected accordingly (see Figure 1.22). Since the formation of the reactive metabolites requires the use of several proteins to catalyze oxidative metabolism, a protein precipitation (or protein crash) is needed to enable the correct downstream study of small metabolites. A common technique is the addition of water-miscible solvents, such as ACN, MeOH or acetone at a 1:1 or 1:3 water-to-organic solvent ratio. Proteins start to aggregate and precipitate, as their hydration layer is reduced and then collected using centrifugation. Soluble stable metabolites and adducts can then be removed from the supernatant and further processed. If need be, the protein pellet can be resuspended using detergents, allowing for proteomics analysis using proteases, subsequent SPE and (2D-)LC-MS/MS. If small molecule analysis is not necessary, protein analysis can be done directly without protein precipitation through in-solution digestion. This helps to avoid the usage of detergents, which are mostly detrimental for LC and ESI-MS peptide analysis through ion suppression effects (Ogorzaiek Loo *et al.*, 1996).

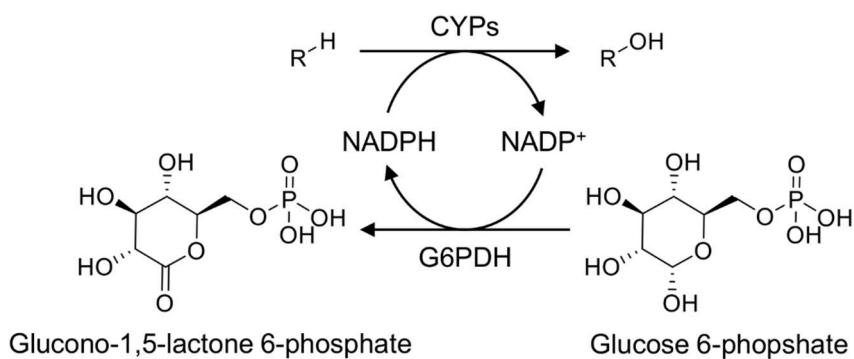


Figure 1.23 NADPH regenerating cycle using glucose 6-phosphate and $NADP^+$ in the CYP-mediated oxidation.

1.3.2 Data processing and treatment

In order to successfully study small molecule adducts and complex modified peptide mixtures, several software packages were used. Most of these software suites included software from Sciex, the manufacturer of the MS systems used in this work. For metabolite identification, MetabolitePilot™ (Sciex) was used. This tool allows to search complex metabolism samples in a targeted but also untargeted fashion. Using control samples for comparison, targeted workflows search for metabolite features (m/z and retention time) based on predicted metabolism in phase I and/or phase II (see Table 1.7) and structural characteristics (*e.g.*, loss of piperazine in CLZ or OLZ). Untargeted workflows can use mass defect, product ion or neutral loss filtering. These can be specifically useful to detect unpredicted GSH adducts. Peptide-based analyses were conducted with ProteinPilot™ (Sciex). This software uses the Paragon™ Algorithm (Shilov *et al.*, 2007) to apply database searching to MS/MS spectra of peptides. In order to detect unknown/uncommon PTMs or artificial modifications on the sequence, such as NAPQI, HNE, CLZox or OLZox adducts, the pre-determined probability of the specific modification was altered in the software-linked files (see overview of searched modification in Table 1.9). This enabled the database search of MS/MS spectra with an artificially increased modification probability of 50–80%. Naturally, this led to many false positives. However, knowledge from preceding GSH and small molecule trapping studies was used to identify amino acid-reactive metabolite specific fragment ions in complex peptide MS/MS. These product ions are generally referred to as diagnostic (fragment) ions, and have proven to be highly useful in reactive metabolite binding studies (Carlsson and Törnqvist, 2017; Takeshita and Kanaly, 2019). Finally, quantitation of modified peptide features was done using MultiQuant™ software (Sciex). Visualization of data was possible using PeakView® and MasterView® (Sciex).

Table 1.9 Brief overview of reactive metabolite-derived modifications of amino acids in protein described in the literature

Source	Reactive metabolite	Modification site	Addition (with replacement of H)	Mass difference (u)
LPO	HNE	Cys, His, Lys	C ₉ H ₁₇ O ₂	+156.1150
APAP	NAPQI	Cys	C ₈ H ₈ NO ₂	+149.0477
CLZ	CLZox	Cys	C ₁₈ H ₁₈ ClN ₄	+324.1142

1.3.3 Research outline

The main focus of this research was the detailed understanding of the source of several reactive metabolites and their direct effects in disease and adverse effects. This research was conducted via two avenues: 1) reactive metabolism on the small molecule level and 2) related effects on the protein-level. Using liver microsomal incubations or oxidations with a specific CYP, the oxidative metabolism of drugs was first elucidated and structural characterized. This was necessary, since reactive metabolite adducts can be derived from multiple steps of metabolism leading to structurally different adducts (*e.g.*, bioactivation of stable DCLZ or CLZ-NO to nitrenium ions). In addition, adducts being structural isomers could also have a direct influence on detection, due to the possibility of chromatographic separation. With this knowledge, it was possible to correctly identify and assign reactive metabolite protein adducts in highly complex samples, even with the potential for many false positives. Using optimized sample preparation strategies combined with state-of-the art LC-MS/MS platforms was another study focus to ensure sensitive assay development. Two MS platforms were used to maximize identification and quantitation yield: 1) a high-resolution QqTOF (TripleTOF[®] 5600⁺, Sciex) for accurate DDA-based identifications, and 2) a high-sensitive QqLIT (also with QqQ function; QTRAP[®] 5500, Sciex) to screen for low abundant features and to precisely quantify modified peptides in MRM mode.

Microsomal samples contain many proteins and other impurities that can be detrimental to instrument sensitivity and feature detection. In proteomics analyses, proper sample purification is one technique to improve reproducibility and lower the limit of detection. However, the more selective a sample preparation protocol is, the higher the risk for important losses of unanticipated yet interesting features. SPE and pre-fractionation of peptides by chromatography (in 2D-LC workflows, for instance) are commonly used to remove impurities, and to lower the complexity in peptide chromatograms and to avoid column overloading effects (Wang and Marcus, 2018). However, the complexity of *in vitro* incubations can be also reduced by using less complex CYP systems, such as recombinant CYPs or Supersomes™ (Corning®). These proteins are available with high purities and low amount of background proteins, thus allowing for an optimized oxidation environment and absence of unnecessary proteins. Incubations using these CYPs might require less purification and thus be more efficient. A combination of these techniques, *in vitro* CYP-specific incubation followed by SPE and multidimensional LC, can be used to determine reactive metabolite binding to specific protein targets of interest, which are added to the incubation systems as purified proteins with increased quantities. This workflow was used in Chapter 3 and 5 to investigate binding to human GSTs of reactive metabolites, respectively, from APAP, and CLZ and OLZ. As an effect of using a very targeted assay with only a couple of potential protein targets, the use of suitable proteases could also be applied to increase the sequence coverage needed to detect all or most of the possible cysteine sites in these GSTs. Hence, cleavage-specific trypsin digestion was paired in parallel with the less specific pepsin digestion yielding variable peptide sequences with different properties. This dual-enzyme approach has the potential for increasing the detection of multiple protein sites hardly accessible by only one protease alone.

Knowledge gained from these types of *in vitro* investigations can then be applied to *in vivo* samples to answer specific questions in disease and adverse effects. For instance, known protein targets of the APAP reactive metabolite NAPQI can be

utilized to monitor the extend of protein binding in liver of patients suffering from APAP intoxication. Especially human serum albumin (hSA or HSA) is known to be a target of hepatic NAPQI binding, which is subsequently released into the circulation (Peters Jr., 1985). Thus, it is possible to apply targeted sample preparation techniques to patient serum samples, to specifically detect and quantify NAPQI-serum albumin adducts, as it was proven in a rodent model (LeBlanc *et al.*, 2014). Therefore, as part of this dissertation (Chapter 2), the previously introduced rodent model was carefully translated to human and successfully applied to serum samples from acute liver failure patients. To enable absolute quantitation capabilities of circulating NAPQI-hSA, a custom-made alkylation agent, based on an iodoacetamide derivative, was used to generate surrogate modified protein standards (see Figure 1.24). An isotope-labeled (d_4) version of that alkylation agent was used to prepare an internal standard for accurate and precise absolute quantitation by LC-MS/MS.

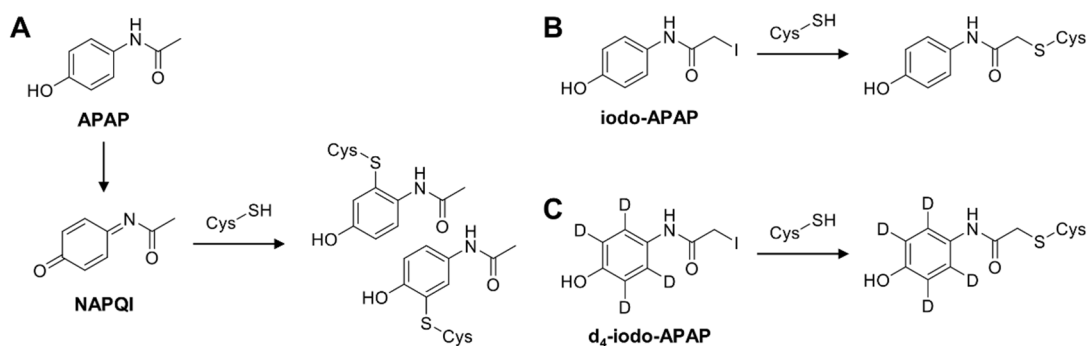


Figure 1.24 Comparison of cysteine binding through (A) the bioactivation of APAP to NAPQI, and the chemically labeling using the custom-made alkylating agents (B) iodo-APAP (*N*-(4-hydroxyphenyl)-2-iodoacetamide) and (C) d_4 -iodo-APAP (*N*-(4-hydroxy[2,3,5,6- d_4]phenyl)-2-iodoacetamide).

In addition, sample preparation and treatment optimization of *in vitro* samples could be used to maximize the detection of low abundant modified peptide species. In

the case of the endogenous reactive metabolite HNE, sample preparation protocols from *in vitro* microsomal binding studies (*i.e.*, tryptic digestion, SPE, SCX and LC-MS/MS) (Golizeh *et al.*, 2016) have been applicable to treatment of post-surgery (discarded) human articular cartilage-derived chondrocytes (Golizeh *et al.*, 2014). In both studies, careful sample preparation has been pivotal to detect HNE-modified proteins with low quantities in either microsomal incubations or in osteoarthritic (OA) chondrocyte extracts. To further investigate the role of HNE in human cartilage degradation, OA chondrocytes were specifically analyzed to pinpoint (nuclear) protein targets of HNE-related binding. Especially nuclear histone proteins, which are crucial for chromatin formation and thus gene regulation, were studied in detail in Chapter 4.

Finally, combining different avenues of *in vitro* metabolism introduced a comprehensive view on APAP, CLZ and OLZ reactive metabolite formation. In addition, differences of reactivities and affinities towards cysteine residues in different protein environments, either in GSH or hepatic proteins, could be helpful information for future studies. Furthermore, the application of these strategies to patient samples could prove important to accurately assess the *in vivo* relevance of binding and answer crucial disease-related questions, such as severity of APAP-induced toxicity and potential outcome, or the involvement of HNE in OA disease. These aspects are discussed in the following Chapter 2, 3, 4 and 5.

CHAPTER II

ABSOLUTE QUANTITATION OF ACETAMINOPHEN-MODIFIED HUMAN SERUM ALBUMIN IN ACUTE LIVER FAILURE PATIENTS BY LIQUID CHROMATOGRAPHY-TANDEM MASS SPECTROMETRY

Timon Geib, André LeBlanc, Tze Chieh Shiao, René Roy, Elaine M. Leslie,

Constantine J. Karvellas and Lekha Sleno

Published in **Rapid Communications in Mass Spectrometry** 2018, **32**, 1573–1582. Available online
at <https://doi.org/10.1002/rcm.8206>.

In this chapter, research was aimed to improve the accuracy of liver failure monitoring related to acetaminophen overdose. A liquid chromatography-tandem mass spectrometry method was developed and validated which allowed for the measurement of acetaminophen-modified human serum albumin in blood, a biomarker for liver protein binding. Goal was to design an approach that is both straightforward and fast to use, without compromising the efficacy. Using previously designed custom standards, a very short sample analysis was achieved which allowed for accurate and precise quantitation of acetaminophen-modified human serum albumin in a clinically relevant time span. This technique was successfully applied to serum samples of a group of acetaminophen-related liver damage patients (treated at the University of Alberta). Ultimately, quantifying modified human serum albumin was able to

distinguish between moderate and severe acute liver failure. The method can help direct clinical care more efficiently and help prevent wrong or ineffective treatment.

Timon Geib, André LeBlanc, Tze Chieh Shiao, René Roy, Elaine M. Leslie, Constantine J. Karvellas and Lekha Sleno are co-authors of this article. Timon Geib conducted the literature survey, prepared experimental protocols, conducted the experiments, processed the data and prepared the original manuscript. André LeBlanc participated in the analytical method development. Tze Chieh Shiao and René Roy synthesized and purified in-house standards iodo-acetaminophen and d₄-iodo-acetaminophen. Elaine M. Leslie and Constantine J. Karvellas supervised the human acute liver failure study (University of Alberta), sampling process and statistical analysis. Lekha Sleno supported and supervised the project, verified data analysis and interpretation of the results, revised and finalized the manuscript.

2.1 Abstract

Rationale: Acetaminophen (APAP) is a well-known analgesic, deemed a very safe over-the-counter medication. However, it is also the main cause of acute liver failure (ALF) in the Western world, via the formation of its reactive metabolite, *N*-acetyl *p*-benzoquinone imine (NAPQI), and its covalent attachment to liver proteins. The aim of this study was to develop a sensitive and robust quantitative assay to monitor APAP-protein binding to human serum albumin (HSA) in patient samples.

Methods: A combination of isotope dilution, peptic digestion and solid-phase extraction coupled to liquid chromatography/multiple reaction monitoring (LC-MRM) was employed. An external calibration curve with surrogate modified protein spiked into blank serum was used for absolute quantitation. Samples were analyzed by LC-

MRM to measure the modified active site peptide of HSA. The LC-MRM assay was validated and successfully applied to serum samples from patients suffering from APAP-induced ALF.

Results: Accuracy ranged from 83.8–113.3%, within-run coefficient of variation (CV) ranged from 0.3–6.9%, and total CVs from 1.6–10.6%. Patient samples ranged from 0.12–3.91 nmol/mL NAPQI-HSA; in-between the assay dynamic range of 0.11–50.13 nmol/mL serum. *In vivo* median concentrations were found to be 0.62 nmol/mL and 0.91 nmol/mL for non-spontaneous survivors ($n = 25$) and individuals with irreversible liver damage ($n = 10$), respectively (p -value = 0.028), demonstrating significant potential as a biomarker for ALF outcome.

Conclusions: A fast and sensitive assay was developed to accurately quantify NAPQI-HSA as a biomarker for APAP-related covalent binding in human serum.

2.2 Introduction

Acetaminophen (APAP, or paracetamol), one of the most commonly used analgesic and antipyretic drugs, is linked to acute liver failure (ALF); in which in extreme cases can lead to death (Hodgman and Garrard, 2012; Larson *et al.*, 2005; Lee, 2004; Ryder and Beckingham, 2001; Sivilotti *et al.*, 2005). Although it is known to be hepatotoxic, APAP is available in many over-the-counter formulations. Though most of its metabolism is via phase II conjugation reactions (sulfation and glucuronidation, see Figure 2.1A), a fraction of APAP transforms into the reactive metabolite *N*-acetyl *p*-benzoquinone imine (NAPQI, Figure 2.1A), via cytochrome P450 (CYP) enzymes (Dahlin *et al.*, 1984; Mitchell *et al.*, 1973a). NAPQI can be conjugated to the tripeptide glutathione (GSH) as a detoxification mechanism (Gibson *et al.*, 1996; Mitchell *et al.*,

1973b). However, upon overdose (>4 g/day) (Mazaleuskaya *et al.*, 2015), GSH depletion (>70%) (Davis *et al.*, 1974; Kalsi *et al.*, 2011; Mitchell *et al.*, 1973b) or induction of CYP enzymes (Prescott, 2000), accumulation of NAPQI may occur. The metabolite is directly linked to APAP-related toxicity, by covalently binding to nucleophilic thiol groups of liver proteins, thus leading to liver failure (Jollow *et al.*, 1973; Pumford *et al.*, 1989).

APAP-induced hepatotoxicity is considered especially problematic as patients often do not seek medical care fast enough. In addition, APAP is known to be the most common cause of ALF in the Western world (Fagan and Wannan, 1996; James *et al.*, 2013; Larson *et al.*, 2005), and clinical care should occur within the first 24–48 h to circumvent possible liver necrosis (Schiødt *et al.*, 1997) and within less than 8 h to avoid any hepatic damage (Beckett *et al.*, 1985). This is challenging, since clinical assays are lacking (particularly in the setting of staggered/inadvertent chronic overuse), and physicians must often wait for symptoms to manifest prior to treatment (Darweesh *et al.*, 2017; Sivilotti *et al.*, 2005). Therefore, with the risk of ALF and the need for fast treatment, accurately monitoring NAPQI-protein binding is of great interest.

The current clinical standard in determining APAP-related hepatotoxicity is the Rumack-Matthew nomogram, which projects APAP concentration in serum against time after ingestion (Rumack *et al.*, 1981). This allows monitoring the half-life of APAP in patients' blood, but is not necessarily reflective of its total protein binding in liver tissue (James *et al.*, 2002). Due to lack in assay specificity, clinicians are not able to circumvent unnecessary or inadequate *N*-acetylcysteine treatment of low-risk or high-risk patients, respectively (Cairney *et al.*, 2016).

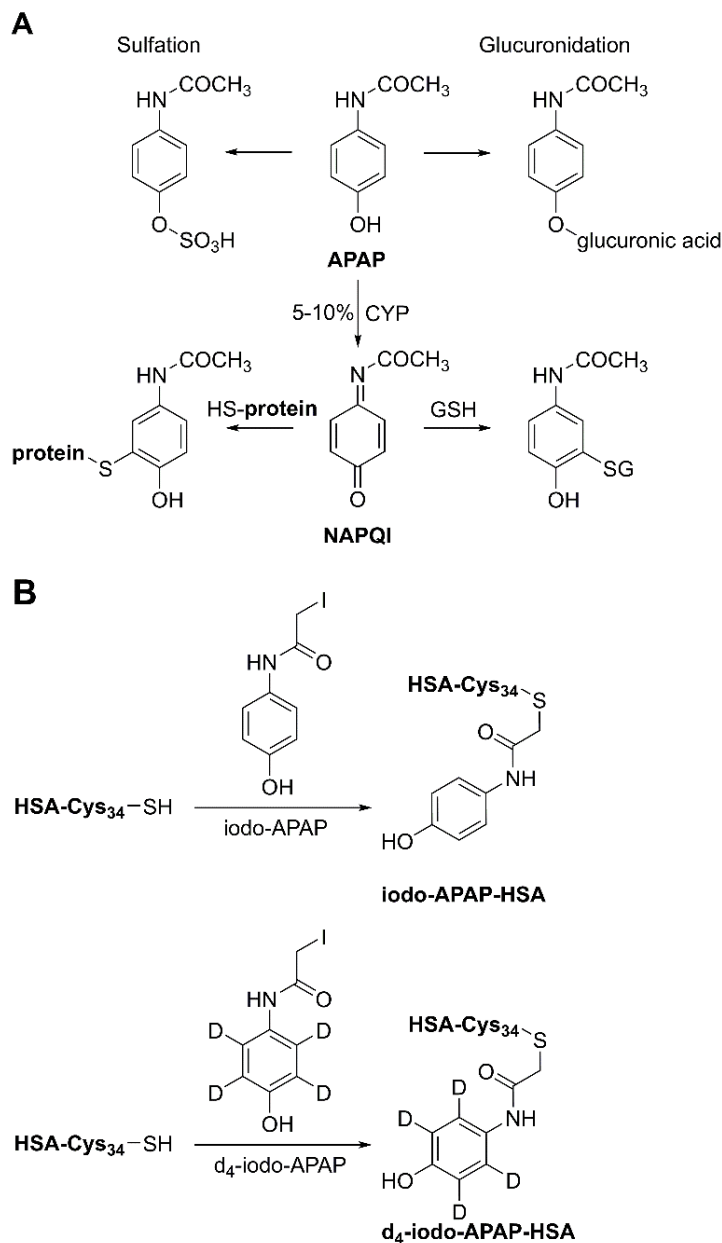


Figure 2.1 (A) Metabolism pathway of APAP, showing sulfation and glucuronidation as the main metabolic pathways and oxidation by CYPs to form NAPQI with subsequent conjugation to GSH. Conjugation of cysteine-containing proteins is also shown as an alternative pathway. (B) Representative alkylation reaction of serum albumin with custom-designed iodo-APAP and d₄-iodo-APAP to yield surrogate calibration standard and IS, respectively.

Other methods have been developed to monitor NAPQI-protein binding. Liquid chromatography coupled to electrochemical detection of APAP-Cys adducts in human serum following the complete digestion of plasma proteins into free amino acids was reported, by Muldrew *et al.* (Muldrew *et al.*, 2002) or Roberts *et al.* (Roberts *et al.*, 2017). Liquid chromatography/tandem mass spectrometry (LC-MS/MS) determination of APAP-Cys in human serum was reported by Cook *et al.* (Cook *et al.*, 2015), whereas Damsten *et al.* focused on the assessment of NAPQI-adducts of serum albumin (Damsten *et al.*, 2007). Serum albumin is especially suitable as a biomarker for NAPQI-protein binding. It is the most abundant serum protein, and the active-site Cys34 has been reported as a target of NAPQI. These adducts are formed in hepatocytes, the major cell-type where serum albumin is synthesized (Peters Jr., 1985). Consequently, NAPQI-serum albumin formation does not require NAPQI to be transported across the cell membrane or to be secreted into the blood circulation (Sabbioni and Turesky, 2017). Therefore, modified serum albumin levels are believed to be a practical marker for APAP-related protein binding occurring in liver. Recent developments in serum albumin biomarker studies have shown great potential in biomarker research (Sabbioni and Turesky, 2017).

Our group has previously introduced a liquid chromatography/multiple reaction monitoring (LC-MRM) assay using a rat model of acetaminophen covalent binding *in vivo* (LeBlanc *et al.*, 2014). The rat assay was used as a starting point for the human model, using the same principle of protein-level standard and isotope dilution. However, based on differences in protein sequence between rat and human albumins, the peptide formed following digestion yields a different target analyte to monitor for the human assay. Also, the needs of a clinically relevant assay are different, since speed of analysis and dynamic range are of utmost importance. For faster analysis, changes in sample preparation workflow and analysis were made, while still maintaining excellent accuracy and precision at relevant concentration levels (Heard *et al.*, 2017). Performance of the assay was evaluated via assessment of calibration curves and

quality controls (QCs). Additionally, a cross-platform validation was realized using high-resolution mass spectrometry (HRMS) on a hybrid quadrupole–time-of-flight platform. Finally, the method was applied to measure NAPQI-HSA levels from a cohort of patients exhibiting ALF.

2.3 Experimental

2.3.1 Chemicals

The standard peptide, LQQCPFEDHVKL, was purchased from Biomatik (Cambridge, ON, Canada). HSA, acetonitrile (ACN), ammonium bicarbonate, ammonium hydroxide, blank serum (from human male AB plasma), dithiothreitol (DTT), formic acid, iodoacetamide (IAM), methanol, and pepsin (from porcine gastric mucosa) were obtained from Sigma-Aldrich (Oakville, ON, Canada). Additional blank male human serum was purchased from BioreclamationIVT (Baltimore, MD, USA). Ultra-pure water was prepared from a Millipore Synergy UV system (Billerica, MA, USA). Iodo-APAP (*N*-(4-hydroxyphenyl)-2-iodoacetamide) and d_4 -iodo-APAP (*N*-(4-hydroxy[2,3,5,6- d_4]phenyl)-2-iodoacetamide) were synthesized in-house (LeBlanc *et al.*, 2014) for chemical labeling of HSA and standard peptide to produce surrogate standard and internal standard (IS, see Figure 2.1B).

2.3.2 Patient samples

Serum samples were obtained from patients taking part in an existing ALF study at the University of Alberta (Edmonton, Canada). The cohort comprised 34 patients suffering from ALF and one suffering from acute liver injury (ALI) due to

APAP. All patients had their blood sampled serially between 1 and 9 days after APAP ingestion and admission to the Intensive Care Unit. Each center implemented monitoring and therapeutic interventions according to institutional standards of care. The study was approved by the University of Alberta Health Research Ethics Board and was conducted in accordance with good clinical practice guidelines as defined in the Declaration of Helsinki.

2.3.3 Participants

For the purposes of this study, ALF was defined as an international normalized ratio ≥ 1.5 and hepatic encephalopathy within the first 26 weeks of liver disease in a patient with an acute hepatic insult (O'Grady *et al.*, 1993). Hepatic encephalopathy grade was defined by the West Haven Criteria (simplified) (Atterbury *et al.*, 1978; Conn and Lieberthal, 1979). Inclusion criteria were: (1) evidence of ALF according to the enrollment criteria for the Acute Liver Failure Study Group (see operational definitions) and (2) age ≥ 18 years; and (3) hepatic encephalopathy, (4) patients with a primary diagnosis of APAP determined by the site investigator. Exclusion criteria were: (1) cirrhosis/acute or chronic liver failure, (2) patients without a primary diagnosis of APAP.

2.3.4 Modified HSA (surrogate standard and IS) preparation

HSA solution (200 μL , 20 mg/mL) in ammonium bicarbonate buffer pH 8.5 (ABC, 100 mM) was combined with DTT (25 μL , 200 mM) and incubated at 37°C (20 min) in a thermomixer (Eppendorf, Mississauga, ON, Canada). ABC (230 μL , 100 mM) and either iodo-APAP or d₄-iodo-APAP (25 μL , 500 mM in ACN) were then added, and the mixture was incubated (37°C, 45 min) in the dark. The resulting

solutions consisted of 125 nmol/mL HSA, modified with either iodo-APAP (for standard solutions) or d₄-iodo-APAP (for IS solution). Standard spiking solutions were diluted with water to appropriate concentrations for each standard and QC prior experiments. Standard and QC stocks were prepared separately. The IS working solution was diluted to 50 nmol/mL.

2.3.5 Modified peptide stock solutions

LQQCPFEDHVKL peptide was prepared as a 1 mg/mL stock solution in 50% methanol. This stock (100 μ L) was then diluted with 190 μ L ABC buffer, and treated with 10 μ L of DTT (50 mM) for 20 min at 37°C. Then, 250 μ L of ABC (100 mM) and 25 μ L of either iodo-APAP or d₄-iodo-APAP (50 mM in ACN) were added and incubated at 37°C for 45 min in the dark. The mixture was diluted with 425 μ L water, and underwent solid-phase extraction (SPE) on OASIS HLB cartridges (1 cc, 30 mg; Waters, Milford, MA, USA), with a water wash step followed by methanol elution (1 mL). The eluate was then dried and reconstituted with 550 μ L of 10% ACN, yielding 125 nmol/mL stock solutions.

2.3.6 Serum sample preparation

Serum samples (100 μ L) were prepared by the addition of 30 μ L ABC buffer and 25 μ L DTT (400 mM) at 37°C for 20 min. Then, 40 μ L of IAM (750 mM in ABC) was added (30 min at 37°C in the dark). After cysteine reduction and alkylation, 40 μ L of water and 20 μ L of IS working solution were added. To adjust the pH, 400 μ L of 1% formic acid in 10% methanol was added and samples were digested for 1 h (at 50°C) by adding 25 μ L of 4 mg/mL pepsin in water. Digestion was quenched with 320 μ L ABC. SPE (as above) was then performed with 10% ACN wash and methanol elution

(1 mL). Extracts were evaporated under vacuum and reconstituted with 100 μ L of 10% ACN.

2.3.7 Calibration standards and QCs

For calibration standards (nine concentrations) and QCs (four concentrations), 100 μ L human blank serum was treated with DTT and IAM as above, followed by the addition of 40 μ L of standard spiking solution and 20 μ L IS working solution. Subsequent steps of digestion and SPE were identical. Calibration standards were prepared and extracted in duplicate, while QCs were in triplicate.

2.3.8 Peptide-level calibration standards

For peptide-level standards, 100 μ L human blank serum was treated the same as explained above. Then 40 μ L of iodo-APAP-LQQCPFEDHVKL stock solution and 20 μ L of d₄-iodo-APAP-LQQCPFEDHVKL IS solution were added. Digestion and SPE were performed as for protein-level standards. Additional samples were prepared by spiking 40 μ L of iodo-APAP-LQQCPFEDHVKL and 20 μ L of d₄-iodo-APAP-LQQCPFEDHVKL stock solution after digestion, prior to SPE.

2.3.9 LC-MS/MS analysis

Samples (10 μ L) were injected in triplicate onto an Aeris PEPTIDE XB-C18 100 \times 2.1 mm column with solid core 1.7 μ m particles (100 Å) fitted with a SecurityGuard ULTRA C18-peptide guard column (Phenomenex, Torrance, CA, USA) using a Nexera UHPLC system (Shimadzu, Columbia, MD, USA) at 40°C with

gradient elution. Mobile phases were water (A) and ACN (B), both containing 0.1% formic acid. The gradient was linearly increased from 5% B to 18% B within 2 min, then to 20% B within 3 min, further increased to 95% B within 1 min, held there for 1.5 min. The flow rate was held at 0.3 mL/min for 6.5 min, then increased to 0.4 mL/min at 7 min, held there for 3 min (for faster re-equilibration), and further decreased to initial conditions. The LC flow to the mass spectrometer was introduced via a diverter valve from 3 to 6 min; the rest was diverted to waste.

A modified gradient (60 min) was employed for MS/MS characterization of modified peptide isomers in samples. The gradient included the same mobile phases. Initial conditions of 5% B were held for 2.5 min and linearly increased to 30% in 37.5 min, then to 50% B in 10 min, further increased to 85% B in 5 min, and held there for 3 min. The gradient was returned to initial conditions for re-equilibration. The flow rate was set at 0.4 mL/min.

MRM experiments were performed on a QTRAP 5500 (Sciex, Concord, ON, Canada) hybrid quadrupole-linear ion trap system with a TurboIonSpray ion source in positive electrospray mode. Source parameters were as follows: ion spray voltage, 5000 V; temperature, 550°C; nebulizer and drying gases (GS1 and GS2), 50 psi; and curtain gas, 35 psi. Declustering, entrance, and collision cell exit potentials were set at 60, 10, and 13 V, respectively. Ion activation via collision-induced dissociation was performed at a collision gas pressure of 5 (arbitrary units). Quantitation was performed using the MRM transitions m/z 535.9 \rightarrow 984.4 (analyte) and m/z 537.2 \rightarrow 984.4 (IS) with collision energy (CE) of 16 V. For qualitative purposes, four additional transitions were monitored (m/z 535.9 \rightarrow 673.9 and 537.2 \rightarrow 675.8, CE = 22 V; and m/z 535.9 \rightarrow 626.1 and 537.2 \rightarrow 626.1, CE = 35 V). The dwell time for each transition was 150 ms, for a total cycle time of 0.9 s. An additional method was tested for higher sensitivity quantitation of 25 μ L sample injections with a dwell time of 500 ms for m/z 535.9 \rightarrow

984.4 and 150 ms for m/z 537.2 \rightarrow 984.4; qualitative transitions were operated with a dwell time of 100 ms.

A Sciex TripleTOF 5600 (quadrupole–time-of-flight) instrument was also used with a DuoSpray ion source in positive mode for additional quantitative data (cross-platform validation) and to conduct HRMS/MS experiments of iodo-APAP-modified LQQCPFEDHVKL and initial testing of human serum digests when optimizing sample preparation conditions, including peptic digestions. HRMS calibration in MS and MS/MS modes was performed after every four injections with an in-house mix of standards. Ion source and transport parameters were as follows: ionspray voltage, 5000 V; temperature, 500°C; curtain gas, 30 psi; GS1 and GS2, 50 psi; declustering potential, 80 V. MS data were obtained from m/z 80–1500 with 250 ms accumulation time and 1.1 s total cycle time, including MS/MS experiments. HRMS/MS was performed for precursor ions m/z 535.9 and 537.3 (CE = 28 V), for iodo-APAP and d₄-iodo-APAP-modified LQQCPFEDHVKL, respectively, over the range m/z 170–1000 using 400 ms accumulation and 1.1 s period cycle time. The high sensitivity MS/MS mode of the instrument was used throughout all experiments. Quantitation was achieved by integrating peak areas from combined extracted ion chromatograms at m/z 626.2569, 673.8135 and 984.5149 (± 0.01 u) for iodo-APAP-modified LQQCPFEDHVKL, and at m/z 626.2569, 675.8261 and 984.5149 (± 0.01 u) for d₄-iodo-APAP-modified LQQCPFEDHVKL. Additionally, qualitative HRMS/MS data over the range m/z 80–1500 with a CE of 30 ± 10 V were collected on the 15 most intense ions from a survey MS experiment (m/z 80–1500). Accumulation times were 250 and 50 ms for MS and HRMS/MS, respectively, with a total cycle time of 1.05 s.

Samples, standards and QCs were analyzed in randomized order. Analyst 1.6 (QTRAP) and 1.7.1 (TripleTOF) was used for data acquisition, and raw data were processed using MultiQuant 3.0.2 (QTRAP) and 2.1 (TripleTOF), and visualized using PeakView 2.2 (Sciex).

2.4 Results

2.4.1 Method development

Reduction, alkylation and digestion of serum samples were optimized using blank serum. Optimal digestion temperature and time were assessed using different proteases (including trypsin, chymotrypsin, GluC and pepsin), to yield an appropriate active-site peptide (data not shown). The aspartic protease pepsin was found to be the most suitable to yield the active-site peptides LQQCPF, LQQCPFEDHVK and LQQCPFEDHVKL, with the latter as its most sensitive peptide signal incorporating Cys34 at the reported conditions. Chromatographic separation was carefully developed to provide good resolution between the chosen analyte peptide and surrounding interferences to yield sufficient signal-to-noise ratio (S/N), while also having fast sample analysis. The optimized gradient yielded sufficient analyte separation in a short cycle time (10.5 min, between injections).

MRM transitions were selected using the $[M+3H]^{3+}$ as a precursor ion, at m/z 535.9 for the analyte. Several product ions were observed in the HRMS/MS spectrum (Figure 2.2), and three product ions were subsequently optimized to find the best CEs for each. The fragment ion at m/z 984.4, the y_8 ion, was chosen as the quantitative transition, due to its higher selectivity and lower surrounding background signals. Two additional transitions were monitored as qualifiers; fragment ions $PFEDH^+$ and $(y_{10}-H_2O)^{2+}$ at m/z 626.1 and 673.9, respectively. Similarly, the IS was monitored at m/z 537.2 with fragments at m/z 984.4, 626.1 and 675.8. For HRMS/MS quantitation, product ions of analyte m/z 626.2569, 673.8135 and 984.5149 (± 0.01 u) were summed to yield comparable sensitivity to MRM experiments, as was done for the IS as well (using the combined area of product ions m/z 626.2569, 675.8261 and 984.5149 (± 0.01 u)). Additional HRMS quantitation results were based on the precursor ion signals at m/z 535.9292 and 537.2709 (± 0.01 u) for iodo-APAP-

LQQCPFEDHVKL (analyte) and d₄-iodo-APAP-LQQCPFEDHVKL (IS), respectively. Monitoring the $[M+3H]^{3+}$ ion without subsequent ion activation did not yield sufficient selectivity and therefore was not considered for quantitation (see Table 2.1 for comparison of LC-HRMS with LC-MRM and LC-HRMS/MS).

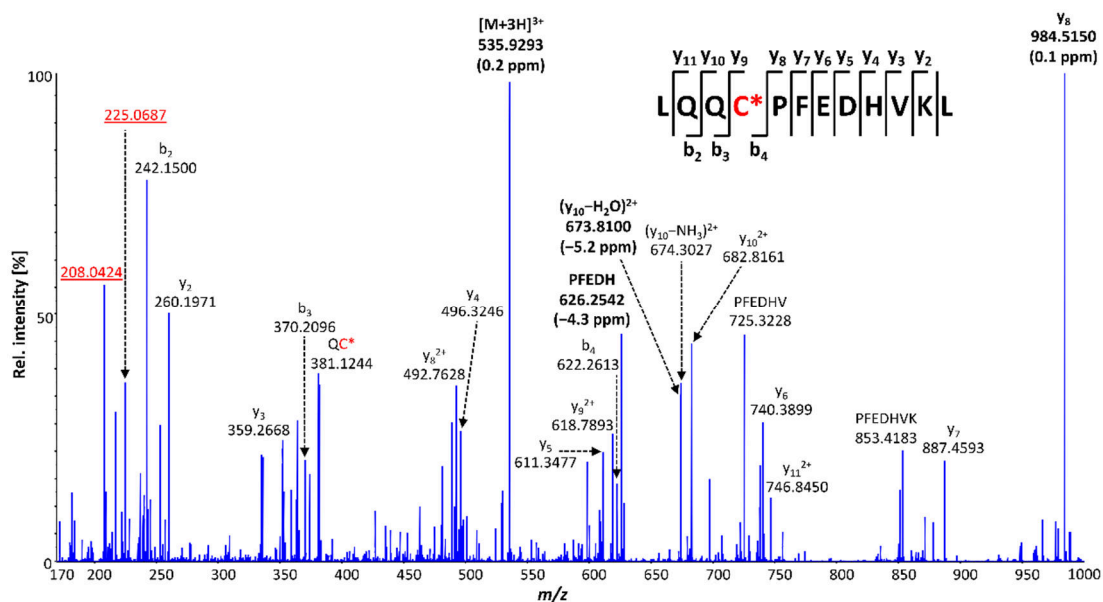


Figure 2.2 High-resolution MS/MS spectrum of iodo-APAP-LQQCPFEDHVKL (theoretical $[M+3H]^{3+}$ precursor at m/z 535.9292) showing three chosen product ions (bold) y_8 , PFEDH and $(y_{10}-H_2O)^{2+}$ at m/z 984.4, 626.1 and 673.9 at CE = 30 V (± 10 V), respectively, and NAPQI-Cys related diagnostic ions (underlined).

2.4.2 LC-MRM method validation

A nine-point calibration (1/x weighting) yielded a linear calibration curve ($y = 0.9013x + 0.0042$) with R^2 of 0.9993. The LC/HRMS/MS assay provided similar linearity as well ($y = 0.7879x + 0.0026$, $R^2 = 0.9989$). The limit of detection, in the MRM assay, was found to be 0.04 nmol/mL (>39 , S/N). The lowest calibration sample (0.11 nmol/mL) was set as the lower limit of quantitation (LLOQ, see Figure 2.3B) for both methods, and yielded the following S/N: LC-MRM, >99 ; LC-HRMS/MS, >30 .

The highest calibration sample (50.13 nmol/mL) was set as the upper limit of quantitation. Detailed method validation results, including accuracies and coefficient of variation (CV) values, can be found in Table 2.2; accuracies were in the range of 83.8–113.3% for LC-MRM, and 91.8–121.3% (LC-HRMS/MS, with two QC injections at LLOQ exceeding 120% accuracy). Values for %CV ($n = 12$ for standards, $n = 18$ for QCs) ranged from 1.6 to 10.6% and 3.5 to 14.4% for LC-MRM and LC-HRMS/MS analyses, respectively. Within-run imprecision was found to be between 0.3% and 6.9% for LC-MRM and 0.5% and 9.6% for LC-HRMS/MS. For cross-validation, linear regression between LC-MRM and LC-HRMS/MS was assessed by comparing calculated concentrations of standards, QCs and patient samples, and a linear agreement (Figure 2.4) between both assays was observed ($y = 1.0003x + 0.0615$; $R^2 = 0.9983$, $n = 91$). LC-MRM selectivity was confirmed by observing co-eluting interferences with low intensity in double blank samples (Figure 2.3A). Additionally, peak purity was confirmed by observing the MRM ion ratio (qualifier-to-quantifier ratio) for standard ($n = 108$) and QC ($n = 72$) samples. The product ion ratio $(y_{10-H_2O})^{2+}/y_8$ was assessed to be 2.42 (± 0.44 ; standard deviation, SD) and 2.49 (± 0.46) for standards and QCs, respectively. The PFEDH/ y_8 MRM transition ratio was found to be 0.92 (± 0.19) for standards and 1.02 (± 0.67) for QCs.

Table 2.1 Comparison of results from LC-MRM, LC-HRMS/MS, LC-HRMS (using MS1 for quantitation)

	LC-MRM	LC-HRMS/MS	LC-HRMS	LC-MRM (lower concentrations)
Linear range (nmol/mL)	0.11–50.13	0.11–50.13	5.41–50.13 ^a	0.02–1.35 ^b
Linear calibration curve (1/x)	$y = 0.9013x + 0.0042$	$y = 0.7879x + 0.0026$	$y = 0.6343x + 0.1067$	$y = 0.7242x + 0.0329$
R^2	0.9993	0.9989	0.9951	0.9983
Accuracy (%)	83.8–113.3	91.8–121.3	92.1–106.1	92.7–112.9
Within-run CV (%)	0.3–6.9	0.5–9.6	3.8–8.6	0.8–6.9

^aLLOQ for the LC-HRMS method was set at 5.41 nmol/mL.

^bLower LLOQ achieved by increasing injection volume and dwell time.

2.4.3 Recovery, matrix effects and comparison of peptide-level to protein-level standards

Comparison of MRM peak areas of iodo-APAP-labeled LQQCPFEDHVKL spiked into matrix before or after peptic digestion of serum matrix exhibited a concentration-dependent peptide signal area decrease between 4.5% and 26.1% (at 0.11, 0.23, 5.38 and 29.96 nmol/mL). This underlined the inherent lack of reproducibility of proteolytic sample preparation techniques, especially the digestion step. Furthermore, we wanted to compare quantitative results for a peptide-level calibration curve (with background digested-serum matrix) to the protein-level quantitation presented in this method. Linear agreement analysis of peptide-level standards against protein-level standards was found to be $y = 1.0261x - 0.3401$ ($R^2 = 0.9992$, $n = 9$), which indicated an underestimation of low-range samples and overestimation of higher concentrations using peptide-level standards for calibration. Extraction recovery (without considering matrix effects) was determined by comparing areas of extracted standard iodo-APAP-

LQQCPFEDHVKL with standard iodo-APAP-LQQCPFEDHVKL. Extraction efficiency was found to be $89.7 \pm 16.9\%$ (SD, $n = 4$). Comparison of peak areas of four peptide-level standards (see above concentrations) with and without blank serum matrix showed a signal decrease due to matrix effects (signal with matrix/signal without matrix) of $67.0 \pm 6.4\%$ and a retention time shift of 0.33 ± 0.06 min to earlier retention. Based on these results, it is clear that protein-level are needed to provide absolute quantitation of our modified protein target.

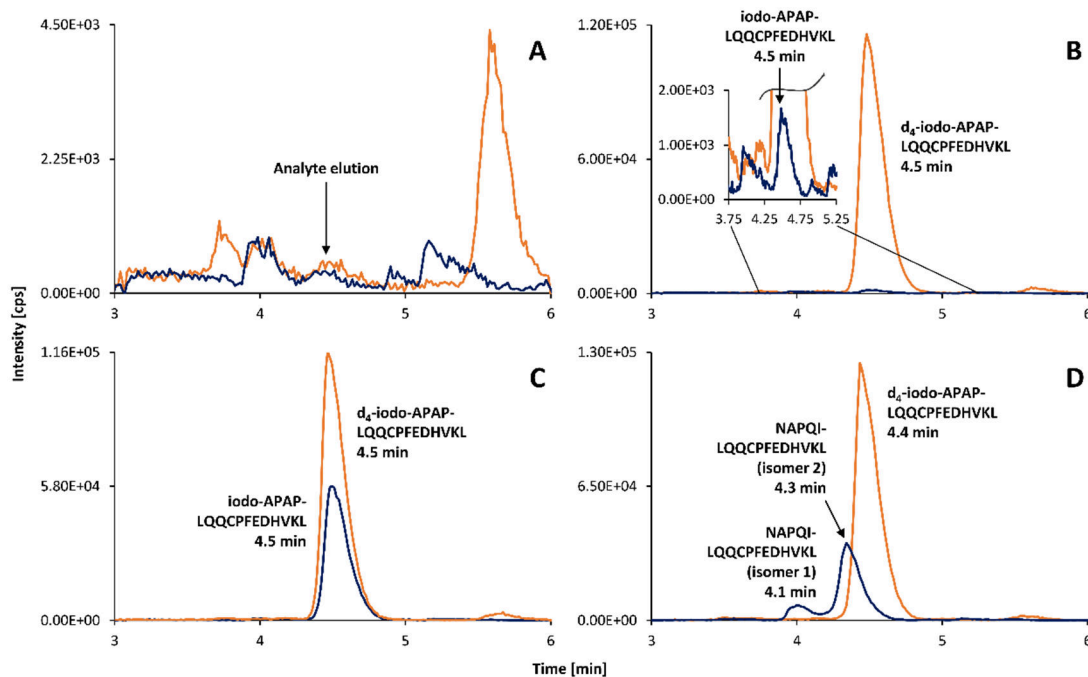


Figure 2.3 MRM chromatograms of double blank sample (A), lowest standard (0.11 nmol/mL, B), mid-range standard (5.41 nmol/mL, C), and a representative patient sample (3.91 nmol/mL, D). MRM transitions were m/z 535.9 \rightarrow 984.4 (dark) for analyte and surrogate standard, and m/z 537.2 \rightarrow 984.4 (light) for IS.

Table 2.2 Accuracy, within-run %CV ($n = 6$ for standards, $n = 9$ for QCs) and total %CV ($n = 12$ for standards, $n = 18$ for QCs) data, obtained from LC-MRM and LC-HRMS/MS evaluation runs

	(nmol/mL)	LC-MRM			LC-HRMS/MS		
		Run 1 – %accuracy (%CV)	Run 2 – %accuracy (%CV)	Total %CV	Run 1 – %accuracy (%CV)	Run 2 – %accuracy (%CV)	Total %CV
Std A	0.11	83.8 (3.5)	85.6 (6.9)	4.9	91.8 (3.9)	92.4 (9.6)	7.5
Std B	0.23	94.4 (6.6)	92.8 (3.8)	5.1	97.2 (3.1)	93.5 (6.4)	4.9
Std C	0.68	107.6 (5.2)	100.9 (3.3)	5.5	104.9 (4.4)	96.4 (4.8)	6.2
Std D	1.35	106.1 (2.1)	105.5 (0.8)	1.6	103.6 (2.2)	103.3 (1.6)	4.8
Std E	5.41	109.9 (1.7)	106.7 (1.3)	2.1	109.8 (2.3)	102.7 (4.3)	4.8
Std F	10.83	104.1 (2.2)	104.2 (1.4)	1.8	104.4 (3.3)	101.9 (3.7)	3.5
Std G	18.05	99.4 (1.6)	103.0 (3.3)	3.1	101.0 (2.2)	99.6 (6.1)	4.4
Std H	30.08	102.2 (1.1)	99.4 (1.0)	1.7	104.6 (1.1)	96.9 (4.3)	5.0
Std I	50.13	97.9 (1.2)	96.3 (1.7)	1.6	101.0 (0.7)	95.1 (3.5)	3.9
QC 1	0.16	113.3 (3.6)	93.2 (4.1)	10.6	121.3 (9.6)	97.5 (8.8)	14.4
QC 2	0.80	112.5 (1.3)	104.1 (1.8)	4.1	110.8 (2.2)	100.4 (4.1)	6.0
QC 3	8.02	113.1 (0.6)	104.8 (1.5)	4.1	113.3 (1.2)	101.3 (3.6)	6.3
QC 4	25.06	106.3 (0.3)	107.8 (2.4)	1.8	108.1 (0.5)	105.0 (4.4)	3.4

2.4.4 APAP hepatotoxicity patient study

The developed assay was applied to a study of 35 patients exhibiting either ALF or ALI (see Table 2.3). In all analyzed samples, two signals for isomeric NAPQI-LQQCPFEDHVKL species were found (see Figure 2.3D), resulting from Michael addition to NAPQI (see Figure 2.1A) in either the ortho or meta position (Damsten *et al.*, 2007). The presence of two NAPQI-LQQCPFEDHVKL isomers in a representative patient sample was analyzed by LC-HRMS/MS using 60 min gradient elution to ensure spectral purity. To verify that signals did not derive from serum-based interferences,

an extracted ion chromatogram and HRMS/MS spectra of both isomers can be found in Figure 2.5. All patient samples showed serum NAPQI-HSA. The $(y_{10}-H_2O)^{2+}/y_8$ ion ratios were 1.42 ± 0.46 (SD, $n = 105$) and 2.27 ± 0.34 for isomer 1 and isomer 2, respectively. The PFEDH/ y_8 MRM transition ratios were found to be 0.65 ± 0.17 for isomer 1 and 0.99 ± 0.10 for isomer 2. Reproducible ion ratios ensured the absence of isobaric interferences. Sample concentrations ranged between 0.12 and 3.91 nmol/mL (isomer 1 and 2 combined), with a maximal SD of repeated injections of 0.10 nmol/mL ($n = 3$). Furthermore, the isomer ratio (isomer 1/isomer 2) was calculated by using the integrated peak areas (A) and the following equation:

$$\text{Isomer ratio} = \frac{A(\text{isomer 1 and 2}) - A(\text{isomer 2})}{A(\text{isomer 2})} \quad (2.1)$$

The isomer ratio was found to be consistently 0.3 (± 0.1 , SD) for all patient samples with isomer 2 peak areas above LLOQ ($n = 32$). Median serum concentrations (see Table 2.3) of isomer 2 and combined isomers of non-spontaneous survivors ($n = 25$) were 0.40 nmol/mL and 0.52 nmol/mL, respectively. For patients exhibiting irreversible liver damage, followed by liver transplantation or fatality, a median serum level of 0.75 nmol/mL was observed by assessing isomer 2; 0.91 nmol/mL by assessing the combined isomers. Null hypothesis analysis (Mann–Whitney U) resulted in a p -value of 0.028 in both cases (isomer 2 only, or combined isomers).

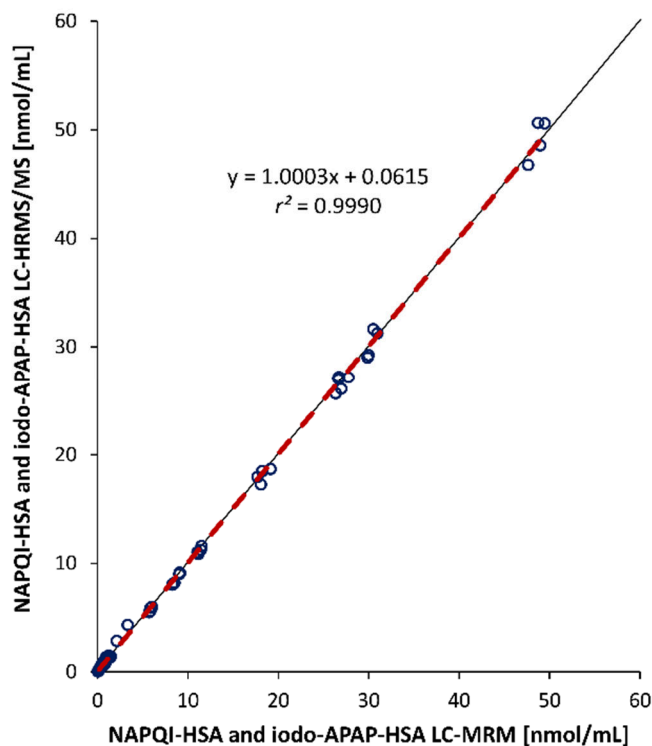


Figure 2.4 Linear agreement (dashed line) between LC-MRM and LC-HRMS/MS results of standards, QCs and patient samples.

Table 2.3 Calculated range, mean, median and SD of NAPQI-HSA concentrations of two patient cohorts

	Non-spontaneous survivors (<i>n</i> = 25)		Patients with irreversible liver damage (<i>n</i> = 10)	
	Main isomer	Two isomers	Main isomer	Two isomers
Range (nmol/mL)	<0.11–2.13 ^a	0.12–2.61	0.25–3.32	0.35–3.91
Mean (nmol/mL)	0.51	0.66	0.95	1.17
Median (nmol/mL)	0.40	0.52	0.75	0.91
SD (nmol/mL)	0.44	0.53	0.87	1.01

Results are based on either NAPQI-HSA main isomer, or isomers 1 and 2 combined

^aTwo patients showed NAPQI-HSA levels below LLOQ. Levels were 0.07 and 0.10 nmol/mL (measured by LC-MRM for lower concentrations).

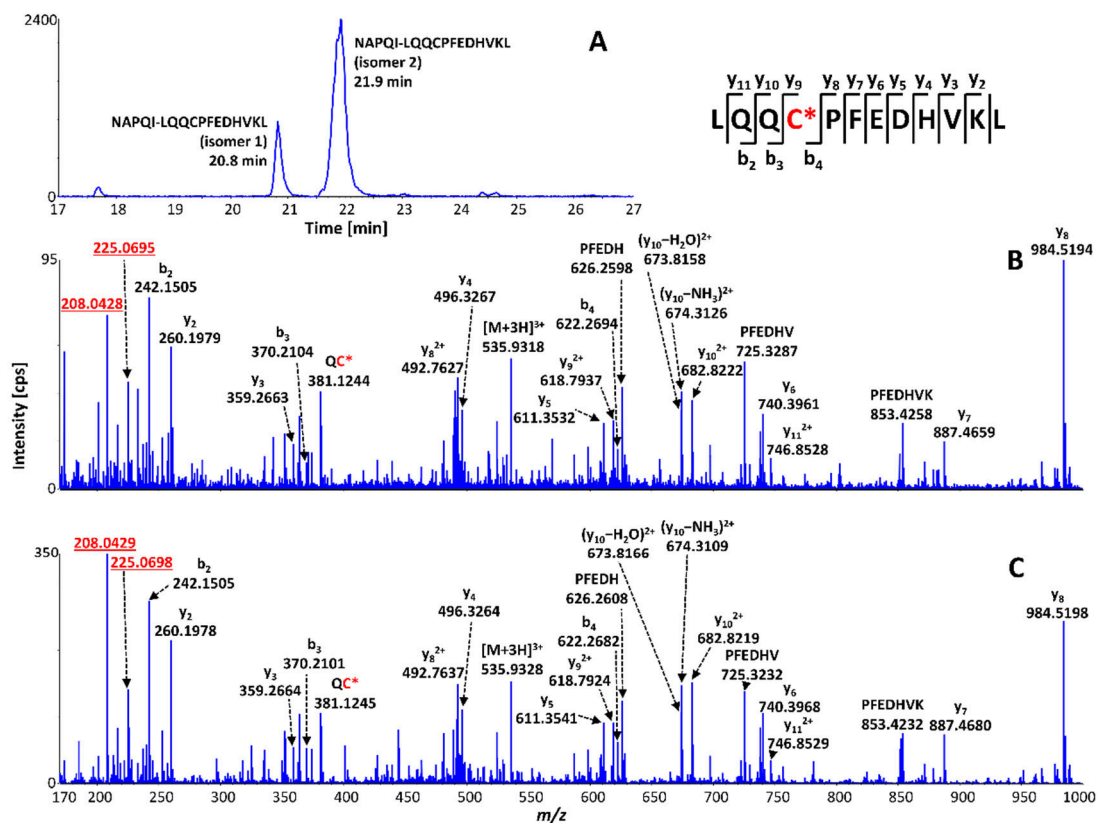


Figure 2.5 (A) Extracted MS/MS chromatogram of a patient sample (3.91 nmol/mL, 60 min gradient), for product ion at m/z 984.5149 (± 0.01 u, CE = 28 V). High-resolution MS/MS spectra of NAPQI-LQQCPFEDHVKL (theoretical $[M+3H]^{3+}$ precursor at m/z 535.9292) showing product ions (in bold) and NAPQI-Cys related diagnostic ions (underlined) of isomer 1 (B) and isomer 2 (C).

2.4.5 LC-MRM quantitation of low level samples

The eight lowest patient samples were also analyzed with 2.5x higher injection volume and increased dwell time for the quantitative MRM transition (500 ms for m/z 535.9 \rightarrow 984.4). The lower linear range (0.02–1.35 nmol/mL, six-point calibration) was set, and additional QCs (at 0.03, 0.11 and 0.23 nmol/mL) were analyzed to validate the obtained results. QCs and all standard samples were in a range of 98.6–112.9% accuracy and 0.8–6.9% within-run CV (see Table 2.1).

2.5 Discussion

This newly developed quantitative assay was successfully used to probe human acetaminophen covalent binding *in vivo*. Validation was achieved by multiple assessments of custom-designed standards and QCs, in combination with linear agreement analysis by HRMS/MS, to investigate the presence of isobaric, serum-derived interferences (Geib *et al.*, 2016; Qi *et al.*, 2015a). The method yielded accuracies and %CVs well within the acceptable limits with fast sample analysis and clinical applicability. We focused on a simple protocol to follow, without the need for extensive fractionation. Digestion, sample preparation and MRM conditions were carefully optimized to probe the modified active-site Cys34 of HSA. The target peptide (NAPQI-LQQCPFEDHVKL) was found to be less acidic than in the rat-based assay (NAPQI-LQKCPYEE) (LeBlanc *et al.*, 2014) and showed different MS properties as well. We also noted chromatographic separation of two isomeric NAPQI-peptides from human samples.

Our new assay focused on modified HSA in blood for more accurate quantitation of direct NAPQI-protein binding than previous assays. HSA is the major protein in blood and is a known target of NAPQI. Total protein adduct quantitation

depends highly on reproducible sample preparation which is limited in the context of complete hydrolysis (to APAP-Cys) without any sample loss or degradation. Furthermore, total NAPQI adduct formation also can include adducts from GSH. The modified HSA strategy presented here incorporates a simple proteolysis step under much less extreme conditions than complete hydrolysis of proteins for quantitative robustness. We were able to combine accurate analysis with a short 1 h digestion and simple SPE protocol. The method yielded comparable results to >18 h digestion of related biomarker assays, as well as other lengthy sample preparation steps, including sample dialysis (Cook *et al.*, 2015; Muldrew *et al.*, 2002) or post-digestion affinity chromatography (Damsten *et al.*, 2007). Furthermore, accuracy and imprecision were comparable to quantitative APAP-Cys analyses (Cook *et al.*, 2015; James *et al.*, 2009; Muldrew *et al.*, 2002). However, we were able to combine these features with high robustness and reliability using a closely co-eluting IS, based on an isotope (d_4) derivative of our surrogate standard, allowing absolute protein-level quantitation.

Protein-level standards allowed for correction of losses during digestion (missed or additional cleavages) and SPE, as well as for ion suppression/enhancement effects during ionization. However, using an isomeric surrogate standard to quantify NAPQI-protein levels necessitated careful evaluation. HRMS/MS analysis of iodo-APAP-LQQCPFEDHVKL (Figure 2.2) confirmed identical fragmentation properties to both NAPQI-LQQCPFEDHVKL species (Figure 2.5B and C), with no differences in relative amounts of fragment ions being due to the slight change in structure. NAPQI-Cys-related fragment ions (Sleno *et al.*, 2007) were observed in both isomer signals as it has been previously reported to confirm NAPQI-protein binding *in vitro* (Golizeh *et al.*, 2015). In addition, NAPQI-peptides yielded similar MRM ion ratios, compared with iodo-APAP-peptides. Mean ion ratios for NAPQI-peptide (isomer 2) deviated by <9% from mean ion ratios of iodo-APAP-peptide, complying with ion ratio thresholds for protein quantitation (Loziuk *et al.*, 2014). Due to the high reactivity and instability of NAPQI, the synthesis of a custom-designed labeled/ unlabeled NAPQI-

HSA standard is not possible. Reproducible synthesis of authentic NAPQI-modified standard, as shown by Damsten *et al.* (Damsten *et al.*, 2007) has been achieved on the peptide-level; however, it is still very challenging. Moreover, the comparison of peptide-level and protein-level standards showed quantitative differences, especially at lower levels. Thus, the use of iodo-APAP-HSA as a more accurate surrogate protein-level standard was considered necessary for absolute quantitation.

Our assay was successfully applied to assess a patient sample cohort of 35 patients to prove sufficient assay applicability especially in terms of dynamic range that would be clinically-relevant. Low limits of quantitation were important, as NAPQI-protein levels in human serum have been found to peak later after ingestion than in rodent models (Xie *et al.*, 2015). A combined assessment of APAP and NAPQI-HSA levels in serum could be a viable clinical approach to monitor early presenting overdose patients. In addition, using our method to analyze the levels of NAPQI-protein adducts over time by serial sampling could provide further insights.

In developing this method, we paid attention to the feasibility and applicability of the assay by reducing digestion time, and having a rapid and simple SPE clean-up for fast sample treatment. A simpler sample clean-up protocol has the potential for important matrix effects and therefore necessitated very careful optimization of chromatographic separation, with a reasonable analysis time (10 min per sample). Blank (IS in analyte-free matrix) and double blank (analyte and IS-free matrix) samples in every batch confirmed the absence of interfering MRM transitions at the analyte's retention time. In addition, we demonstrated assay linearity in lower NAPQI-HSA concentrations (0.02–1.35 nmol/mL) by altering the final LC-MRM method with the exact same sample preparation. The calibration range is therefore very flexible, and customizable for future applications.

Finally, we successfully developed a LC-MRM-based assay to accurately quantify NAPQI-modified HSA in ALF patients, as a potent method to monitor APAP-related hepatotoxicity. The strength of our novel design is that a good balance of accuracy and applicability was found. The given dynamic range enabled adequate quantitation of NAPQI-HSA with a low SD, thus allowing accurate monitoring of APAP-protein binding. In addition, two isomeric species of NAPQI-HSA were found to be separated, with a consistent isomer ratio in all patient samples.

This assay is applicable to many investigations into APAP-related human hepatotoxicity from a simple blood test, including those at sub-toxic doses and those investigating potential drug-drug (or drug-diet) interactions, as well as disease states with potential effects on drug metabolism and increased susceptibility for APAP-related toxicity. Subsequently, investigation of the kinetics and stability of protein-bound NAPQI in hepatocytes and the systemic circulation can also be further investigated using this assay.

2.6 Acknowledgements

The Natural Sciences and Engineering Research Council of Canada (NSERC, Discovery grant Nos. 355933-2011 & RGPIN 2016-06034) is acknowledged for financial support of this research. T.G. acknowledges the *Fondation Hydro-Québec*, Université du Québec à Montréal, and the *Groupe de Recherche Axé sur la Structure des Protéines* (GRASP), funded by the FRQS (*Fonds de recherche du Québec – Santé*), for scholarships. E.M.L. was an Alberta Innovates Health Solutions Scholar.

CHAPTER III

LIQUID CHROMATOGRAPHY-TANDEM MASS SPECTROMETRY ANALYSIS OF ACETAMINOPHEN COVALENT BINDING TO GLUTATHIONE S-TRANSFERASES

Timon Geib, Cristina Lento, Derek J. Wilson and Lekha Sleno

Published in **Frontiers in Chemistry** 2019, 7, 558. Supporting information partly included in

Appendix A and online at <https://doi.org/10.3389/fchem.2019.00558>.

In this chapter, covalent adducts formed between the reactive metabolite of acetaminophen and key cellular defense enzymes against toxicity, the glutathione *S*-transferases, were characterized *in vitro*. Bottom-up proteomics combined with liquid chromatography-tandem mass spectrometry analyses revealed four different cytosolic glutathione *S*-transferases as targets. Modifications were identified at the exact cysteine site. Furthermore, two different mass spectrometry systems, targeted multiple reaction monitoring on a quadrupole linear ion trap and untargeted data-dependent acquisition on a quadrupole–time-of-flight platform, were compared for general performance and sensitivity. Comparing the detection of low abundant drug-protein adducts allowed for a detailed demonstration of limitations and strengths of both untargeted and targeted approaches.

Timon Geib, Cristina Lento, Derek J. Wilson and Lekha Sleno are co-authors of this article. Timon Geib conducted the literature survey, prepared experimental protocols, conducted the experiments, processed the data and prepared the original manuscript. Cristina Lento and Derek J. Wilson performed recombinant expression and purification of glutathione *S*-transferase proteins. Lekha Sleno supported and supervised the project, verified data analysis and interpretation of the results, revised and finalized the manuscript.

3.1 Abstract

Acetaminophen (APAP)-induced hepatotoxicity is the most common cause of acute liver failure in the Western world. APAP is bioactivated to *N*-acetyl *p*-benzoquinone imine (NAPQI), a reactive metabolite, which can subsequently covalently bind to glutathione and protein thiols. In this study, we have used liquid chromatography-tandem mass spectrometry (LC-MS/MS) to characterize NAPQI binding to human glutathione *S*-transferases (GSTs) *in vitro*. GSTs play a crucial role in the detoxification of reactive metabolites and therefore are interesting target proteins to study in the context of APAP covalent binding. Recombinantly-expressed and purified GSTs were used to assess NAPQI binding *in vitro*. APAP biotransformation to NAPQI was achieved using rat liver microsomes or human cytochrome P450 Supersomes in the presence of GSTA1, M1, M2, or P1. Resulting adducts were analyzed using bottom-up proteomics, with or without LC fractionation prior to LC-MS/MS analysis on a quadrupole-time-of-flight instrument with data-dependent acquisition (DDA). Targeted methods using multiple reaction monitoring (MRM) on a triple quadrupole platform were also developed by quantitatively labeling all available cysteine residues with a labeling reagent yielding isomerically-modified peptides following enzymatic digestion. Seven modified cysteine sites were confirmed,

including Cys112 in GSTA1, Cys78 in GSTM1, Cys115 and 174 in GSTM2, as well as Cys15, 48, and 170 in GSTP1. Most modified peptides could be detected using both untargeted (DDA) and targeted (MRM) approaches, however the latter yielded better detection sensitivity with higher signal-to-noise and two sites were uniquely found by MRM.

3.2 Introduction

Hepatotoxicity induced by acetaminophen (APAP), a widely used analgesic and antipyretic, presents major health care challenges in Western societies (Fagan and Wannan, 1996; James *et al.*, 2013; Larson *et al.*, 2005; Lee, 2004; Sivilotti *et al.*, 2005). At therapeutic doses, APAP is considered harmless (Mazaleuskaya *et al.*, 2015). However, at higher doses, it can act as a potent hepatotoxin, and cause cell necrosis (McGill *et al.*, 2013) and acute liver failure (Lee, 2004). Liver failure induced by APAP correlates often with overdose or misuse, including chronic overuse (Lee *et al.*, 2008b). This often results in difficulties in diagnosis and treatment (Cairney *et al.*, 2016).

APAP is mostly detoxified via phase II metabolism; with direct glucuronidation (~55%) and sulfation (~40%) (Mazaleuskaya *et al.*, 2015; Mitchell *et al.*, 1973a). However, up to 10% undergoes bioactivation to *N*-acetyl *p*-benzoquinone imine (NAPQI), a highly reactive electrophile, which is known to covalently bind to nucleophilic centers, including cysteine thiols in liver proteins (see Figure 3.1) (Dahlin *et al.*, 1984; Gibson *et al.*, 1996; Jollow *et al.*, 1973). At higher doses, the fraction of oxidized APAP can increase up to 15%, due to saturation of the sulfation pathway (Mazaleuskaya *et al.*, 2015). The formation of NAPQI is mediated by the cytochrome P450 (CYP) superfamily (Potter *et al.*, 1973), with CYP1A2, 2D6, 2E1, and 3A4

isoforms as the major APAP oxidizing enzymes (Dong *et al.*, 2000; Laine *et al.*, 2009; Manyike *et al.*, 2000; Mazaleuskaya *et al.*, 2015; Patten *et al.*, 1993; Preissner *et al.*, 2010; Raucy *et al.*, 1989). NAPQI can be detoxified by subsequent phase II metabolism via conjugation with glutathione (GSH), partly mediated by different glutathione *S*-transferase (GST) isozymes (Figure 3.1) (Mitchell *et al.*, 1973b).

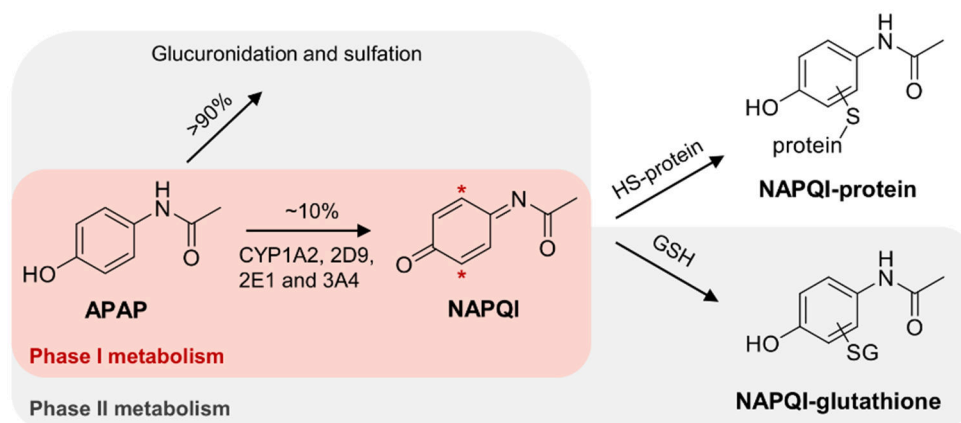


Figure 3.1 Simplified scheme of APAP metabolism, leading to the formation of NAPQI with subsequent GSH conjugation. Hepatotoxicity of NAPQI is linked to protein binding to cysteine sites.

GSTs represent major detoxification enzymes with a protein size of ~25 kDa (Eaton and Bammler, 1999) and multifunctional purposes, including induction of microsomal peroxidation (Strange *et al.*, 2000) and heavy metal resistance (Cao *et al.*, 2017; Zhang *et al.*, 2013), as well as possible roles in diseases, such as pulmonary fibrosis (He *et al.*, 2019). Members of cytosolic GSTs tend to dimerize with subunits of the same class, which results in a larger number of enzyme possibilities than genes (Sheehan *et al.*, 2001). Different genetic variants of GST have shown varying effectiveness in the detoxification of NAPQI. The isozymes GST mu 1, pi 1, and theta 1 (GSTM1, P1, and T1) have been found to be most effective (Coles *et al.*, 1988).

However, due to staggered or inadvertent APAP overuse, cellular GSH can be depleted and the GSH conjugation pathway can be saturated, resulting in NAPQI accumulation, leading to increased protein binding (Mitchell *et al.*, 1973b). NAPQI modifications of certain proteins can alter critical cellular functions (Liebler, 2008) and NAPQI-protein adducts have been found to accumulate in hepatocytes (Jollow *et al.*, 1973). Thus, functional and conformational protein changes may ultimately lead to subsequent cell death in liver (Kon *et al.*, 2004). In a previous study, we demonstrated a dose response to protein binding, using absolute quantitation of NAPQI-adducts to Cys34 in rat serum albumin *in vivo* (LeBlanc *et al.*, 2014). A subsequent related study quantifying modified human albumin in patient plasma samples was able to distinguish between moderate and severe APAP-induced acute liver failure (Geib *et al.*, 2018).

Several NAPQI-protein adducts have been identified previously in mouse, rat, and human (Cohen *et al.*, 1997; Copple *et al.*, 2008; Damsten *et al.*, 2007; James *et al.*, 2003; Jan *et al.*, 2014; Qiu *et al.*, 1998; Wendel and Cikryt, 1981). These protein targets consist mostly of cytoplasmic liver proteins, most likely due to the increased solubility and detectability of these proteins. Included in these identified targets is mouse GSTP1 (Qiu *et al.*, 1998). *In vitro* binding studies have also shown NAPQI-GST adducts, using ¹⁴C-APAP metabolism in mouse liver homogenates (Wendel and Cikryt, 1981). In a previous study in rat liver microsomes (RLM), we reported that rat microsomal GST 1 (MGST1) was a target of NAPQI (Golizeh *et al.*, 2015). A subsequent paper confirmed rat MGST1 as well as GSTM1 as targets (Leeming *et al.*, 2017). Binding to human MGST1 was observed by Shin *et al.* (Shin *et al.*, 2007) studying human liver microsomes incubations of APAP. Boerma *et al.* (Boerma *et al.*, 2011) found recombinant human GSTP1 modified after NAPQI formation by a CYPB3 mutant *in vitro*. Certain of these previous reports were able to pinpoint the specific cysteine residues which were modified in the GSTs, namely Cys50 in rat and human MGST1 (Golizeh *et al.*, 2015; Shin *et al.*, 2007), and Cys48 in human GSTP1 (Boerma *et al.*, 2011). All of these cysteines are significant for enzyme function and alkylation would

therefore result in inhibition (Jenkins *et al.*, 2008; Lemercier *et al.*, 2004; Shin *et al.*, 2007). Since GSTs play a significant role in detoxification, further research into the susceptibility of different GST isozymes to being modified by NAPQI remains of high interest.

The analysis of proteins and their modifications benefits from continual advancements in liquid chromatography-tandem mass spectrometry (LC-MS/MS), a broadly used tool for proteomic investigations (Aebersold and Mann, 2003). Constant improvements in sensitivity and selectivity have made LC-MS/MS an invaluable method to characterize proteins and study their post-translational modifications (Aebersold and Mann, 2016). The development of high-resolution mass spectrometry (HRMS) (Mehmood *et al.*, 2015), data-dependent acquisition (DDA) (Mann *et al.*, 2001), targeted multiple reaction monitoring (MRM) (Gillette and Carr, 2013; Picotti and Aebersold, 2012), and multidimensional LC (Di Palma *et al.*, 2012) have all contributed significantly to MS-based proteomics for highly sensitive detection of proteins and their modifications. As a result of its unique ability to distinguish changes in exact sites in the protein sequence (Larsen *et al.*, 2006), MS/MS has become especially vital in post-translational modification studies.

In this work, several analytical approaches (Figure 3.2) were investigated combining different techniques for sample preparation and LC-MS/MS analysis to identify APAP-related covalent binding to purified human GSTs (overview in Table 3.1, note: Met1 is considered here as the first amino acid in protein sequences throughout the whole manuscript). Strength of our study was not needing to use radioactivity or a fluorescence tag to selectively detect modified proteins or peptides (a brief overview of protein detection methods can be found in Table S1). *In vitro* NAPQI-protein binding to four GSTs was investigated (GST alpha 1 (A1), M1, M2, and P1). APAP oxidation was performed *in vitro* using RLM or CYP3A4 Supersomes. Then, NAPQI-modified proteins were digested via two proteases (trypsin and pepsin) in

parallel and analyzed by two-dimensional LC-MS/MS, using high-pH reversed-phase (RP) offline fractionation. Results of fractionated and non-fractionated samples were compared. MS/MS was employed with DDA on a high-resolution quadrupole-time-of-flight platform. High-sensitivity MRM measurements were then used for targeted analysis of modified peptides, using reference standards of all possible cysteine modified peptides.

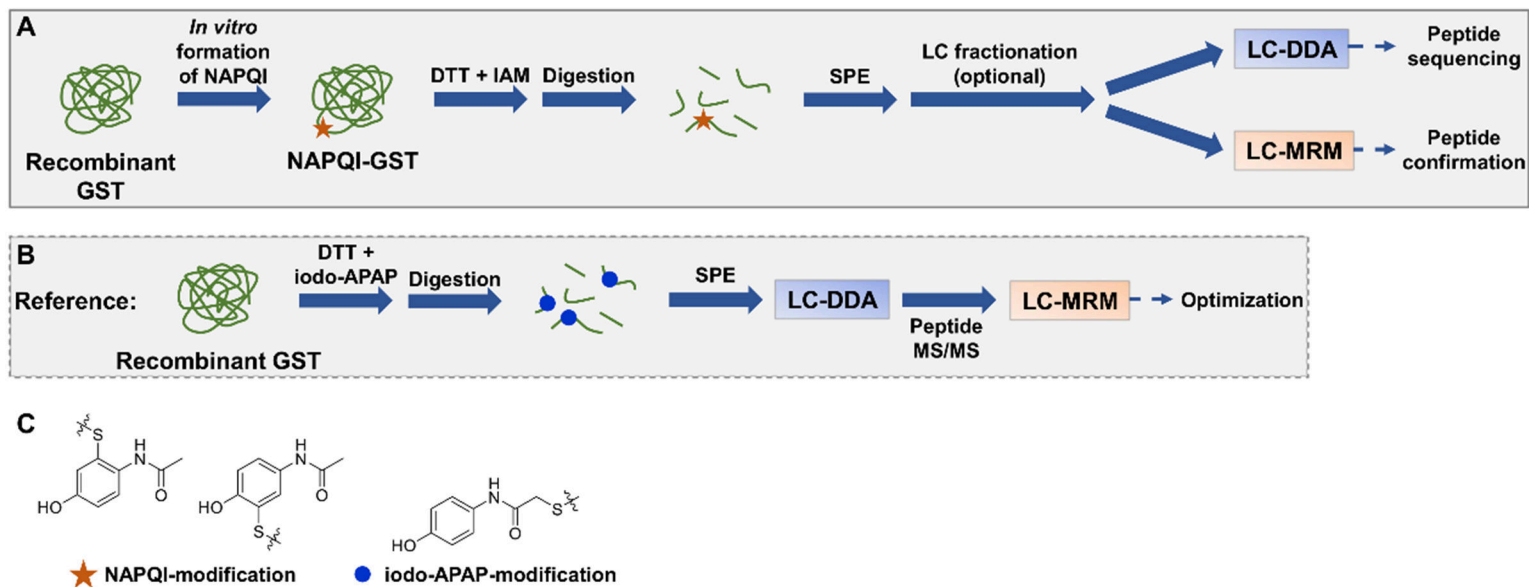


Figure 3.2 Representative workflow of *in vitro* NAPQI binding to recombinant GSTs followed by reductive alkylation and digestion (trypsin or pepsin), SPE with optional LC fractionation, and LC-MS/MS analysis (A). NAPQI generation was achieved by activation of APAP with either RLM or CYP3A4 Supersomes. MRM methods were based on isomeric iodo-APAP-GST standard, digested and first analyzed by DDA to investigate ionization and fragmentation properties of iodo-APAP-peptides (B). Then, MRM transitions were built and optimized for each peptide individually. Cysteine alkylation reagent iodo-APAP yields positional isomer label to NAPQI-modified cysteine (C).

Table 3.1 Overview of studied human GST enzymes^a

GST	Accession number	Molecular weight [Da]	pI	Active site (function)	Cysteine site	References
A1	P08263	25,631	8.22	Tyr9 and Arg45 (GSH binding)	Cys112	(Balogh <i>et al.</i> , 2009)
M1	P09488	25,712	5.99	Lys50 (GSH binding) and Tyr116 (substrate binding)	Cys78, 87, 115 and 174	(Johnson <i>et al.</i> , 1993; Patskovsky <i>et al.</i> , 2006)
M2	P28161	25,745	5.79	Lys50 (GSH binding), Tyr116 (substrate binding) and Thr210 (substrate specificity)	Cys87, 115 and 174	(Johnson <i>et al.</i> , 1993)
P1	P09211	23,356	5.29	Tyr8, Arg14, Trp39 and Lys45 (GSH binding)	Cys15, 48, 102 and 170	(Ang <i>et al.</i> , 2009; Federici <i>et al.</i> , 2009; Ji <i>et al.</i> , 1994; Oakley <i>et al.</i> , 1997b, 1997a; Prade <i>et al.</i> , 1997)

^a*Met1* is considered here as first entry in the amino acid sequence.

3.3 Materials and methods

3.3.1 Chemicals and materials

Aroclor 1254-induced male Sprague-Dawley rat liver microsomes (RLM) (part no.: M10001, lot no.: QEB and OTS) were purchased from BioreclamationIVT (Baltimore, MD). Human CYP3A4 Supersomes (also containing oxidoreductase and cytochrome *b*₅, part no.: 456202, lot no.: 7304001) were from Corning (Corning, NY). Cysteine alkylating agent iodo-APAP (*N*-(4-hydroxyphenyl)-2-iodoacetamide) was synthesized in-house as previously described (LeBlanc *et al.*, 2014). *Escherichia coli* cells were from laboratory stocks. Magnesium chloride and potassium phosphate (dibasic) were from Anachemia (Montréal, QC). Trypsin (TPCK-treated, from bovine pancreas), pepsin (from porcine gastric mucosa), dithiothreitol (DTT), acetaminophen (APAP), HPLC-grade acetonitrile (ACN) and methanol (MeOH), iodoacetamide (IAM), glucose-6-phosphate dehydrogenase (type XV, from baker's yeast), and other chemicals were purchased from Sigma-Aldrich (St. Louis, MO). Ultrapure water was from a Millipore Synergy UV system (Billerica, MA).

3.3.2 GST expression and purification protocols

Recombinant human GSTA1, M1, M2, and P1 proteins were expressed in *E. coli* and purified using a modification of published protocols (Groom *et al.*, 2014; Mukanganyama *et al.*, 2002). Overnight induction was proceeded when the culture reached OD₆₀₀ = 0.6. Cells were lysed as previously described (Mukanganyama *et al.*, 2002). Protein concentration was determined with the Bradford assay, using bovine serum albumin as reference standard (Habig *et al.*, 1974). GST affinity purification was performed on a GSH-agarose column (Groom *et al.*, 2014). Purified GSTs were

dialyzed to remove GSH by 3 L changes against 500 μ L into ammonium acetate for 48 h. Proteins were stored at -80°C .

3.3.3 Preparation of alkylated GSTs using iodo-APAP or IAM

Reductive alkylation of human GSTA1, M1, M2, or P1 (1.8–3.6 nmol) was performed in 100 mM ammonium bicarbonate (ABC, pH 8.5) using DTT (250 nmol; 20 min, 37°C), and either iodo- APAP (750 nmol in ACN; 45 min,) or IAM (750 nmol; 30 min) at 37°C (in dark). Alkylated proteins were incubated with either 10 μ g trypsin (4 h at 37°C) in ABC buffer, or 10 μ g pepsin (1 h at 37°C) with added 1% formic acid in 10% MeOH to obtain pH 2 during digestion. Trypsin digests were diluted with water; pepsin digests with ABC (100 mM), prior to solid-phase extraction (SPE) on 1 cc (30 mg) OASIS HLB cartridges (Waters, Milford, MA) eluted with 100% MeOH (1 mL). Eluates were dried and then resolubilized in 100 μ L of 10% ACN prior to LC-MS/MS analysis.

3.3.4 NAPQI-GST formation by RLM incubation

RLM (1 mg/mL protein) and APAP (100 μ M) were incubated (37°C and 500 rpm) in the presence of NADP^+ (500 μ M), and a NADPH-regenerating system: glucose 6-phosphate (10 mM), glucose-6-phosphate dehydrogenase (2 U/mL) and magnesium chloride (5 mM). Human GST (A1, M1, M2, or P1) in 100 mM phosphate buffer (pH 7.4, 1.8–3.6 nmol protein amount) was added to react with produced NAPQI for 3 h. The final incubation volume was 200 μ L. Then, proteins were diluted in ABC (100 mM); 200 and 150 μ L for tryptic and peptic digestion, respectively.

3.3.5 NAPQI-GST formation by CYP3A4

CYP3A4 Supersomes (1 mg/mL protein, 125 pmol/mL CYP3A4 final concentration) and APAP (100 μ M) were incubated (37°C and 500 rpm) in the presence of NADPH (1 mM in phosphate buffer). Then, GST (same as above) was added to react with produced NAPQI and diluted after 3 h (as above).

3.3.6 Digestion of NAPQI-GST

Reductive alkylation was performed using 10 μ L DTT (25 mM; 20 min, 37°C) and 10 μ L IAM (63 mM, 30 min, 37°C, in dark). All samples were then digested with either 10 μ g trypsin (4 h at 37°C), or with 400 μ L solution of 1% formic acid in 10% MeOH with 10 μ g pepsin (1 h at 37°C). Trypsin digestion was diluted with 500 μ L water, pepsin digestion with 200 μ L ABC (100 mM). Digests were then cleaned-up by SPE and reconstituted as above.

3.3.7 High-pH RP peptide fractionation

Dried extracts were reconstituted in 10% ACN (120 μ L) for injection (100 μ L) onto a ZORBAX Extend-C18 column (250 \times 4.6 mm; Agilent Technologies, Palo Alto, CA) with 5 μ m (100 Å) particles on an Agilent 1200 series HPLC equipped with a temperature-controlled autosampler (at 8°C), binary pump, degasser, diode array detector, and cooled fraction collector (at 8°C). High-pH RP fractionation was performed at a flow rate of 0.6 mL/min with a gradient starting at 5% B for 2 min, increased to 50% B in 12 min, to 70%B within 0.5 min, and held for 6.5 min. Mobile phase A was 10 mM ammonium acetate (pH 10, adjusted with ammonium hydroxide) in water and mobile phase B was prepared with 10% A / 90% ACN. UV absorbance

was monitored at 220 and 280 nm. Then, 16 (1 min) fractions were collected from 3 to 19min. Fractions were concatenated (fraction 1+9, 2+10, ...) into eight final fractions, dried and reconstituted in 100 μ L 10% ACN.

3.3.8 LC-MS/MS analysis with DDA

Samples were injected (30 μ L) onto an Aeris PEPTIDE XB- C18 100 \times 2.1 mm column, with solid core 1.7 μ m particles (100 \AA) fitted with a SecurityGuard ULTRA C18-peptide guard column (Phenomenex, Torrance, CA) using a Nexera UHPLC system (Shimadzu, Columbia, MD) with water (A) and ACN (B), both containing 0.1% formic acid, at a flow rate of 0.3 mL/min (40°C). The gradient started at 5% B (held for 2.5 min) and was linearly increased to 30% B within 37.5 min, to 50% B within 10 min, then to 85% B within 5 min (held for 3 min). MS and MS/MS spectra were collected on a high-resolution TripleTOF 5600 system (quadrupole–time-of-flight; Sciex, Concord, ON) equipped with a DuoSpray ion source in positive mode set at 5 kV source voltage, 500°C source temperature, and 50 psi GS1/GS2 gas flows, with a declustering potential of 80 V. The instrument performed a survey MS acquisition (TOFMS) from m/z 120–1,250 (250 ms accumulation time), followed by MS/MS (high sensitivity mode) from m/z 80–1,500 on the 15 most intense precursor ions (excluded for 20 s after two occurrences) using information dependent acquisition with dynamic background subtraction. Each MS/MS acquisition had an accumulation time of 50 ms and a collision energy (CE) of 30 \pm 10 V. The total cycle time was 1.05 s. MS and MS/MS calibration was performed after every four injections with a set of in-house standards, using an automatic calibrant delivery system. Sciex Analyst software version 1.7.1 (TripleTOF) was used for data acquisition. Raw data was visualized with PeakView 2.2.

Human files were searched against the UniProtKB/Swiss-Prot protein database (release date: 07/18/2018, including common protein contaminations) by ProteinPilot 5.0 software (Sciex) using the Paragon Algorithm (Shilov *et al.*, 2007). To find potential APAP-related adducts, the feature probability was altered to 50% for NAPQI on cysteine (addition of $C_8H_7NO_2$). The search was performed for +2 to +4 charge states at a MS tolerance of 0.05 u on precursor ions and 0.1 u on fragment ions. Peptides and proteins were identified with a 1% false discovery rate (FDR) (Tang *et al.*, 2008) using a target-decoy database search algorithm.

3.3.9 LC-MS/MS analysis in MRM mode

LC-MRM experiments were performed on an identical LC platform and column, and a QTRAP 5500 (Sciex, Concord, ON) hybrid quadrupole-linear ion trap system with a TurboIonSpray ion source in positive mode. For fractionated samples, a shorter LC gradient (~28 min) was used. The gradient started at 5% B (held for 2.5 min) and was linearly increased to 30% B within 21.5 min, to 50% B within 2 min, then to 85% B within 0.5 min (held for 2 min). Source parameters were as follows: ion spray voltage, 5 kV; temperature, 550°C; GS1 and GS2, 50 psi; and curtain gas, 35 psi. Entrance and collision cell exit potentials were set at 10 and 13 V, respectively. Ion activation via collision-induced dissociation was performed at collision gas pressure of 5 (arbitrary units). Individual MRM transitions with corresponding CE settings can be found in Table S2. MRM transitions of modified peptides were integrated using Sciex MultiQuant 2.1. Sciex Analyst software version 1.6 was used for data acquisition. Raw data was visualized with PeakView 2.2.

3.4 Results

3.4.1 Method development

Optimal *in vitro* metabolism of APAP was examined by GSH trapping experiments (data not shown). Oxidizing RLM and CYP3A4 Supersomes were each tested with either NADPH, or NADP⁺ and a NADPH regenerating system. RLM incubation in combination with a NADPH regenerating system and 3A4 Supersomes in the presence of NADPH yielded optimal conditions for APAP *in vitro* metabolism. For both strategies, a combination of 1 h open tube incubation followed by 2 h closed tube was found best for oxidation. It must be noted that GST stock solutions contained reduced GSH, which also bound to NAPQI (data not shown). Denaturation and excessive buffer exchange of GSTs, to yield completely GSH-free stocks, did not permit the study of binding capabilities based on protein structure. Additionally, excessive treatment of proteins led to important sample loss, different for each protein (data not shown). Furthermore, inclusion of a His-tag during expression (for subsequent Ni-nitrilotriacetic acid purification) might alter protein folding and thus binding results (Ledent *et al.*, 1997). The use of non-mutant GSTs purified over GSH affinity combined with solvent-free elution seemed optimal in this study. These facts were considered and APAP concentrations in final incubations were adjusted accordingly to assure detectable amounts of NAPQI-GST being formed. Subsequently, protein digestion, SPE and offline fractionation were optimized for highest sequence coverage of target GST from database search results of DDA runs. Trypsin and pepsin digestion (4 and 1 h, respectively) in parallel was found optimal to yield a sequence coverage >83% (data not shown). Standard iodo-APAP-GST was used to test cysteine coverage and detection of all possible modified cysteine (see Table 3.2). Only the sites Cys15 and 102 were detected with a confidence <95%, based on small sequence size and low fragmentation of tryptic C¹⁵(iodo-APAP)AALR, and poor abundance of peptic GVEDLRC¹⁰²(iodo-APAP)KYISL. For peptide separation, high-pH RP and fraction

concatenation was used as an alternative strategy to conventional ion exchange offline fractionation (Yang *et al.*, 2012; Zhou, 2003). This enabled orthogonal separation to online (low-pH) RP chromatography without a desalting SPE step, thus reducing potential sample loss (Di Palma *et al.*, 2012; Wang *et al.*, 2011).

MRM experiments were based on initial DDA results of digested iodo-APAP-GST standards. After database searching, iodo-APAP-modified peptides were investigated for each cysteine site (data not shown). Based on signal abundance and MS/MS properties, up to three modified peptides per cysteine site were chosen (see Table S2); peptide precursor with more than seven residues (Liebler and Zimmerman, 2013) and a charge state of +2 and +3 were preferred. Then, final transitions were based on the three most intense fragment ions (in DDA runs, with $m/z < 1250$) with fragment $m/z >$ precursor m/z . An additional transition was based on the most intense fragment (no m/z restriction). CE was further optimized for highest signal abundance of each transition.

Table 3.2 Coverage of iodo-APAP-cysteine sites in DDA HRMS/MS

GST	Cys	Peptide	z	Peptide confidence [%]	(DDA) absolute precursor area [cps]	RT [min]
Trypsin digestion						
M1	78	ITQSNAILC(iodo-APAP)Y	+2	95	6.48E+06	24.4
	87	HNLC(iodo-APAP)GETEEEEK	+3	99	1.21E+06	7.0
	115	GMIC(iodo-APAP)YNPEFEK	+2	99	7.99E+05	21.6
	174	C(iodo-APAP)LDAFPNLK	+2	99	1.76E+06	23.8
M2	87	HNLC(iodo-APAP)GESEK	+3	99	9.63E+05	3.4
	115	LC(iodo-APAP)YDPDFEK	+2	95	5.56E+07	20.8
	174	NQVFEPSC(iodo- APAP)LDAFPNLK	+3	99	1.60E+07	32.0
P1	15	C(iodo-APAP)AALR	+2	36	1.92E+07	5.6
	48	ASC(iodo-APAP)LYGQLPK	+2	98	1.11E+07	19.4
Pepsin digestion						
A1	112	PVC(iodo-APAP)PPEEKDAKL	+2	99	3.34E+06	14.4
M1	115	GMIC(iodo-APAP)YNPEF	+2	99	6.89E+05	27.9
M2	87	IARKHNLC(iodo- APAP)GESEKEQIRE	+2	99	5.10E+05	7.4
	115	AKLC(iodo-APAP)YDPDF	+2	98	1.28E+07	21.9
	174	ERNQVFEPSC(iodo-APAP)L	+2	99	3.77E+07	23.9
P1	102	GVEDLRC(iodo-APAP)KYISL	+3	32	7.18E+04	23.6
	170	IHEVLAPGC(iodo-APAP)L	+2	99	3.30E+06	23.8

3.4.2 Protein analysis by DDA and detection of NAPQI binding

The number of found total proteins within 1% FDR ranged from 135 to 356 for RLM incubated, non-fractionated samples; from 40 to 80 for Supersomes incubations. Applying offline fractionation lead to an average increase in found proteins at 1% FDR of 23.7% and 28.5% for RLM and Supersomes incubated samples, respectively. NAPQI-alkylated peptides found by database searching were confirmed by using the following criteria: 1) precursor mass error <10 ppm, 2) MS/MS spectral confidence >95%, 3) the presence of one diagnostic production (see Figure 3.3) (Golizeh *et al.*, 2015; Sleno *et al.*, 2007), and 4) <0.5 min retention time deviation from iodo-APAP standard (for human GSTs). A total of six NAPQI-modified peptides of five distinct cysteine sites of three GSTs were found based on above criteria (see Table 3.3). Overlaid extracted ion chromatograms of all six peptides can be found in Figure 3.4A. Found diagnostic fragment ions can be found in Table 3.4. Additional MS and MS/MS spectra are available in Figure 3.4B and C, and Figure S1. In addition, NQVFEPSC*LDAFPNLK from human GSTM2 and one peptide from rat MGST1 (from RLM background) were identified without detection of diagnostic fragment ions (Figures S2 and S3). MS/MS of modified rat MGST1 peptide, VFANPEDC*AGFGK, was confirmed by comparison to previously analyzed standard peptide (Golizeh *et al.*, 2015). A comparison of NAPQI-modified peptides from human GSTs to their confidently identified carbamidomethylated variants can be found in Table 3.5. An overview of all carbamidomethylated GSTs can be found in Table S3.

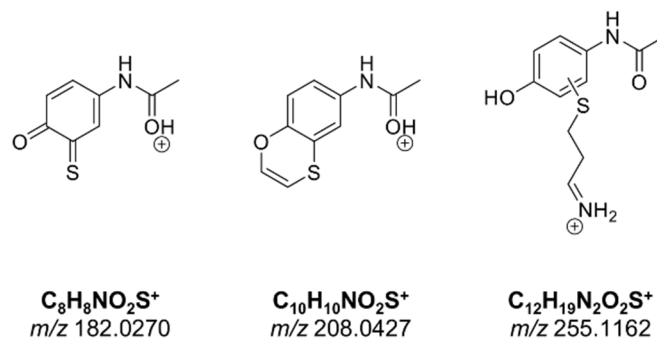


Figure 3.3 Proposed structures of diagnostic fragment ions.

3.4.3 Confirmation of NAPQI binding by MRM strategies

NAPQI-modified peptides were identified in MRM experiments by following criteria: 1) signal-to-noise (S/N) of all transitions >10, 2) <17.2% deviation of relative abundance (see Equation 3.1) (Loziuk *et al.*, 2014) of two highest transitions (with fragment m/z > precursor m/z) from iodo-APAP-modified peptide standard, and 3) <0.5 min retention time deviation of all transitions from iodo-APAP standard. After data filtration, MRM strategies yielded 10 NAPQI-modified peptides of seven cysteine sites of four GSTs (see Table 3.3). Overlaid MRM chromatograms can be found in Figures S4–S7. The relative abundance of transitions was calculated through the ratio of its integrated peak area and the peak area sum of all three transitions (with fragment m/z > precursor m/z) (Loziuk *et al.*, 2014):

$$\text{Relative abundance} = \frac{A_x}{\sum_{i=1}^3 A_i} \quad (3.1)$$

Table 3.3 NAPQI-GST peptides confirmed by DDA and MRM methods^a

GST	Cys	Peptide	DDA				MRM			
			RLM (1D)	RLM (2D)	3A4 (1D)	3A4 (2D)	RLM (1D)	RLM (2D)	3A4 (1D)	3A4 (2D)
A1	112	PVC*PPEEKDAKL		✓			✓	✓		✓
		PVC*PPEEKDAKLAL	✓				✓	✓		
M1	78	ITQSNAILC*Y					✓		✓	✓
M2	115	AKLC*YDPDF						✓		✓
		LC*YDPDFEK		✓						
	174	ERNQVFEPSC*L				✓	✓	✓	✓	✓
		DVLERNQVFEPSC*								✓
		NQVFEPSC*LDAFPNLK	✓	✓			✓	✓	✓	✓
P1	15	C*AALR								✓
		48	ASC*LYGQLPK				✓			✓
		170	IHEVLAPGC*L	✓				✓	✓	✓

^aRLM (1D): RLM incubation without fractionation, RLM (2D): RLM incubation with fractionation, 3A4 (1D): CYP3A4 Supersome incubation without fractionation, 3A4 (2D): CYP3A4 Supersome incubation with fractionation, DDA: confirmed by DDA, MRM: confirmed by MRM.

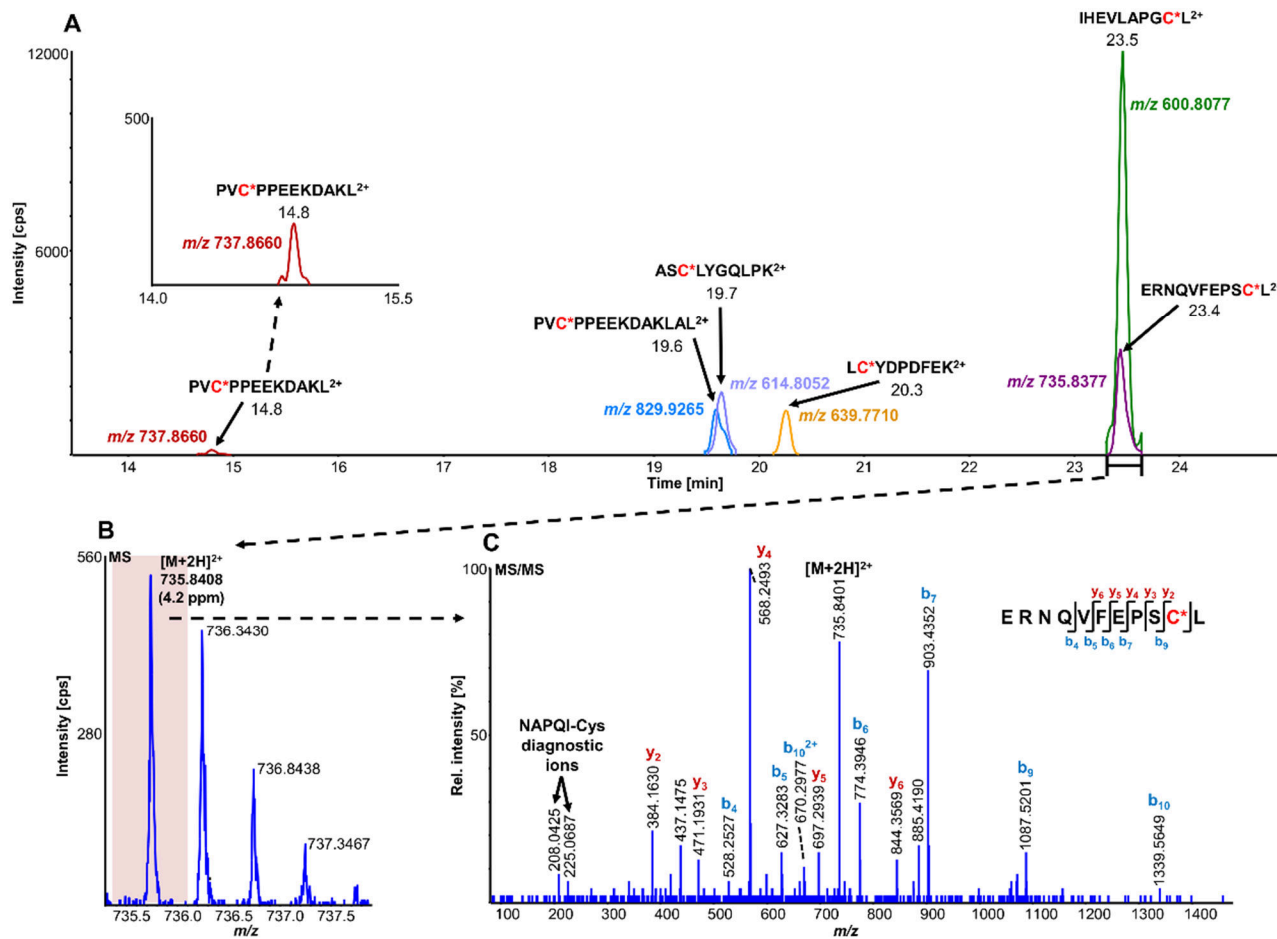


Figure 3.4 Overlaid high-resolution extracted ion chromatograms (± 0.01 u) of detected modified peptide precursors (A). Confirmation was based on high-resolution accurate mass TOFMS (B) and triggered (DDA) MS/MS (C) analyses, including diagnostic NAPQI-cysteine fragment ions.

Table 3.4 NAPQI-cysteine diagnostic fragment ions (MS2) detected in HRMS/MS experiments

GST	Cys	Peptide	Diagnostic ion (ppm)		
			<i>m/z</i> 182.0270	<i>m/z</i> 208.0427	<i>m/z</i> 225.0692
A1	112	PVC*PPEEKDAKL		✓ (-2.4)	✓ (-0.4)
		PVC*PPEEKDAKLAL		✓ (-1.9)	✓ (-1.8)
M2	115	LC*YDPDFEK			✓ (1.8)
	174	ERNQVFEPSC*L		✓ (-1.0)	✓ (-2.2)
P1	48	ASC*LYGQLPK	✓ (5.5)		✓ (5.8)
	170	IHEVLAPGC*L		✓ (-9.6)	

3.4.4 Comparison of different strategies

A total of 11 distinct peptides comprising seven unique cysteine sites were found as NAPQI-modified, two of which, Cys78 in GSTM1 and Cys15 in GSTP1, were uniquely found by MRM strategies. Thus, CYP3A4 incubations combined with high-pH RP fractionation and MRM analysis was found most suitable with a total of nine found distinct peptides, including all seven distinct cysteine sites. This combination reflects the least biological background, reduced matrix effects by offline fractionation and more certain detection by following selective transitions at matching retention times of peptides modified by the isomeric labeling reagent. Peptides ERNQVFEPSC*L, NQVFEPSC*LDAFPNLK (both Cys174 in GSTM2), and IHEVLAPGC*L (Cys170 in GSTP1) were identified using all four tested MRM strategies. Using MRM techniques demonstrated that dilution effects during offline fractionation, in the case where a specific peptide can elute over neighboring fractions (see Figure S8), could lead to target signal intensities below detection limits ($S/N < 10$) and thus missing identification in DDA and MRM experiments. This was observed in RLM incubations of GSTM1. Peptide ITQSNAILC*Y was only detected in MRM

experiments without LC fractionation (see Table 3.3). Furthermore, DDA experiments showed higher susceptibility to interfering compounds, even when detection limits were not an issue. Co-eluting, high abundant interferences in TOFMS survey scans resulted in missed MS/MS acquisition of target peptides. A visual representation of missed fragmentation of a NAPQI-peptide target (IHEVLAPGC*L), compared to a positive MRM identification, can be found in Figure 3.5. Missing MS/MS acquisition of the IHEVLAPGC*L peptide precursor at m/z 600.8077 was caused by a higher abundant interference at m/z 601.3123, overlapping with the peptide $[M+1+2H]^{2+}$ signal. In that case, only the highly abundant interference was analyzed in MS2 leading to a MS/MS spectrum of interference fragments and low abundant $[M+1+2H]^{2+}$ fragments, not allowing confident identification. One peptide, LC*YDPDFEK (Cys115 in GSTM2), was found only through DDA efforts, which was based on susceptibility of MRM transitions to isobaric interferences. The peptide was ultimately identified through HRMS/MS sequencing only (see Figure S1C). These circumstances lead to differences between DDA or MRM analyses (*e.g.*, RLM (1D) compared to 3A4 (1D) in Table 3.3), leading to more found modified sites with RLM incubations than with Supersomes, even though the latter were less complex incubations. Overall, NAPQI-peptide MRM signals reached higher signal abundance as extracted precursor ion (± 0.01 u) signals in DDA survey scans (TOFMS) with comparable S/N. The use of both trypsin and pepsin as proteases was shown to be complementary. Several sites were uniquely found using either one of the two proteases. NAPQI-modified Cys15, 48, and 78 were uniquely found in trypsin digests, whereas Cys112 and 170 were only found after pepsin digestion. Cys115 and 174 in GSTM2 were the only sites with detectable NAPQI peptides from both protease treatments; AKLC*YDPDF and LC*YDPDFEK, and ERNQVFEPSC*L and NQVFEPSC*LDAFPNLK, respectively.

GSTP1 sequence:

MPPYTVVYFPVVRGRCAALRMLLADQGQSWKEEVTVETWQEGSLKASCLYGQLPKFQDGLTLY
QSNILRHLGRTLGLYGKQQEAALVDMVNDGVEDLRCKYISLIYTNYEAGKDDYVKALPGQLKPF
ETLLSQNQQGKTFIVGDQISFADYNLLDLLLIHEVLAPGC*LDAFPLLSAYVGRLSARPKLKAFLASP
EYVNLPIPINGKQK

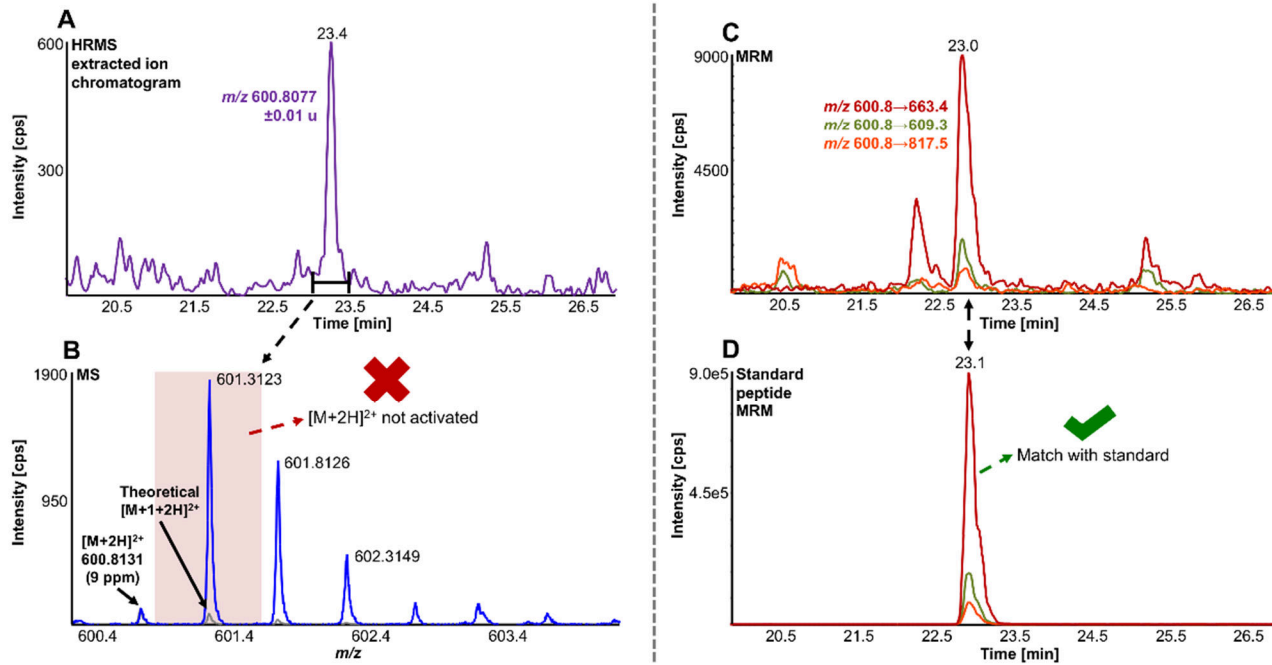


Figure 3.5 Comparison of LC-DDA and LC-MRM results, used to identify NAPQI-modified GSTP1 peptide IHEVLAPGC¹⁷⁰L (underlined) from *in vitro* incubation with CYP3A4 (Supersomes). DDA analysis of the target peptide (theoretical $[M+2H]^{2+}$ at m/z 600.8077) eluting at 23.4 min (A) did not yield MS/MS acquisition (B). Fragmentation was triggered by an interfering ion at m/z 601.3123, which resulted in a MS1 isolation window (red rectangle) not incorporating target peptide. MRM analysis (C) confirmed presence of IHEVLAPGC*L²⁺ by comparing to iodo-APAP-GST (D).

Table 3.5 Comparison of NAPQI-peptide to the IAM-modified (CAM) version found with >95% confidence in the same DDA experiments

GST	Cys	Peptide	NAPQI modification		CAM modification	
			RT [min]	Absolute peptide intensity [cps] (z)	RT [min]	Absolute peptide intensity [cps] (z)
A1	112	PVC*PPEEKDAKL	14.8	9.96E+02 (+3)	12.1	8.63E+03 (+3)
		PVC*PPEEKDAKLAL	19.6	6.61E+03 (+3)	17.1	1.77E+04 (+2)
M2	115	LC*YDPDFEK	20.3	3.83E+02 (+2)	17.2	5.86E+04 (+2)
		174 ERNQVFEPSC*L	23.4	1.27E+03 (+2)	19.3	3.19E+05 (+2)
		NQVFEPSC*LDAFPNLK	31.6	1.84E+03 (+2)	28.9	2.68E+05 (+2)
P1	48	ASC*LYGQLPK	19.7	5.82E+02 (+2)	15.5	1.09E+04 (+2)
		170 IHEVLAPGC*L	23.5	3.87E+03 (+2)	19.5	1.00E+02 (+1)

3.5 Discussion

The GST family is an essential, multifunctional set of enzymes, crucial in many detoxification and binding reactions in liver and other tissues. GSTs are involved in the metabolism of many substances and xenobiotics, including reactive metabolites such as NAPQI. The understanding of NAPQI binding to GSTs is thus a logical step toward understanding its hepatotoxicity. This study used several approaches for targeted and untargeted identification of modified peptides from *in vitro* incubations. The use of different methodologies yielded complementary findings but also allowed a critical view on performance and inherent limitations of each method.

3.5.1 Performance of different strategies

This study highlighted the importance of using complementary proteases to better cover potential modification sites. Pre-fractionation of peptides was mostly beneficial for identifying adducted peptides. The double protease approach substantially increased protein sequence coverage. Multiple protease digestion can be easily applied in proteomics workflows and is highly flexible, due to wide range of specific and less specific enzymes with diverse cleavage behavior. Pre-fractionation increased peptide coverage and improved NAPQI-peptide discovery due to better resolution of peptides, thus reducing matrix effects in both MRM and DDA. Benefits from better peptide resolution in multiplexed LC outweighed the potential for sample loss and dilution effects introduced through fractionation and concatenation. These sample preparation techniques are viable approaches to broaden the potential for identification of low abundant modifications on proteins.

Targeted MRM-based methods are most easily developed with the availability of purified proteins, whereas untargeted DDA analyses offer a more flexible, universal application without time-consuming optimization steps. GSTs are relatively easy to purify via GSH affinity chromatography and thus represent ideal proteins for reference standard preparation to build and optimize MRM methods. Untargeted DDA with subsequent database searching did not require any custom-made standards. Furthermore, DDA allowed for the analysis of protein binding beyond recombinant GST as the only target during incubations. For example, database searching for NAPQI-modified RLM proteins detected modified rat MGST1. Moreover, DDA and MRM strategies did not only differ in terms of applicability but also performance. This was rooted in differences in both MS platforms, as well as the two different acquisition types. Low resolving triple quadrupole systems (here a quadrupole-linear ion trap hybrid) generally reach lower limits of detection based on a higher duty cycle in optimized MRM modes. In comparison, quadrupole-time-of-flight instruments are less sensitive (Geib *et al.*, 2016) but offer higher mass accuracy and the possibility for structural characterization by MS/MS. The difference in sensitivity is a crucial factor in characterizing low abundant protein modifications. In our findings, MRM strategies generally reached superior detection limits and thus led to two uniquely found modified peptides. In addition, even when detection limits were surpassed, low abundance of NAPQI-peptides resulted in missed peptide precursor fragmentation in DDA and thus were not identified. The final number of found modified sites, confirmed by DDA, was ultimately achieved here by using multiple attempts, which highlighted the limitations of unsupervised DDA in covalent adduct analysis. Furthermore, DDA relies on automatically triggered high quality MS/MS of modified peptides. This can be a challenge in complex biological samples, especially for low-abundant modifications, since so many peptides are eluting off the analytical column together. Even though high-speed high-resolution mass spectrometers, such as the one used in this work, have the ability to acquire spectra very fast and with high sensitivity, there are still many

peptides not triggered for MS/MS acquisition under these conditions. MRM, on the other hand, does not suffer from this caveat. If a given peptide is present, above a certain threshold, it should be detected by MRM. This method still suffers from matrix effects (ion suppression) but is not competing with co-eluting species for MS/MS acquisition. In general, MRM methodologies offer higher robustness and reproducibility. However, it should be noted that the use of a semi-targeted DDA, using an inclusion list of putative modified peptides could potentially increase reproducibility. Furthermore, susceptibility of low mass resolving MRM to isobaric interferences might obstruct confident identification and quantitation in some cases, which is less likely in HRMS. Also constant improvements in instrumentation and software are improving DDA performances and the development of all-ion fragmentation in data-independent acquisition (Bruderer *et al.*, 2015) will certainly be viable avenues for future applications of HRMS in protein binding studies. In conclusion, MRM and DDA are powerful MS tools in proteomics, both of which have intrinsic advantages and disadvantages.

3.5.2 Putative NAPQI-cysteine sites in GST

In this study we characterized seven cysteine sites from four cytosolic human GSTs by NAPQI *in vitro*. NAPQI binding to human GSTA1, M1, and M2 had not been reported previously. Only binding to Cys48 and 102 in human GSTP1 was previously confirmed (Boerma *et al.*, 2011; Jenkins *et al.*, 2008). In one of their studies, Boerma *et al.* (Boerma *et al.*, 2011) also reported binding of clozapine metabolites to Cys48, as well as metabolized troglitazone to Cys15, 48, and 102 by *in vitro* incubation, tryptic digestion, affinity removal of background protein and LC-MS/MS analysis. In a follow-up study Boerma *et al.* (Boerma *et al.*, 2012) confirmed also diclofenac-related binding to Cys15 and 48. Using GSTP1 in a protein trapping study, binding of the

reactive diquinone methide of raloxifene was also observed to Cys48 (Yukinaga *et al.*, 2012). Here, we detected modified Cys48 and additional target sites of NAPQI in GSTP1 by using pepsin as an additional protease with different cleavage specificity than trypsin. We observed Cys15, 48, and 170 as NAPQI target sites in GSTP1. Boerma *et al.* (Boerma *et al.*, 2011) stated that alkylation of Cys48 lead to complete inhibition of GSTP1, based on the close proximity to GSH binding sites (Reinemer *et al.*, 1991; Vega *et al.*, 1998), as well as subsequent disruption of the active GSTP1-1 dimer (Jenkins *et al.*, 2008). Additionally, modification on Cys170 is believed to influence activity as well (Orton and Liebler, 2007), which is also explained by its importance in dimerization (Chang *et al.*, 2001). Furthermore, Cys15 is in direct proximity to Arg14 which is also involved in GSH binding (Ang *et al.*, 2009; Federici *et al.*, 2009; Ji *et al.*, 1997; Oakley *et al.*, 1997a, 1997b; Prade *et al.*, 1997). It is possible that alkylation of multiple sites combined leads to full enzymatic inhibition. Binding analysis of Cys102 presented several challenges in this study. The site was inaccessible via tryptic digestion and peptic peptides showed the lowest signal intensity of all screened sites. Sufficient recovery of Cys102 requires other proteases or potentially more limited proteolysis. Jenkins *et al.* (Jenkins *et al.*, 2008) used Asp-N to confirm binding of NAPQI to Cys102. However, it was reported that Cys102 binding occurred only with high molar ratios of NAPQI to protein. Alkylation reactions of Cys102, being more solvent exposed, was believed to play a minor role in enzymatic activity (Lemercier *et al.*, 2004).

Previous alkylation studies of GSTA1 focused on *in vivo* binding of bromobenzene metabolites to Cys112 in rat (Koen *et al.*, 2006). Detection of these low abundant peptide modifications was enabled by GSH affinity purification, tryptic digestion and capillary LC-MS. Human and rat GSTA1 share a high identity of 76%, including Cys112, which was found NAPQI-modified in our work. The relatively long distance between Cys112 and the active sites, Tyr9 and Arg45 (Balogh *et al.*, 2009),

was believed to ensure activity even after cysteine alkylation (Koen *et al.*, 2006). However, Cys112 is in range to Met94, Phe136, and Val139, which are associated to a hydrophobic pocket, important in dimerization (Vargo *et al.*, 2004). Alkylation of Cys112 could therefore compromise the formation of the GSTA1-1 dimer. However, further activity studies of NAPQI-modified GSTA1 are needed to investigate this.

In comparison to our findings of NAPQI-modified Cys78 in GSTM1, Nerland *et al.* (Nerland *et al.*, 2001) found rat GSTM1 (Cys87) modified *in vivo* by acrylonitrile using a combination of radiolabeling, affinity purification and LC-MS. Modification of Cys87 in rat was also observed by a recent study of Leeming *et al.* (Leeming *et al.*, 2017), using *in vitro* metabolism of APAP and LC-MS/MS. Rat GSTM1 is missing Cys78, though Cys87 is identical in human and rat. Hence, an interspecies comparison of cysteine reactivity is not trivial, since both sites, Cys78 and 87, might compete for binding reactions. However, Nerland *et al.* (Nerland *et al.*, 2001) hypothesized that the reactivity of Cys87 is based on possible interactions with His85, which is only found in rat. Missing His85 could explain a lower reactivity of Cys87 in human GSTM1 (and M2). Nevertheless, the extent of enzyme inhibition after modification needs further study. Nerland *et al.* (Nerland *et al.*, 2001) observed loss in rat GSTM1 activity only after IAM alkylation of Cys115 (identical in human GSTM1) and not Cys87. A possible explanation might be the close active site Tyr116, which is vital for substrate binding (Johnson *et al.*, 1993). Binding to Cys115 in human GSTM1 was not observed in our experiments. However, we could identify Cys115 and 174 as putative targets in human GSTM2. Koen *et al.* (Koen *et al.*, 2006) studied *in vivo* binding of 4-bromophenol in rat GSTM2 and confirmed adducts by radioactive labeling, tryptic digestion and LC-MS/MS. Based on cysteine mutant studies of human GSTM2, it has been stated that Cys115 might be involved in enzyme activity (Norrgård *et al.*, 2011), based on the mu class active site Tyr116 (Johnson *et al.*, 1993). The effect of binding to GSTM2 needs further research, especially with regards to distinguishing both

modified sites found in this study, Cys115 and 174. Furthermore, the difference of NAPQI binding properties of GSTM1 and GSTM2 are also crucial to investigate in future studies, since they share very high sequence homology.

In conclusion, we used *in vitro* incubations to identify adduct formation with NAPQI. Further research of *in vivo* and *in vitro* treated hepatocytes and liver fractions would complement our findings. The techniques shown here were designed to help study protein adduct formation and to guide subsequent research. Furthermore, a combination of our methods with targeted sample preparation and enrichment tools (*e.g.*, immunoaffinity) could be applied to analyze the NAPQI binding affinity of GST and various proteins of interest in the future. A similar strategy can be used to find NAPQI-protein targets in more complex samples and unknown protein targets, while pinpointing binding sites. The novel use of an isomeric labeling reagent with identical chromatographic elution of NAPQI-modified cysteine containing peptides is invaluable for confirming the identity of modified peptides.

3.6 Data availability

The datasets generated for this study are available on request to the corresponding author.

3.7 Author contributions

LS and TG conceived the research. CL and DW performed recombinant expression and purification of GST proteins. TG carried out further sample preparation, experiments, analyses, and data treatment. TG and LS wrote the paper. All authors made substantial, direct and intellectual contribution to the work, and revised the manuscript.

3.8 Funding

This work was funded by the Natural Sciences and Engineering Research Council of Canada (NSERC, Discovery grant nos. 355933-2011 & RGPIN 2016-06034). TG acknowledges the *Fondation Hydro-Québec*, Université du Québec à Montréal, FRQNT (*Fonds de recherche du Québec – Nature et technologies*), and the *Groupe de Recherche Axé sur la Structure des Protéines* (GRASP), funded by the FRQS (*Fonds de recherche du Québec – Santé*), for scholarships.

3.9 Supplementary material

The Supplementary Material for this article can be found online at: <https://www.frontiersin.org/articles/10.3389/fchem.2019.00558/full#supplementary-material>

Additional information on protein detection methods, MRM transitions and identified carbamidomethylated GST peptides; figures of peptide chromatograms, MS and MS/MS spectra, and peptide distribution in concatenated fractions.

CHAPTER IV

IDENTIFICATION OF 4-HYDROXYNONENAL-MODIFIED PROTEINS IN HUMAN OSTEOARTHRITIC CHONDROCYTES

Timon Geib, Cristiana Iacob, Rihab Jribi, Julio Fernandes, Mohamed Benderdour and
Lekha Sleno

Submitted for publication in **Journal of Proteomics**, April 2020. Supporting information partly
included in Appendix B.

In this chapter, the relation of osteoarthritis and the reactive lipid peroxidation product, 4-hydroxynonenal, was studied in human chondrocytes. Specific western blot analysis was combined with an untargeted bottom-up proteomics liquid chromatography-tandem mass spectrometry method to analyze 4-hydroxynonenal-protein adducts. These assays were successfully used to analyze modified proteins in chondrocytes from discarded knee cartilage samples of osteoarthritis patients and non-disease subjects (treated at the Hôpital du Sacré-Coeur de Montréal). Finally, several protein 4-hydroxynonenal-modifications were detected unique to osteoarthritis, including the exact site of modification. Modified proteins included DNA-associated proteins, the histones, highly important for nucleosome and chromatin formation, which might play an important role in osteoarthritis pathogenesis.

Timon Geib, Cristiana Iacob, Rihab Jribi, Julio Fernandes, Mohamed Benderdour and Lekha Sleno are co-authors of this article. Timon Geib and Cristiana Iacob contributed equally to this work. Both conducted the literature survey, prepared experimental protocols, conducted the experiments, processed the data and prepared the original manuscript. Rihab Jribi performed additional sample preparation and protein extraction. Julio Fernandes provided human cartilage samples for the study (from patients treated at the Hôpital du Sacré-Coeur de Montréal). Mohamed Benderdour and Lekha Sleno supported and supervised the project, verified data analysis and interpretation of the results, revised and finalized the manuscript.

4.1 Abstract

The α,β -unsaturated aldehyde 4-hydroxynonenal (HNE) is formed through lipid peroxidation during oxidative stress. As a highly reactive electrophile, it is able to form adducts with various biomolecules, including proteins. These protein modifications could modulate many signaling pathways, as well as cell differentiation and proliferation, and thus could be highly important in the context of the extracellular matrix and degradation of articular cartilage. This study specifically investigated the role of HNE as a bioactive molecule in chondrocytes of OA patients. Chondrocyte extracts of OA and non-OA patients were analyzed for HNE binding using Western blot and bottom-up LC-MS/MS analyses. HNE-modified histones, H2A and H2B, and histone deacetylase were identified using anti-HNE antibodies. Furthermore, peptide sequencing and database searching revealed 95 distinct HNE-modified proteins and their exact modification sites, with 88 protein adducts being unique to OA chondrocytes. HNE-proteins of specific interest included histone H2A, H2B and H4, collagen alpha-3(VI) chain, eukaryotic initiation factor 4A-I, and nucleolar RNA

helicase 2. These six HNE-proteins were further validated by comparing with HNE-modified standard peptides to confirm their MS/MS spectra.

4.2 Introduction

Oxidative stress modulates various signaling cascades responsible for crucial cellular functions such as apoptosis, cellular proliferation and inflammatory responses. Free radicals resulting from an imbalance between antioxidant and pro-oxidant systems induce lipid peroxidation (LPO). This mechanism can be described as a process under which free radicals attack unsaturated lipids in the cellular membrane, producing a wide variety of oxidation products including 4-hydroxynonenal (HNE) (Esterbauer *et al.*, 1991; Schaur, 2003). HNE is considered the most toxic α,β -unsaturated aldehyde formed from LPO of both ω -3 and ω -6 polyunsaturated fatty acids. Its highly reactive nature allows it to covalently bind to a variety of biomolecules, such as proteins, lipids and nucleic acids (Poli *et al.*, 2008; Schaur, 2003). HNE binds to specific nucleophilic amino acids in proteins through Michael-type additions. Precisely, HNE adduction of proteins can occur on the imidazole ring nitrogen of histidines (His), the sulfhydryl group of cysteines (Cys) and the ϵ -amino group of lysines (Lys). Reversible Schiff base reactions can also occur with lysines, the guanidine nitrogen of arginines and N-terminal amines, although these modifications are much less prevalent and stable (Bruenner *et al.*, 1995; Uchida and Stadtman, 1992).

HNE naturally induces diverse biological effects in the cell through its electrophilic nature by modulating various signaling pathways, thereby causing apoptosis as well as alterations in cell differentiation and proliferation. Studies have shown that antioxidant agents, such as *N*-acetyl-cysteine or nuclear GSTA4-4, can

suppress HNE production, and inhibit apoptosis in cell lines (Cheng *et al.*, 2001; Ruef *et al.*, 2001; Vaillancourt *et al.*, 2008). Additionally, HNE can inhibit the inducible form of nitric oxide synthase by modulating the nuclear factor-kappa B signaling pathway in chondrocytes (Vaillancourt *et al.*, 2007). Furthermore, another study has shown that HNE induces a dual effect on platelet-derived growth factor receptor beta (PDGFR- β) (Lee *et al.*, 2010), which plays a role in the smooth muscle cell (SMC) migration and proliferation. A short incubation of SMCs with HNE activates the PDGFR- β pathway, but a long incubation triggers a desensitization of this receptor to its agonist. However, in a few instances, activation of enzymes may occur. In a recent study, we observed that there are significantly more HNE-protein adducts in osteoarthritic (OA) synovial fluid compared to normal subjects (Morquette *et al.*, 2006). HNE binds to the matrix metalloproteinase 13 (MMP-13) *in vitro* (Morquette *et al.*, 2006). It also induces a PTM of type II collagen (COL2), both of which resulting in the degradation of the articular cartilage in OA.

To gain additional insight into the potential role of HNE in osteoarthrosis, the role that HNE plays as a bioactive molecule in chondrocytes by modifying specific proteins was investigated. This PTM could have a role in the degradation of human cartilage by causing an imbalance in the chondrocytes' usual epigenetic modifications. HNE-protein adducts have been detected in OA and non-OA (from healthy controls) chondrocytes using western blotting and bottom-up proteomics. For the latter, cell extracts were proteolytically digested prior to LC-MS/MS analysis on a quadrupole-time-of-flight platform. High sequence coverage was achieved by data-dependent acquisition (Mann *et al.*, 2001) enabling the detection of a high amount of HNE-modified peptides.

4.3 Materials and methods

4.3.1 Chemicals and materials

Trypsin (TPCK-treated, bovine pancreas), pepsin (porcine gastric mucosa), collagenase (type IV, from *Clostridium histolyticum*), pronase (from *Streptomyces griseus*), dithiothreitol (DTT), acetic acid, ACN, ammonium bicarbonate, ammonium hydroxide, formic acid, iodoacetamide (IAM), methanol and other chemicals were from Sigma-Aldrich (St. Louis, MO). Recombinant histone H2AX was purchased from Abcam (Cambridge, MA). Fetal bovine serum (FBS), Tris-buffered saline (TBS), penicillin and streptomycin were obtained from Wisent Bioproducts (Saint-Jean-Baptiste, QC, Canada). HNE was from Cayman Chemical (Ann Arbor, MI). Standard peptides (>82% purity) were ordered from Biomatik (Cambridge, ON, Canada). Ultrapure water was from a Millipore Synergy UV (Billerica, MA).

4.3.2 Cartilage samples

Human OA cartilage was obtained from thirteen advanced OA patients and two healthy controls (64 ±6 years) having undergone total knee arthroplasty. Informed consent was acquired from patients and OA diagnosis was given according to American College of Rheumatology criteria (Altman *et al.*, 1986). The Clinical Research Ethics committee of Montréal's Hôpital du Sacré-Coeur approved the study protocol as well as the use of human articular tissues. A brief overview of cartilage chondrocyte samples can be found in Table S1.

4.3.3 Chondrocyte culture conditions

Cartilage was dissected from bone under aseptic conditions within 24 h of surgery, diced and rinsed with phosphate buffered saline (PBS) supplemented with 500 U/mL penicillin and 500 µg/mL streptomycin. OA chondrocytes were extracted from cartilage explants by enzymatic digestion with 1 mg/mL pronase (1 h, 37°C), and 2 mg/mL collagenase (4 h, 37°C), in DMEM (Wisent Bioproducts) supplemented with 10% inactivated FBS, 100 U/mL penicillin and 100 µg/mL streptomycin. Isolated chondrocytes were seeded at high density in DMEM with 1% antibiotics and 10% FBS. The cells were cultured at 37°C in a humidified atmosphere (5% carbon dioxide/95% air) until they reached confluence. Only first-passaged cells were used.

4.3.4 Protein extraction and HNE treatment

Samples consisted of isolated nuclear and cytosolic protein extracts, as well as whole cell protein lysates. Confluent chondrocytes were detached by trypsinization. Cell pellets were washed and resuspended in PBS. Cellular protein fractionation was achieved using a commercial nuclear extraction kit (Cayman Chemical), where isolated nuclei and cytoplasm were obtained. Nuclear chondrocyte extracts contained <0.5% NP-40, 2% HEPES, 1% NaF, 1% EDTA and 0.2% Na₂MoO₄. Cytosolic extracts constituted of 0.5% NP-40, 2.6% HEPES, 0.5% EDTA, 5.3% NaCl, 0.5% EDTA, 0.5% MgCl₂ and 15.8% glycerol. The nuclear pellet was resuspended in PBS, and the proteins were extracted using three repeated cycles of snap freezing in liquid N₂ and thawing at 37°C, followed by brief sonication and centrifugation. Similarly, whole cell protein lysates were extracted from resuspended chondrocytes using three cycles of snap freezing/thawing, as above. Total extracts contained <0.5% NP-40, 2.5% HEPES, 5% NaCl, 0.5% MgCl₂, 0.5% EDTA and 15% glycerol. Cell protein lysates, recombinant histone H2AX and commercial standard peptides were all incubated in

PBS for 2h at 37°C with HNE at different concentrations. All samples were subsequently stored at -80°C.

4.3.5 Protein quantitation and western blot analysis

Protein quantitation and western blot details can be found in the supporting information.

4.3.6 Immunoprecipitation and HDAC activity

Immunoprecipitation details of HNE-histone deacetylase 2 (HDAC2) and HNE-histone adducts as well as HDAC activity assay method can be found in the supporting information.

4.3.7 Protein digestion and peptide standard sample preparation

All extracts (~7–80 µg protein) and recombinant histone H2AX (50 µg) were diluted in 400 µL ammonium bicarbonate buffer (ABC; 100 mM, pH 8.5). Reductive alkylation was performed at 1 mM DTT (20 min, 37°C) and 2.5 mM IAM (30 min, 37°C; in dark). Proteins were then incubated with 2.5–10 µg trypsin (4 h, 37°C and 500 rpm). One set of total cell extracts (see Table S1) was also digested using 2.5–10 µg pepsin after adding 400 µL 2% formic acid in 20% methanol (4 h, 37°C). Tryptic digests were diluted with 500 µL 1% formic acid in 10% methanol and subjected to SPE on OASIS MCX cartridges (1 cc, 30 mg, Waters, Milford, MA). Pepsin digests were diluted with 350 µL ABC (100 mM, pH 8.5) followed by SPE on OASIS HLB

cartridges. Dried extracts were reconstituted in 100 μ L 10% ACN prior to LC-MS/MS analysis.

HNE-treated standard peptides (10 μ g) were diluted in 500 μ L loading buffer (MCX or HLB, for tryptic and peptic peptides, respectively) and subjected to SPE as above.

4.3.8 LC-MS/MS analysis and data processing

Samples were injected (20 μ L) onto an Aeris PEPTIDE XB-C18 100 \times 2.1 mm, 1.7 μ m column, with a SecurityGuard ULTRA C18-peptide guard column (Phenomenex, Torrance, CA) using a Nexera UHPLC system (Shimadzu, Columbia, MD) with water (A) and ACN (B), both containing 0.1% formic acid, as mobile phase at a flow rate of 0.3 mL/min (40°C). The gradient started at 5% B, was held for 2.5 min, and was linearly increased to 30% B within 37.5 min, to 50% B within 10 min, then to 85% B within 5 min and held there for 3 min (total gradient 58 min), and re-equilibrated for 8 min between injections.

High-resolution TOF-MS and MS/MS spectra were collected on a hybrid quadrupole-time-of-flight mass spectrometer, TripleTOF 5600 (Sciex, Concord, ON), equipped with a DuoSpray ion source in positive mode with 5 kV source voltage, 500°C source temperature, and 50 psi GS1/GS2 gas flows, and declustering potential of 80 V. The instrument performed a survey TOF-MS acquisition from m/z 120–1250 (250 ms), followed by MS/MS on the 15 most intense ions from m/z 80–1500 using data-dependent acquisition with dynamic background subtraction. MS/MS acquisition (50 ms each) used a collision energy of 30 \pm 10 V. HNE-modified standard peptides were analyzed via targeted product ion scans with TOF-MS (m/z 170–1000, 500 ms)

and MS/MS acquisition (m/z 50–1500, 500 ms) with collision energy set at 28 V. The total cycle time in each experiment was 1.05 s.

LC-MS/MS files were searched against the human UniProtKB/Swiss-Prot database (release date: 07/18/2018, including common protein contaminations) by ProteinPilot 5.0 (Sciex). To identify potential HNE-adducts (from Michael addition), the protein search algorithm was changed to consider a probability of 50% for HNE modification (addition of $C_9H_{16}O_2$) on histidine, cysteine and lysine. The search was performed at a MS tolerance of 0.05 u on precursor ions and 0.1 u on fragment ions. Proteins and peptides were identified with a local 1% false discovery rate (FDR) (Tang *et al.*, 2008) using a target-decoy database search algorithm. The online tool WebGestalt (Zhang *et al.*, 2005) was used for enrichment analysis using right-sided hypergeometric testing and Benjamini-Hochberg (BH) correction. Manual data verification and visualization was done with PeakView 2.2 and MasterView 1.1 (Sciex).

4.4 Results

Our complete study cohort consisted of chondrocyte samples from 13 OA patients and two healthy (non-OA) subjects. Different cell extraction techniques were used to yield nuclear ($n = 6$), cytosolic ($n = 2$) and total cell ($n = 5$) extracts of OA patient samples to increase coverage of HNE-proteins from different cell compartments. Extracted chondrocytes were subjected to western blot and LC-MS/MS analysis, focusing on HNE adduct formation. Identified HNE-proteins from OA samples were compared to those found in total cell extracts of healthy controls ($n = 2$).

4.4.1 HNE induces modification of nuclear proteins

HNE's ability to form adducts with nuclear proteins was verified in isolated human OA chondrocytes. In HNE untreated cells, the corresponding profile of the HNE-protein adducts that was generated at the basal level following incubation of OA chondrocytes with HNE is shown in Figure 4.1A. As can be seen, the intensity of immunoreactive bands increased in the presence of 10 μ M HNE, and most had a molecular weight less than 60 kDa.

We then tested the hypothesis that among nuclear proteins, histones are modified by HNE. These proteins provide structural support to DNA and their PTMs play a key role in DNA replication and transcription. As illustrated in Figure 4.1B, the immunoprecipitation assay indicated that histone H2A and H2B were targeted by HNE binding and that the level of HNE-histone H2A and HNE-histone H2B adducts is higher in HNE-treated isolated OA chondrocytes.

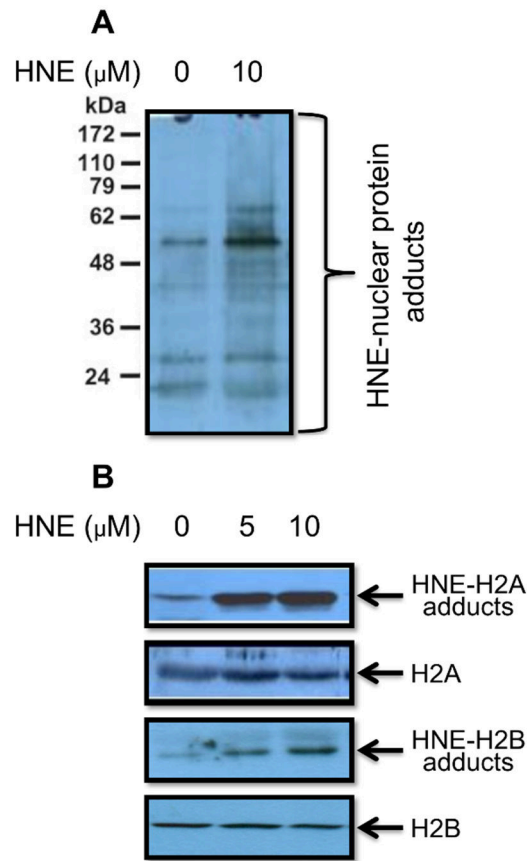


Figure 4.1 Immunoreactive HNE-protein adduct profile of OA chondrocytes without and with 10 μM HNE treatment (A). Immunoprecipitation of HNE-H2A and HNE-H2B adducts and western blot analysis of total histone H2A and H2B in nuclear extracts from human OA chondrocytes treated with HNE (0, 5 and 10 μM) (B).

4.4.2 HNE inhibits HDAC activity by HNE-HDAC adduct formation

In a follow-up experiment, the effect of HNE on HDAC activity in OA human chondrocytes was considered. HDACs are key enzymes involved in histone deacetylation. As shown in Figure 4.2A, the addition of HNE significantly reduced total HDAC activity in a dose-dependent manner. At 10 μM , HNE suppressed total HDAC activity by 80%.

To confirm the formation of HNE-HDAC2 adducts, OA human chondrocytes were incubated with increasing doses of HNE for 24 h and nuclear protein extracts were immunoprecipitated with mouse anti-HDAC2 antibody and subjected to western blotting. Using an anti-HNE antibody, our results revealed a signal corresponding to HNE-HDAC2 conjugates, the intensity of which increased with HNE concentration (Figure 4.2B). Nuclear extracts from non-treated OA chondrocytes showed a very low signal for the modified protein.

4.4.3 Effect of HNE on histone acetylation status

The influence of HNE on histone acetylation in HNE-treated human OA chondrocytes was verified and results are shown in Figure 4.2C and D. Levels of acetylated histone H2A (K5) and histone H2B (K20) were higher as HNE concentration increased, up to 10 μ M, and then decreased at 20 μ M HNE. In contrast, the levels of total histone H2A and H2B were relatively stable as HNE increased.

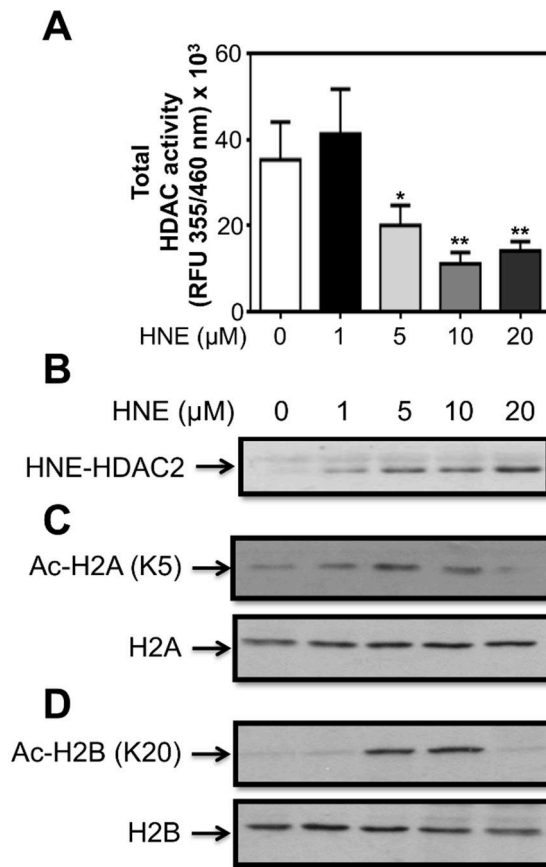


Figure 4.2 Total HDAC activity in HNE-treated OA human chondrocytes at different concentrations of HNE (0–20 μ M; *, p -value ≤ 0.05 ; **, p -value ≤ 0.01) (A). Immunoprecipitation followed by western blot analysis of HNE-HDAC2 adduct formation in nuclear protein extracts, monitored at different doses of HNE (0–20 μ M) for 24 h (B). Histones H2A and H2B acetylation levels in HNE-treated human OA chondrocytes. Levels of acetylated histone H2A (K5) (C) and H2B (K20) (D) were analyzed in nuclear extract of human OA chondrocytes by western blot analysis at different levels of HNE (0–20 μ M) treatment.

4.4.4 LC-MS/MS analysis of HNE-modified proteins

A minimum of 1,188 peptides and 309 proteins were identified in each sample analyzed (see data for individual samples in Table S1), of which a total of 252 HNE-modified peptides (see Table S2) from 95 distinct proteins, modified at 198 sites (see Table S3) were confirmed in OA samples using the following criteria (Golizeh *et al.*, 2016): 1) precursor mass error within 10 ppm (MS) and spectral confidence >95% (MS/MS), 2) presence of at least one diagnostic fragment ion (m/z 139.1118 or 266.1863, see Figure 4.3) (Roe *et al.*, 2007), 3) removal of uncommon PTMs and 4) located in associated extracted cell components (nuclear, cytosolic or total extracts). In total, 88 distinct HNE-modified proteins were unique to OA disease samples (all extracts combined). In addition, most HNE-proteins were identified in total chondrocyte extracts. Of the total 91 distinct HNE-modified proteins (191 modified sites) found in total cell OA chondrocytes ($n = 5$): 35 proteins (68 sites) were shared between at least two extracts. Of 88 proteins unique to OA samples, 81 (and 185 sites) were identified in total OA chondrocyte extracts ($n = 5$), of which 31 proteins (63 sites) were common in at least two samples.

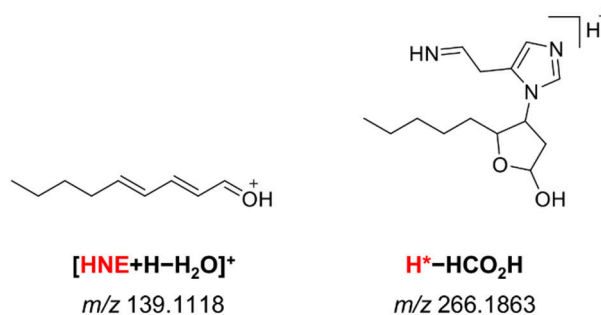


Figure 4.3 Proposed diagnostic fragment ion structures at m/z 139.1118 and 266.1863, resulting from HNE and the HNE-histidine adduct (H*), respectively.

4.4.5 Enrichment analysis of proteins related to OA disease and HNE binding

We investigated further the 81 distinct HNE-modified proteins from total chondrocyte extracts ($n = 5$) unique to OA disease using gene enrichment analysis (right-sided hypergeometric), by submitting the list to WebGestalt for analyzed of over-representation in the human genome (reference set: genome protein-coding) with BH correction (Benjamini and Hochberg, 1995) for multiple comparisons (significance level: $FDR \leq 0.05$). In total, 49 gene ontology (GO) terms and six pathways (from WikiPathways) were over-represented, based on identified HNE-modified proteins unique to OA disease. An overview of enriched GO terms and pathways can be found in Tables S4A and S5A, respectively. However, we also observed a bias (over-representation) of genes in our list of all identified proteins, HNE-modified or not. We saw multiple GO terms and pathways enriched in our data in either OA patients or healthy controls (data not shown). Thus, to compensate for this, the enrichment of HNE-protein binding unique to OA disease was also analyzed against a custom reference set of total identified proteins in total OA chondrocyte extracts. In total, 12 GO terms (Table S4B) and one pathway (Table S5B) were found to be over-represented. A visual representation of these statistically-significant GO term enrichment ratios can be found in Figure 4.4.

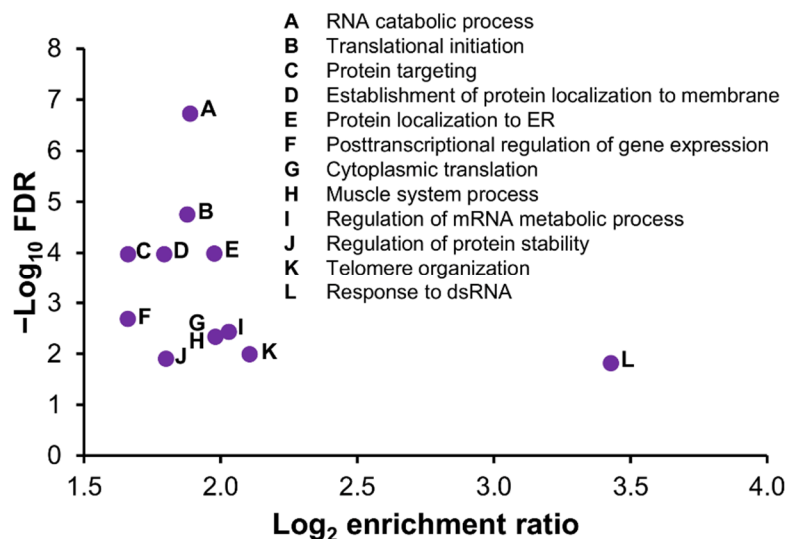


Figure 4.4 Scatter plot of significantly enriched GO terms (FDR ≤ 0.05 , against reference of all proteins identified in all samples) of HNE-modified proteins unique to OA-related samples (total chondrocyte extracts).

4.4.6 HNE-peptide adduct confirmation with *in vitro* modified peptides

Several HNE-modified histones (H2A, H2B and H4) were found after data processing and filtering (see Table S3). Of these histones, H2A and H2B were identified in two out of five total chondrocyte extracts, and H4 in one of the five extracts. Modified peptides, H*AVSEGTK and AKH*AVSEGTKA (His110 in histone H2B), QVH*PDTGISSK (His50 in histone H2B), H*LQLAIR (His83 in histone H2A), and DAVTYTEH*AK (His76 in histone H4), were subsequently confirmed by comparison of MS and MS/MS spectra to HNE-modified commercially-available standard peptides (see Figures S1–5). Probing HNE binding to recombinant histone H2AX confirmed the identification of modified H*LQLAIR (His83) peptide from cell extracts. In addition, recombinant H2AX was also found to be modified at Lys96 and 119.

Moreover, one HNE-modified collagen protein, COL6A3, was confidently detected. HNE-modified COL6A3, modified at Lys2027, was confirmed via MS and MS/MS comparison to standard peptide LNLDDL DYELAEQLDNIAEK* (see Figure S6).

Standard peptides were also obtained for the protein nucleolar RNA helicase 2 (DDX21) and eukaryotic translation initiation factor 4A1 (EIF4A1). Fragmentation spectra of analyzed patient samples matched well with standard GAVEALAAALAH*ISGATSVDQR for DDX21 (at His617, see Figure S7) and LQMEAPH*IIVGTPGR for EIF4A1 (at His153, see Figure S8).

4.5 Discussion

Chondrogenic differentiation and function are regulated by intricate epigenetic modifications, affecting the expression of specific genes. Histones are targeted by multiple PTMs, including acetylation, methylation, and nitrosylation (Sen, 2015). A specific goal of this study was to verify HNE binding to nuclear proteins, especially in the context of OA. Through its role in epigenetic modification, HNE could alter chondrocyte-related gene expression.

4.5.1 HNE-nuclear protein adducts

Several nuclear proteins were modified by HNE, including histones and HDAC2. HNE binding reduced HDAC2 activity and consequently enhanced the acetylation levels of histone H2A and H2B. Reactive species can influence epigenetic

modifications, including methylation/acetylation, and lead to changes in gene expression (Moldogazieva *et al.*, 2018). For example, nitric oxide is involved in epigenetic modifications through nitrosylation (Illi *et al.*, 2009). HDAC nitrosylation is a key mechanism of epigenetic regulation involved in gene expression. Nott *et al.* demonstrated that neurotrophic factors promote chromatin remodeling and the activation of genes associated with neuronal development through HDAC2 nitrosylation (Nott *et al.*, 2013). To the extent of our knowledge, the role of HNE in chromatin remodeling has yet to be investigated. In Raw264.7 macrophages, Galligan *et al.* reported that histones are HNE targets, without investigating the impact on gene expression (Galligan *et al.*, 2014).

From our LC-MS/MS results, 95 distinct HNE-modified proteins were identified in our analyses, with 88 HNE-proteins being uniquely found in OA samples. All protein adducts were relevant *in vivo* and did not occur as a result of post-surgery cell treatment. These proteins include three histone variants (H2A, H2B and H4). Codreanu *et al.* had found several histone H2As and H2Bs to be targeted by HNE (Codreanu *et al.*, 2014). We could identify five histone HNE-peptides (encompassing four unique sites). The four modified histidine residues, His50, 76, 83 and 110, are located in the center and C-terminal end of the protein sequences. These parts are known to form the DNA-binding helix-turn-helix-turn-helix motif (Brennan and Matthews, 1989). Alkylation of residues in this motif would likely alter DNA-binding properties and the ability to form nucleosomes and thus gene expression (Barter *et al.*, 2012; Drake *et al.*, 2004). Sequence recovery of the N-terminal region was challenging due to the high amounts of lysine and arginine, resulting in low coverage after tryptic digestion. Hence, analysis of residues near the N-terminus was not fully possible. Even parallel pepsin digestion with low cleavage specificity yielded a limited increase in total sequence coverage for these proteins (see Table 4.1). The acetylation (and methylation) of histone N-terminal tails influences the structure of histones which, in

effect, allows for modulation and regulation of their function (Morales and Richard-Foy, 2000). Formation of HNE-histone adducts at N-terminal tails might obstruct acetylation and remains interesting for future studies, especially since this could act in combination with changes in HDAC activity. We were not able to recover substantial amounts of HDAC from samples to study HNE-HDAC binding via LC-MS/MS. HNE binding in nuclear cells was however confirmed through specific HDAC2 activity testing and western blotting (see Figure 4.2A,B), as well as HNE-dependent effects on histone acetylation states (see Figure 4.2C,D).

Table 4.1 Overview of histones (H1–4), histone deacetylase (HDAC) and collagen (COL) sequence coverage from LC-MS/MS analyses of OA disease and healthy control samples

Sample	Digestion	Best sequence coverage [%]						
		H1	H2A	H2B	H3	H4	HDAC	COL
Disease nuclear ($n = 6$)	Trypsin	24	53	40	43	64	0	50
Disease cytosolic ($n = 2$)	Trypsin	0	43	9	0	10	0	11
Disease total ($n = 5$)	Trypsin	29	64	42	38	53	20	54
	Pepsin	21	60	68	37	18	4	4
Recombinant H2AX	Trypsin	-	55	-	-	-	-	-
	Pepsin	-	79	-	-	-	-	-
Healthy ($n = 2$)	Trypsin	0	52	14	18	20	0	17
	Pepsin	15	43	9	24	9	2	2

A connection of HNE-histone formation and the development of several diseases has been reported. Alzolibani *et al.* confirmed HNE-histone H2A in patients with systemic lupus erythematosus, using autoantibodies against HNE-modified

histone H2A. HNE binding to histone H2A was postulated to initiate or promote disease (Alzolibani *et al.*, 2013). Drake *et al.* examined the connection of HNE with Alzheimer's disease, suggesting HNE-histone adducts affected protein conformation (Drake *et al.*, 2004). These adducts affected the ability to bind DNA, and thus to form nucleosomes. The formation of HNE-histones alter hydrophobicity and charge state, having a direct effect on electrostatic interactions with DNA (Nightingale *et al.*, 1998). HNE exposure was correlated to phosphorylation of histone H2AX in mice. Chaudhary *et al.* postulated that DNA double strand breaks were introduced by phosphorylation as well as comet tail formation (Chaudhary *et al.*, 2013).

4.5.2 Other HNE-modified proteins

HNE-alkylated proteins found here in OA chondrocytes overlapped with previous global proteomic studies (Codreanu *et al.*, 2009, 2014). Codreanu *et al.* investigated HNE-protein binding in HNE-treated human RKO cells by biotinylation and subsequent streptavidin capture, gel electrophoresis and trypsin digestion, and LC-MS/MS (Codreanu *et al.*, 2009). A small overlap can be seen to a bottom-up approach using click chemistry for enrichment, investigating binding of an alkyne-containing HNE analog to RKO proteins (Yang *et al.*, 2015). In OA samples, glyceraldehyde-3-phosphate dehydrogenase (GAPDH) was modified by HNE at several sites. Binding of HNE to this protein was also previously studied *in vitro* (Ishii *et al.*, 2003; Uchida and Stadtman, 1993). HNE adduction to rabbit GAPDH was also detected at many sites, including three analogous residues to those found in our human study (Cys245, His165 and 328) using trypsin and V8 protease digestion with LC-MS/MS. While studying hydroxyurea exposure to CD1 mice, Schlisser *et al.* observed HNE-protein adducts in embryos (Schlisser *et al.*, 2010). Eight HNE-modified proteins were identified, including mouse GAPDH. It was shown that HNE binding significantly decreased

GAPDH activity. Furthermore, HSP90 α and HSP90 β were potentially modified at multiple sites (note: human HSP90 α and β are 86% identical). Carbone *et al.* studied chronic alcohol-induced oxidative stress and observed HNE modified cytosolic rat HSP72 (Carbone *et al.*, 2004), correlating with decreased affinities for ATP. Rat HSP90 has also been found to be HNE-modified at Cys572 (Carbone *et al.*, 2005). HNE-HSP90 α was studied in RKO colorectal cancer cells and His450 and 490 were confirmed as modification sites (Connor *et al.*, 2011). Unfortunately, we could not recover the sequence of HSP90 α having His450 and 490. HSP90 β was found modified at several sites, namely His171, 442, 458, 625 and 632. We could confirm binding to all of these sites, except His442. Furthermore, human HSP90 β was identified as a HNE target by investigating HNE-treated human THP-1 monocytes via a gel-based approach, anti-HNE immunostaining and targeted MS/MS (Chavez *et al.*, 2010). Over 30 HNE-proteins were identified, including some site-specific determinations. We could confirm six of these proteins and two specific modification sites, including 14-3-3 protein beta/alpha, actin (cytoplasmic 1, at His40), tubulin alpha-1B chain and vimentin (at Cys328). The authors stated that HNE-modified proteins associated with the cytoskeleton are important for maintaining cell shape and intracellular transport (Papakonstanti and Stournaras, 2008). It was also observed that HNE obstructs assembly of tubulins, by studying exposure of HNE to rat brain cells, causing impaired microtubule formation (Kokubo *et al.*, 2008).

Gene enrichment analysis of the HNE-modified proteins in OA samples revealed several statistically-significant GO terms and pathways (see Tables S4 and S5). Among these proteins, translational initiation factors and ribosomal proteins were enriched. These proteins comprised at least five elongation and translation factors (including EIF4A1), and 17 ribosomal proteins. These vital proteins have previously been shown to modified by reactive metabolites, leading to functional inhibition. Argüelles *et al.* observed that HNE and malondialdehyde modified elongation factor 2

(EEF2) in a rat model (Argüelles *et al.*, 2009). We observed HNE binding to Cys131 and potentially Lys333 in human EEF2. Reed *et al.* found HNE-modified elongation factor Tu and translation initiation factor alpha in patient brains with mild cognitive impairment (Reed *et al.*, 2008). Several ribosomal protein subunits (RPSA1A, RPS12, RPL3, RPL4A and RPL17B) were also previously found to be HNE-modified in yeast (Roe *et al.*, 2007), partly overlapping with our findings in human. The authors applied a pattern analysis of HNE adduct formation, compared to a non-treated yeast lysate control. It was postulated that HNE-modified sequences had a higher number of basic residues (Lys and Arg) positioned within four residues of the HNE-histidine. Increased removal of the histidine imidazole hydrogen, from a highly basic environment, was believed to lower the pK_a and thus increase nucleophilic attack on HNE. These effects might partly explain the prominence of highly basic ribosomal proteins as being modified by HNE (Roe *et al.*, 2007). This circumstance could apply to histones as well.

4.5.3 Target proteins linked to OA pathogenesis

The effect of HNE on the turnover of COL2 (found as an HNE target in this work) and MMP-13 expression in the context of OA was previously investigated (Morquette *et al.*, 2006). During cartilage degeneration, HNE is produced in OA synovial cells. *In vitro* HNE binding to MMP-13 activated the enzyme, and HNE modification of COL2 accelerated its degradation by MMP-13. Increased levels of HNE in OA cartilage and the ability of HNE to induce transcriptional modifications and PTMs of COL2 and MMP-13 suggest HNE is involved in OA (Morquette *et al.*, 2006). In addition, *in vitro* formation of HNE-COL2 resulted in multiple phenotypic abnormalities of OA chondrocytes. However, the dipeptide carnosine, an efficient HNE-trapping agent, was able to counteract these effects (El-Bikai *et al.*, 2010). HNE was shown to accelerate COL2 degradation and MMP-13 activation, as well as

inhibiting the expression of both. HNE-protein adducts increased in OA synovial fluid and chondrocyte samples. Induction of MMP-13 correlated with COL2 HNE modification, and also induced intercellular adhesion molecule 1 and integrin alpha1beta1 (El-Bikai *et al.*, 2010). Since the activation of MMP-13 was believed via HNE modification, the modified sites of MMP-13 were determined by LC-MS/MS in a subsequent study (Golizeh *et al.* 2014) (Golizeh *et al.*, 2014). Furthermore, an *in vivo* dog study (Shi *et al.* 2014) showed decreased OA severity and HNE-protein adduct formation using carnosine as a HNE-trapping agent (Shi *et al.*, 2014). In a chick embryo study, Fernandez *et al.* suggested that type I and II collagen gene regulation during chondrocyte differentiation and dedifferentiation could occur through DNA methylation (Fernandez *et al.*, 1985). In the current study, translation factors, such as EIF4A1, were found to be HNE targets. The *EIF4A1* gene was identified among 26 genes as differentially expressed in OA patients by Mahr *et al.* (Mahr *et al.*, 2006). Tsolis *et al.* observed quantitative changes between OA patients and controls at the protein level, including EIF4A1 and several other proteins and translation factors (Tsolis *et al.*, 2015).

Histone modification has been linked to OA disease progression. Methylation (K4) in histone H3 contributed to IL-1 β -induction of iNOS and COX-2 expression (El Mansouri *et al.*, 2011). Further results indicated that histone H3 demethylation (K9) contributed to IL-1 β -induced microsomal prostaglandin E synthase 1 expression (El Mansouri *et al.*, 2014). Here, an increase in acetylation of histone H2A and H2B was observed, possibly in conjunction with HNE-HDAC2 binding.

4.6 Conclusion

HNE has been observed to form adducts to multiple proteins in OA chondrocytes. Using straightforward protein extraction, western blot and bottom-up proteomics LC-MS/MS, we could pinpoint various modification sites of these proteins, including histones and collagen. Through enrichment analysis, we could also identify several over-represented protein targets, which included multiple translation factors and ribosomal proteins. This underlined an important role of HNE in cartilage OA chondrocytes, as it is largely known that protein-bound HNE alters conformation and function of proteins (Hellberg *et al.*, 2010; Reed *et al.*, 2009; Siems *et al.*, 1989; Subramaniam *et al.*, 1997). The present study allowed the detection of HNE-nuclear protein adducts, but also helped us better understand the participation of this aldehyde in gene expression through epigenetic modification during physiological and pathophysiological processes, such as cell differentiation, cell metabolism, inflammation, apoptosis. In particular, insights into the molecular mechanisms underline the effect of HNE-modified histones and HDACs in the modulation of epigenetic modifications involved in chondrocytes differentiation and metabolism under oxidative stress. Research progress on how HNE modulates chondrocyte-related gene expressions, as well as the identification of potential HNE-targeted histones and HDACs, may confirm the physiological and pathophysiological role of HNE in the modulation of cell differentiation and function under adaptive response to oxidative stress. These results will undoubtedly open new avenues to elucidate the role of specific enzyme-related HNE detoxification pathways, involving GSTA4-4 for instance, in the control of HNE-induced epigenetic modifications.

4.7 Acknowledgements

This work was funded by the *Fonds de Recherche en Orthopédie*, Hôpital du Sacré-Cœur de Montréal. We would like to acknowledge a scholarship for TG from the *Fonds de Recherche du Québec – Nature et Technologies*.

CHAPTER V

INVESTIGATION OF CLOZAPINE AND OLANZAPINE REACTIVE METABOLITE FORMATION AND PROTEIN BINDING BY LIQUID CHROMATOGRAPHY-TANDEM MASS SPECTROMETRY

Timon Geib, Madhuranayaki Thulasingham, Jesper Z. Haeggström and Lekha Sleno

Published in **Chemical Research in Toxicology** 2020. Supporting information partly included in

Appendix C and online at <https://pubs.acs.org/doi/10.1021/acs.chemrestox.0c00191>.

In this chapter, reactive metabolite formation of the atypical antipsychotics clozapine and olanzapine was studied using *in vitro* incubations and glutathione trapping. In addition, covalent adducts formed between these reactive metabolites and key cellular defense enzymes against toxicity, the glutathione *S*-transferases, as well as human serum albumin were characterized *in vitro*. Glutathione adducts were analyzed using a small molecule approach, whereas modified proteins were subjected to bottom-up proteomics. Both analyses used liquid chromatography-tandem mass spectrometry analyses to reveal multiple reactive metabolites of clozapine and olanzapine and multiple adducts to human glutathione *S*-transferases, as well as human serum albumin. Modifications were identified at the exact cysteine site. Additionally, untargeted data-dependent acquisition was paired with targeted tandem mass spectral analysis on a

quadrupole–time-of-flight platform, to significantly increase modified protein detection.

Timon Geib, Madhuranayaki Thulasingham, Jesper Z. Haeggström and Lekha Sleno are co-authors of this article. Timon Geib conducted the literature survey, prepared experimental protocols, conducted the experiments, processed the data and prepared the original manuscript. Madhuranayaki Thulasingham and Jesper Z. Haeggström performed recombinant expression and purification of human microsomal glutathione *S*-transferase 1 protein. Lekha Sleno supported and supervised the project, verified data analysis and interpretation of the results, revised and finalized the manuscript.

5.1 Abstract

Drug-induced toxicity has, in many cases, been linked to oxidative metabolism resulting in the formation of reactive metabolites and subsequent covalent binding to biomolecules. Two structurally related antipsychotic drugs, clozapine (CLZ) and olanzapine (OLZ), are known to form similar nitrenium ion reactive metabolites. CLZ-derived reactive metabolites have been linked to agranulocytosis and hepatotoxicity. We have studied the oxidative metabolism of CLZ and OLZ as well as two known metabolites of CLZ, desmethyl-CLZ (DCLZ), and CLZ-N-oxide (CLZ-NO), using *in vitro* rat liver microsomal (RLM) incubations with glutathione (GSH) trapping of reactive metabolites and liquid chromatography-high resolution tandem mass spectrometry (LC-HRMS/MS). Reactive metabolite binding to selected standard peptides and recombinant purified human proteins was also evaluated. Bottom-up proteomics was performed using two complementary proteases, prefractionation of

peptides followed by LC-HRMS/MS for elucidating modifications of target proteins. Induced RLM was selected to form reactive metabolites enzymatically to assess the complex profile of reactive metabolite structures and their binding potential to standard human proteins. Multiple oxidative metabolites and several different GSH adducts were found for CLZ and OLZ. Modification sites were characterized on human glutathione S-transferase (hGST) alpha 1 (OLZ- modified at Cys112), hGST mu 2 (OLZ at Cys115), and hGST pi (CLZ, DCLZ, CLZ-NO and OLZ at Cys170), human microsomal GST 1 (hMGST1, CLZ and OLZ at Cys50), and human serum albumin (hSA, CLZ at Cys34). Furthermore, two modified rat proteins, microsomal GST 1 (CLZ and OLZ at Cys50) and one CYP (OLZ-modified, multiple possible isoforms), from RLM background were also characterized. In addition, direct effects of the reactive metabolite modifications on proteins were observed, including differences in protease cleavage specificity, chromatographic behavior, and charge-state distributions.

5.2 Introduction

The atypical antipsychotics clozapine (CLZ) and olanzapine (OLZ) are both used in the treatment of schizophrenia and paranoia (Akamine *et al.*, 2017; Ciudad *et al.*, 2005). However, both differ in their efficacy, side effects, and usage restrictions. CLZ is used as a third-line medication in treatment-resistant cases (Baldessarini and Frankenburg, 1991; Curto *et al.*, 2015; Kane *et al.*, 1988), even though it is considered more effective than any other standard neuroleptic available (Fehsel *et al.*, 2005; Saha *et al.*, 2005). Its restricted use is due to its potential to cause agranulocytosis in up to 1% of patients (Ingimarsson *et al.*, 2016). As a result, constant blood monitoring is mandatory (Nielsen *et al.*, 2016). Furthermore, in several other cases, CLZ-induced venous thromboembolism (Hägg *et al.*, 2009), diabetic ketoacidosis (Vuk *et al.*, 2017),

eosinophilic myocarditis and cardiomyopathy (Kilian *et al.*, 1999), neuroleptic malignant syndrome (Leonardo *et al.*, 2017), and hepatotoxicity (Hummer *et al.*, 1997; Tucker, 2013; Wu Chou *et al.*, 2014) have been observed. Most of its toxic effects are believed to be caused by immune-mediated responses and/or the formation of an unstable nitrenium ion, formed via oxidative metabolism (Liu and Uetrecht, 1995). This electrophilic intermediate can covalently bind to biomolecules, including cysteine residues in proteins (Boerma *et al.*, 2011). In contrast, OLZ is known to cause less severe side-effects (Fulton and Goa, 1997), and is thereby used as a first-line medication (Murray, 2006; Schwenger *et al.*, 2011). In addition, OLZ is also a treatment for mood disorders (Luan *et al.*, 2017; Samara *et al.*, 2017), anorexia nervosa (Attia *et al.*, 2019) and chemotherapy-induced nausea (Navari *et al.*, 2016; Sutherland *et al.*, 2018). Both of these drugs are known to form structurally similar nitrenium ions (CLZox and OLZox, respectively) (Gardner *et al.*, 1998b), via phase I metabolism in the liver. In addition, the nitrenium ion species can also be formed by myeloperoxidase-derived hypochlorous acid (Lobach and Uetrecht, 2014; Uetrecht, 1996), and is suspected to cause covalent binding in neutrophils, with subsequent agranulocytosis and neutropenia in CLZ administration (Gardner *et al.*, 1998a).

Several stable phase I metabolites are also formed following the administration of CLZ and OLZ. The most prevalent ones include demethylated (DCLZ, DOLZ) and *N*-oxide (CLZ-NO, OLZ-NO) metabolites as well as 2-hydroxymethyl olanzapine (2-OH-OLZ). These products are formed via cytochrome P450 (CYP)-mediated metabolism (Korprasertthaworn *et al.*, 2015; Lu *et al.*, 2016; Murray, 2006; Okubo *et al.*, 2016; Wagmann *et al.*, 2016). Flavin-containing monooxygenases (FMOs) are also known to contribute to the formation of *N*-oxides (Fang *et al.*, 1998; Korprasertthaworn *et al.*, 2015; Okubo *et al.*, 2016). Some of these stable metabolites are known to be pharmacologically-active (*e.g.*, DCLZ) (Lameh *et al.*, 2007). Furthermore, studies with CLZ-NO have shown that it can be partly reduced back to CLZ (Manvich *et al.*, 2018).

In general, reactive metabolites are effectively detoxified through glutathione (GSH) conjugation, partly mediated by glutathione *S*-transferases (GSTs) during phase II metabolism (Dragovic *et al.*, 2010). However, upon depletion of reduced GSH, drug-protein adducts can accumulate and cause severe tissue injury (Hadi *et al.*, 2013b). Thus, identifying all potential reactive metabolites and studying the formation of protein adducts is crucial to understanding drug-related toxicity. Especially interesting here is the comparison of CLZ to the structurally similar OLZ. A previous rat model with equimolar doses of both drugs showed that only CLZ had a significantly detrimental effect on neutrophil kinetics (Ng *et al.*, 2014).

Using rat liver microsomes (RLM), we studied oxidative metabolism and GSH adduct formation of CLZ and OLZ. Standard peptides and recombinant proteins, including several GST isozymes and human serum albumin, were tested individually to probe for covalent binding. Metabolites, GSH conjugates, and peptide adducts were analyzed directly, whereas protein adducts were subjected to a protein digestion using two complementary proteases (trypsin and pepsin) and prefractionation of peptides prior to LC-HRMS/MS analyses.

5.3 Experimental procedures

5.3.1 Chemicals and materials

Aroclor 1254-induced male Sprague–Dawley RLM (part no.: M10001) were purchased from BioreclamationIVT (Baltimore, MD). Magnesium chloride and potassium phosphate (dibasic) were from Anachemia (Montréal, QC). CLZ, CLZ-NO, DCLZ, and OLZ, trypsin (TPCK-treated, bovine), pepsin (porcine), human serum albumin (hSA), and other chemicals were purchased from Sigma-Aldrich (St. Louis,

MO). Standard peptides were purchased from Biomatik (Cambridge, ON). Ultrapure water was from a Millipore Synergy UV system (Billerica, MA).

5.3.2 Purified protein preparation

Proteins hGSTA1, M2 and P1 were prepared by recombinant expression in *Escherichia coli* and purified through GSH affinity chromatography, as previously reported (Geib *et al.*, 2019). Detailed information on hMGST1 expression can be found in the Supporting Information. The expression and solubilization conditions were essentially as previously described for MGST2 (Ahmad *et al.*, 2013).

5.3.3 *In vitro* metabolism and GSH trapping

RLM (1 mg/mL protein) and CLZ, OLZ, DCLZ or CLZ-NO (each 10 μ M) were incubated (37°C, 2 h) in the presence of a NADPH-regenerating system, containing NADP⁺ (500 μ M), glucose 6-phosphate (10 mM), glucose-6-phosphate dehydrogenase (2 U/mL) and magnesium chloride (5 mM). A negative control was prepared in each case without NADP⁺. GSH (2.5 mM) was added to trap reactive metabolites. The incubation was quenched with equal volume ice-cold ACN and centrifuged (8 min, 4°C, 14,000 rpm). Supernatant was then removed and dried under vacuum. Dried samples were re-solubilized in 100 μ L of 5% ACN prior to LC-MS/MS analysis.

5.3.4 Peptide and protein binding protocol

A final concentration of 50 µg/mL of hSA-related standard peptides (containing active site Cys34), LQQCPFEDHVKL and LQQCPFEDHVK, were incubated with either CLZ or OLZ in RLM under the same conditions as above (instead of GSH).

Similar RLM incubations were also performed to test binding to standard recombinant human proteins with either CLZ or OLZ (250 µM final concentration). Several proteins were added individually into incubations, namely hGSTA1, hGSTM2, hGSTP1, hMGST1, or hSA (each ~9 nmol/mL) (200 µL incubation volume). Following a 2 h incubation, an equal volume of 100 mM ammonium bicarbonate (ABC buffer, pH 8.5) was added, followed by DTT (250 nmol, for 20 min at 37°C) and IAM (750 nmol, for 30 min at 37°C, in the dark) for reductive alkylation of cysteines. Trypsin (10 µg) digestion was then performed for 4 h at 37°C. For pepsin digestion, samples were diluted with 1% formic acid solution in 10% MeOH to obtain pH 2.5 and digested with 10 µg pepsin (1 h at 37°C). Prior to solid-phase extraction (SPE), pepsin digests were neutralized with ABC. Digests were cleaned-up on 1 cc (30 mg) OASIS HLB cartridges (Waters, Milford, MA), with a 100% MeOH (1 mL) elution step, and dried under nitrogen. Incubations with hSA and hGSTA1 were only digested with pepsin, based on previous knowledge that trypsin digested did not add any coverage of cysteine sites of interest (Geib *et al.*, 2018, 2019).

5.3.5 Metabolite and standard peptide analysis

Analysis of metabolites, as well as GSH and peptide adducts was performed by injecting dried incubation supernatants (10 µl) onto an Aeris PEPTIDE XB-C18 100 × 2.1 mm column, with solid core 1.7 µm particles (100 Å) fitted with a SecurityGuard ULTRA C18-peptide guard column (Phenomenex, Torrance, CA) using a Nexera

UHPLC system (Shimadzu, Columbia, MD). Mobile phases consisted of water (A) and ACN (B), both containing 0.1% formic acid, at a flow rate of 0.3 mL/min and a column temperature of 40°C. Details on the gradient used for separation can be found in the Supporting Information. High-resolution MS and MS/MS spectra were collected on a TripleTOF 5600 quadrupole–time-of-flight system (Sciex, Concord, ON) equipped with a DuoSpray ion source in positive mode, in data-dependent acquisition (DDA) mode with dynamic background subtraction. Instrument parameters and MS acquisition details can be found in the Supporting Information.

Metabolite samples were screened for possible metabolism products using MetabolitePilot 1.5 software (Sciex) using a set of known drug biotransformations (including oxidative and dealkylation reactions and GSH conjugates). The list of features of interest were confirmed and expanded upon using PeakView 2.2 and MasterView 1.1, based on precursor ion accurate mass, isotope pattern and MS/MS analysis.

5.3.6 Bottom-up proteomics analysis

Dried digests were reconstituted in 10% ACN and pre-fractionated using a ZORBAX Extend-C18 column (250 × 4.6 mm; Agilent Technologies, Palo Alto, CA) with 5 µm (100 Å) particles on an Agilent 1200 series HPLC with mobile phases consisting of 10 mM ammonium acetate (pH 10, adjusted with ammonium hydroxide) in water (mobile phase A). Mobile phase B was prepared with a 1:9 ratio of mobile phase A/ACN. LC fractionation conditions were based on an previously published method (Geib *et al.*, 2019). A brief overview of the gradient used can be found in the Supporting Information.

Dried fractions were reconstituted in 10% ACN and injected (30 μ L) onto the same LC-MS/MS system with the same column and mobile phases, as mentioned above for metabolite analysis. The details on the LC gradient and the MS parameters used for proteomic analysis can be found in the Supporting Information. Selected samples were also analyzed via targeted product ion scans, for those modified peptides that were not initially triggered automatically by data-dependent acquisition, as specified in the Results and Discussion section.

Raw data files from each protein digest (all fractions combined) were searched against the UniProtKB/Swiss-Prot human (*Homo sapiens*) and rat (*Rattus norvegicus*) protein database (release date: 04/10/2019, including common protein contaminations) by ProteinPilot 5.0 software (Sciex) using the Paragon Algorithm (Shilov *et al.*, 2007). To find potential reactive metabolite adducts, the feature probability was altered to 50% for each individual metabolite binding to cysteine. Potential cysteine binding of CLZ-2H (addition of C₁₈H₁₇CIN₄), CLZ-NO-2H (C₁₈H₁₇CIN₄O), DCLZ-2H (C₁₇H₁₅CIN₄), CLZ-HCl (C₁₈H₁₈N₄), CLZ+O (C₁₈H₁₉CIN₄O) and CLZ-C₅H₁₀N₂+O-2H (C₁₃H₇CIN₂O), and OLZ-2H (C₁₇H₁₈N₄), oxidized OLZ-2H (C₁₇H₁₈N₄O), DOLZ-2H (C₁₇H₁₆N₄), OLZ+O (C₁₇H₂₀N₄O) and OLZ-C₅H₁₀N₂+2O (C₁₂H₁₀N₂O₂) were searched separately. Trypsin digests were searched with specifying trypsin as protease; pepsin digests without specifying any protease. The search was performed for +2 to +4 charge states at a MS tolerance of 0.05 u on precursor ions and 0.1 u on fragment ions. Peptides and proteins were identified at a 1% false discovery rate (Tang *et al.*, 2008) using a target-decoy database search algorithm. Using target-decoy database searching facilitates the validation of peptide and protein identification by estimating the false discovery rates. Intentionally incorrect decoy protein sequences are added to the database of correct protein sequences. Identified proteins and peptides from that decoy database are considered false positives. Then, the false discovery rate can be estimated by dividing the number of false

positives by the number of total positives (true positives and false positives combined) (Elias and Gygi, 2010).

5.4 Results and discussion

5.4.1 Metabolites and GSH adducts identification

Phase I oxidative metabolites and GSH adducts were curated based on the following criteria: (1) MS1 mass error within 10 ppm, (2) MS1 isotope ratio (M:M+1) difference <20%, (3) chromatographic peak signal-to-noise ratio >10, and (4) sample/control area ratio >5. False-positives from in-source fragmentation were excluded. A list of all confirmed metabolites of CLZ, CLZ-NO, DCLZ, and OLZ incubations can be found in Tables S1–S2. Overlaid chromatograms depicting peaks of all metabolites and parent compounds can be found in Figure 5.1 (GSH adducts) and Figure S1 (stable metabolites).

GSH-related adducts were investigated for their potential to form structural isomers and characteristic MS/MS fragment ions (see Figure 5.2 and Figure 5.3, and Figure S2). Nitrenium-related CLZ reactive metabolites formed multiple well-resolved GSH adducts. Incubations with CLZ, CLZ-NO, and DCLZ each led to the formation of three isomeric ‘-2H+GSH’ adducts and one dechlorinated GSH adduct (-HCl+GSH). In OLZ incubations, four isomeric ‘OLZ-2H+GSH’ adducts were identified as well as four oxidized GSH conjugates (+O-2H+GSH). Three demethylated adducts (OLZ-CH₂-2H+GSH) were also observed. Both CLZ and OLZ were found to form ‘+O+GSH’ adducts as well as a related ‘-Cl+OH+GSH’ adduct for CLZ. These latter adducts are presumably via the formation of an arene epoxide reactive metabolite (Maggs *et al.*, 2000; Reddy *et al.*, 2004), and followed similar

fragmentation behavior (Figure S2D) as nitrenium-related GSH adducts. An overview of selected postulated fragment ion structures and exact masses can be found in Figure 5.2 and Figure 5.3, and Table S3, respectively. Unique OLZ-GSH fragment ions were found at m/z 254.0746 and 311.1325 (see Figure 5.3). Specific ions for 'CLZ+O+GSH' adducts were found at m/z 275.0040 and 301.0197 (see Figure S2D). In addition, several other GSH-related adducts were observed. These adducts included '+O+GSH', '-PIP+O-2H+GSH' resulting from CLZ and OLZ-related incubations and '-PIP+2O+GSH' in OLZ experiments. An overview of stable metabolites and adducts can be found in Figure 5.4.

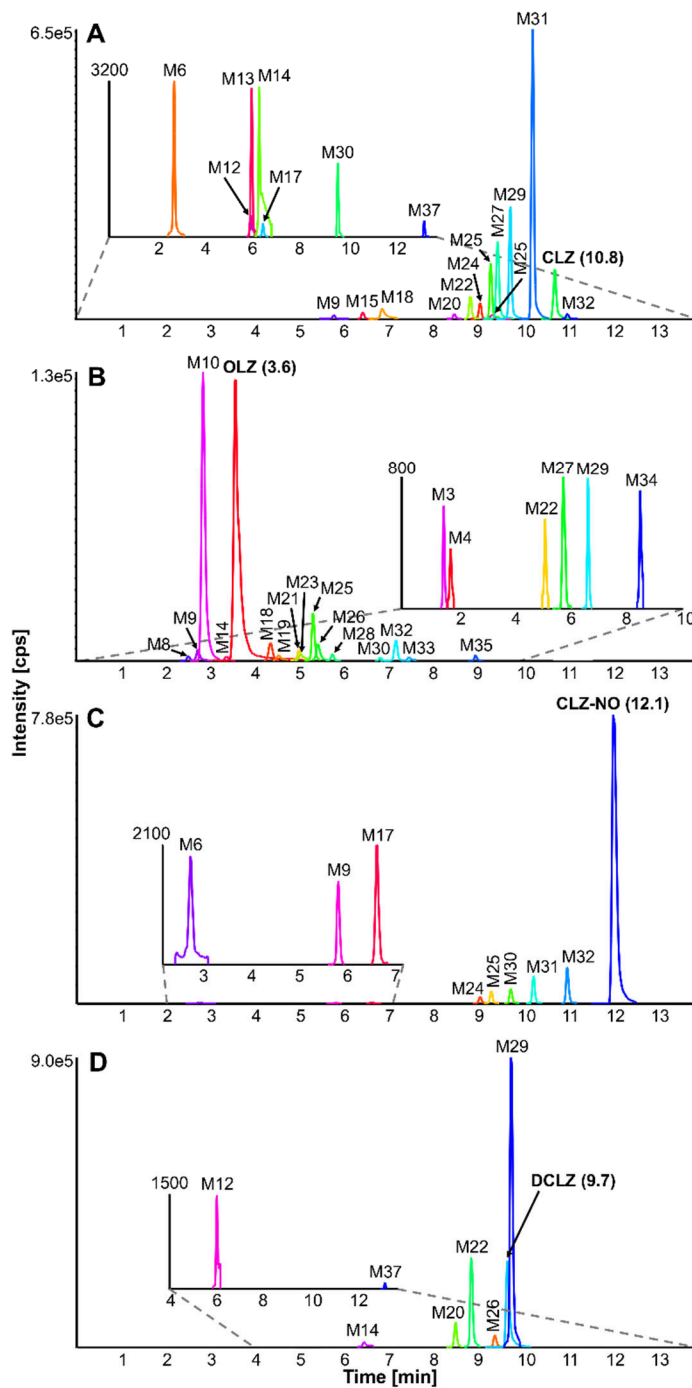


Figure 5.1 Extracted ion chromatograms of $[M+2H]^{2+}$ of GSH adducts in incubations of (A) CLZ, (B) OLZ, (C) CLZ-NO and (D) DCLZ with RLM. Retention times in parentheses. Metabolite IDs can be found in Tables S1–2.

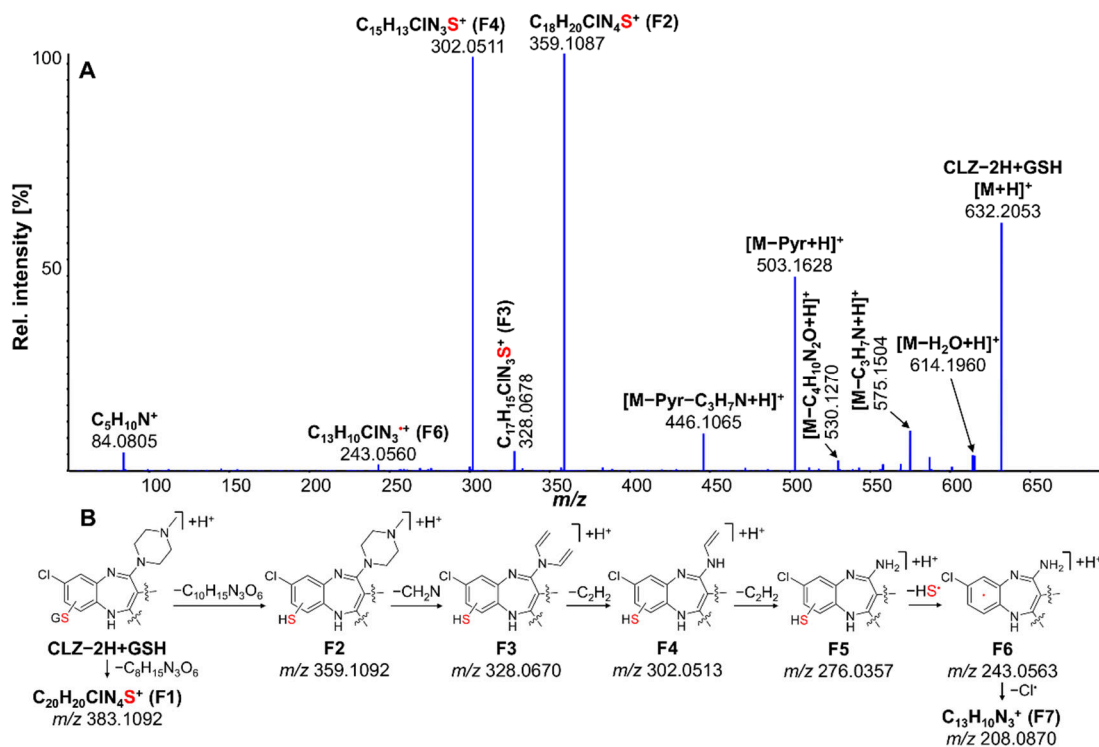


Figure 5.2 (A) MS/MS spectrum of $[M+H]^+$ of the ‘CLZ-2H+GSH’ adduct (at 10.3 min) and (B) proposed fragmentation scheme.

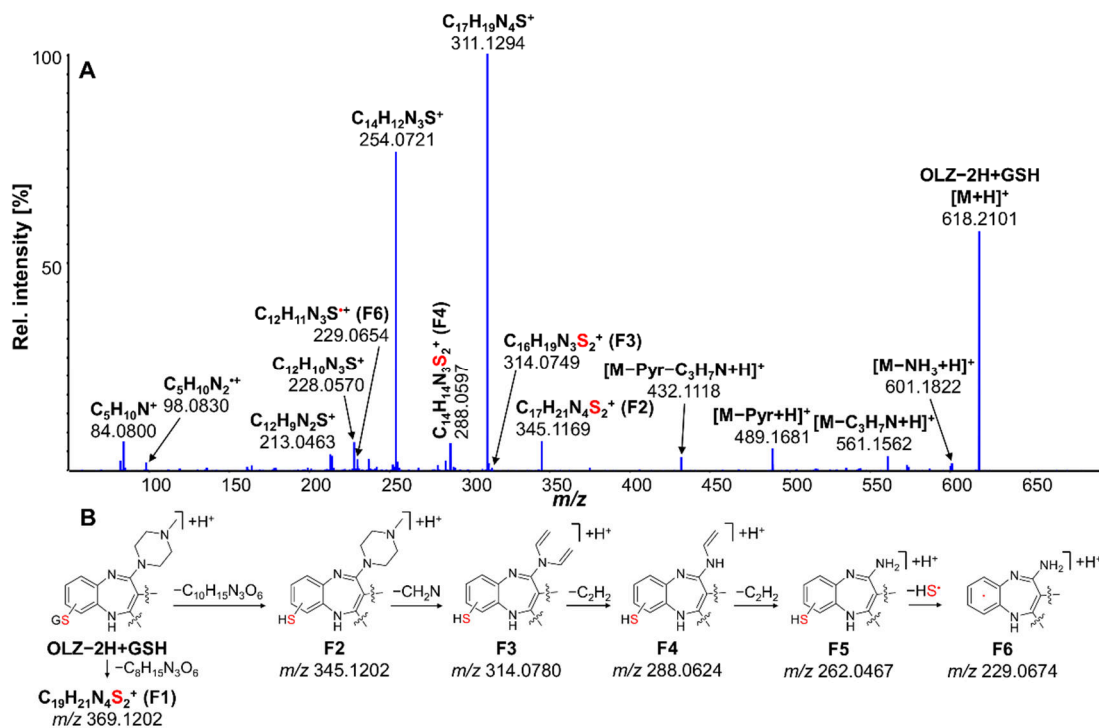


Figure 5.3 (A) MS/MS spectrum of $[M+H]^+$ of the 'OLZ-2H+GSH' adduct (at 2.9 min) and (B) proposed fragmentation scheme.

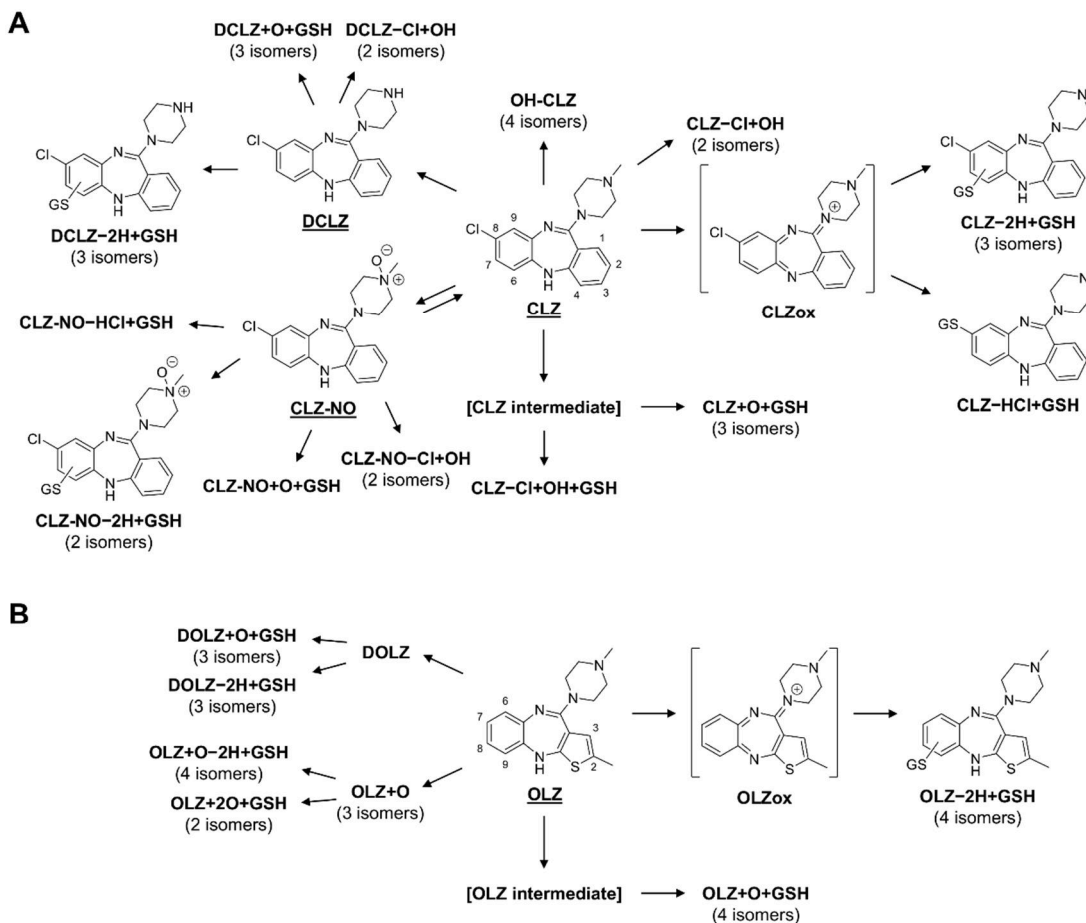


Figure 5.4 Selection of stable metabolites and GSH adducts found in (A) CLZ, CLZ-NO and DCLZ, and (B) OLZ incubations (parents underlined). Adduct '+O+GSH' were presumed to be derived from a novel intermediate.

5.4.1.1 Oxidative metabolism

Various stable metabolites, via demethylation, loss of C_2H_2 (Dragovic *et al.*, 2010), oxidation (+O and +2O), and oxidative dechlorination ($-Cl+OH$ with CLZ only) were identified from OLZ and CLZ (see Tables S1–2). This latter metabolite has not been previously reported, but correlates with phase I metabolism of other aryl chlorinated compounds, including infigratinib (Al-Shakliah *et al.*, 2020). One reason for potentially not being detected in past experiments is the relatively high polarity compound of the dechlorinated metabolite. Further corroboration of this reaction resulted from detecting analogous metabolites from CLZ-NO and DCLZ incubations (see Table S1). We also observed reduction of CLZ-NO to its parent CLZ *in vitro* ($-O$), as previously seen in *in vivo* in rat (Lin *et al.*, 1996) and human (Chang *et al.*, 1998). Also, a dechlorinated hydroxylated ($-Cl+OH$) metabolite was observed in our incubations, potentially through oxidation of the chlorinated ring, followed by chlorine elimination, as observed in the case of chlorophenols by a flavin-dependent monooxygenase (Pimviriyakul *et al.*, 2017). Observing two distinct peaks (see Figure S1), also hints at an arene oxide intermediate (Ahlborg *et al.*, 1992). This *in vitro* metabolism study demonstrated the complexity of CLZ and OLZ oxidative biotransformations. It is important to note that Aroclor 1254- induced RLM has increased CYP levels and therefore affects the metabolic profiles seen here (Dubois *et al.*, 1996; Easterbrook *et al.*, 2001). These conditions were chosen to increase the yield of reactive metabolites and thus better detect potential protein modifications by LC-MS/MS.

5.4.1.2 Reactive metabolite and GSH adduct formation

In total, 10 and 7 different GSH adducts were identified from CLZ and OLZ incubations, respectively. These adducts resulted from direct bioactivation of CLZ and

OLZ and also via bioactivation of their stable metabolites. Most GSH adducts were formed from a nitrenium intermediate. The presence of '+O+GSH' or '-Cl+OH+GSH' conjugates indicates a possible arene oxide intermediate (Grimm *et al.*, 2015; Quinete *et al.*, 2017; Reddy *et al.*, 2004). However, these adducts are normally unstable and dehydrate quickly to rearomatized GSH adducts (Maggs *et al.*, 2000). Maggs *et al.* (Maggs *et al.*, 1995) postulated that the 'CLZ+O+GSH' adduct (at a neutral mass of 649 Da) was formed via *N*-demethylation, oxidation at the 2' position to a carbonyl and subsequent lactam hydrolysis to a carboxylic acid. This is an unlikely explanation in this study, since '+O+GSH' adducts were observed from CLZ, CLZ-NO, DCLZ and OLZ. Especially, DCLZ '+O+GSH' adducts with neutral masses of 635.1928 u (see Table S1) was an indicator that these conjugates were not formed through demethylation. Other '+O+GSH' adducts combined with (*N*-methyl)piperazine loss (-PIP) were also observed for CLZ, DCLZ and OLZ. However, low abundance of these metabolites did not allow for acquisition of high quality MS/MS data.

With demethylation and *N*-oxidation products representing major circulating metabolites, subsequent bioactivation may play an important role in covalent binding *in vivo*. The fact that CLZ and OLZ form many structurally different GSH adducts, including many isomeric species, presents an impressive challenge for the detection of modified proteins.

Detailed analysis of the MS/MS fragmentation behavior of these GSH adducts was used to find diagnostic ions for confirming modified peptides. CLZ and OLZ-derived modifications are relatively large and offered several fragment ions, including several piperazine ring fragmentations (see Figure 5.2 and Figure 5.3). Standard peptides were employed to study the effect of the modifications on fragment ion formation with precursor ions of differing charge states (+2 to +4), which were used for subsequent protein binding experiments.

5.4.2 Standard peptide adducts

Two standard peptides containing the active site cysteine of hSA, LQQCPFEDHVKL, and LQQCPFEDHVK were used to analyze the effects of CLZ and OLZ-related modifications on peptide charge distribution and retention time. Carbamidomethylated peptides were compared to cysteine modifications from CLZ and OLZ reactive metabolites. In general, an overall increase in charge state was noted for all drug-derived modifications of both peptides (see Figure S3). In addition, CLZ-related modifications increased peptide retention, whereas OLZ-related binding uniformly decreased retention (data not shown).

5.4.3 Protein adducts

Modified peptides found by database searching were selected by the following criteria: (1) MS1 precursor mass accuracies <10 ppm and (2) MS2 spectral identification confidence >95%. To identify modified peptides missed by database searching based on poor quality or unacquired MS/MS, MS1 data of DDA runs were manually searched for all possible modifications from peptides with predicted cysteine modification sites (see Figure 5.5 for example). Predicted peptides were based on either modified (CLZ or OLZ) peptides identified with <95% confidence, peptides found in previous covalent binding studies (Geib *et al.*, 2019; Golizeh *et al.*, 2015), or confidently identified carbamidomethylated (CAM) peptides. If at least two charge states coeluted and MS1 mass accuracies were within 10 ppm (exception: (CLZ-2H)-QQC*PFEDHVKLVNE, at 10.9 ppm), peptides were then subjected to targeted MS/MS. MS2 data was curated for diagnostic fragment ions followed by manual sequencing (Figure 5.5). MS/MS spectra for all found modified peptides have been compiled in Figures S4–16.

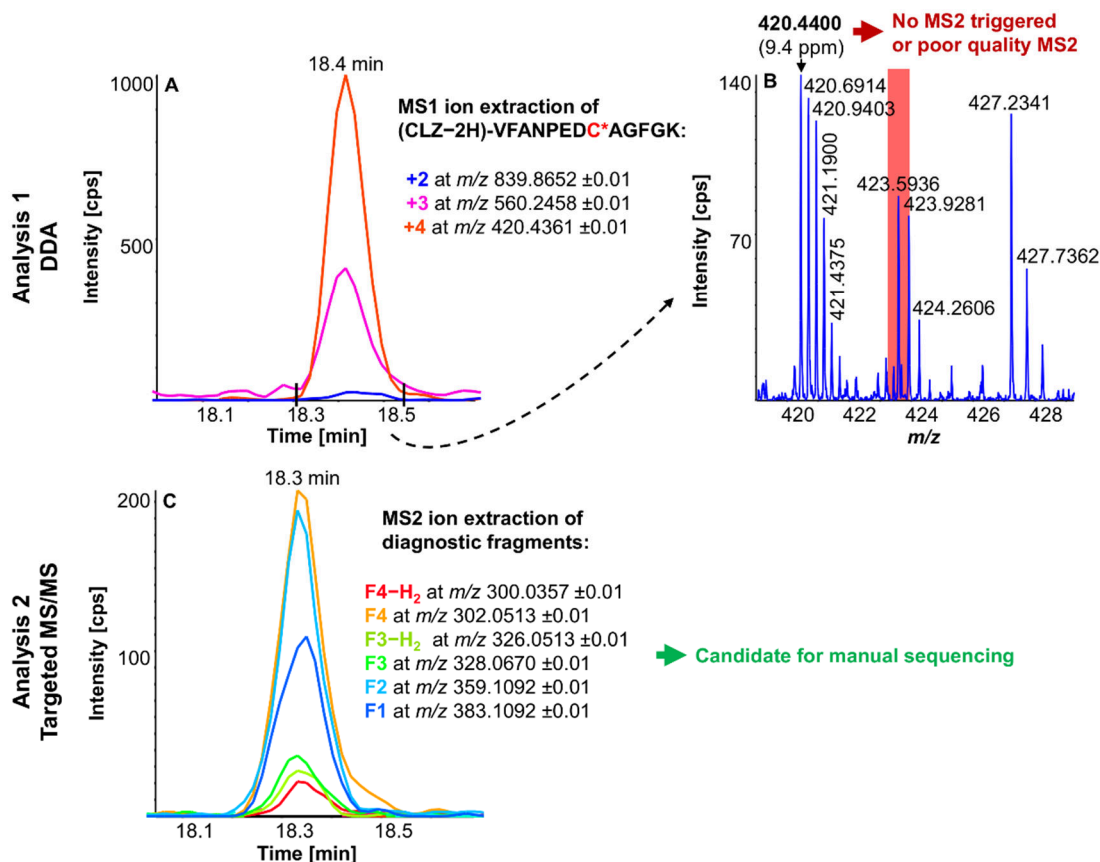


Figure 5.5 General workflow for modified peptide manual identification using DDA and targeted MS/MS data. First, DDA runs were analyzed for potential peptide ions (+2 to +4) in MS1 (A) and further verified through mass accuracy (B). Then, potential peptides with missing or poor MS2 data were selected for targeted MS/MS analyses (triggered DDA MS/MS of an unrelated feature at m/z 423.5936 highlighted as red square). Candidates for manual peptide sequencing were based on MS2 extracted ion chromatograms with co-eluting diagnostic fragment ions (C, targeted MS/MS of activated $[M+4H]^{4+}$).

A total of 15 reactive metabolite-modified peptides (Figure S17) from five human and two rat proteins, with distinct modification sites, were identified (see Table 5.1). These included one (OLZ-2H)-peptide associated with hGSTA1 (modified at Cys112), with two resolved peaks observed when the precursor ion and two diagnostic fragment ions from the cysteine modification were extracted (see Figure S18). Other modified peptides included a hGSTM2 peptide (Cys115), with four modified forms of the same peptide, from CLZ-2H, CLZ-NO-2H, DCLZ-2H, and OLZ-2H as well as a peptide from the addition of CLZ+O onto hGSTP1 (at Cys170). A peptide containing Cys50 of hMGST1 was modified by both CLZ-2H and OLZ-2H. One CLZ-2H modified peptide was identified containing the active site Cys34 of hSA. In addition, Cys50 of rMGST1 was modified by both CLZ-2H and OLZ-2H. One of three rat CYP isozymes (CYP2B1, 2B22, or 2C11) with a high sequence homology was modified by OLZ-2H.

In summary, adducted proteins were observed from nitrenium ions of CLZ, CLZ-NO, DCLZ, and OLZ as well as one CLZ+O modification. Specific diagnostic product ions were found in all targeted MS/MS spectra (Table S4). Furthermore, a shift in peptide charge distribution (see Figure 5.6) and retention time was observed based on the different modifications, similarly to when standard peptides were tested. Compared to their CAM variants, the majority of CLZ-2H, CLZ-NO-2H, DCLZ-2H and CLZ+O, and OLZ-2H modifications on cysteine resulted in increased charge states of peptides, due to the increase in size and relative basicity. Only the CLZ-2H addition on the QQC*PFEDHVKLVNE peptide from hSA did not affect its charge-state distribution, potentially as a result of its relatively acidic nature.

Table 5.1 Found peptides from screened protein targets and RLM proteins modified by CLZ or OLZ reactive metabolites

protein	protease	% sequence coverage	peptide	mod.	z	site	accuracy [ppm]	no. diagnostic ions
hSA	pepsin	77.2	QQC*PFEDHVKLVNE ^c	CLZ-2H	2	Cys34	10.9	1
hGSTA1	pepsin	75.2	PVC*PPEEKDAKL ^a	OLZ-2H	4	Cys112	5.4	4
hGSTM2	pepsin	96.3	C*YDPDF ^a	OLZ-2H	2	Cys115	0.4	5
hGSTP1	pepsin	85.2	IHEVLAPGC*L ^a	CLZ-2H	4	Cys170	5.1	8
	pepsin	85.2	IHEVLAPGC*L ^a	CLZ-NO-2H	4		4.9	7
	pepsin	85.2	IHEVLAPGC*L ^c	DCLZ-2H	4		6.1	6
	pepsin	90.0	IHEVLAPGC*L ^c	OLZ-2H	2		-0.5	2
	pepsin	85.2	LIHEVLAPGC*L ^b	CLZ+O	3		4.0	4
hMGST1	trypsin	83.9	VFANPEDC*VAFGK ^d	CLZ-2H	4	Cys50	2.7	6
	trypsin	83.2	VFANPEDC*VAFGK ^d	OLZ-2H	3		0.9	4
	trypsin	83.2	VFANPEDC*VAF ^d	OLZ-2H	3		0.4	2
	trypsin	83.2	KVFANPEDC*VAFGK ^d	OLZ-2H	4		2.2	2
rCYP2B1/2B2 or 2C11	trypsin	74.5, 74.5 or 82.2	IQEEAQC*LVEELR ^d	OLZ-2H	4	Cys152 or 151	3.0	3
rMGST1	trypsin	67.7	VFANPEDC*AGFGK ^a	CLZ-2H	4	Cys50	9.4	6
	trypsin	78.1	VFANPEDC*AGFGK ^b	OLZ-2H	3		2.9	2

^a<25% peptide confidence or not found by database searching, ^b25–80%, ^c80–95%, ^d>95%

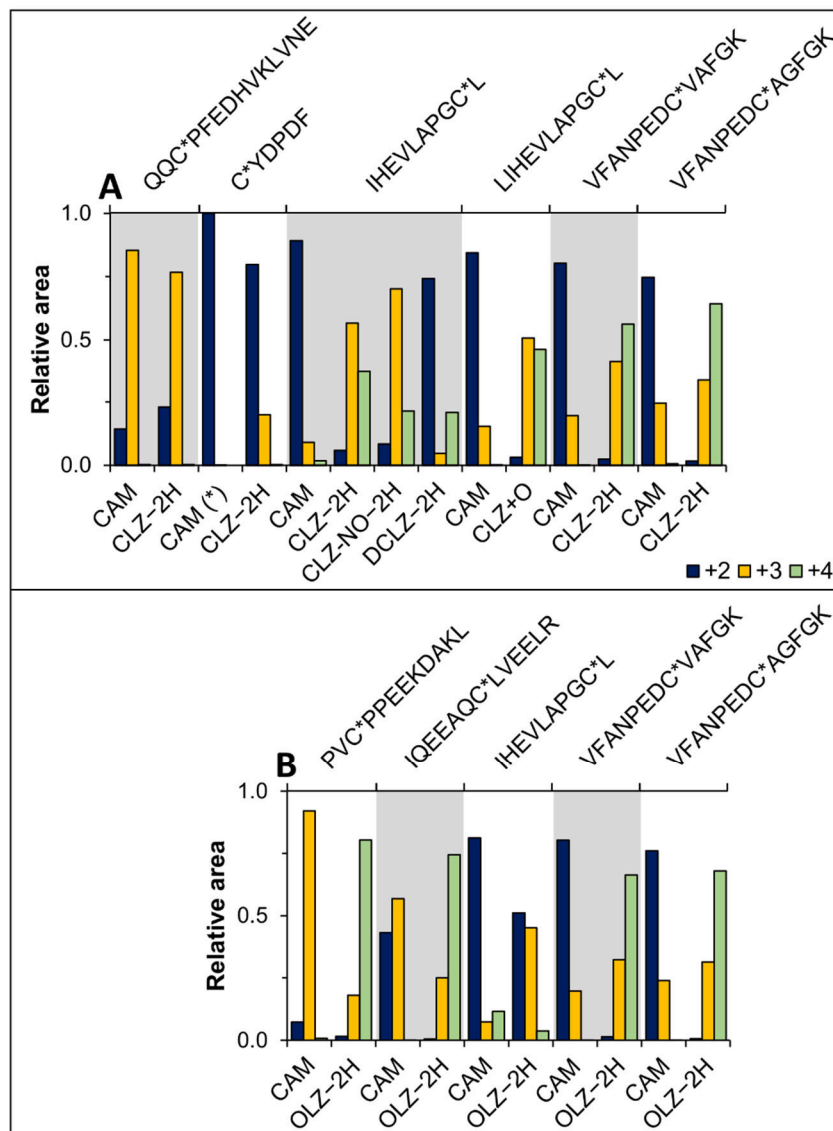


Figure 5.6 Peptide precursor ion charge distribution (+2 to +4) of CAM-peptides, and corresponding (A) CLZ and (B) OLZ reactive metabolite-peptide adducts from digests of hGSTA1, hGSTM2, hGSTP1, hMGST1 and hSA, and rat proteins. (OLZ-2H)-hGSTM2 CAM-peptide (*) was found singly and doubly charged only.

5.4.3.1 Binding to purified human proteins

In this study, covalent protein binding was assessed using Aroclor 1254-induced RLM incubations and with purified human proteins: hGSTA1, hGSTM2, hGSTP1, hMGST1, and hSA. Figure S17 shows extracted ion chromatograms of all confirmed modified peptides. These human proteins were chosen specifically as they represent interesting covalent binding targets, especially in the context of liver toxicity. HSA is a valuable blood biomarker for protein binding occurring in the liver (Sabbioni and Turesky, 2017), and GSTs are highly involved in the detoxification of reactive species and phase II metabolism (Dragovic *et al.*, 2010, 2014; Vredenburg *et al.*, 2013). Furthermore, hSA and hGSTP1 have been previously observed to be (CLZ-2H) modified (Boerma *et al.*, 2011; Lohmann *et al.*, 2008). Boerma *et al.* studied the binding of APAP, troglitazone, and CLZ to hGSTP1 *in vitro*, using a bacterial CYPBM3 mutant, tryptic digestion, and LC-MS/MS (Boerma *et al.*, 2011). Cys48 was found to be modified by CLZ, APAP, and troglitazone. Diclofenac (Boerma *et al.*, 2012) and raloxifene (Yukinaga *et al.*, 2012) have also been confirmed to bind to the same cysteine residue. Most of these studies were conducted using mostly trypsin as the protease of choice, leaving some other cysteine sites less accessible for detection via LC-MS/MS analysis. In a previous study of APAP covalent binding, multiple modification sites (Cys15, 48, and 170) in hGSTP1 were found using a double-protease approach with trypsin and pepsin (Geib *et al.*, 2019). APAP adducts of hGSTA1 (at Cys112), hGSTM1 (Cys78), and hGSTM2 (Cys115 and 174) were also detected. In the current study, Cys170 in hGSTP1 was modified by CLZ-2H, CLZ+O, CLZ-NO-2H, DCLZ-2H, and OLZ-2H, showing a high affinity of Cys170 toward electrophilic species. Using recombinant hGSTP1, Cys170 has been observed to be more highly reactive toward APAP's reactive metabolite than Cys15 and Cys48 (data not shown). OLZ adducts were also identified to Cys112 in hGSTA1 and Cys115 in hGSTM2 as well as CLZ-2H and OLZ-2H adducts to Cys50 in hMGST1. The latter was also previously found to be APAP-modified by Shin *et al.* using HLM incubations

and LC-MS/MS analysis (Shin *et al.*, 2007). MGST1 is especially interesting, since it is induced by oxidative stress and directly activated by covalent modifications (Aniya and Imaizumi, 2011; Morgenstern *et al.*, 2011; Wallin and Morgenstern, 1990). The conserved Cys50 in human (and rat) MGST1 proteins is essential for activity of the homotrimeric detoxification enzyme (Busenlehner *et al.*, 2004; Ji *et al.*, 2006; Svensson *et al.*, 2000). Thus, observing CLZ and OLZ-related binding to Cys50 might yield further insight in the detoxification process.

5.4.3.2 Binding to microsomal rat proteins

CLZ and OLZ binding to rat microsomal proteins was also investigated without added target human proteins. Rat microsomal GST1 (rMGST1) was modified at Cys50 by both CLZ-2H and OLZ-2H reactive metabolites. An OLZ-modified rat CYP was also found, belonging to either CYP2B1/2 or 2C11 (at Cys152 or 151, respectively). These three CYP isozymes are highly homologous, with 97% shared sequences between 2B1 and 2B2 and 55% between 2B2 and 2C11. In a previous study, we identified APAP-modified rCYP2C6 *in vitro* at Cys372 (not included in its 73% shared sequence with 2C11) (Golizeh *et al.*, 2015). The 2C subfamily is a highly complex set of rat CYP isozymes (Martignoni *et al.*, 2006). CYP2C7 and 2C11 in rat were previously reported to be targeted *in vivo* by reactive metabolites of teucrin A (Druckova *et al.*, 2007) and diclofenac (Shen *et al.*, 1997), respectively, without the modification sites being specified

5.4.4 Potential link between reactive metabolite-protein adducts and toxicity

Covalent binding of reactive metabolites has been associated with CLZ toxicity in many previous studies *in vitro* and *in vivo* studies. CYP-dependent CLZ-related

toxicity has been confirmed in rat hepatocytes (Lu *et al.*, 2008) as well as human liver microsomes (Pirmohamed *et al.*, 1995). Depleted GSH levels have been reported following treatment with CLZ in rat hepatocytes (Lu *et al.*, 2008). Accordingly, adding exogenous GSH has shown to protect from CLZ and DCLZ toxicity and increase cell viability (Williams *et al.*, 1997). Additional *in vitro* studies have linked CLZ and its oxidative metabolism to toxicity through bioactivation, including the induction of human neutrophil apoptosis (Williams *et al.*, 2000) as well as a dose-dependent decrease of human bone marrow stromal cell viability (Pereira and Dean, 2006). Interestingly, stromal cell death was unique to CLZ bioactivation, compared to OLZ and other antipsychotics. The formation of CLZ reactive metabolites has been investigated in liver microsomes, neutrophils, and myeloid cells where one GSH adduct was mostly observed as well as evidence for protein binding (Maggs *et al.*, 1995). In a study, a link between the formation of CLZ reactive metabolites and liver toxicity was based on increased carbonyl content, malondialdehyde and GST activity, and decreased GSH levels in CLZ-treated rats (Zlatković *et al.*, 2014). These histopathological changes correlated with liver damage observed in a study of patients receiving CLZ therapy (Dorta *et al.*, 1989; Schmidt *et al.*, 1987).

In general, covalent binding to biomolecules has often been reported in the occurrence of drug-related idiosyncratic toxicity (Utrecht, 2008; Walgren *et al.*, 2005; Zhou *et al.*, 2005). CLZ and OLZ, though very structurally similar, exhibited differences in toxicity at equimolar doses in rat (Ng *et al.*, 2014). In this study, both drugs formed multiple GSH and protein adducts *in vitro*, under oxidative conditions. However, we also observed a lower depletion of the OLZ parent in incubations compared to CLZ (see Figure 5.1 and Figure S1), showing potentially less phase I metabolism *in vitro*, paired with a higher hydrophilicity of OLZ and therefore potential for increased clearance of the parent drug, compared to CLZ. The significance of the

identified adducts described here remains to be seen, requiring further *in vivo* investigations.

5.4.5 Comparison of untargeted DDA and targeted MS/MS of modified peptides from protein digests

In order to increase the identification yield of low abundant modified peptide features of spiked-in human proteins in complex sample digests, a two-step MS/MS-based workflow was applied (Figure 5.5). This technique was employed due to insufficiencies in DDA to trigger MS/MS acquisition of low abundant peptide species (Michalski *et al.*, 2011; Tabb *et al.*, 2010). Previously, we have developed a targeted multiple reaction monitoring method for identifying APAP-modified peptides by using an isomerically labeled protein standard (Geib *et al.*, 2019). Due to the lack of an appropriate alkylating reagent to produce standard CLZ-modified peptides, targeted high-resolution MS/MS was employed as a complementary tool to increase modification coverage. In total, 15 distinct CLZ or OLZ-related modified peptides were identified: Five of which were confidently identified through DDA with database searching, seven (low-confidence peptides from DDA) after additional targeted MS/MS and manual sequencing, and three solely through targeted MS/MS. Targeted MS/MS allows for MS2 spectra for a given precursor ion to be acquired over the whole chromatographic peak. This strategy was used to correctly identify (OLZ-2H)-modified hGSTA1 peptic peptide PVC¹¹²PPEEKDAKL (Figure S18) with a less ideal peak shape, potentially as a result of different peptide conformers from multiple prolines in each sequence (Glover *et al.*, 2015; O'Neal *et al.*, 1996). Similar chromatographic effects were previously observed for another peptide with multiple prolines (LLAHAFPPGP) (Golizeh *et al.*, 2014). Therefore, overlapping MS1 and MS2 chromatograms also facilitates feature identification of non-ideal peaks. Nevertheless,

limit of detection, chromatography, and fragmentation behavior remained challenging in both untargeted and targeted acquisitions. For instance, (CLZ–2H)-modified Cys48 in hGTSP1, observed by Boerma *et al.* (Boerma *et al.*, 2011), was not detected in the current study. Complex proteomic samples are highly affected by extraction recoveries, dilution factors from sample preparation, and fractionation, and ion suppression from coeluting highly abundant peptides affect the detection of each modified peptide.

5.4.6 Effects of CLZ and OLZ modifications on proteomic analysis

Effects on pepsin cleavage specificity were observed as a result of cysteine modifications by CLZ and OLZ. The hSA peptide from pepsin digestion previously found to be modified by APAP, LQQC(APAP)PFEDHVKL (Geib *et al.*, 2018), is also consistently the active site Cys containing peptide with the highest signal intensity for carbamidomethylated hSA. However, in the case of CLZ, the modified peptide QQC*PFEDHVKLVNE was detected. This latter sequence was not found as a carbamidomethylated peptide with sufficient confidence and significant abundance. The modification with the relatively large and hydrophobic CLZ moiety changes the cleavage specificity of pepsin, and we can thus not rely on which peptides are observed in their unmodified forms to search modification sites. A similar difference in cleavage specificity was also seen in (OLZ–2H)-modified Cys115 in hGSTM2, with the resulting formation of C*YDPDF, instead of AKLC¹¹⁵YDPDF (Geib *et al.*, 2018). These differences were specifically observed in pepsin samples, as a function of the more flexible cleavage specificity of this enzyme. Tryptic digestion was much less susceptible to changes in the cleavage site based on cysteine modification (see tryptic peptides of hMGST1, rMGST1, and rCYP in Table 5.1). Pepsin digests of CLZ and OLZ-modified hGSTA1 (Cys112) and hGSTP1 (Cys170) resulted in the formation of anticipated peptide sequences. PVC*PPEEKDAKL and IHEVLAPGC*L, respectively,

were identical to previously identified APAP-modified peptides (Geib *et al.*, 2019); and identical to highest abundant CAM peptides from our data. Since these modifications add hydrophobicity, pepsin cleavage occurs closer to the cysteine site, thus influencing the pepsin cleavage of hGSTM2 and hSA, but not hGSTA1 and P1.

CLZ and OLZ modifications increased peptide mass and basicity and consequently showed an effect on HPLC retention and MS ionization. CLZ-modified peptides were more highly charged than OLZ peptides. All or some of these effects might explain differences in peptide identification outcome in the presence of large modification groups. As a result, CLZ and OLZ-related protein binding demonstrated multiple analytical challenges, necessitating careful evaluation and unambiguous peptide identification. These effects also have an important effect on the possibility for relative quantitation of unmodified vs modified peptides.

5.5 Conclusion

The oxidative metabolism of CLZ and OLZ was studied *in vitro* in induced RLM with multiple reactive metabolite-related covalent adducts with GSH, with the identification of peptides and proteins. These findings provided further insight into the formation and reactivity of nitrenium ions as well as the potential formation of arene oxide intermediates. Site-specific modifications were identified for human serum albumin and multiple GST enzymes. Understanding the reactive behavior of these metabolites and related protein binding requires further study to better understand a potential link to toxicity. For instance, comparing the covalent binding levels of CLZ and OLZ *in vitro* in human hepatocytes or neutrophils would allow a good comparison for toxicological risk assessment. GSTs, such as MGST1, are important targets of reactive metabolites in the context of liver toxicity. It remains highly interesting to

study covalent binding for these two compounds specifically related to agranulocytosis. The evidence provided here for multiple GSH adduct structures and their distinct MS/MS fragmentation patterns can be useful to support further covalent binding studies.

5.6 Associated content

5.6.1 Supporting information

The Supporting Information is available free of charge at <https://pubs.acs.org/doi/10.1021/acs.chemrestox.0c00191>.

Supporting Figures S1–S18 include metabolite and adduct chromatograms, modified peptide MS/MS, modified peptide chromatograms, and comparison of MS1 and MS2 ion extractions (PDF)

Supporting Tables S1–S4 include identified CLZ and OLZ metabolites in RLM incubations, diagnostic fragment ions found in GSH adduct MS/MS, and reactive metabolite-cysteine MS2 diagnostic fragment ions detected in targeted MS/MS experiments of modified peptides (XLSX)

5.7 Author information

5.7.1 Funding

This work was funded by the Natural Sciences and Engineering Research Council of Canada (NSERC, Discovery grant no. RGPIN 2016-06034). T.G. acknowledges FRQNT (*Fonds de recherche du Québec – Nature et technologies*) for scholarships.

5.7.2 Notes

The authors declare no competing financial interest.

5.8 Acknowledgment

The authors acknowledge Cristina Lento and Derek J. Wilson for assistance in recombinant expression of cytosolic GSTs.

CHAPTER VI

SUMMARY AND CONCLUSIONS

In the preceding chapters, the *in vitro* reactive metabolite formation of two antipsychotics, CLZ and OLZ, was analyzed using GSH trapping. Also, related protein binding of these antipsychotics and the analgesic APAP to phase II enzymes, the GSTs, was determined. Circulating *in vivo* APAP-hSA adducts were quantified in the serum of ALF patients. In addition, the LPO reactive metabolite HNE was studied. The effects of *in vivo* HNE-chondrocyte protein adducts in relation to OA were evaluated. Throughout all these studies the following research objectives were consistently followed:

1. Optimal sample preparation for adequate recovery of low abundant analytes
2. Optimal offline and online LC settings for abundant feature signals with reduced complexity
3. Selection of the most suitable MS/MS platform and acquisition method
4. Straightforward data mining and data analysis of complex data sets
5. Correct data validation, and determination of false positives and outliers
6. Adequate interpretation of *in vitro* and *in vivo* findings

To achieve the above goals successfully, each study was designed based on at least one of the following aspects: 1) technical improvement in small molecule and/or proteomics LC-MS/MS analyses and sample preparation, and 2) answering

biologically relevant questions. This chapter will outline these results and will discuss follow-up research, as well as limitations and possible improvements.

6.1 Summary of findings

All findings can be categorized into either *in vitro* reactive metabolite identification (CLZ and OLZ in Chapter 5), *in vitro* investigation of reactive metabolite binding to (recombinant) proteins (APAP in Chapter 3, and CLZ and OLZ in Chapter 5), reactive metabolite protein target identification *in vivo* (HNE in Chapter 4), or quantitation of known reactive metabolite-protein targets *in vivo* (APAP-hSA in Chapter 2) (see Figure 6.1). Accordingly, these chapters will be discussed in that order.

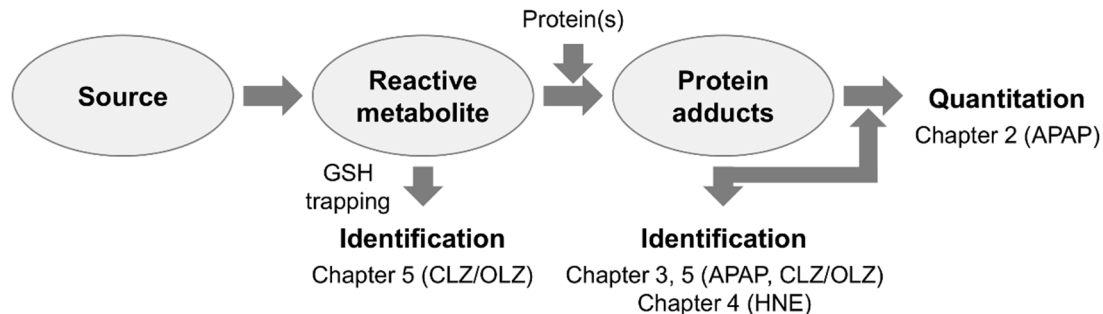


Figure 6.1 Categorization of thesis research on *in vitro* reactive metabolite formation of APAP, CLZ and OLZ, and investigation of OA-related *in vivo* protein binding of reactive HNE. *In vivo* quantitation was possible by monitoring APAP-hSA in ALF patient serum. Reactive metabolite sources were CYP oxidations or LPO.

6.1.1 Identification of drug reactive metabolism and protein binding

The reactive metabolite formation of the atypical antipsychotics CLZ and OLZ was studied using CYP incubations and GSH trapping (Chapter 5). Several GSH adducts related to CLZox and OLZox were observed, which complied with literature findings. In addition, multiple novel reactive metabolite-GSH adducts from CLZ's primary metabolites CLZ-NO and DCLZ were also identified, as well as possible arene oxide-derived GSH adducts. These findings were confirmed on the protein-level as well. CLZ and OLZ binding was studied using recombinant hGSTA1, M2 and P1, and hMGST1, as well as purified hSA. These adducts were detected using RLM bioactivation of CLZ and OLZ, addition of individual proteins, dual-enzyme bottom-up proteomics (trypsin and pepsin in parallel), high-pH offline fractionation and LC-MS/MS in DDA mode on a QqTOF system. Moreover, in order to maximize the identification yield of low reproducible DDA peptide detection (Michalski *et al.*, 2011), dedicated HRMS product ion scans were used. Dedicated MS/MS was based on pre-existing reactive metabolite-GST binding knowledge (*i.e.*, from APAP-related binding), prediction of possible modified peptides and manual MS1 data evaluation. The use of dedicated MS/MS allowed for a significant increase in spectral quality of peptide MS/MS. Thus, multiple modified peptides were only identified through these efforts. In total, 11 different modified cysteine sites were identified, alongside adducts to rat proteins from Aroclor 1254-induced RLM incubations (rMGST1 and rCYP). Especially, Cys170 in hGSTP1 formed multiple covalent adducts, including adducts derived from CLZ, CLZ-NO, DCLZ and OLZ nitrenium ions, and one modification possibly from an arene oxide intermediate of CLZ (modification: CLZ+O).

The same workflow was also applied to study APAP-related reactive metabolite binding to GSTs (Chapter 3). A total of seven different covalent adducts (different modification sites) were observed, studying hGSTA1, M1, M2 and P1. Several aspects of the general workflow were tested for possible improvements. These aspects included

the CYP source for *in vitro* metabolism, offline fractionation and the MS acquisition (DDA on QqTOF and MRM on QqLIT). In terms of CYP sources, Aroclor 1254-induced RLM were compared to recombinant hCYP3A4 (Supersomes™). Using purified hCYP3A4 led to a decrease in protein complexity before proteolysis, allowing for a more sensitive peptide analysis after digestion. In addition, hCYP3A4 is known to be the most effective enzyme for APAP oxidative metabolism *in vitro* (Laine *et al.*, 2009). Purified hCYP3A4 was more effective compared to higher complex rat liver fractions (here RLM) containing many different CYP isoforms and other enzymes (see Figure 1.9). Lower protein complexity in hCYP3A4 incubations resulted in a higher recovery of low abundant modified peptide features after digestion. In addition, improvements from pre-fractionation were compared to workflows without offline fractionation. Overall, fractionation reduced peptide complexity, through two dimensions of orthogonal separation. In addition, fractionation increased probabilities for target peptide MS/MS acquisition. More time spent on online LC per sample also increased the amounts of acquisition cycles per sample. Finally, DDA performance on a QqTOF was compared to MRM acquisition on a QqQ platform with identical Q₁ and q₂ build (5000 MS series from Sciex). Due to the superior duty cycle and sensitivity of QqQ systems in MRM mode (Geib *et al.*, 2016), more modified peptides were detected using MRM with increased reproducibility. MRM methods were based on isomeric standards based on an alkylating reagent (iodo-APAP) labeling each possible cysteine site in purified hGSTs. This also allowed for testing the recovery and possible detection of each modified cysteine site. Apart from one cysteine site in hGSTP1 (Cys102), most iodo-APAP-modified sites were recovered with an adequate signal.

6.1.2 Identification of HNE protein binding

Another study focused on detecting HNE-modifications to proteins in the knee cartilage of OA patients (Chapter 4). Cartilage of 13 patients was extracted, and chondrocyte proteins analyzed. Different extraction techniques were used to yield nuclear, cytosolic or total chondrocyte protein extracts to aid detection of HNE-modified proteins in bottom-up proteomics and LC-MS/MS analysis using DDA (QqTOF). Identified HNE-proteins were compared to total chondrocyte extracts of two healthy subjects. A total of 88 HNE-proteins were unique to OA disease, with 81 HNE-proteins found in total extracts. These 88 modified proteins included histones H2A, H2B and H4. This agreed with western blot results identifying H2A and H2B as targets of HNE, using anti-HNE antibodies. Additionally, western blot efforts identified HDAC2 (histone deacetylase 2) as another target of HNE, which also had direct effects on the acetylation of histones H2A and H2B. These results underlined a possible connection of OA and HNE-protein binding. Based on the involvement of histones in chromatin formation (see Figure 6.2), HNE-histone modifications might play a crucial role in the onset or progression of OA (Shen *et al.*, 2017; Shi *et al.*, 2014).

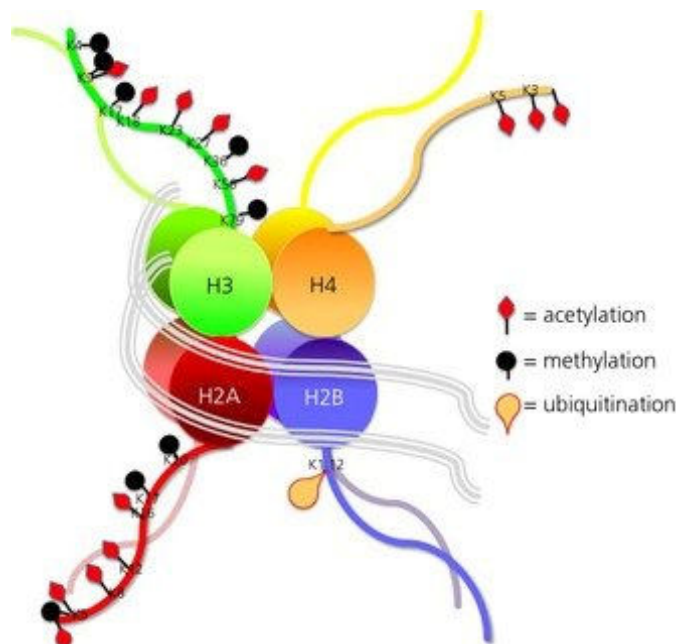


Figure 6.2 A nucleosome consisting of a segment of DNA (grey) wound around an octamer of histones of four variants (H2A, H2B, H3 and H4). With the addition of histone H1, nucleosomes coil into a 30 nm helical structure, the chromatin. PTMs can alter the electric charge of the core histones which either repels or attracts molecules and transcription factors (taken from (McCarthy and Nugent, 2013)).

6.1.3 Quantification of APAP-related binding to hSA

One other important aspect of reactive metabolite-protein binding studies is the accurate quantitation of modified proteins. Therefore, APAP-related binding to a known protein target, hSA, was analyzed in serum of ALF patients suffering from APAP overdose (Chapter 2). The formation of NAPQI-hSA is known to occur in liver tissue. The protein adduct is then secreted into blood circulation, which makes NAPQI-hSA a viable blood biomarker for protein binding in the liver. In this study, serum samples were collected from 34 ALF patients and one suffering from an acute liver injury (ALI). Sampling occurred 1 to 9 days after APAP ingestion and admission to the

Intensive Care Unit. Serum was analyzed using a fast and specifically optimized bottom-up proteomics (pepsin digestion) and LC-MRM assay. The cysteine labeling agents iodo-APAP and d₄-iodo-APAP were used to prepare standard modified hSA with known concentrations, to be used as calibration standards and internal standards. The assay was successfully applied to screen a 450-fold NAPQI-hSA concentration range and to quantify absolute NAPQI-hSA serum levels in all 35 ALF/ALI patients. Grouping these patients into two groups, 25 non-spontaneous survivors and 10 individuals with irreversible liver damage, demonstrated that significant differences in NAPQI-hSA levels between both groups were present, potentially allowing to predict the outcome of ALF/ALI after APAP misuse by monitoring modified hSA.

In summary, several LC-MS/MS strategies were developed and specifically optimized to identify reactive metabolite formation and reactive metabolite-protein adducts and to quantify circulating adducts to assess relations in adverse effects and disease. These methods can be adapted to analyze similar sample types with various complexity *in vitro* and *in vivo*. These perspectives, alongside important limitations, will be discussed in the following sections.

6.2 Limitations and perspectives

Reactive metabolite formation and reactivity are complex research topics. Several factors are important key elements to fully elucidate certain effects related to reactive metabolites and their reactions. These factors include correct structural characterization of the reactive metabolite, reactivity assessment, binding target identification, adduct quantitation and evaluation of cellular damage (Dalvie *et al.*, 2015; Grillo, 2015; Thompson *et al.*, 2016). Each of these factors represents an

individual challenge in and of itself but are all necessary to fully understand possible effects resulting from xenobiotic bioactivation. In this work, the focus was set on the structural investigation of reactive metabolite-amino acid adducts and covalent protein adduct formation with specific targets, presumed to play a role in related disease and toxicity in different tissues. Furthermore, quantitative analysis of circulating reactive metabolite-protein adducts was used to study the correlation of binding and severity of toxicity.

6.2.1 Sample preparation workflow applicability

In Chapters 3 and 5, a total of five recombinant GST proteins were identified to be modified by APAP (Chapter 3), CLZ and/or OLZ (both Chapter 5) using *in vitro* incubations, bottom-up proteomics and (2D-)LC-MS/MS. Several limitations can be discussed here. Both studies are specifically aimed at identifying spiked-in (GST) protein targets of CYP-derived reactive metabolites of these three drugs *in vitro*. This allowed for a very detailed but also narrow view on covalent binding to phase II GSTs in the setting of an artificial scenario in specific CYP environments (Supersomes™ or RLM). Since these recombinant GSTs were purified through GSH-affinity, possible GSH and GST binding competition was assumed. Thus, GSTs were spiked-in at high concentrations to improve the detection of low abundant peptide adducts, resulting from binding competition. This workflow, or parts of it, can be theoretically applied to every compound which undergoes (bio)chemical activation to a reactive intermediate that potentially binds to a mix of proteins or to individually purified protein isoforms. In general, the workflow included: 1) *in vitro* activation of the compound, 2) addition of protein target and incubation, 3) reductive alkylation and proteolysis, 4) SPE using a hydrophilic-lipophilic balance (HLB, see Figure 6.3 for SPE resin overview), 5) optional high-pH RP fractionation, and 6) LC-MS/MS with DDA. However, certain

limitations apply, based on the given scenario. If the protein targets of interest are known to have specific features and properties which are incompatible with the workflow, adaptations must be made. In Chapter 4 for instance, *in vivo* HNE adducts with nuclear histones in chondrocytes were the main study focus. Histones are basic, nuclear proteins (Manning and Manning, 2018) requiring careful protein extraction techniques and careful sample preparations. Nuclear protein extraction techniques often include LC-MS-incompatible detergents, such as NP-40 (nonyl phenoxyethoxyethanol; used in this study), or polysorbate 20 (Tween[®]-20) or Triton[™] X-100. These types of non-ionic detergents have detrimental effects on ESI and LC retention (Yeung *et al.*, 2008), and are not properly removed by HLB-SPE. Thus, the proteomics workflow was changed to analyze *in vivo* HNE-modified chondrocyte extracts. Instead of HLB, mixed-mode strong cation-exchange (MCX, see Figure 6.3A) extraction was employed, which utilizes separation principles similar to SCX chromatography, well suited for basic peptides as a result of histone digestion. In addition, offline fractionation was not used to reduce potential loss of low abundant protein quantities and dilution effects. This was possible because low protein amounts ($\leq 80 \mu\text{g}$) and complexity did not require multiplexed LC, as it was necessary, for instance, in a preceding HNE-microsomal protein (500 μg) *in vitro* binding study (Golizeh *et al.*, 2016). Sample loss and analyte recovery are both important factors in the successful detection of low abundant features. Each step of sample preparation (*e.g.*, digestion, SPE and offline LC) and analysis (*e.g.*, online LC) can potentially lead to a significant reduction or complete loss of final analyte signals (Feist and Hummon, 2015). This is especially difficult to evaluate in untargeted or semi-targeted analyses where standard materials are less or not available. Only in the case of APAP-related binding to GSTs (Chapter 3) it was possible to generate custom-made standard material using iodo-APAP alkylation reagent and recombinant GSTs, which was used to test for peptide signal intensity and workflow optimization. Analyses of HNE-binding (Chapter 4) and CLZ/OLZ-related binding (Chapter 5) could not be fully evaluated in

that regard. One viable alternative to account for potential analyte losses in a specific workflow is applying one or multiple complementary techniques. For instance, LC-MS/MS proteomics was accompanied by western blot in Chapter 4. Through western blotting HNE-HDAC2 adducts were observed which was not possible in bottom-up proteomics LC-MS/MS experiments due to very low protein amounts and low protein recoveries after digestion. Yet, immunoaffinity assays are highly dependent on the availability of selective antibodies. In terms of studying reactive metabolite-protein binding, not many antibodies are available. APAP, CLZ or OLZ-modification specific antibodies are not commercially available, but they could increase detection of very low abundant peptide adduct species in immunoaffinity assays and in immunoaffinity purification techniques coupled with LC-MS/MS (Grønborg *et al.*, 2002). Such antibodies could theoretically be prepared by immunization against reactive metabolite-protein, peptides or amino acid antigens in an animal model (Houen, 2015; Maleki *et al.*, 2013).

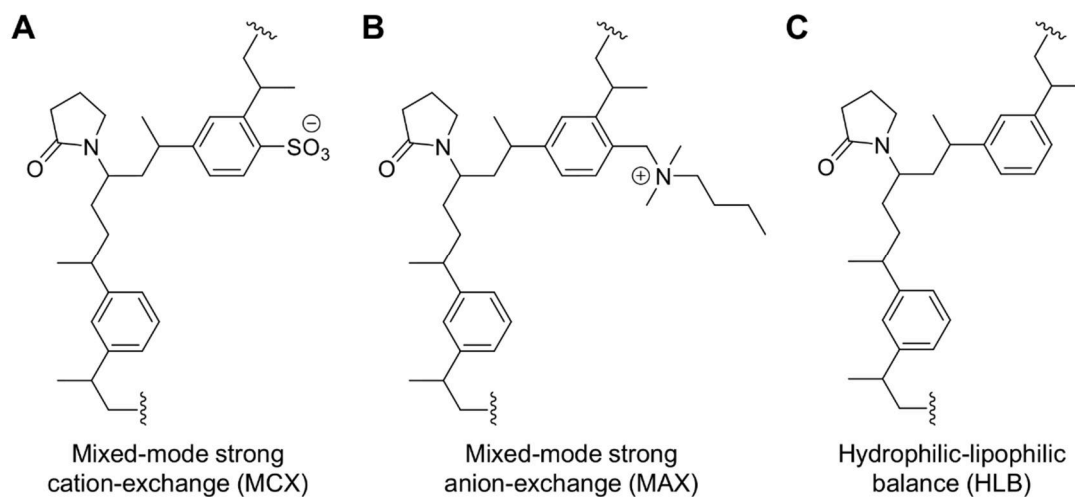


Figure 6.3 Chemical structures of (A) mixed-mode strong cation-exchange (MCX), (B) mixed-mode strong anion-exchange (MAX) and (C) hydrophilic-lipophilic balance (HLB) SPE polymer resins.

6.2.2 Limitations in reactive metabolite-GSH and GST adduct identification

The reactive metabolite formation of CLZ and OLZ was studied using GSH trapping and peak intensity-based DDA experiments. Resulting GSH adducts were analyzed based on pre-existing knowledge of biotransformation and anticipated metabolites (see Table 1.7). This enabled the identification of several reactive metabolite-GSH adducts, including adducts of primary metabolites (*e.g.*, ‘DCLZ–2H+GSH’ adducts). However, this did not include potential unforeseen metabolites and adducts which could have been formed through novel/unknown routes of biotransformation. Only a fully unbiased data acquisition or data mining strategy could answer these questions. In the investigation of reactive metabolite-protein adducts, several recombinant hepatic GSTs were identified as targets of APAP, CLZ and OLZ reactive metabolites. As briefly stated before, this allowed for a detailed view of *in vitro* reactivity and possible covalent binding *in vivo*. However, increased levels of target protein, as well as reactive metabolite, might have had direct effects on the reactive metabolite-protein binding outcome. To fully understand covalent binding, *in vivo* or cell culture follow-up studies under physiological conditions are needed. These studies are complicated due to high cost of proper cell material or lack thereof, or due to ethical boundaries to conduct human liver *in vivo* studies. Nevertheless, cell metabolism and viability studies are crucial to classify protein binding targets and their adducts as factors in toxicity, adverse effects or pathogenesis. This became apparent in the comparison of CLZ and OLZ toxicity with regards to the number of identified protein adducts. More OLZ-related modified proteins than CLZ-modified proteins were detected. However, OLZ is known to be less toxic at equimolar concentrations (Ng *et al.*, 2014) and is leading to less severe adverse effects (Fulton and Goa, 1997). Thus, the detection of many reactive metabolite-protein adducts without quantitative information did not allow for direct correlation with toxicity. These effects could be based on technical/instrumental differences and insufficiencies. Based on differences in metabolism, structure, and effects of sample preparation and analysis, OLZ-related

adducts presented fewer challenges in identification than CLZ-related binding. For instance, an increased $[M+2+nH]^{n+}$ isotope signal from ^{37}Cl might have led to possible difficulties in isotope pattern recognition in DDA experiments. Detrimental effects on isotope pattern recognition might have also had detrimental effects on untargeted MS/MS acquisition.

Furthermore, other sample preparation aspects need to be discussed in detail as well. Using two proteases in parallel has proven to be a useful tool to improve GST sequence coverage of cysteine residues. However, several cysteine sites remained challenging. Most prominently, Cys102 in GSTP1 was not recovered after trypsin digestion (theoretical tryptic peptide: CK) and peptides from pepsin digestion were found to be low abundant. It was not possible to confidently detect any reactive metabolite binding to this cysteine site in both studies (APAP and CLZ/OLZ). In contrast, Jenkins *et al.* were able to confirm the binding of APAP's reactive metabolite NAPQI to Cys102 using AspN (Jenkins *et al.*, 2008) (see protease overview in Table 1.8). Thus, assay flexibility could be significantly increased by using additional or different proteases in combination with trypsin and pepsin. In addition, CLZ-related binding to GSTP1 was found only at Cys170, not Cys48 which Boerma *et al.* previously stated (Boerma *et al.*, 2011). This hinted at possible recovery and detection limiting effects which might have hindered modified peptide detection, even using appropriate proteases.

6.2.3 Challenges in HNE-chondrocyte protein analysis

Since HNE is a naturally occurring reactive compound and HNE-modifications appear under physiological conditions (Siems and Grune, 2003), identification of HNE-protein adducts related to specific OA-related questions necessitated non-OA

control samples. In Chapter 4 chondrocyte samples from 13 OA patients were compared to samples from two non-OA patients. Access to non-OA knee cartilage samples was limited due to low frequencies of OA-unrelated knee surgeries and low accessibility to discarded cartilage. An equally sized control group would have been more preferred and would have increased the significance of identified HNE-proteins unique to OA. In addition, an increased number of control samples would have allowed for relative quantitation of protein amounts in OA compared to non-OA, using label-free proteomics (Megger *et al.*, 2013). This could have given additional insight on OA-specific protein expression levels and could have complemented HNE-protein binding findings, without any additional sample preparation step. In addition, specific limitations in HNE-protein, especially HNE-histone, detection were prevalent as well. In general, histone sequence coverage was limited, not including the very basic histone tails in trypsin (and pepsin) digestions. Therefore, HNE-modifications potentially located at these histone tails could not be fully investigated, even though they are the main targets of regulative PTMs and vital factors in chromatin folding (Bannister and Kouzarides, 2011). Potential HNE binding to these sites remains interesting for future research.

6.2.4 Limitations in APAP-protein quantitation

Using a specifically optimized method to detect one NAPQI-hSA-derived peptide through pepsin digestion, limits the applicability of the assay in multiple regards. The assay was developed to answer NAPQI-hSA quantitative questions in a rapid manner (<24 h) with a sufficient assay dynamic range (7.65 $\mu\text{g/mL}$ to 3.48 mg/mL NAPQI-hSA in serum). As an effect, digestion, LC and MRM parameters would be significantly different for other NAPQI-modified proteins and would require a completely re-evaluated workflow. In addition, an isomeric cysteine labeling agent

(iodo-APAP) was used to prepare standards. This alkylation agent is only applicable in APAP-related binding studies and would not allow accurate quantitation of other reactive metabolite modifications (*e.g.*, from CLZ/OLZ metabolism or by HNE). In addition, limitations were present even in the quantitation of APAP-related binding. The used alkylating agent yielded a positional isomer to the actual NAPQI-Cys modification (see Figure 1.24). This had direct effects on LC elution of the standards, compared to the analyte. Slightly different elution times generally result in differences of ionization through differences in ESI droplet behavior and ion evaporation. Thus, isomeric iodo-APAP-standard and d₄-iodo-APAP-internal standard peptides could not fully correct for these effects. Another study limitation arose from the variability in patient serum sampling time. Sampling occurred between 1 and 9 days after APAP ingestion. This led to a relatively large range of NAPQI-hSA levels in both groups, non-spontaneous survivors and individuals with irreversible liver damage. A uniform sampling procedure could have potentially increased the significance of differences between NAPQI-hSA levels of both groups. Finally, the assay's quantitative performance can also be compared to related quantitative assays. Dynamic range and lower limit of quantitation (LLOQ) were compared to a preceding NAPQI-rat serum albumin (rSA) study (LeBlanc *et al.*, 2014). With a 450-fold dynamic range and an LLOQ of 7.65 µg/mL, the NAPQI-hSA assay was inferior to the NAPQI-rSA assay (0.30 µg/mL LLOQ and 700-fold dynamic range; >24 h analysis). However, certain adaptations to the human assay were possible by simple changes in the MRM dwell time settings. The assay was specifically altered to also cover lower concentration levels down to 1.39 µg/mL.

6.2.5 Perspectives and improvements

In order to discuss challenges and limitations properly, appropriate improvements need to be mentioned as well. Some perspectives were already briefly mentioned in the previous sections. An overview of perspectives and improvements, including aspects, which will be discussed in subsequent paragraphs, can be found in Table 6.1.

Table 6.1 Brief overview of possible improvements and their theoretical benefits

Improvement	Possible benefit
Immunoaffinity protein/peptide extraction	Increase in sensitivity and selectivity
Multiple protease proteomics	Increase in coverage of important binding sites
Accompanying toxicity and protein inhibition assessment	Correlation of protein binding with possible adverse effect mechanism
<i>In vivo</i> studies with appropriate cohort and control group size	Ideal scenario to study complex protein binding in comparison to control groups
Absolute or relative quantitation of modified proteins using appropriate standard material	Direct and accurate quantitative information of protein binding on the protein-level (or peptide-level)
GSH adduct detection via neutral loss and precursor ion scan	High sensitivity and unbiased detection of GSH adducts
GSH and protein adduct analysis via DIA-MS/MS	Fully unbiased and untargeted analysis of adduct MS2, and the possibility to use diagnostic ion finding strategies

GSH adduct analysis, as in Chapter 5, could be easily improved using available MS technologies (QTRAP[®] 5500) and data mining tools (MetabolitePilot[™]). Using a QqQ (or QqLIT) platform would enable the application of specific and sensitive neutral loss and precursor ion scans (see Figure 1.18). In studies by Dieckhaus *et al.* and Jian *et al.*, a negative and positive ion mode, analysis of $[M+nM]^{n+}$ and $[M-nM]^{n-}$ through fast polarity switching, was used to study unknown GSH adducts (Dieckhaus *et al.*, 2005; Jian *et al.*, 2012). GSH adducts were detected using a positive mode neutral loss scan of 129 u combined with a negative mode precursor ion scan of product ions at m/z 272 (see Table 1.6). This scanning technology enables highly sensitive detection of low abundant, also unpredicted GSH adduct species. In addition, using a QqLIT (such as the QTRAP[®] 5500) would allow for DDA-style analysis using a 129 u neutral loss survey scan and enhanced product ion scan for structural analysis via LIT-MS/MS acquisition with higher mass resolution (Jian *et al.*, 2012). If a QqQ platform would not be available, regular intensity-/isotope pattern-/mass defect-based DDA on a high-resolution QqTOF or Orbitrap MS could be paired with post-acquisition neutral loss and product ion filtering techniques. This would only be possible if GSH adduct MS/MS data is available. However, due to a lack of sufficient precursor sampling of low abundant species, MS/MS information might be missing for certain adducts. Thus, novel all ion fragmentation HRMS acquisition strategies, such as DIA (see Figure 6.4) (Ludwig *et al.*, 2018), could be paired with post-acquisition MS2 data filtration techniques. In these all ion fragmentation analyses, multiple precursor ions are isolated through a large Q_1 isolation window. This enables the fragmentation of all ions in MS1 in relatively reasonable cycle time. This could be used to detect low abundant and unpredicted GSH adducts, and also to collect high-resolution fragmentation spectra for structural elucidation.

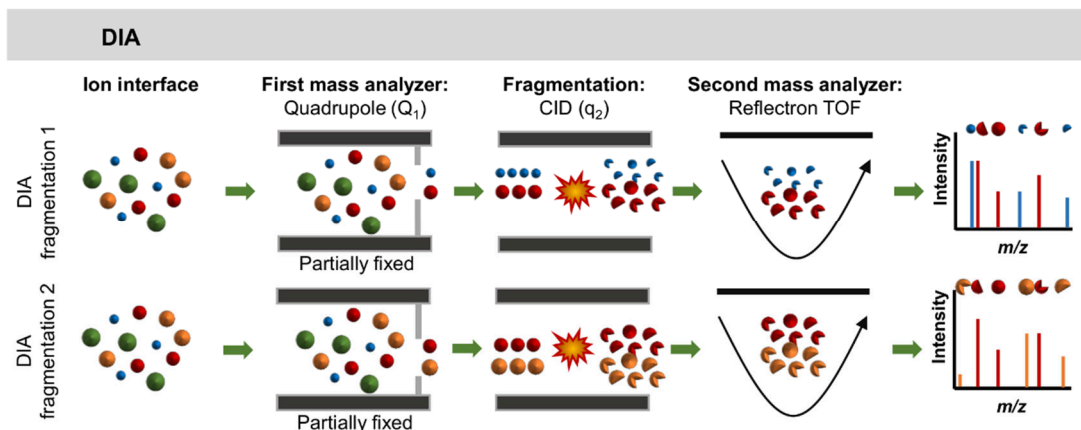


Figure 6.4 Exemplary principle of DIA MS/MS analysis on a QqTOF platform. All or a selection of precursor ions are sequentially fragmented by isolating multiple precursor ions at once through Q_1 windows of multiple mass units. Generally, these isolation windows are sequentially scanned in each acquisition cycle and normally overlap (~ 1 u) to allow homogenous precursor sampling. Resulting MS/MS are normally composite MS/MS of multiple precursors.

In terms of detecting low abundant modified peptides in complex peptide mixtures, some technical MS developments could improve data acquisition limits. Regular peptide DDA is limited in terms of reproducibility and coverage of low abundant features (Michalski *et al.*, 2011). Good quality MS/MS of modified peptides is necessary to identify the reactive metabolite-peptide and its modification site accurately. Furthermore, the detection of diagnostic fragment ions, related to the reactive metabolite-amino acid bond, is highly important for confident identification. These factors could be theoretically improved by DIA techniques as well. An all ion fragmentation analysis would theoretically lead to the collection of all detectable reactive metabolite-peptide MS/MS throughout the whole cycle time, which then can be analyzed on the presence of specific diagnostic fragment ions. However, in addition to highly complex composite MS/MS and missing MS1-MS2 spectra pairs, current MS

acquisition speeds and sophisticated software packages are not fully available. However, constant improvement in hardware and software might open novel, highly sensitive strategies using DIA analysis in (modified) peptide detection in future applications.

Another important limitation in modified peptide studies is often the lack of quantitative information. ESI-MS signals are not directly dependent on analyte concentration and make quantitative conclusions without the use of internal standards highly difficult, up to impossible. In addition, proteolytic specificities and peptide recovery effects do not permit trivial comparison of multiple binding sites in the same protein (*e.g.*, NAPQI-modification at Cys15, 48 and 170 in hGSTP1). Notwithstanding, a quantitative understanding of protein binding is one of the first steps in understanding potential protein inhibition effects. One way to follow up on reactive metabolite-protein binding studies could be an absolute or relative quantitation study, analyzing protein adducts using calibration standards and internal standards. Depending on availability, an ideal scenario would involve a standard as the modified protein in purified form with known concentration. However, this is very difficult to obtain. Alternatives could be isomeric modified proteins, modified peptides or chemical analogs on the protein or peptide-level. Taking advantage of the cysteine alkylating agents iodo-APAP and d₄-iodo-APAP it would be, therefore, possible to create isomeric standard material by labeling purified proteins or peptides. This could be a viable addition to the findings in Chapter 3. By labeling recombinant GSTs with iodo-APAP and d₄-iodo-APAP, custom-made standard materials could be used for absolute peak signal calibration at relevant levels, or for relative quantitation. Theoretically, these isomeric labeling agents would be possible for other reactive metabolites too, such as nitrenium ions or HNE, but would need sophisticated and careful chemical synthesis.

Finally, as briefly discussed in Section 6.2.2, *in vitro* studies are limited on several aspects: 1) no exact replication of cellular conditions, 2) no or incomplete cellular response to stimuli, 3) gradual reduction of enzyme expression/activity in cell cultures, 4) missing compound flow and extraction mechanism, and 5) only the possibility of single/simplified cell cultures and missing combination of multiple tissues/organs with different properties (Gómez-Lechón *et al.*, 2003). Thus, findings of *in vitro* studies, in most cases, require validation through *in vivo* studies. However, clinical *in vivo* studies of reactive metabolite formation in human are often hindered by low predictability of outcome and the danger of potential harm. Thus, animal models are one common option to account for *in vivo* metabolism of drugs and other compounds. These studies often include a rodent model in rat or mouse, even though significant differences between species exist (Lewis *et al.*, 1998). Nevertheless, in some cases *in vivo* reactive metabolite or drug toxicity studies are possible. Especially in the scenario of (involuntary) overdose/misusage (as described in Chapter 2), valuable information might be accessible. However, in these scenarios, participant selection and reproducible sampling protocols are often impeded or simply not feasible. Ideal human clinical studies are rarely applicable in drug toxicity and IADR assessment but would yield valuable information to better understand these effects and to better predict them in (drug) preapproval testing (Splawiński *et al.*, 2006).

APPENDIX A

FIGURES OF APAP-PEPTIDE CHROMATOGRAMS, MS AND MS/MS SPECTRA, AND PEPTIDE DISTRIBUTION IN CONCATENATED FRACTIONS

The complete Supplementary Material for this article can be found online at: <https://www.frontiersin.org/articles/10.3389/fchem.2019.00558/full#supplementary-material>.

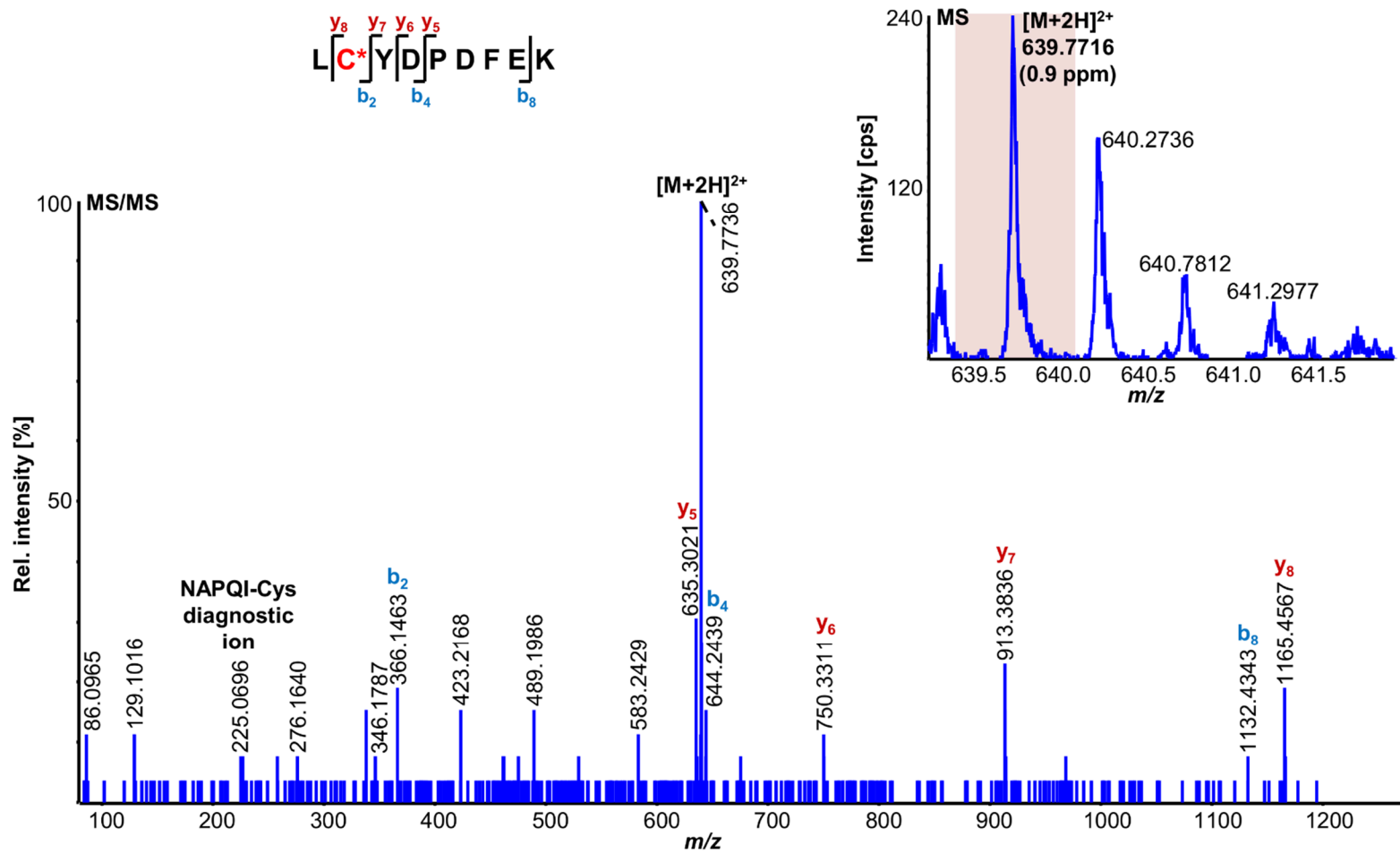


Figure S1C DDA spectra of NAPQI-GSTM2 tryptic peptide LC*YDPDFEK (acquired at 20.3 min).

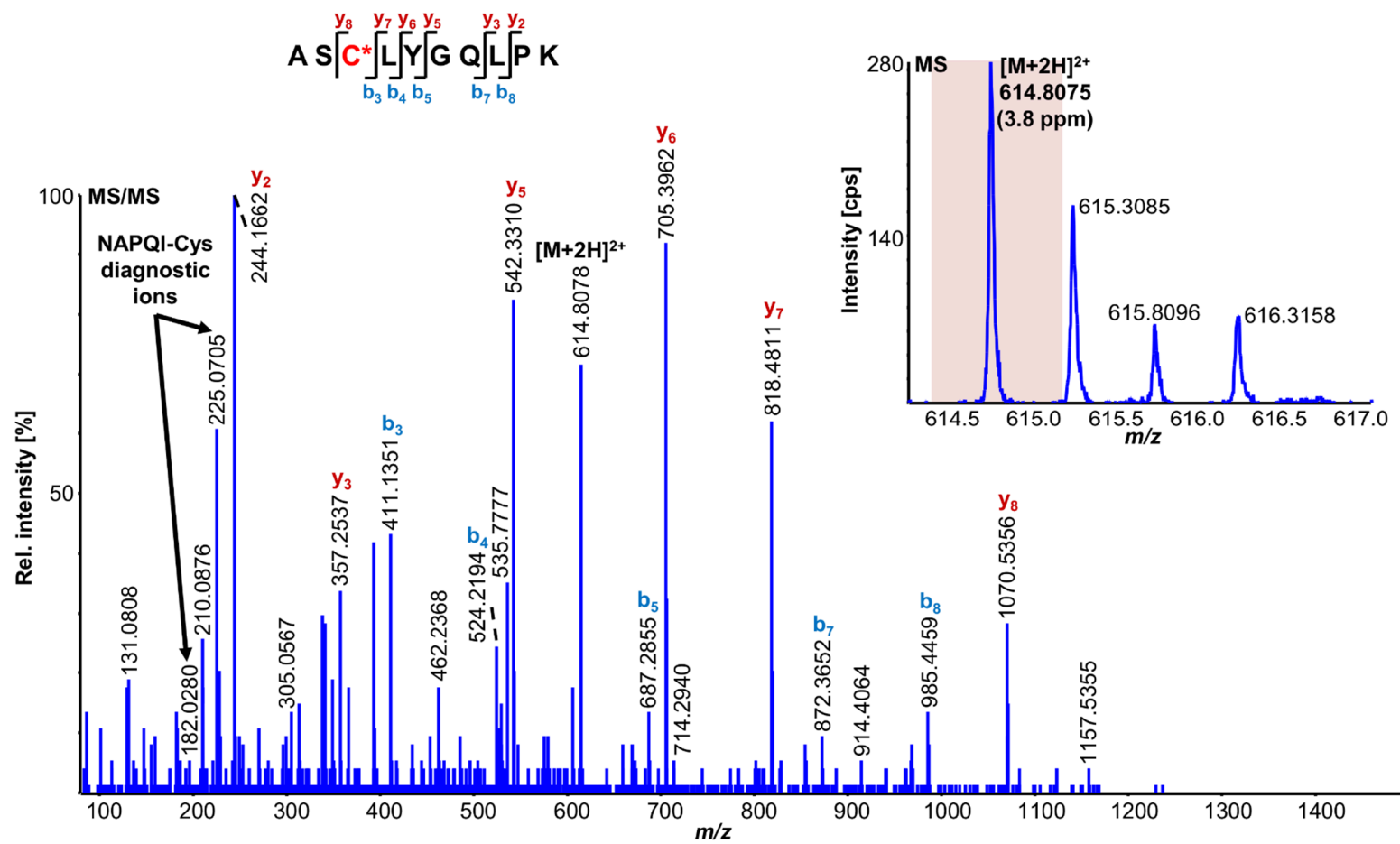


Figure S1D DDA spectra of NAPQI-GSTP1 tryptic peptide ASC*LYGQLPK (acquired at 19.7 min).

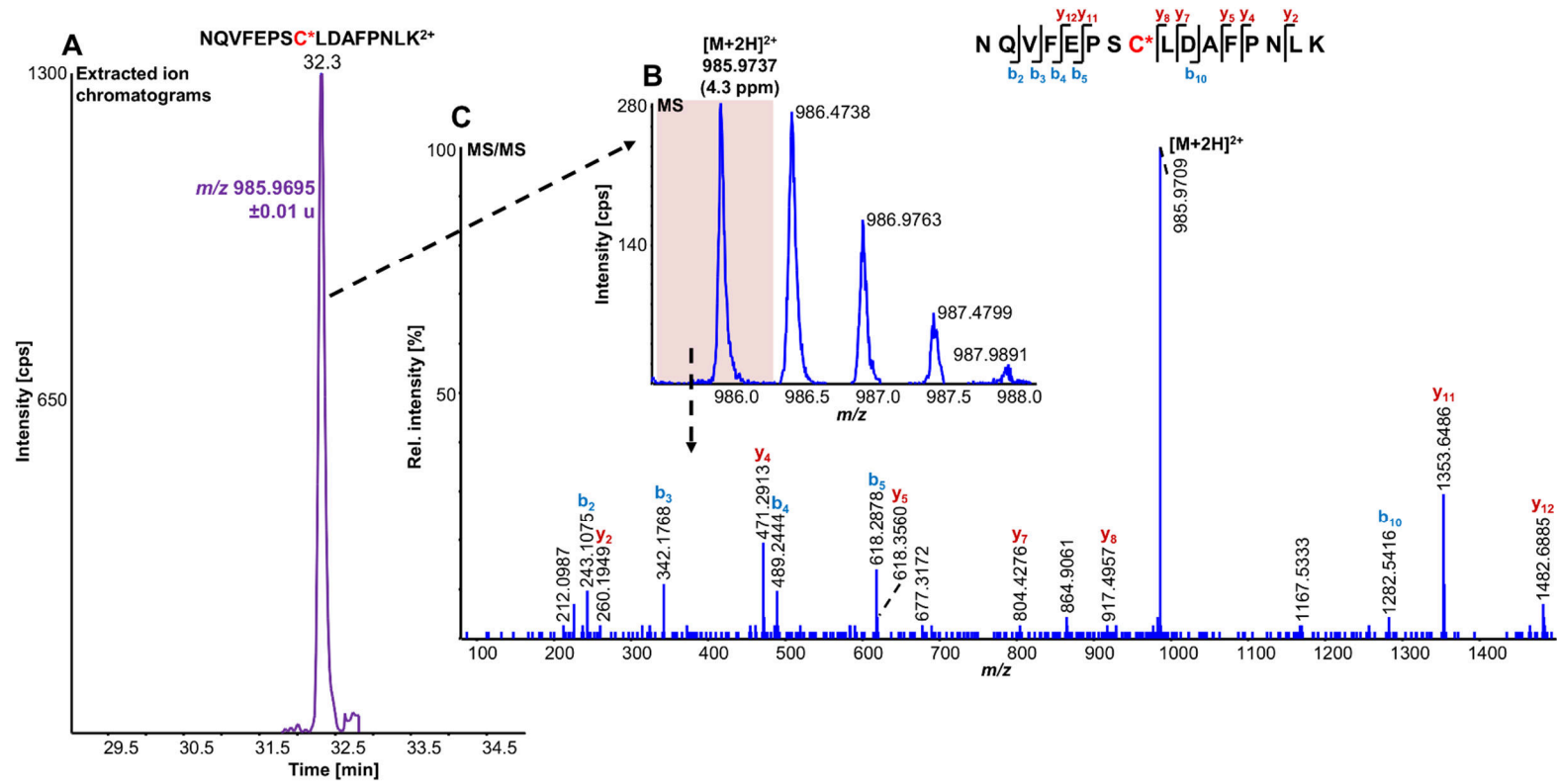


Figure S2 Extracted ion chromatogram of NAPQI-GSTM2 tryptic peptide NQVFEPSC*LDAFPNLK (A), including survey scan MS (B) and triggered MS/MS (C).

MGST1_RAT
Cys50

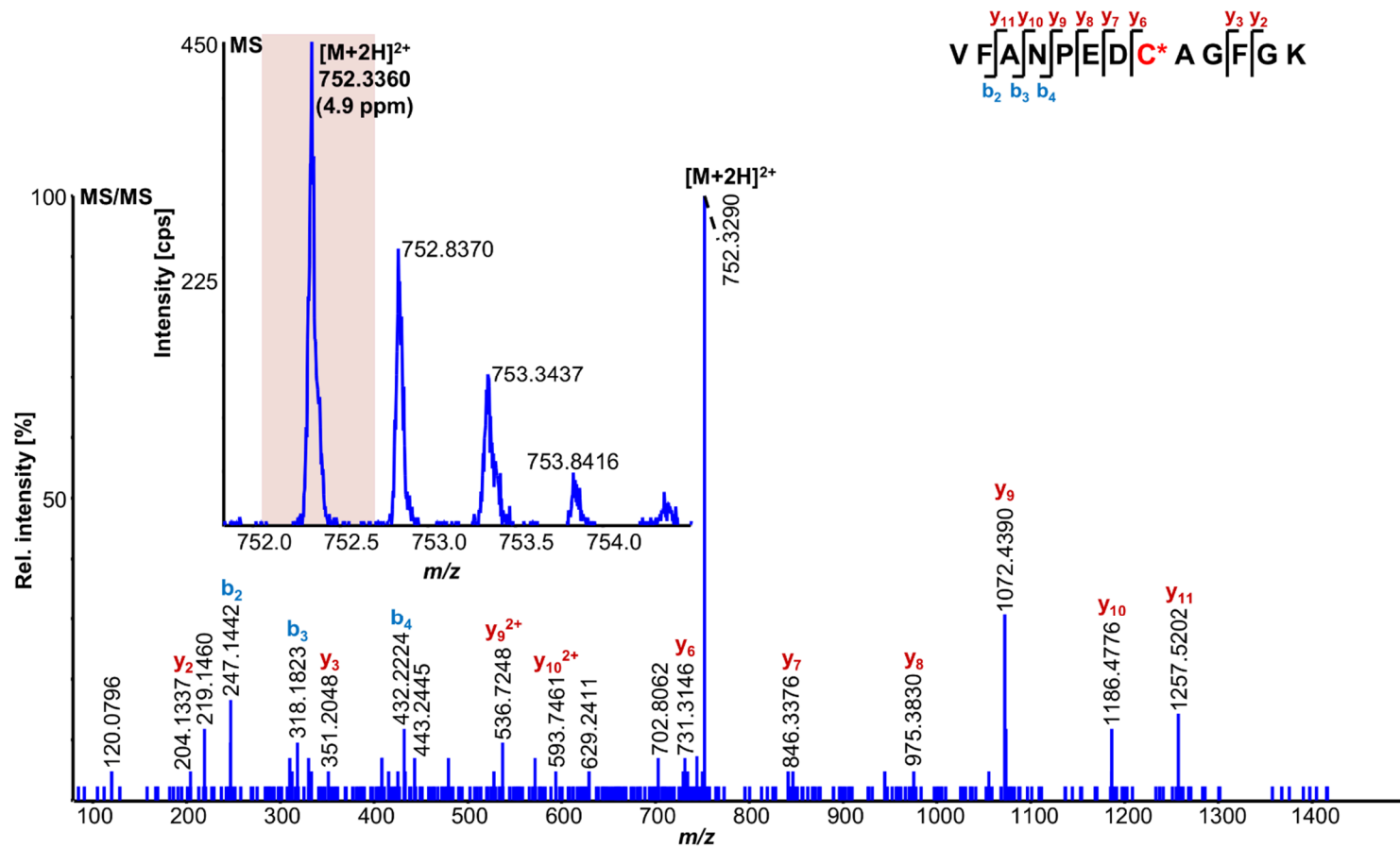


Figure S3 DDA spectra of NAPQI-rat MGST1 tryptic peptide VFANPEDC*AGFGK (acquired at 22.0 min).

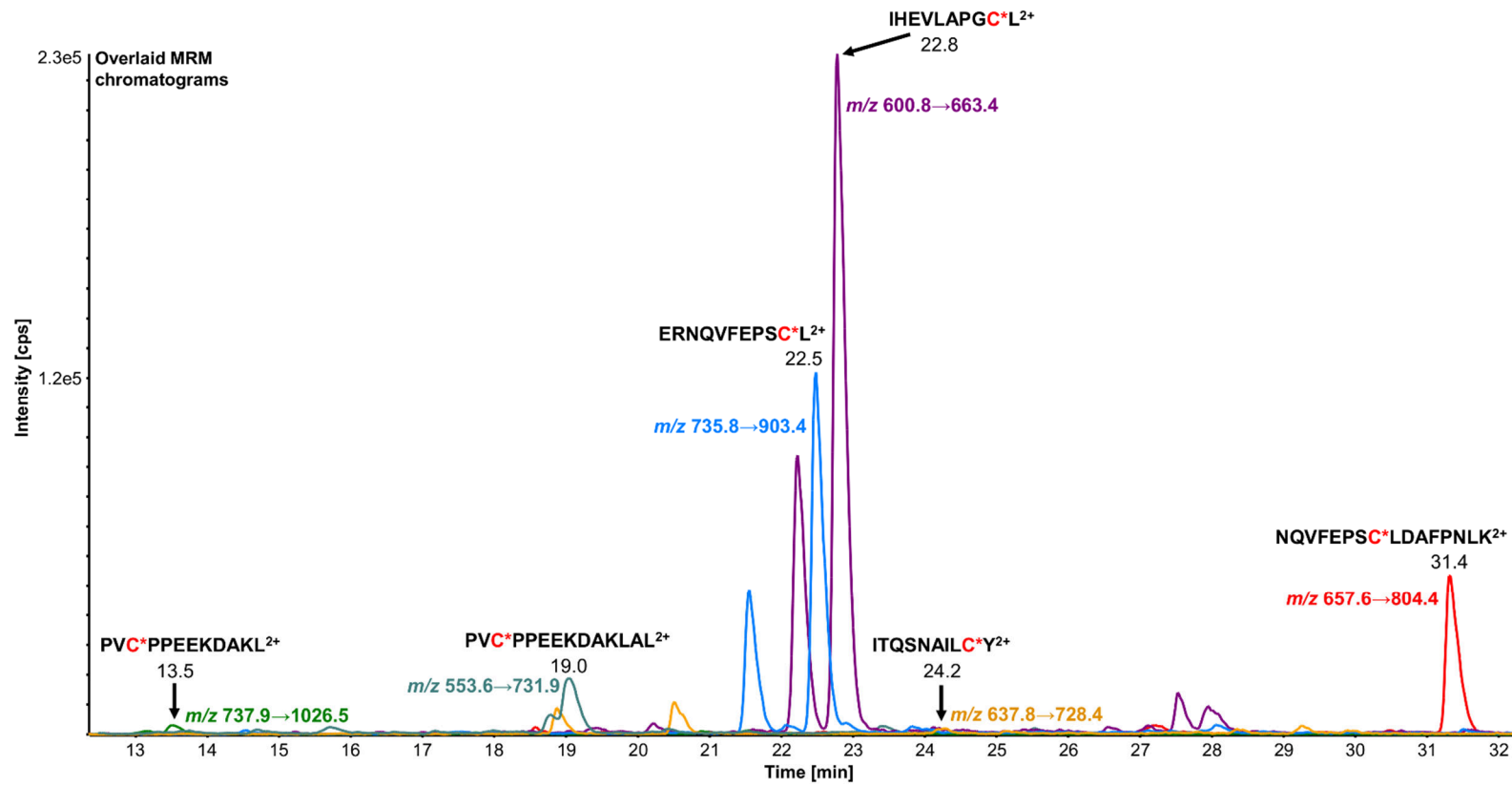


Figure S4 Overlaid MRM chromatograms (60 min LC) of found modified peptides using RLM incubation and SPE purification.

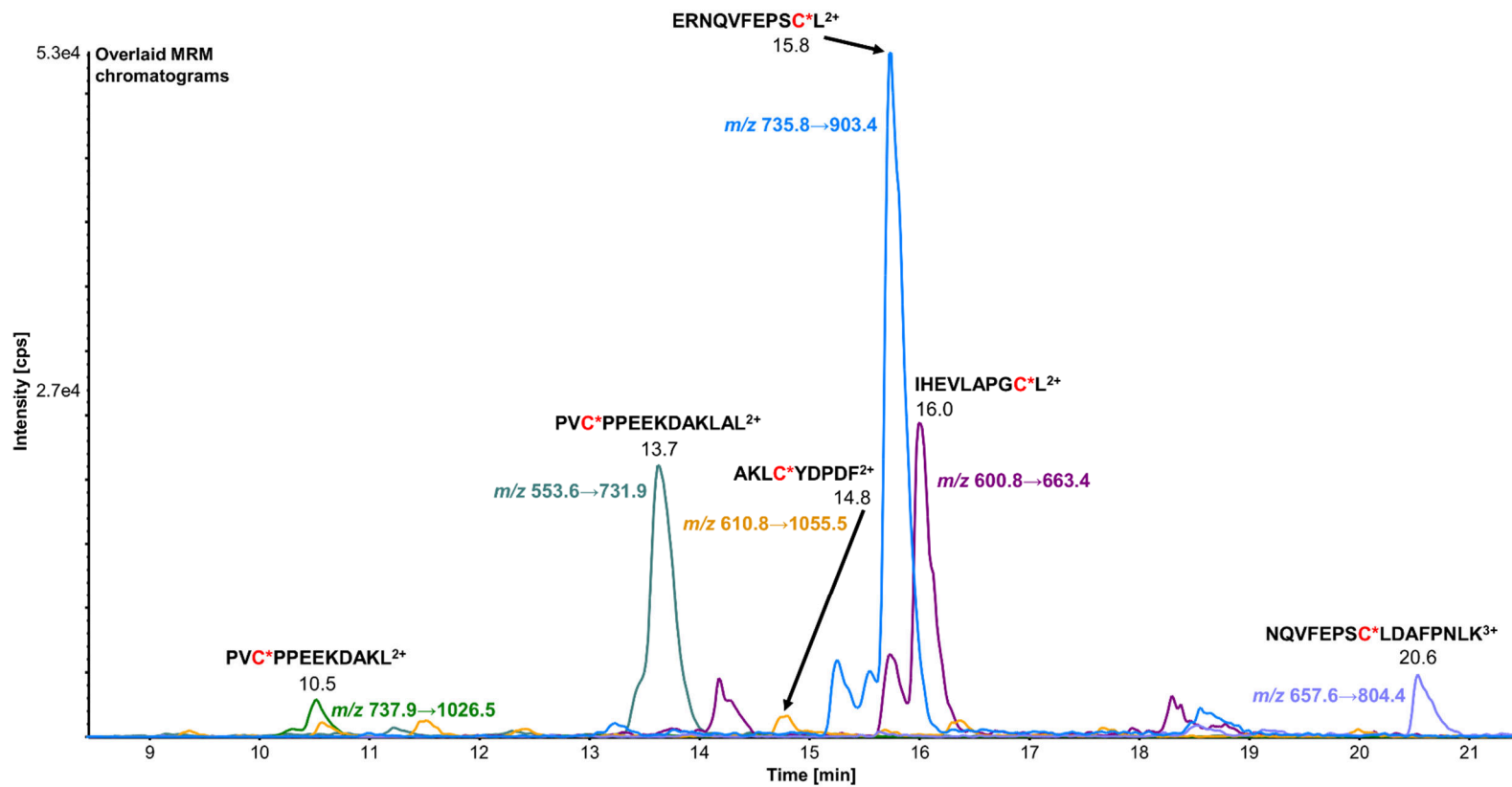


Figure S5 Overlaid MRM chromatograms (30 min LC) of found modified peptides using RLM incubation, SPE purification and high-pH RP fractionation.

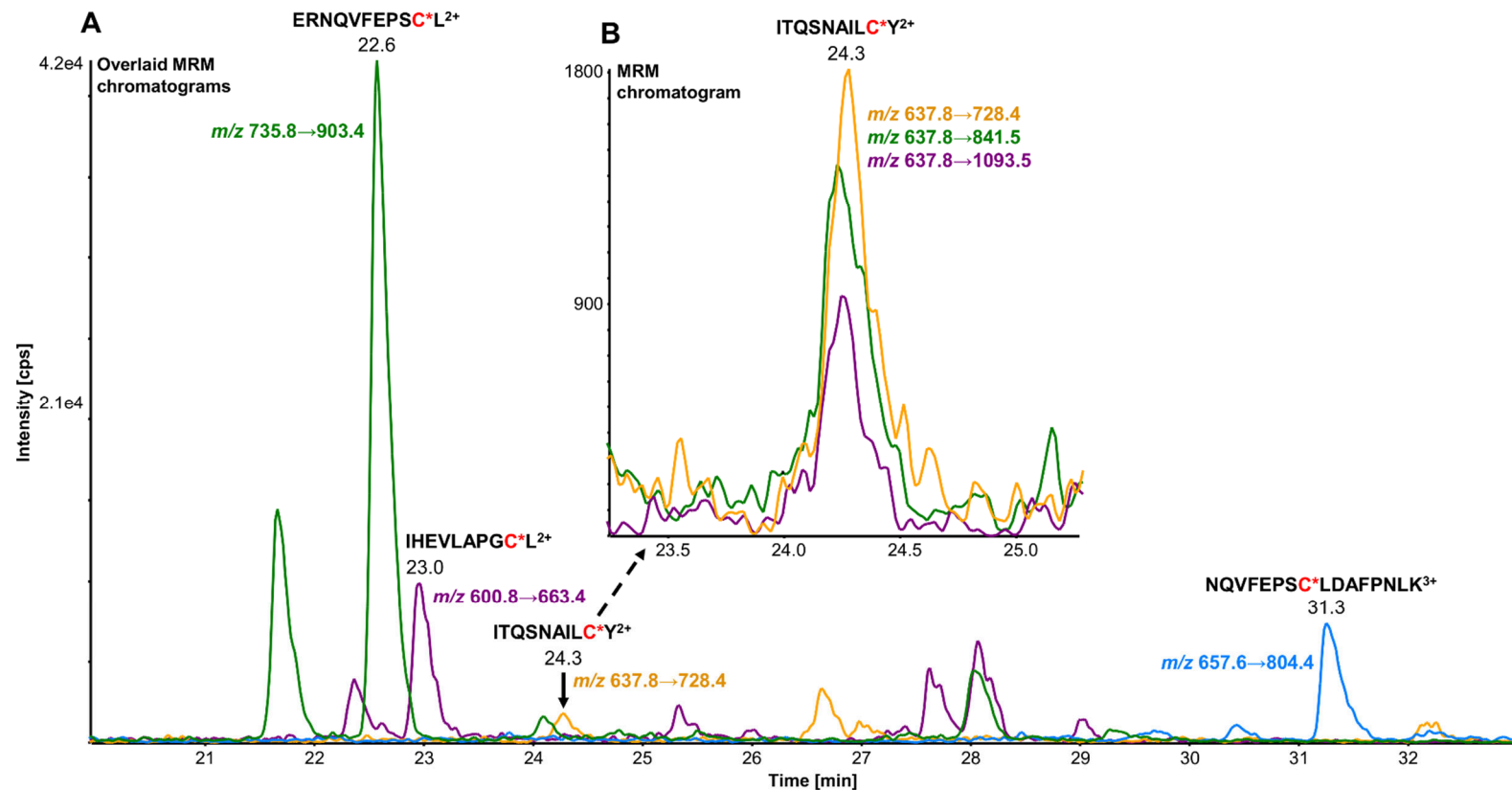


Figure S6 Overlaid MRM chromatograms (60 min LC) of found modified peptides using CYP3A4 Supersomes incubation and SPE purification (A), including peptide ITQSNAILC*Y (B).

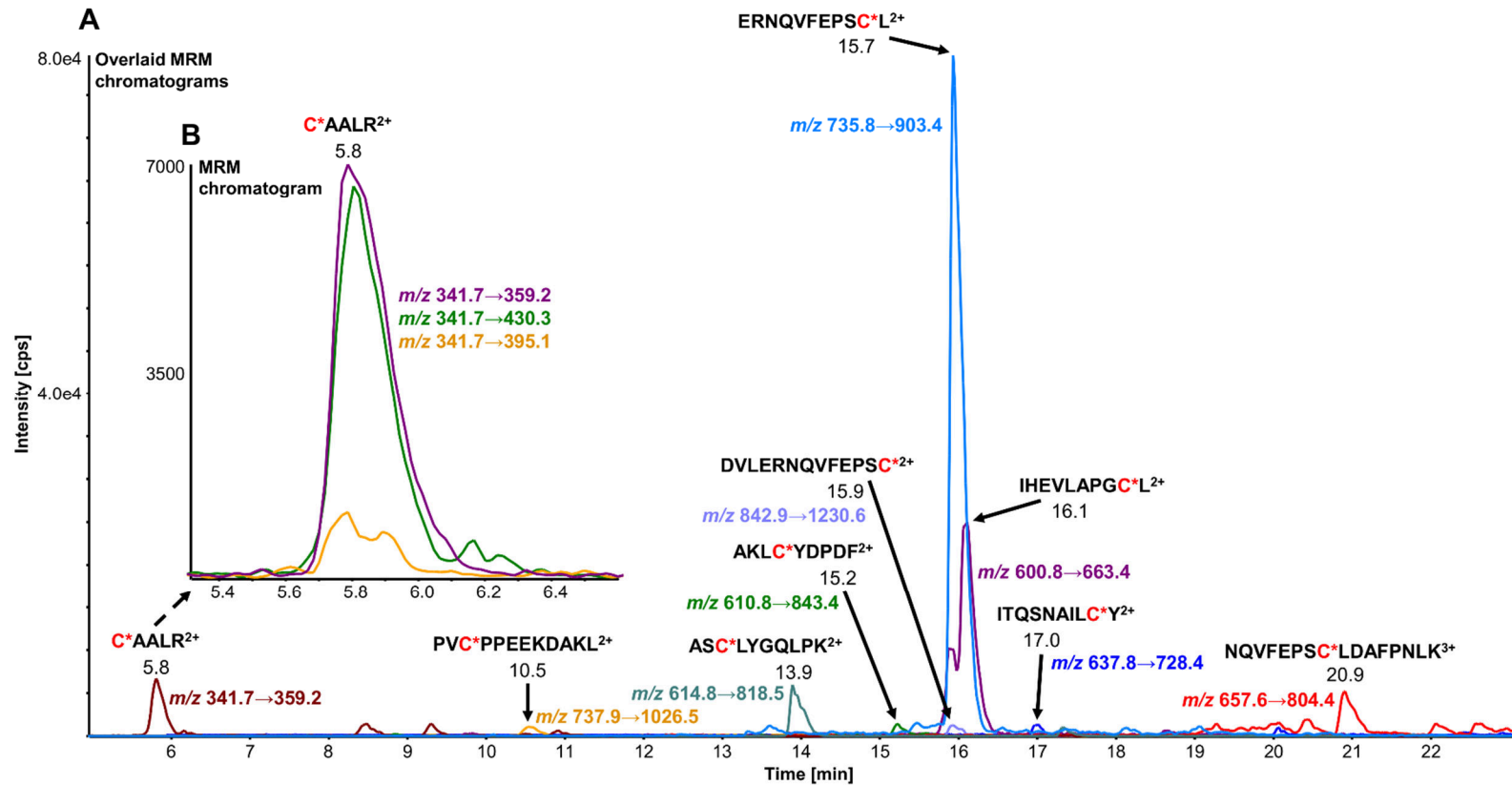


Figure S7 Overlaid MRM chromatograms (30 min LC) of found modified peptides using CYP3A4 Supersomes incubation, SPE purification and high-pH RP fractionation (A), including peptide C*AALR (B).

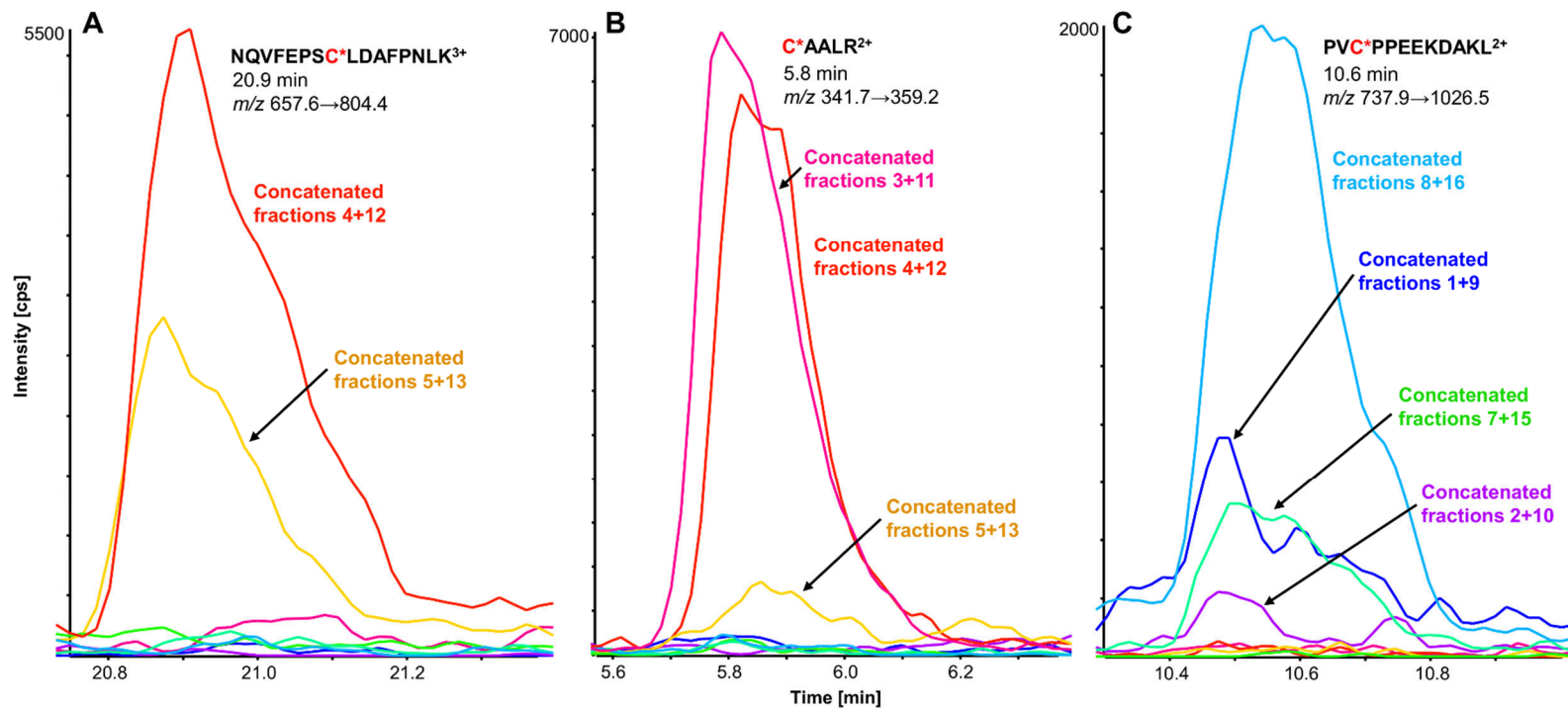


Figure S8 Distribution of selected MRM transitions over all concatenated fractions of peptides NQVFEPSC*LDAFPNLK (A), C*AALR (B) and PVC*PPEEKDAKL (C), showing individual differences in elution during high-pH RP fractionation.

APPENDIX B

METHODS OF HNE-CHONDROCYTE PROTEIN QUANTITATION, WESTERN BLOT, AND MS/MS SPECTRA AND ENRICHMENT ANALYSIS RESULTS

The complete Supplementary data to this article can be found online after publication at <https://www.journals.elsevier.com/journal-of-proteomics>.

Protein quantitation and western blot analysis

Protein concentrations were determined using bicinchoninic acid (BCA) method (Pierce, Rockford, IL). Nuclear, cytosolic or whole cell protein extracts (20 µg) were subjected to a discontinuous 4–12% SDS-PAGE, then electrotransferred to a nitrocellulose membrane (Bio-Rad Laboratories, Hercules, CA). After protein transfer, membranes were blocked overnight in 5% (w/v) skim milk, washed with TBS (pH 7.5 with 0.1% (v/v) Tween-20), and incubated for 2 h with a polyclonal rabbit anti-HNE primary antibody (1:1,000 dilution). After additional washes, membranes were incubated with a horseradish peroxidase-conjugated secondary anti-rabbit IgG antibody for 1 h at 22°C, and washed again. Protein detection was carried out using SuperSignal chemiluminescent substrates (Thermo Fisher Scientific, Waltham, MA), followed by exposing the membranes to HyBlot CL autoradiography film (Denville Scientific Inc., Holliston, MA). The films were subjected to an X-ray film processor (AFP Manufacturing, Peachtree City, GA).

Immunoprecipitation and HDAC activity assay

To identify the formation of HNE-histone deacetylase 2 (HDAC2) and HNE-histone adducts, human OA chondrocytes (1.5×10^6 cells/well) were incubated with increasing concentrations of HNE (0, 1, 5, 10 and 20 μM) for 24 h at 37°C in the presence of 5% carbon dioxide/95% air. Culture medium was collected, and cells lysed using cold radioimmunoprecipitation assay buffer (RIPA) (150 mM NaCl, 1 mM EDTA, 40 mM Tris, pH 7.6, Triton X-100 at 1%) supplemented with a protease inhibitor cocktail (Sigma-Aldrich) (Bentz *et al.*, 2012). Following 15 min on ice and samples were mixed and centrifuged (4°C, 10 min, 12,000 rpm). The supernatant was recovered, and the protein concentration quantified by BCA. Then, 50 μg of total proteins were immunoprecipitated using mouse anti-human HDAC2, mouse anti-human histone H2A and H2B (R&D Systems, Minneapolis, MN), and anti-acetylated histone H2A (K5) and anti-acetylated histone H2B (K20) (Cell Signaling Technology) at 1 $\mu\text{g}/\text{mL}$ (overnight, 4°C) followed by a 2 h incubation with protein A-Agarose resin (Santa Cruz Biotechnology, Santa Cruz, CA). The resin was washed several times with RIPA and immunoprecipitates were collected (1,000 rpm) and analyzed by Western blotting using anti-HNE rabbit antibody at 1:1,000 dilution. The membranes were washed again and incubated with the secondary antibody goat anti-mouse immunoglobulin G conjugated to horseradish peroxidase (1:5,000 dilution; Jackson ImmunoResearch, West Grove, PA). Immunoreactive proteins were detected with SuperSignal Blotting substrate (Thermo Fisher Scientific) and exposed to Kodak X-Omat film (Denville Scientific Inc.). Total histone H2A and H2B was revealed by incubation of nitrocellulose membrane with mouse anti-human histone H2A and H2B antibody followed by the secondary anti-rabbit IgG antibody.

First-passage OA chondrocytes were seeded at 1.2×10^6 cells/well in 6-well tissue culture plates and incubated for 48 h. The experiments were performed in

DMEM with 1 % FBS and antibiotics. Cells were treated with increasing concentrations of HNE (1–20 μ M) for 16 h. Then, culture medium was removed and cells washed three times with PBS and incubated with lysis buffer (40 mM Tris (pH 8.0), 250 mM NaCl, 0.1% NP-40, 5 mM EDTA, 5 mM EGTA, 10 mM β -glycerophosphate, 10 mM sodium fluoride, 0.3 mM sodium orthovanadate, 1 mM DTT) supplemented with protease inhibitor cocktail. Protein concentration of the cell lysates was measured by BCA assay and total HDAC activity was assessed with a commercial kit (Cayman Chemical). Absorbance was measured with a micro-ELISA Vmax photometer (BioTek Instruments, Winooski, VT).

Supporting tables

Table S1 List of peptides and proteins identified through LC-MS/MS proteomics and database searching

Sample (extract)	Protein quantity [µg]	Protease	Peptides at local 1% FDR	Proteins at local 1% FDR	Sample note
Disease nuclear 1	7.3	Trypsin	2385	310	
Disease nuclear 2	13.0	Trypsin	3172	379	
Disease nuclear 3	58.4	Trypsin	4077	520	
Disease nuclear 4	46.6	Trypsin	2850	328	
Disease nuclear 5	48.0	Trypsin	2974	366	
Disease nuclear 6	100.4	Trypsin	3403	434	
Disease cytosolic 1	14.8	Trypsin	3395	553	
Disease cytosolic 2	13.1	Trypsin	5054	727	
Disease total extract 1	11.7	Trypsin	3199	434	
Disease total extract 2	62.5	Pepsin	1230	312	Samples split in two for trypsin and pepsin digestions
	62.5	Trypsin	6108	636	
Disease total extract 3	72.5	Pepsin	1766	369	
	72.5	Trypsin	6303	824	
Disease total extract 4	57.5	Pepsin	1766	369	
	57.5	Trypsin	5319	808	
Disease total extract 5	80.0	Pepsin	1188	309	
	80.0	Trypsin	5311	826	
Healthy total extract 1	52.5	Pepsin	1313	300	
	52.5	Trypsin	5186	710	
Healthy total extract 2	77.5	Pepsin	1538	388	
	77.5	Trypsin	5289	777	

Table S4A List of enriched GO terms (against total protein-coding genome) related to HNE-protein binding unique to OA disease (without **overlap** and **associated genes**)

Gene set	Description	-Log₁₀ FDR	Log₂ enrichment ratio
GO:0006401	RNA catabolic process	15.50	3.80
GO:0006413	Translational initiation	15.50	4.27
GO:0070972	Protein localization to endoplasmic reticulum	15.40	4.45
GO:0090150	Establishment of protein localization to membrane	11.84	3.42
GO:0006605	Protein targeting	11.84	3.17
GO:1903311	Regulation of mRNA metabolic process	9.64	3.41
GO:0002181	Cytoplasmic translation	9.35	4.40
GO:0010608	Posttranscriptional regulation of gene expression	8.66	2.78
GO:0008380	RNA splicing	6.91	2.76
GO:0032200	Telomere organization	4.94	3.44
GO:0022613	Ribonucleoprotein complex biogenesis	4.90	2.49
GO:0031647	Regulation of protein stability	4.66	2.86
GO:0006397	mRNA processing	4.44	2.34
GO:0071826	Ribonucleoprotein complex subunit organization	4.13	2.85
GO:0002446	Neutrophil mediated immunity	3.64	2.21
GO:0036230	Granulocyte activation	3.63	2.20
GO:0019058	Viral life cycle	3.63	2.63
GO:0051169	Nuclear transport	3.61	2.45
GO:0034248	Regulation of cellular amide metabolic process	3.33	2.33
GO:0071897	DNA biosynthetic process	3.33	2.91
GO:0003012	Muscle system process	2.98	2.20

Table S4A Continued

Gene set	Description	-Log₁₀ FDR	Log₂ enrichment ratio
GO:0006090	Pyruvate metabolic process	2.73	3.20
GO:0009141	Nucleoside triphosphate metabolic process	2.69	2.38
GO:0009123	Nucleoside monophosphate metabolic process	2.53	2.31
GO:0035966	Response to topologically incorrect protein	2.50	2.71
GO:0046390	Ribose phosphate biosynthetic process	2.50	2.47
GO:0072522	Purine-containing compound biosynthetic process	2.37	2.40
GO:0017038	Protein import	2.23	2.55
GO:0043331	Response to dsRNA	2.21	3.76
GO:0043900	Regulation of multi-organism process	2.20	2.11
GO:0072524	Pyridine-containing compound metabolic process	2.20	2.79
GO:0006403	RNA localization	2.09	2.44
GO:0007568	Aging	2.09	2.22
GO:0051052	Regulation of DNA metabolic process	1.93	1.97
GO:0060249	Anatomical structure homeostasis	1.92	1.96
GO:0009259	Ribonucleotide metabolic process	1.91	1.82
GO:1901293	Nucleoside phosphate biosynthetic process	1.78	2.04
GO:0034504	Protein localization to nucleus	1.75	2.21
GO:0030048	Actin filament-based movement	1.70	2.74
GO:0009895	Negative regulation of catabolic process	1.63	2.13
GO:0045088	Regulation of innate immune response	1.62	1.93
GO:0010639	Negative regulation of organelle organization	1.62	1.93
GO:1903320	Regulation of protein modification by small protein conjugation or removal	1.54	2.29

Table S4A Continued

Gene set	Description	-Log₁₀ FDR	Log₂ enrichment ratio
GO:2001233	Regulation of apoptotic signaling pathway	1.53	1.87
GO:0015931	Nucleobase-containing compound transport	1.41	2.18
GO:0046939	Nucleotide phosphorylation	1.40	2.88
GO:0016072	rRNA metabolic process	1.40	2.16
GO:0007178	Transmembrane receptor protein serine/threonine kinase signaling pathway	1.34	1.91
GO:0071103	DNA conformation change	1.33	2.11

Table S4B List of enriched GO terms (against list of identified proteins in OA samples) related to HNE-protein binding unique to OA disease (without **overlap** and **associated genes**)

Gene set	Description	-Log₁₀ FDR	Log₂ enrichment ratio
GO:0006401	RNA catabolic process	6.73	1.89
GO:0006413	Translational initiation	4.76	1.88
GO:0070972	Protein localization to endoplasmic reticulum	3.99	1.98
GO:0090150	Establishment of protein localization to membrane	3.98	1.79
GO:0006605	Protein targeting	3.98	1.66
GO:0010608	Posttranscriptional regulation of gene expression	2.72	1.50
GO:1903311	Regulation of mRNA metabolic process	2.69	1.66
GO:0002181	Cytoplasmic translation	2.43	2.03
GO:0003012	Muscle system process	2.34	1.98
GO:0032200	Telomere organization	1.99	2.11
GO:0031647	Regulation of protein stability	1.91	1.80
GO:0043331	Response to dsRNA	1.82	3.43

Table S5A List of enriched pathways (against list of identified proteins in OA samples) related to HNE-protein binding unique to OA disease (without **overlap** and **associated genes**)

Gene set	Description	-Log₁₀ FDR	Log₂ enrichment ratio
WP477	Cytoplasmic ribosomal proteins	13.32	4.00
WP534	Glycolysis and gluconeogenesis	2.55	3.49
WP107	Translation factors	2.36	3.28
WP438	Non-homologous end joining	2.23	5.17
WP411	mRNA processing	2.02	2.42
WP4018	Pathways in clear cell renal cell carcinoma	1.46	2.57

Table S5B List of enriched pathways (against list of identified proteins in OA samples) related to HNE-protein binding unique to OA disease (without **overlap** and **associated genes**)

Gene set	Description	-Log₁₀ FDR	Log₂ enrichment ratio
WP477	Cytoplasmic ribosomal proteins	3.16	1.72

Supporting figures

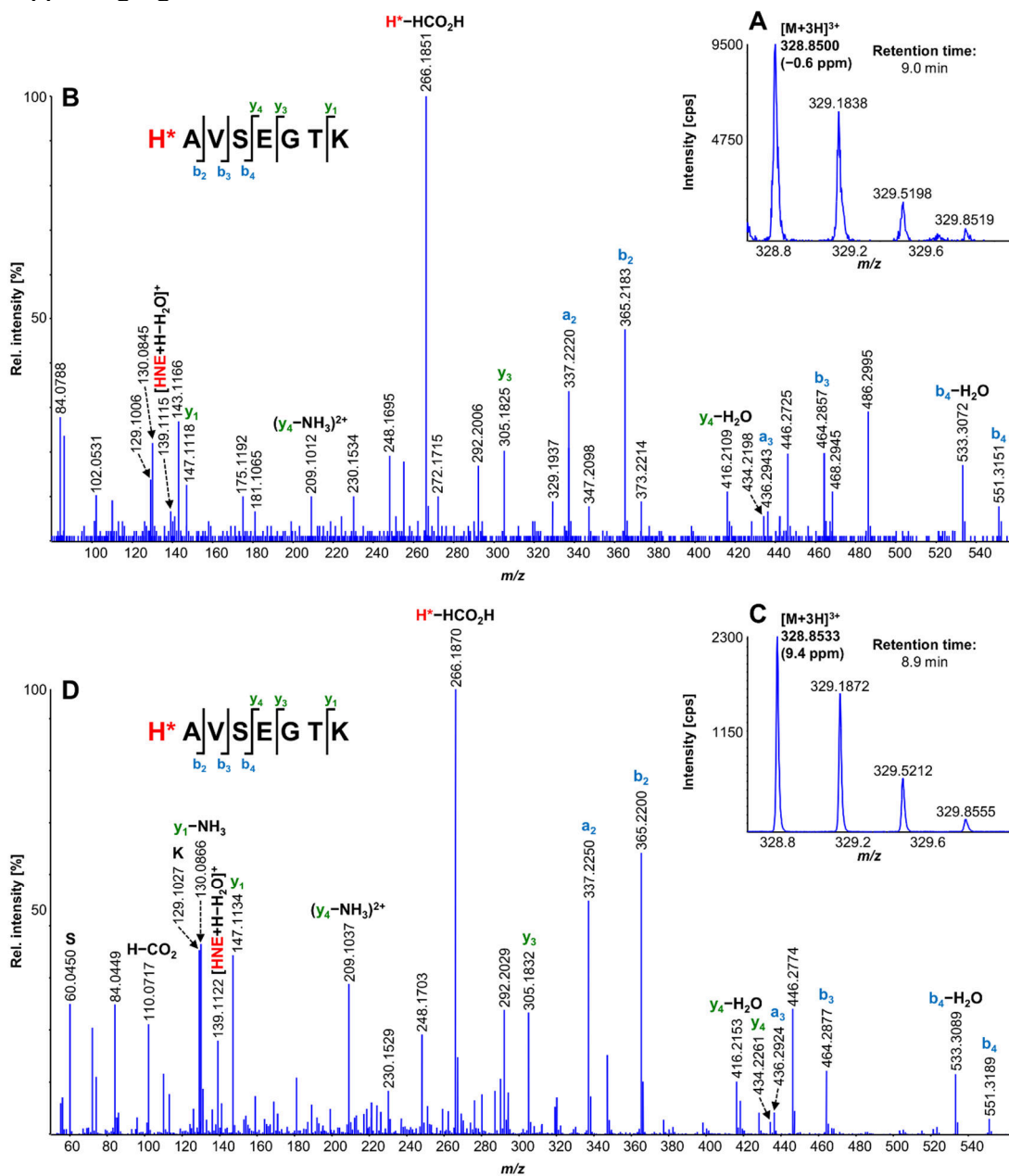


Figure S1 MS (A) and MS/MS (B) spectra of HNE-modified histone peptide H*AVSEGTK (His110 in histone H2B) identified in OA chondrocytes (not HNE-treated), compared to modified standard peptide (C and D).

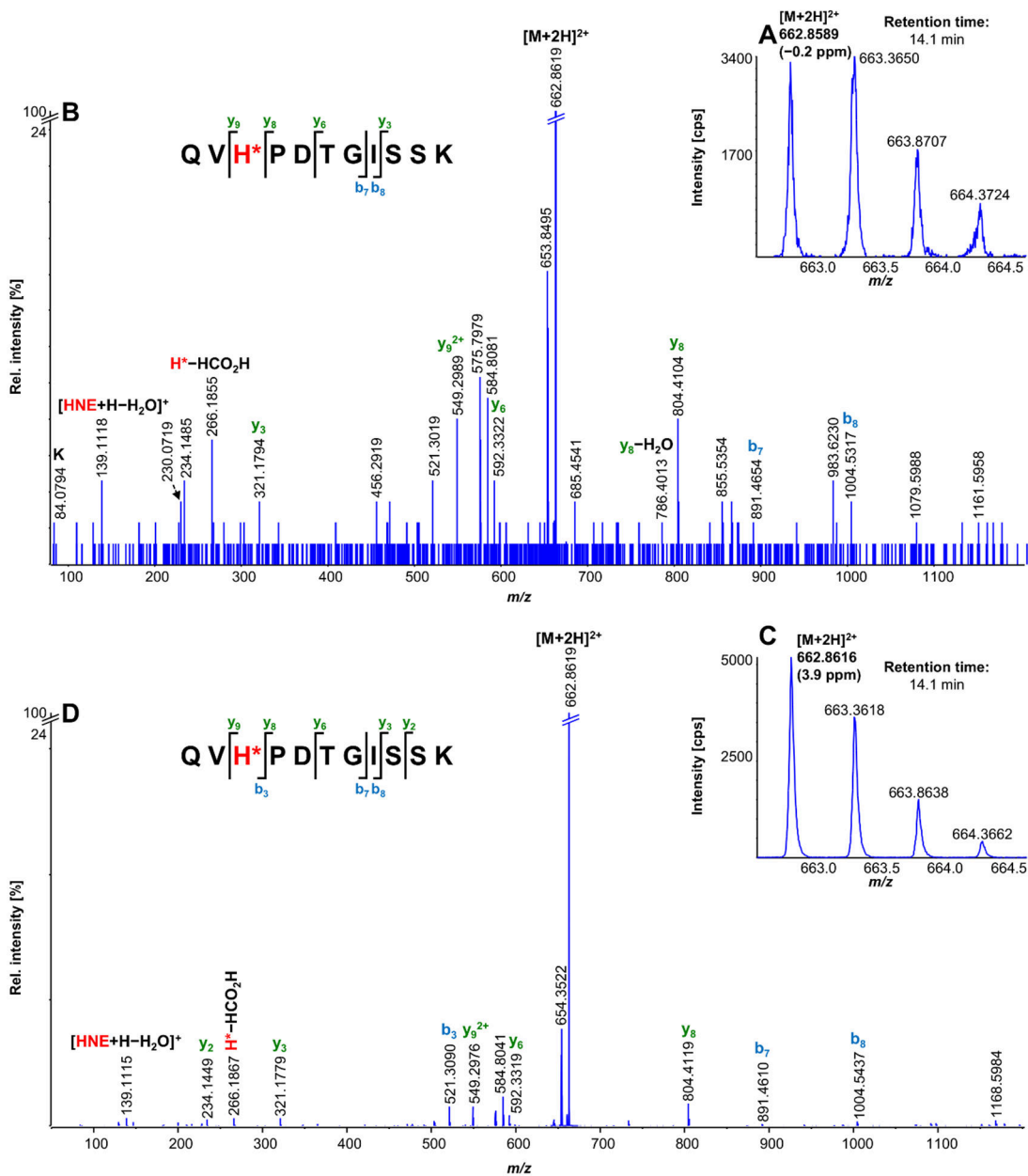


Figure S2 Comparison of MS (A) and MS/MS (B) spectra of HNE-modified histone peptide QVH*PDTGISSK (His50 in histone H2B) identified in OA chondrocytes (not HNE-treated), compared to modified standard peptide (C and D).

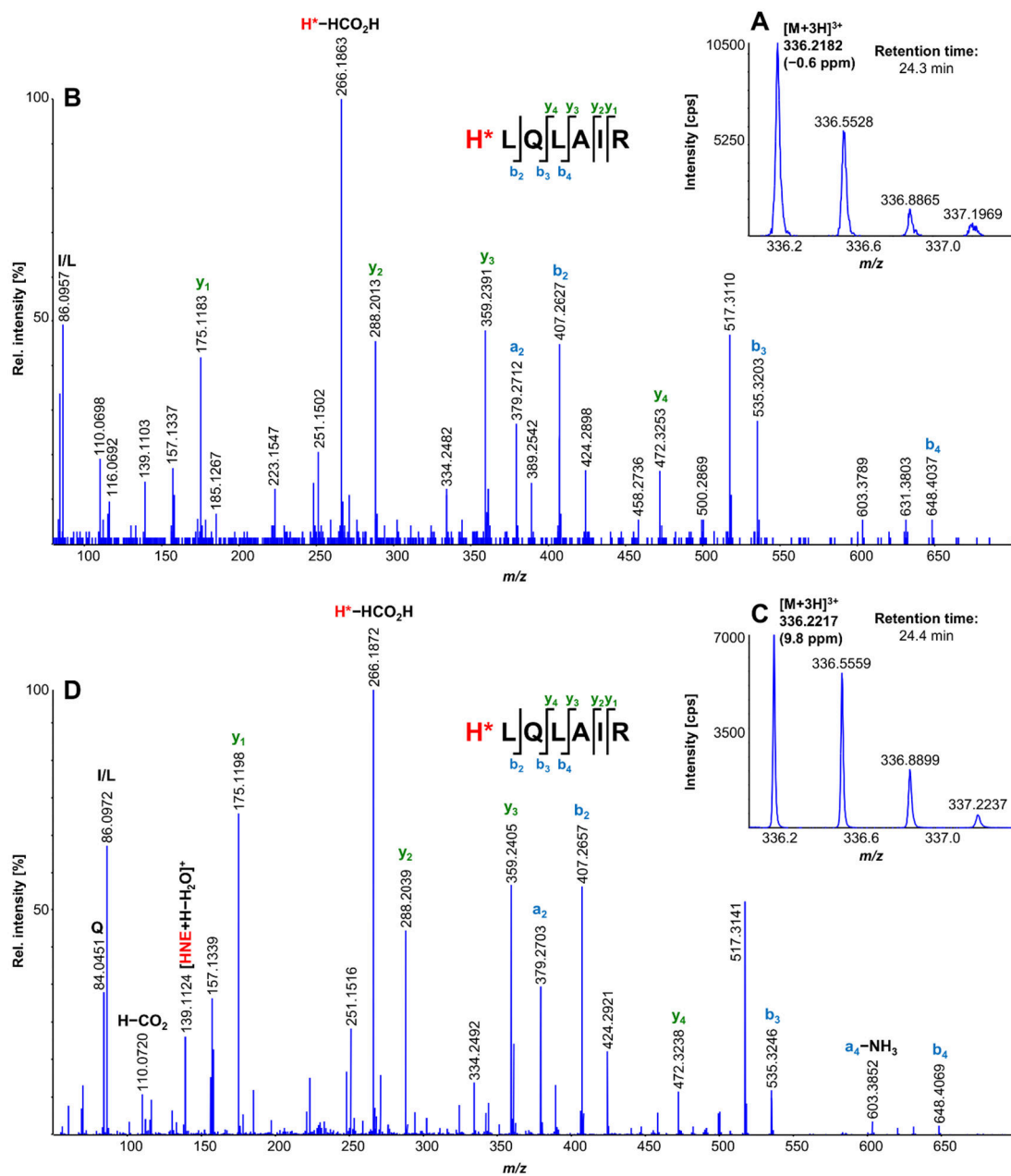


Figure S3 Comparison of MS (A) and MS/MS (B) spectra of HNE-modified histone peptide $H^*LQLAIR$ (His83 in histone H2A) identified in OA chondrocytes (not HNE-treated), compared to modified standard peptide (C and D).

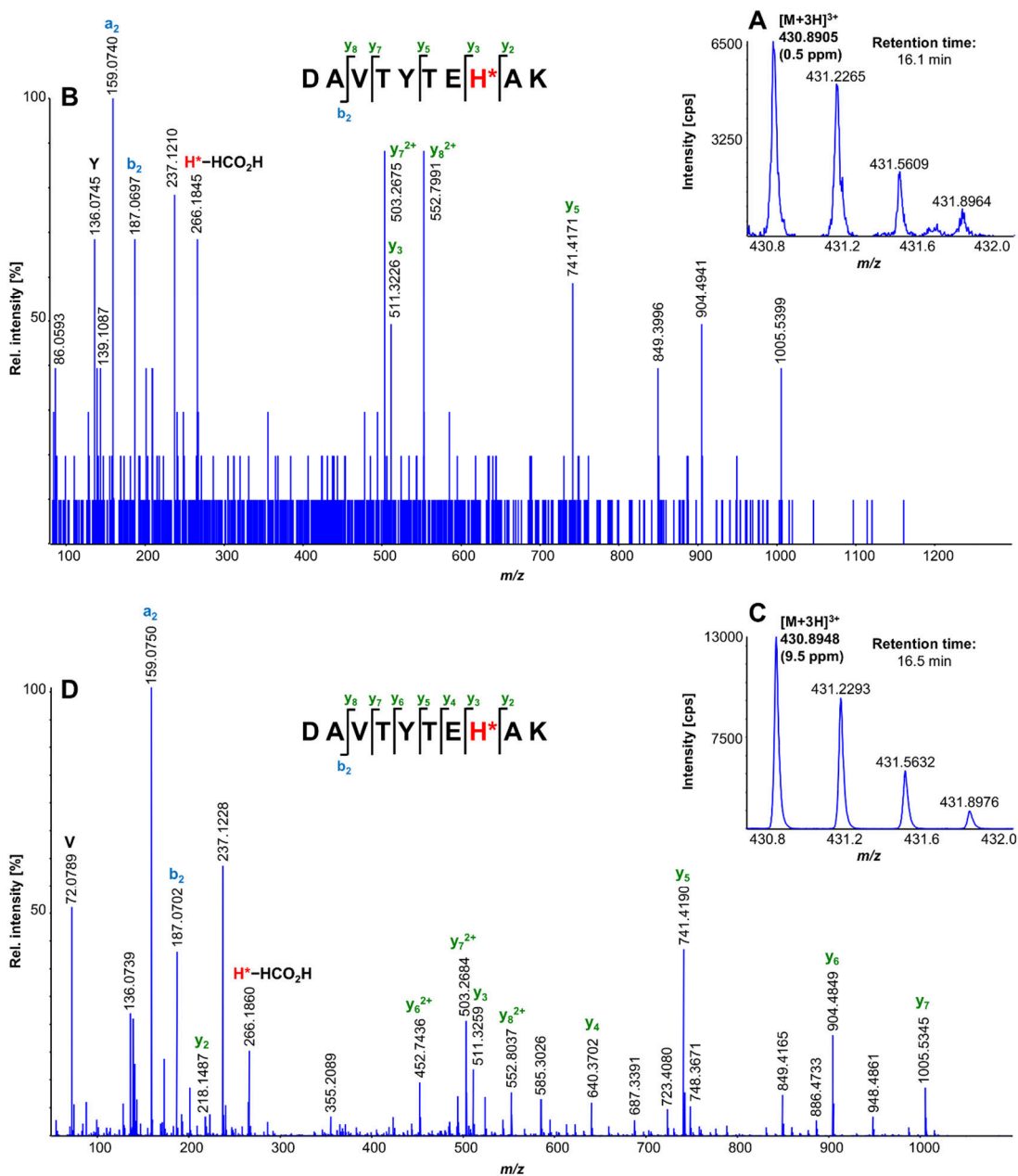


Figure S4 Comparison of MS (A) and MS/MS (B) spectra of HNE-modified histone peptide DAVTYTEH*AK (His76 in histone H4) identified in OA chondrocytes (not HNE-treated), compared to modified standard peptide (C and D).

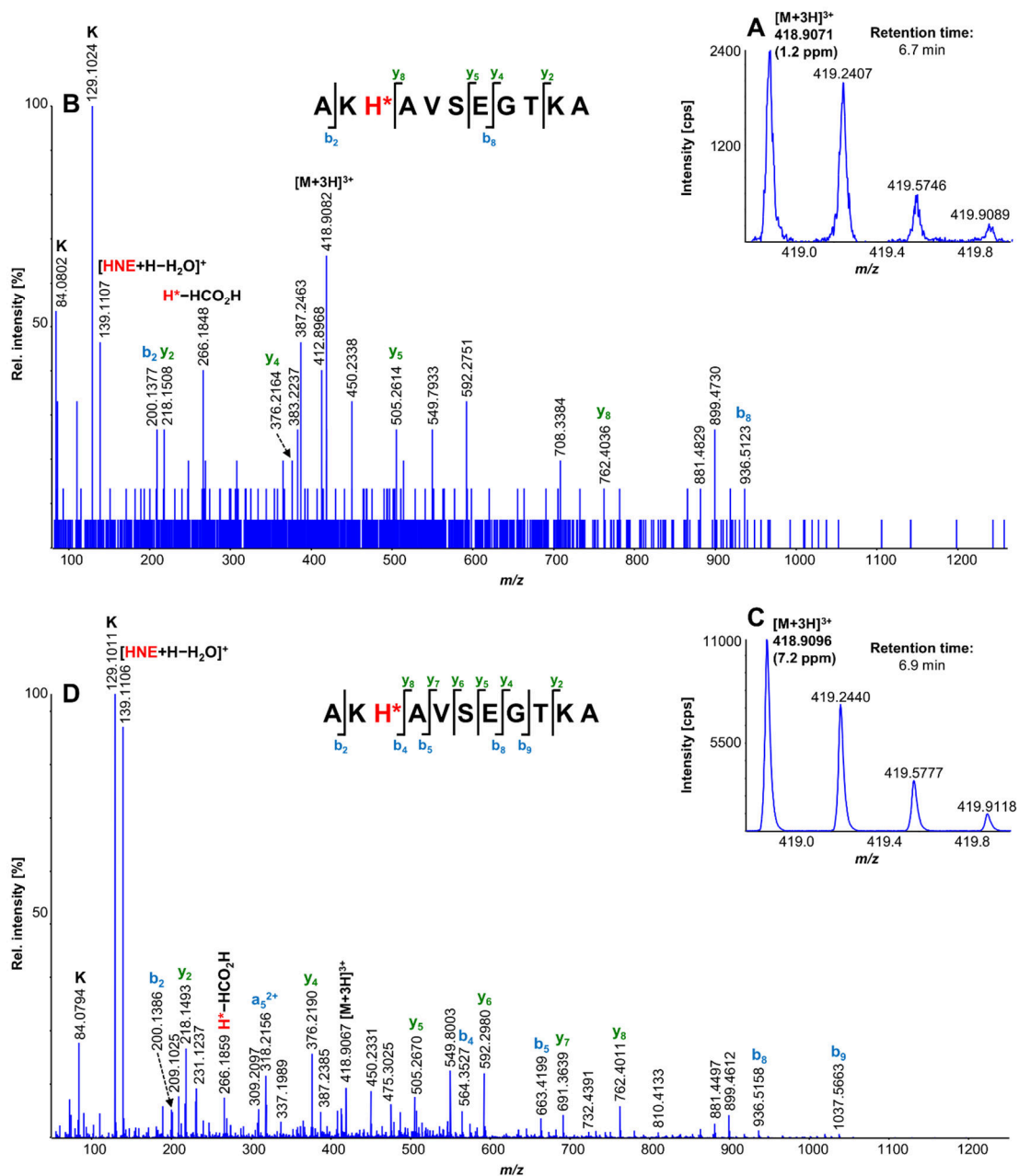


Figure S5 Comparison of MS (A) and MS/MS (B) spectra of HNE-modified histone peptide AKH*AVSEGTKA (His110 in histone H2B) identified in OA chondrocytes (not HNE-treated), compared to modified standard peptide (C and D).

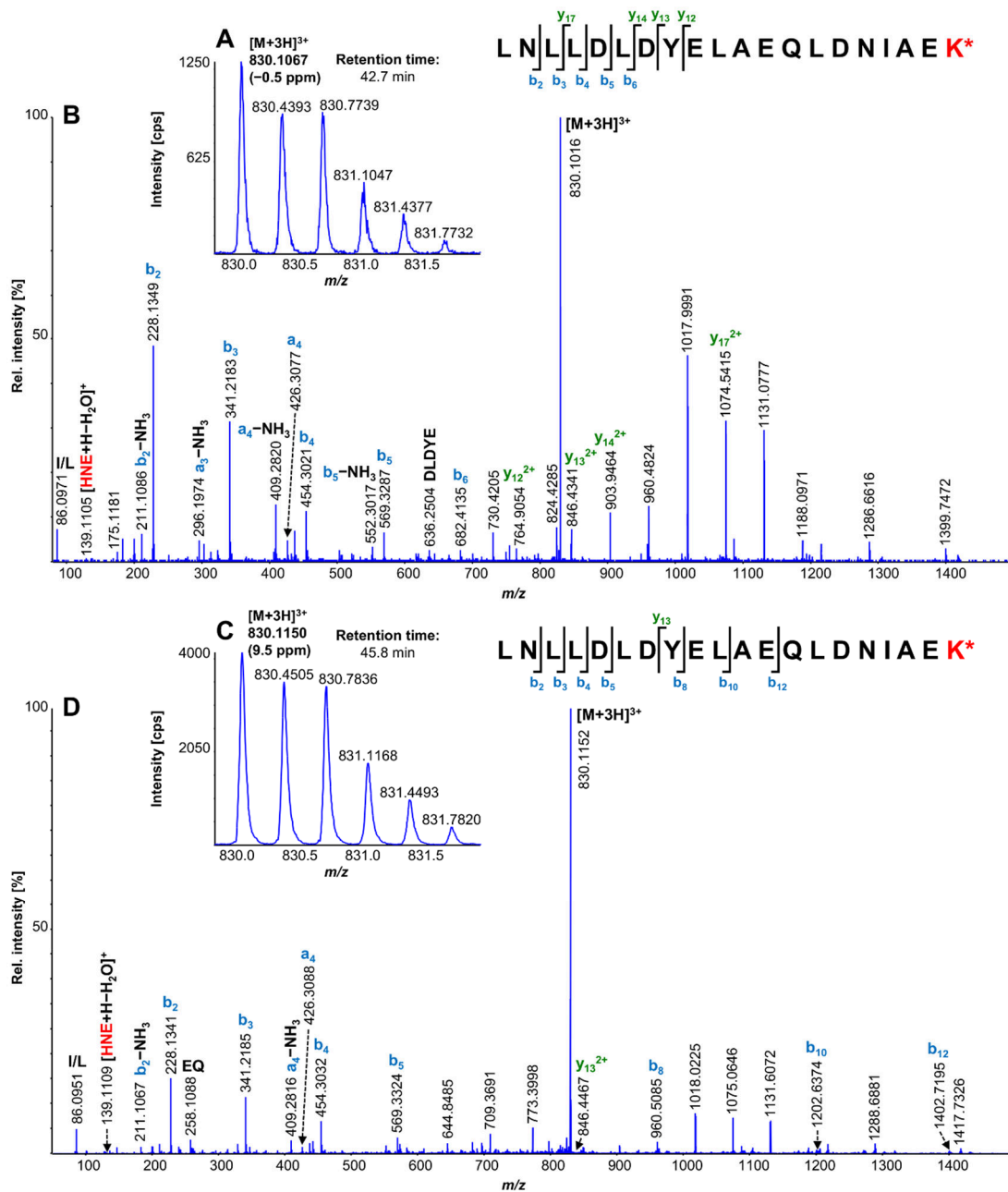


Figure S6. Comparison of MS (A) and MS/MS (B) spectra of HNE-modified collagen peptide LNLLDLDYELAEQLDNIAEK* (Lys2027 in COL6A3) identified in OA chondrocytes (not HNE-treated), compared to modified standard peptide (C and D).

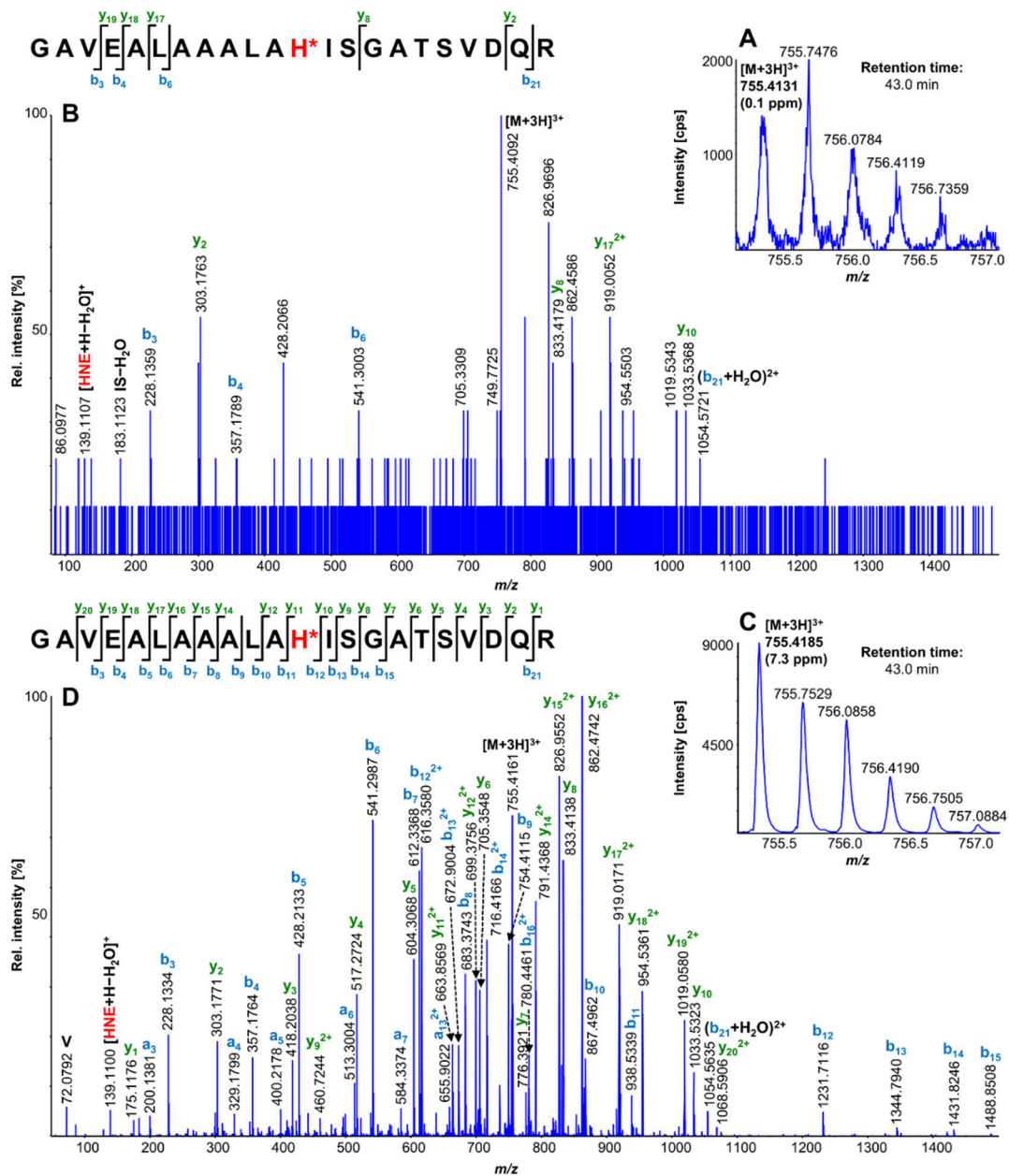


Figure S7 Comparison of MS (A) and MS/MS (B) spectra of HNE-modified nucleolar RNA helicase peptide GAVEALAAALAH*ISGATSVDQR (His617 in DDX21) identified in OA chondrocytes (not HNE-treated), compared to modified standard peptide (C and D).

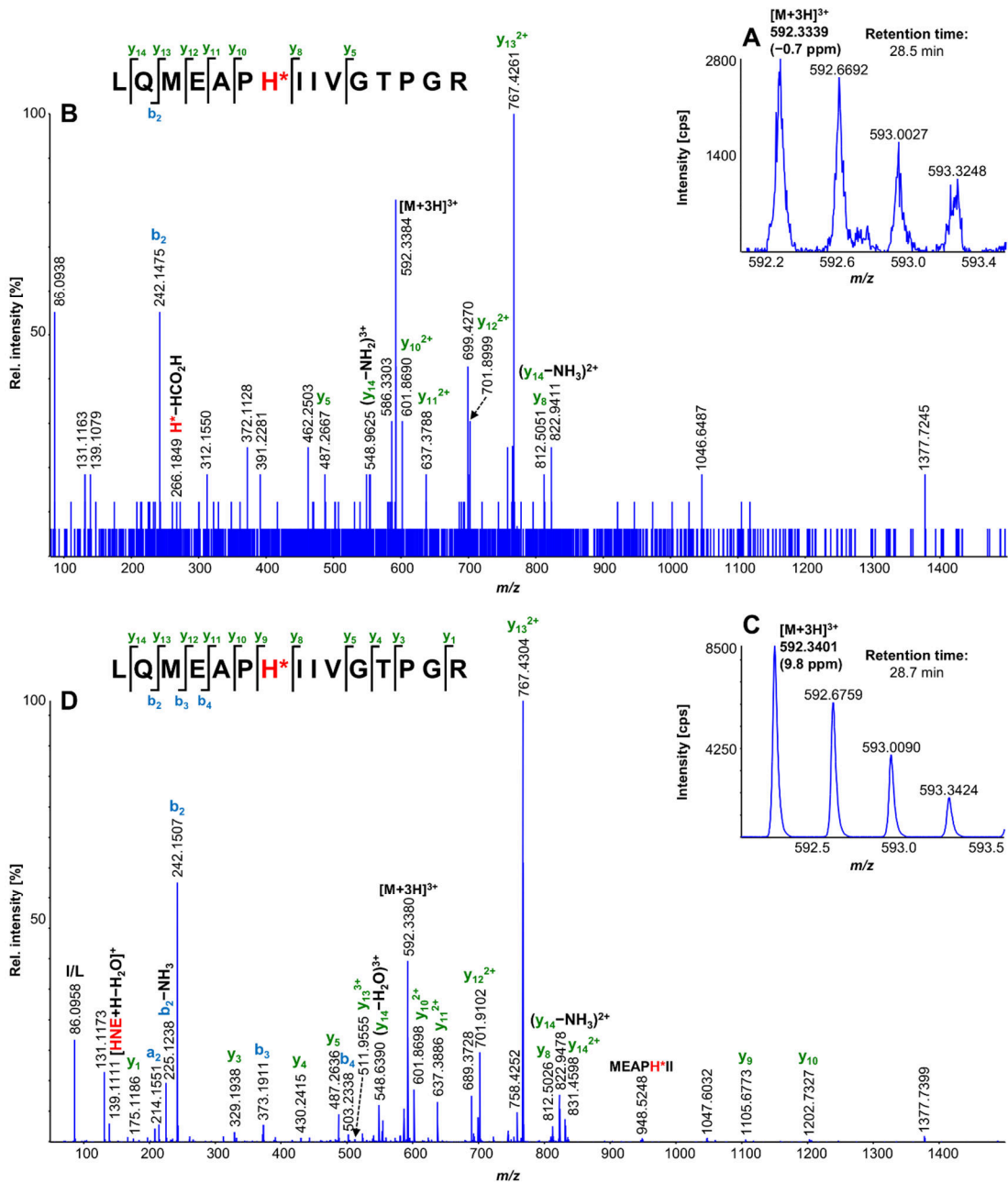


Figure S8 Comparison of MS (A) and MS/MS (B) spectra of HNE-modified translation initiation factor peptide LQMEAPH*IIVGTPGR (His153 in EIF4A1) identified in OA chondrocytes (not HNE-treated), compared to modified standard peptide (C and D).

APPENDIX C

ADDITIONAL PROTEIN EXPRESSION PROTOCOL, GSH ADDUCT SPECTRA,
MODIFIED PEPTIDE SPECTRA, CHROMATOGRAMS AND FOUND
DIAGNOSTIC FRAGMENT IONS, AND CHARGE DISTRIBUTION OF
MODIFIED STANDARD PEPTIDES

The complete material is available free of charge after publication via the
Internet at <https://pubs.acs.org/doi/10.1021/acs.chemrestox.0c00191>.

Purified hMGST1 preparation

Human *MGST1* gene was cloned in pPICZA vector (Invitrogen, Carlsbad, CA) and expressed in yeast *Pichia pastoris*. The solubilized protein was passed through Ni Sepharose 6 Fast Flow column (GE Healthcare, Chicago, IL). The column was washed with five column volumes of buffer containing 25 mM Tris-hydrochloride (pH 7.8), 500 mM sodium chloride, 10% glycerol, 5 mM 2-mercaptoethanol, 0.05% *n*-dodecyl- β -D-maltopyranoside (DDM; Anatrace, Maumee, OH), 0.1 mM GSH and 20 mM imidazole followed by three column volumes of same buffer having 40 mM imidazole instead of 20 mM concentration and hMGST1 protein was finally eluted in buffer containing 300 mM imidazole. The peak fractions were pooled and passed through *S*-hexylglutathione agarose column (Abcam, Cambridge, United Kingdom; and GE Healthcare) after equilibration. The column was washed with three column volumes of buffer containing 25 mM Tris-hydrochloride (pH 8.0), 500 mM sodium chloride, 10% glycerol, 5 mM 2-mercaptoethanol, 0.05% DDM and 0.1 mM GSH. Protein was eluted with the same buffer containing 30 mM probenecid but without sodium chloride. The eluate was concentrated using Amicon Ultra-15 30 kDa centrifugal filter device (MilliporeSigma, Burlington, MA) and purified further by size exclusion chromatography using HiLoad 16/600 Superdex 200 pg (GE Healthcare) column. The final buffer used for size exclusion chromatography contained 25 mM Tris-hydrochloride (pH 8.0), 100 mM sodium chloride, 10% glycerol, 0.1 mM tris(2-carboxyethyl)phosphine, 0.03% DDM and 0.1 mM GSH. The final fractions containing pure hMGST1 were concentrated to 32 mg/mL by ultrafiltration and stored at -80°C . Protein concentration was measured by UV spectrophotometry and purity was analyzed by sodium dodecyl sulfate-polyacrylamide gel electrophoresis.

Offline LC peptide purification

Fractionation was performed with a gradient starting at 5% B (2 min), to 50%B (within 12 min), to 70%B (within 0.5 min), and held for 6.5 min at 0.6 mL/min. Fractions were concatenated (1+9, 2+10, ...) into eight final fractions, dried under vacuum and reconstituted in 100 μ L 10% ACN.

LC-MS/MS

LC gradient for metabolites started at 5% B (held for 2.5 min) and linearly increased to 50% B within 23.5 min, then to 85% B within 2 min (held for 2 min). Ionization source was set at 5 kV, 500°C temperature, and 50 psi GS1/GS2 gas flows, with a declustering potential of 80 V. The instrument performed a survey MS acquisition (TOFMS) from m/z 50–700 (350 ms accumulation time), followed by MS/MS (high sensitivity mode) from m/z 50–700 on the 5 most intense precursor ions (within m/z 100–700, excluded for 20 s after two occurrences) Each MS/MS acquisition had an accumulation time of 100 ms and a collision energy (CE) of 30 \pm 10 V. The total cycle time was 0.9 s.

The peptide gradient started at 5% B (held for 2.5 min) and was linearly increased to 30% B within 21.5 min, to 50% B within 2 min, then to 85% B within 0.5 min, then to 95% B within 0.1 min (held for 1.4 min), and then returned to initial conditions. Source parameters were the same as above. TOFMS acquisition was from m/z 120–1,250 (250 ms), followed by MS/MS (CE = 30 \pm 10 V), DDA in high sensitivity mode with background subtraction) from m/z 80–1,500 on the 15 most

intense precursor ions (within m/z 250–1,250, excluded for 20 s after two occurrences), and an accumulation time of 50 ms each MS/MS. The total cycle time was 1.05 s.

During each analysis MS and MS/MS calibration were performed after every four injections with a set of in-house standards, using an automatic calibrant delivery system. Sciex Analyst software version 1.7.1 was used for data acquisition. Raw data was visualized and integrated with Sciex PeakView 2.2 and MultiQuant 3.0.3, respectively.

Supporting figures

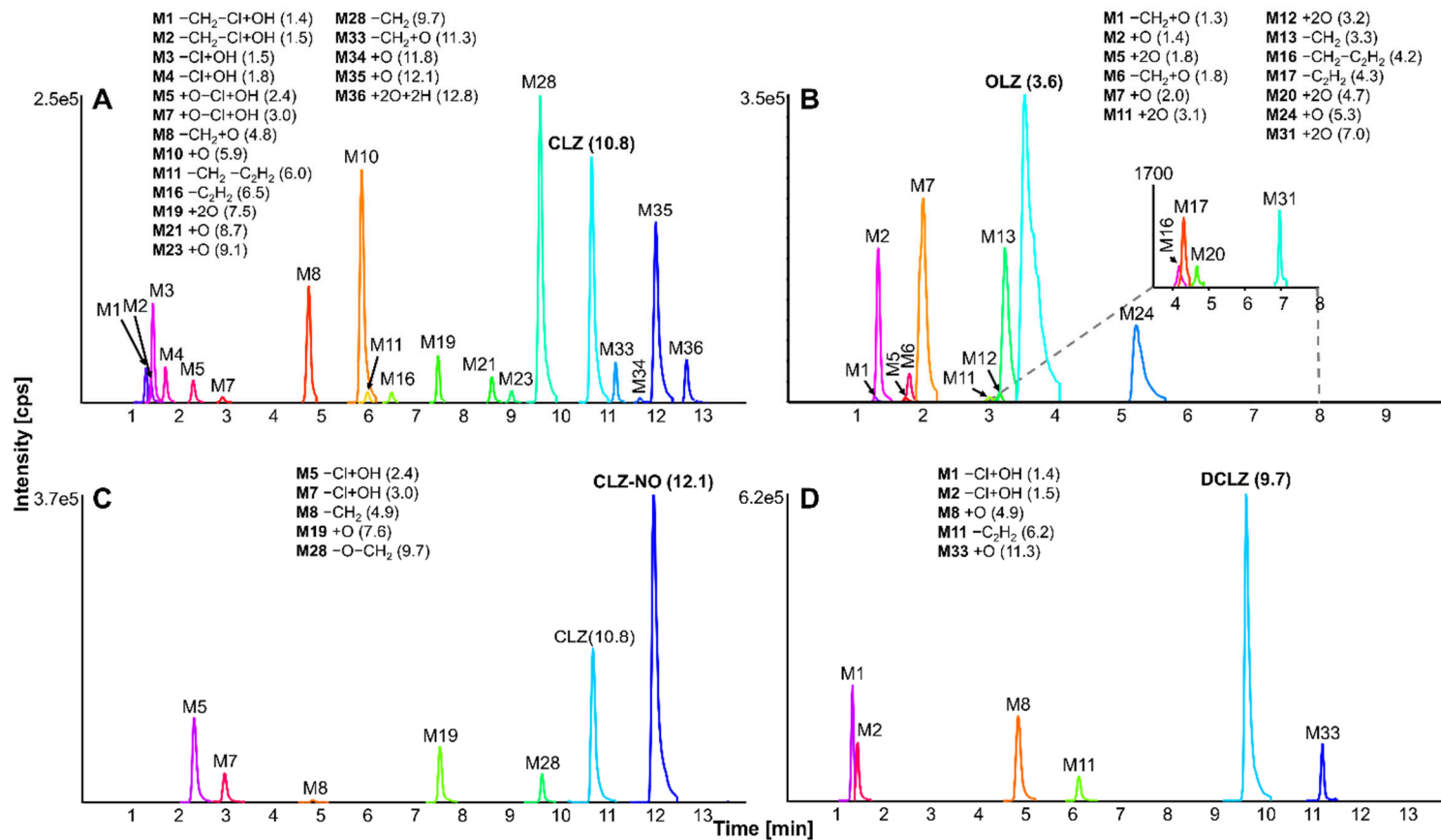


Figure S1 Extracted ion chromatograms of $[M+H]^+$ of stable oxidative metabolites in incubations of (A) CLZ, (B) OLZ, (C) CLZ-NO and (D) DCLZ with RLM. Retention times in parentheses.

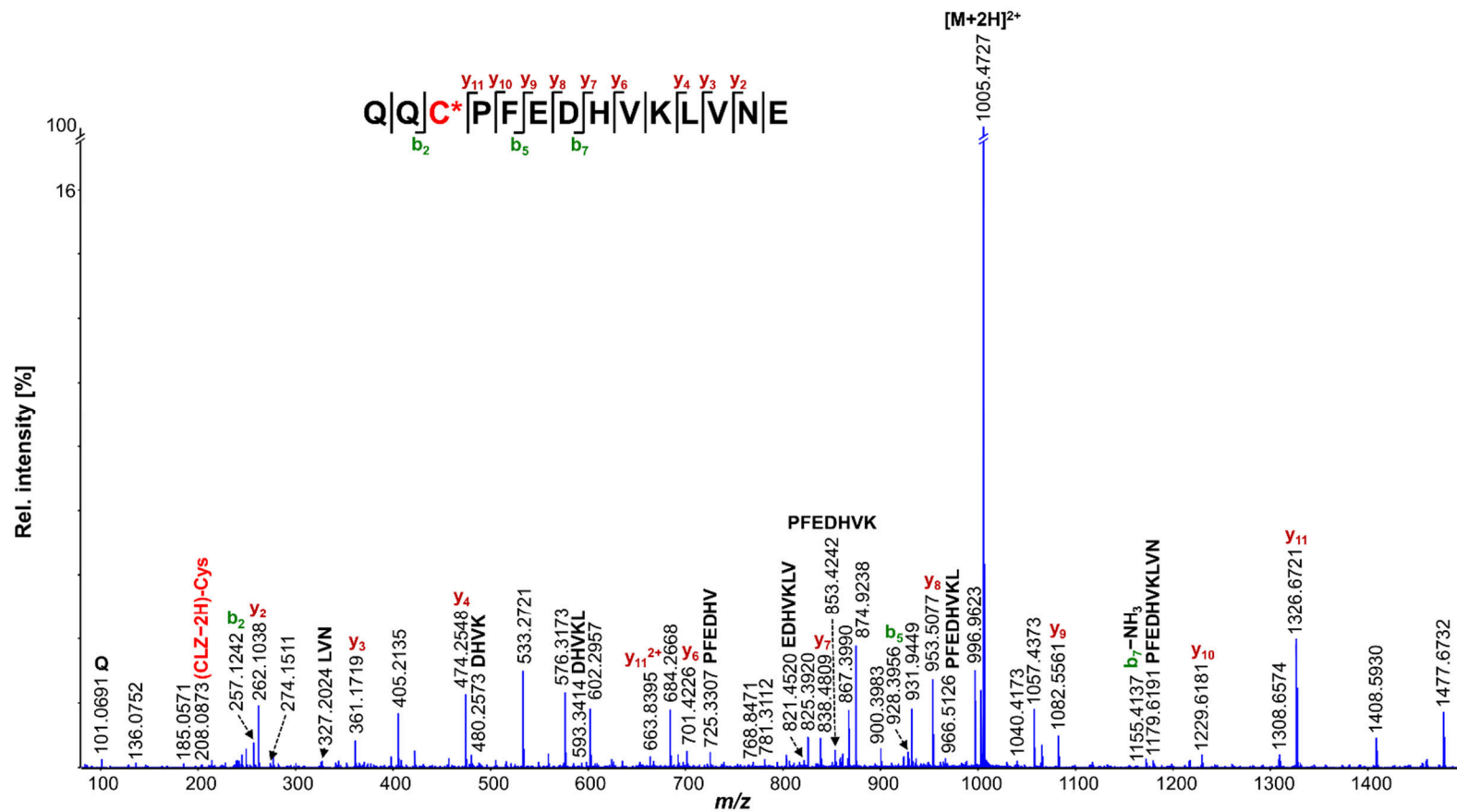


Figure S4 Identified (CLZ-2H)-hSA peptide QQC*PFEDHVKLVNE (modified at Cys34, pepsin digestion) MS/MS spectra. Targeted MS/MS was acquired for $[M+2H]^{2+}$ at m/z 1005.5.

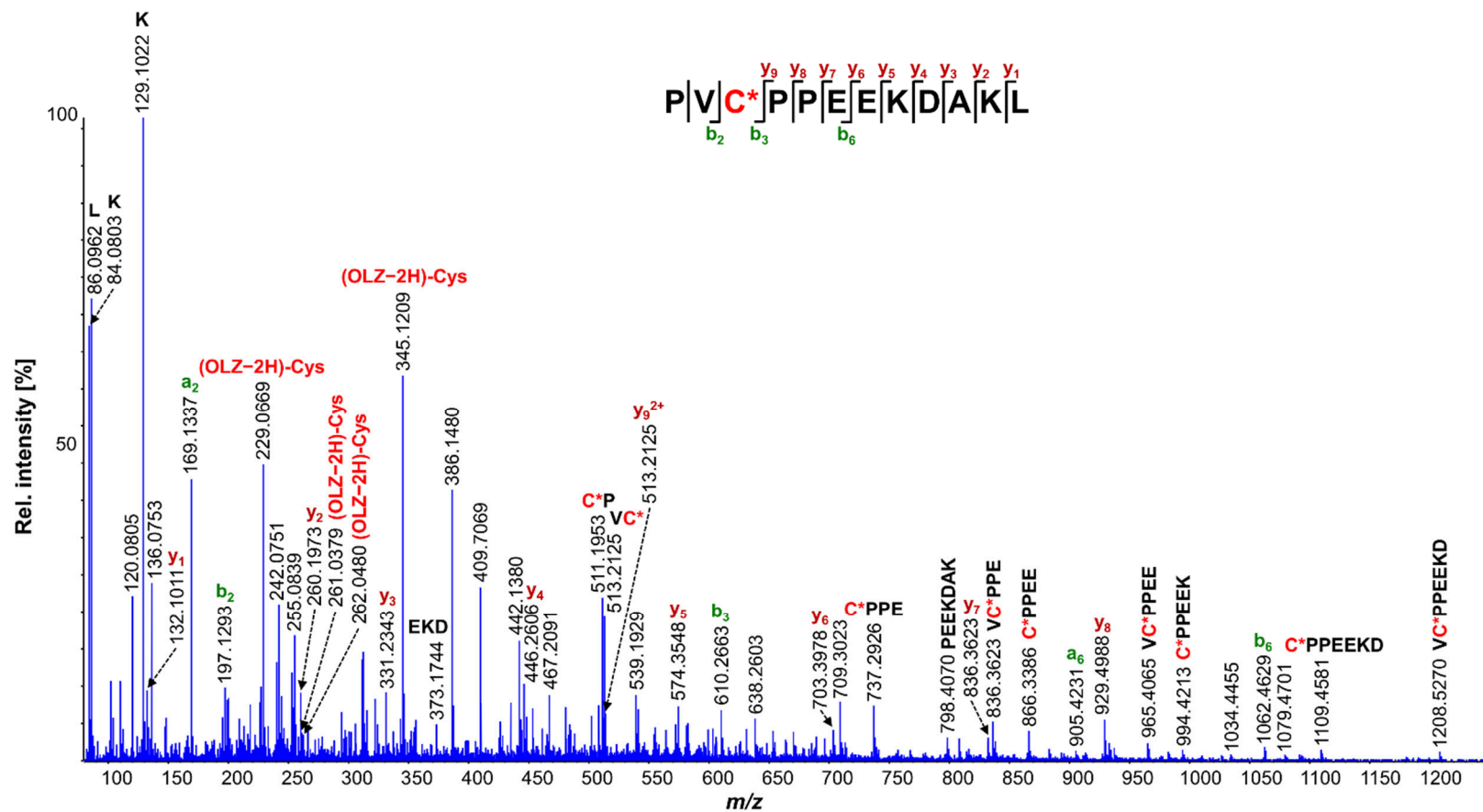


Figure S5 Identified (OLZ-2H)-hGSTA1 peptide PVC*PPEEKDAKL (modified at Cys112, pepsin digestion) MS/MS spectra. Targeted MS/MS was acquired for $[M+4H]^{4+}$ at m/z 409.7.

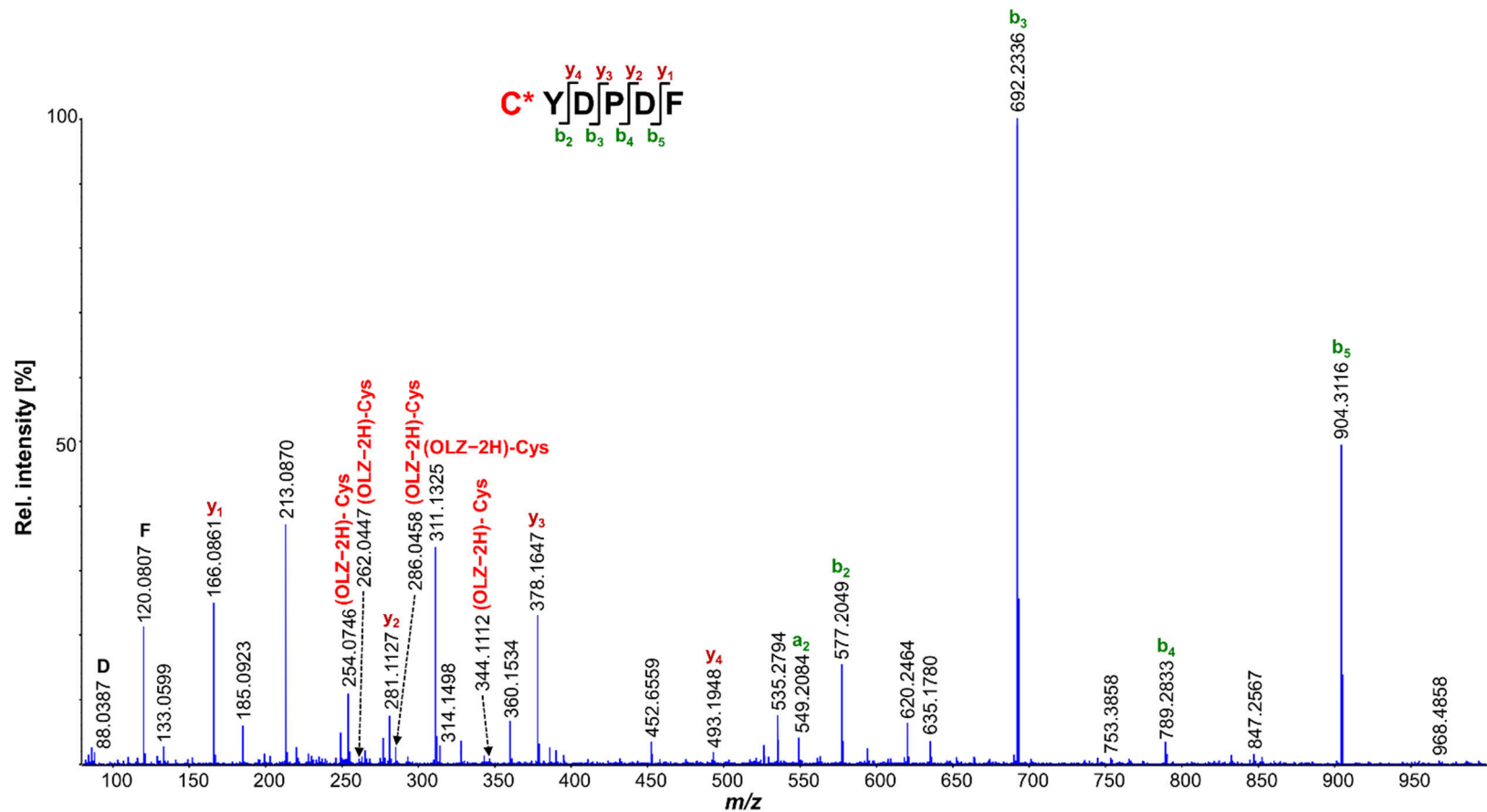


Figure S6 Identified (OLZ-2H)-hGSTM2 peptide C*YDPDF (modified at Cys115, pepsin digestion) MS/MS spectra. Targeted MS/MS was acquired for $[M+2H]^{2+}$ at m/z 535.2.

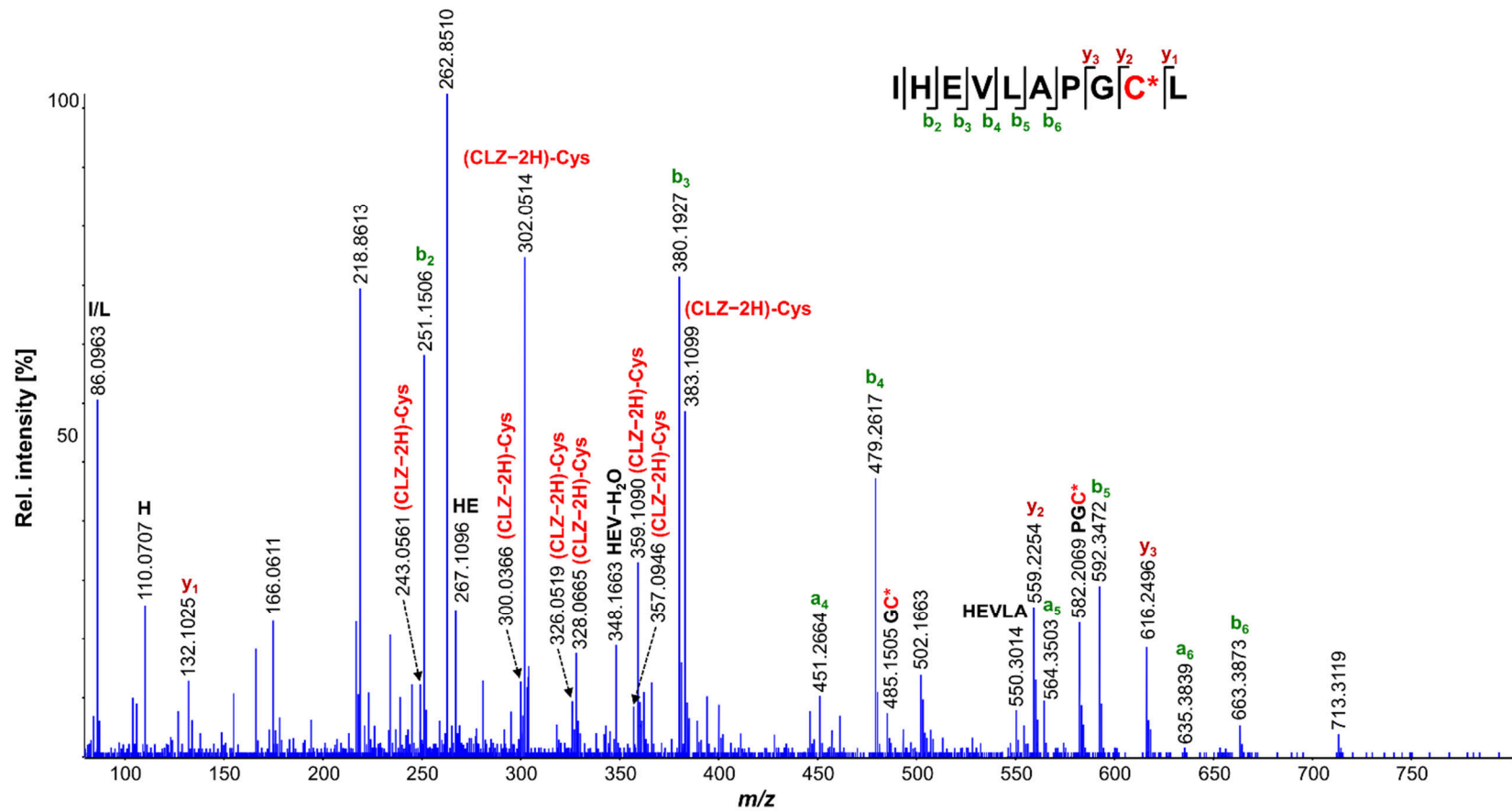


Figure S7 Identified (CLZ-2H)-hGSTP1 peptide IHEVLAPGC*L (modified at Cys170, pepsin digestion) MS/MS spectra. Targeted MS/MS was acquired for $[M+4H]^{4+}$ at m/z 344.7.

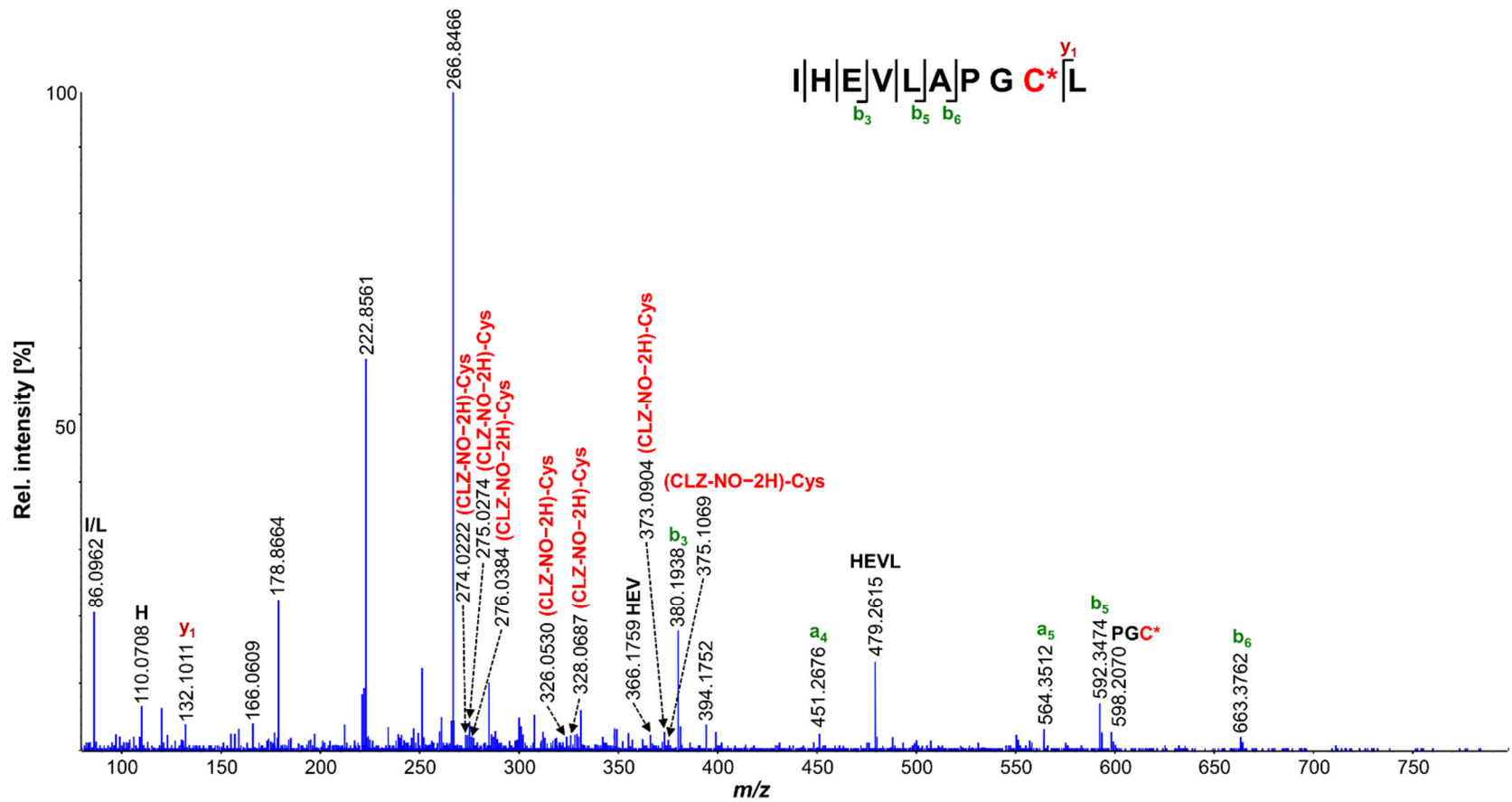


Figure S8 Identified (CLZ-NO-2H)-hGSTP1 peptide IHEVLAPGC*L (modified at Cys170, pepsin digestion) MS/MS spectra. Targeted MS/MS was acquired for $[M+4H]^{4+}$ at m/z 348.7.

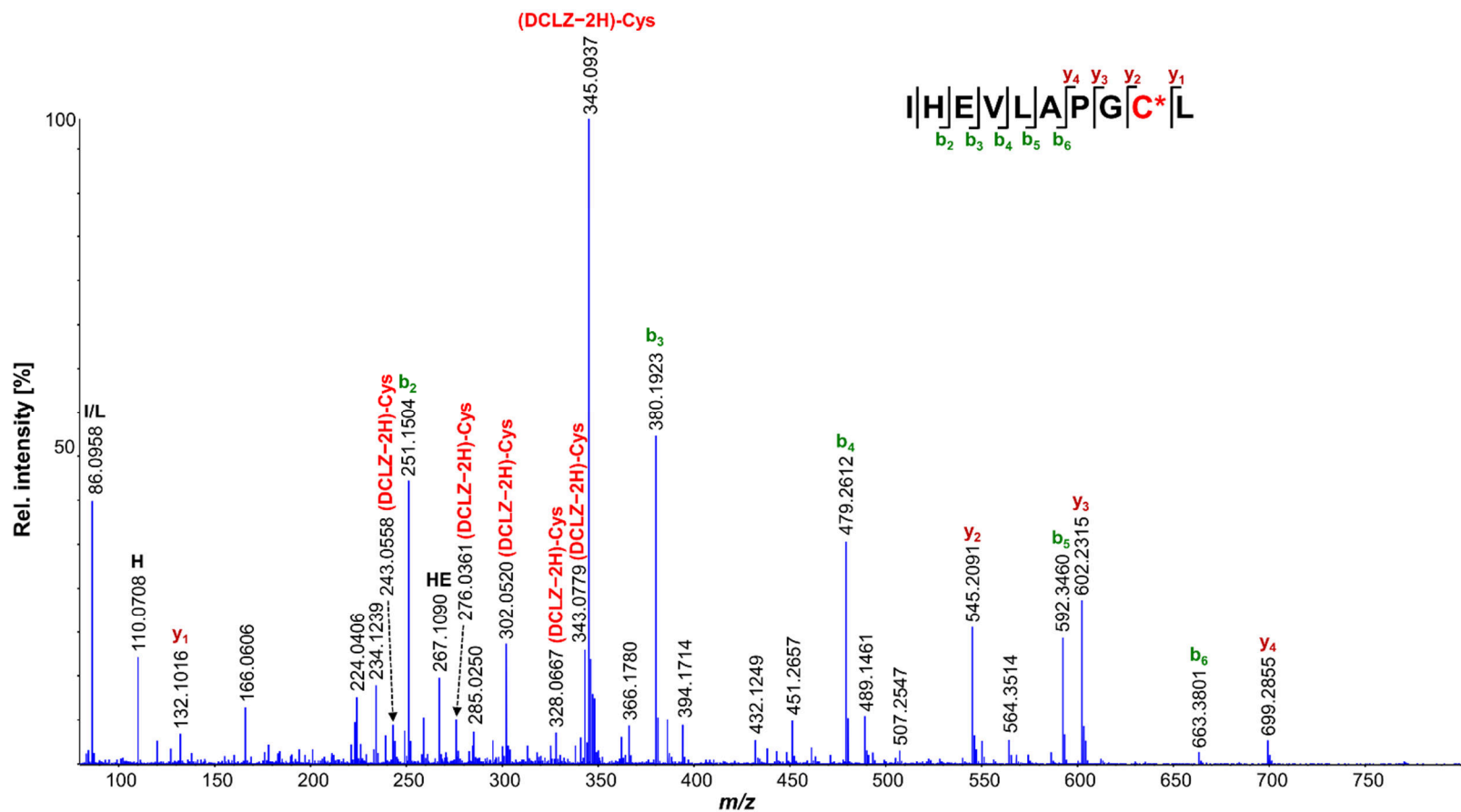


Figure S9 Identified (DCLZ-2H)-hGSTP1 peptide IHEVLAPGC*L (modified at Cys170, pepsin digestion) MS/MS spectra.

Targeted MS/MS was acquired for $[M+4H]^{4+}$ at m/z 341.2.

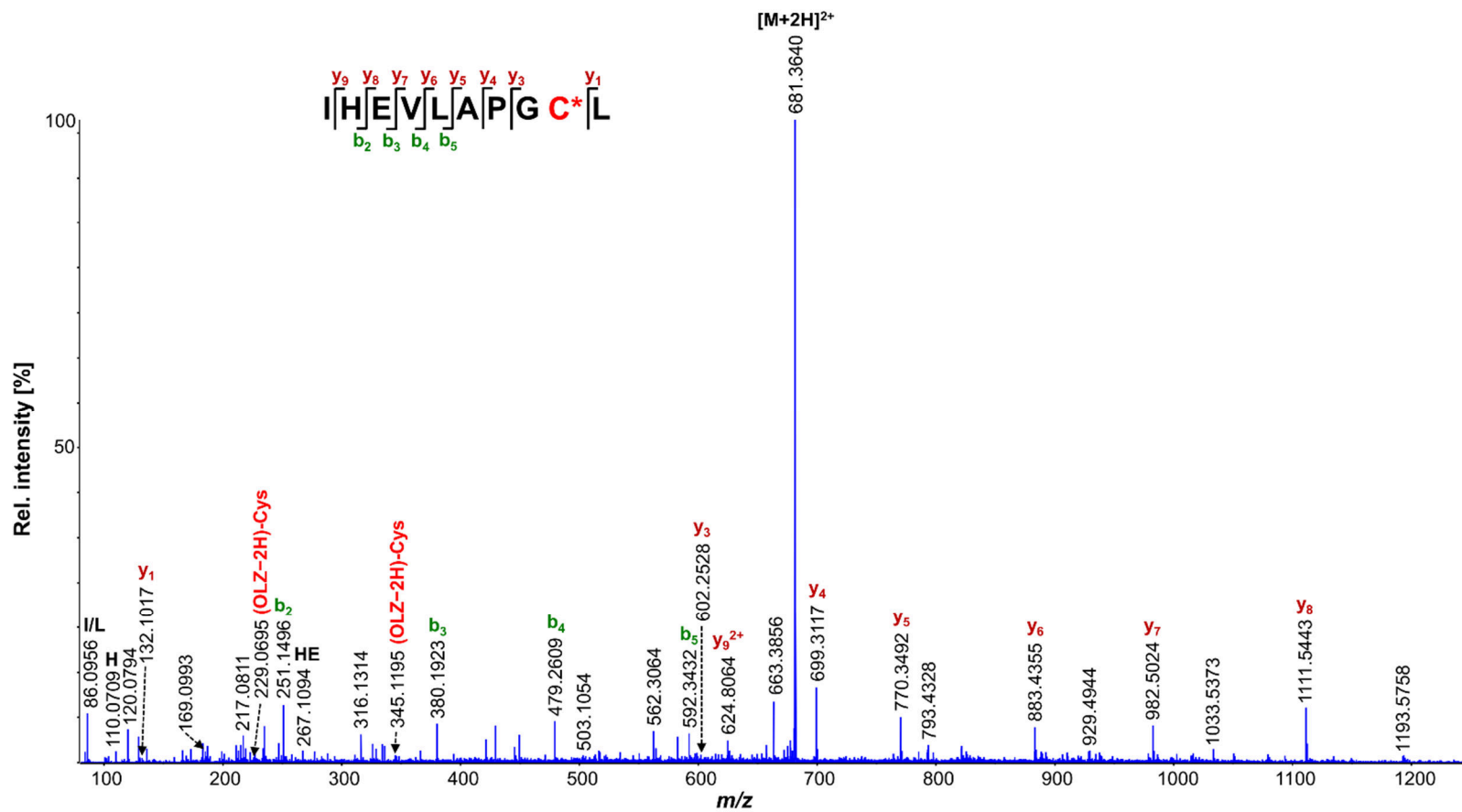


Figure S10 Identified (OLZ-2H)-hGSTP1 peptide IHEVLAPGC*L (modified at Cys170, pepsin digestion) MS/MS spectra. Targeted MS/MS was acquired for $[M+2H]^{2+}$ at m/z 681.3.

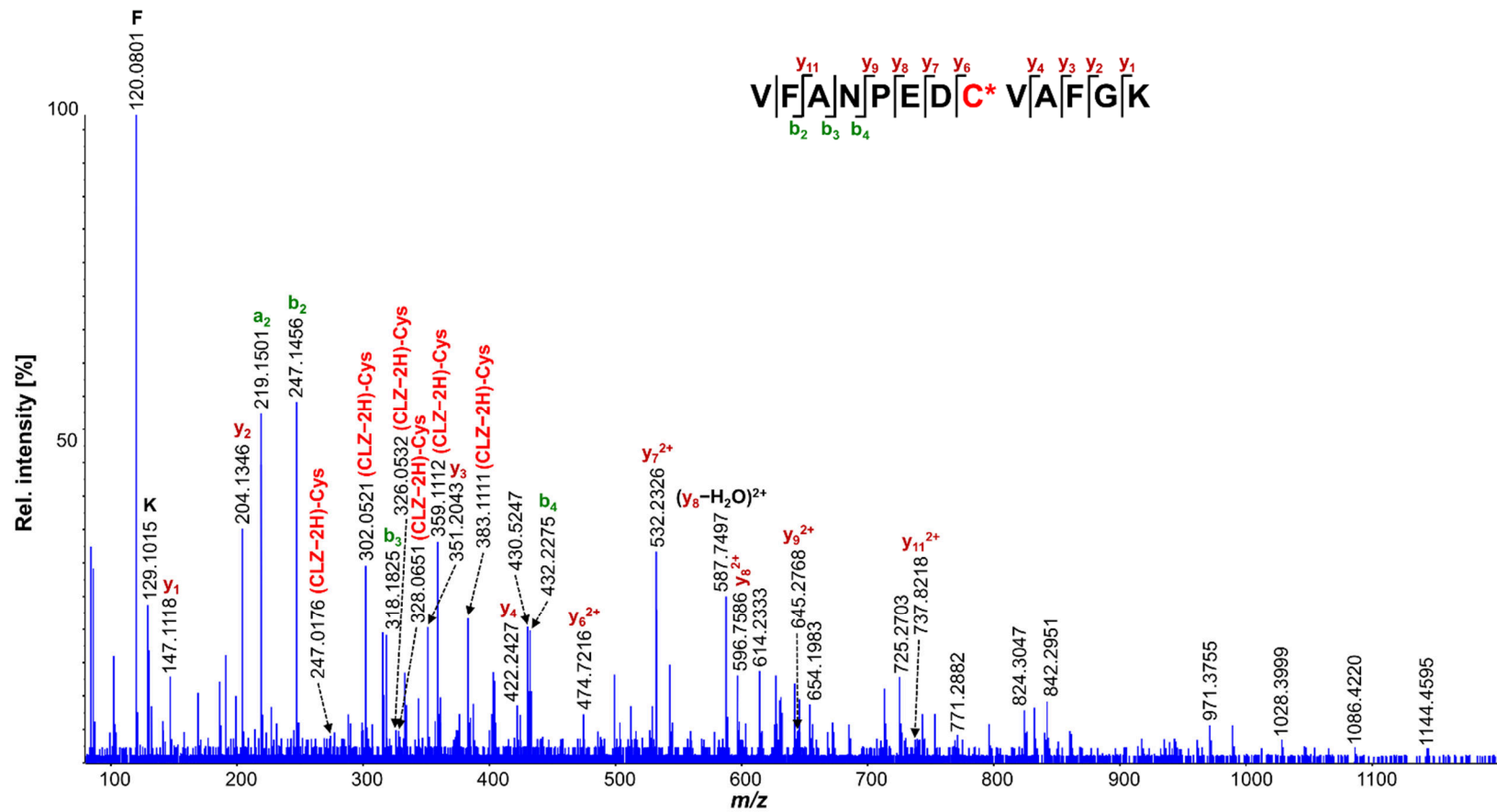


Figure S11 Identified (CLZ-2H)-hMGST1 peptide VFANPEDC*VAFGK (modified at Cys50, trypsin digestion) MS/MS spectra. Targeted MS/MS was acquired for $[M+4H]^{4+}$ at m/z 430.9.

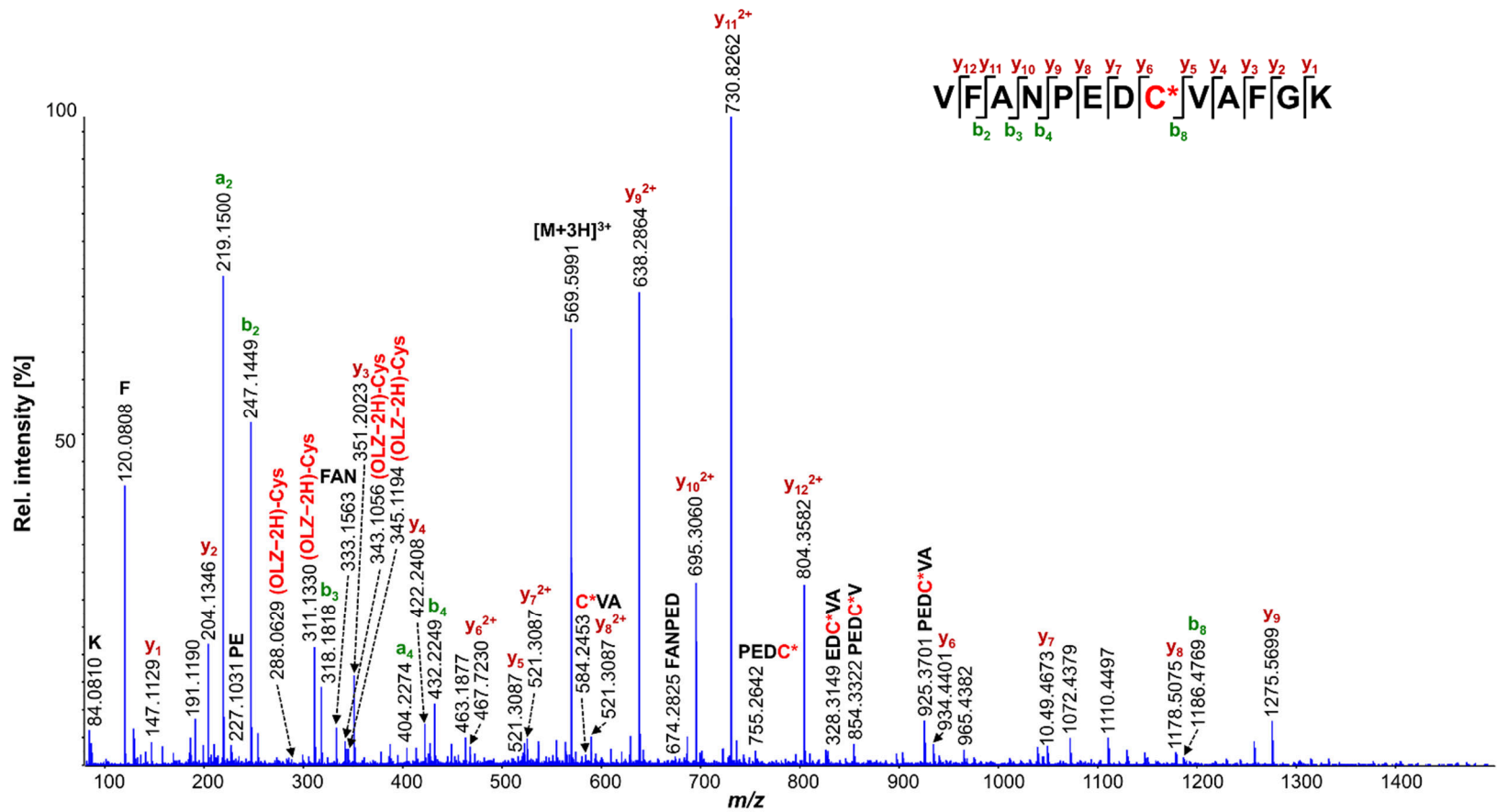


Figure S12 Identified (OLZ-2H)-hMGST1 peptide VFANPEDC*VAFGK (modified at Cys50, trypsin digestion) MS/MS spectra. Targeted MS/MS was acquired for $[M+3H]^{3+}$ at m/z 569.6.

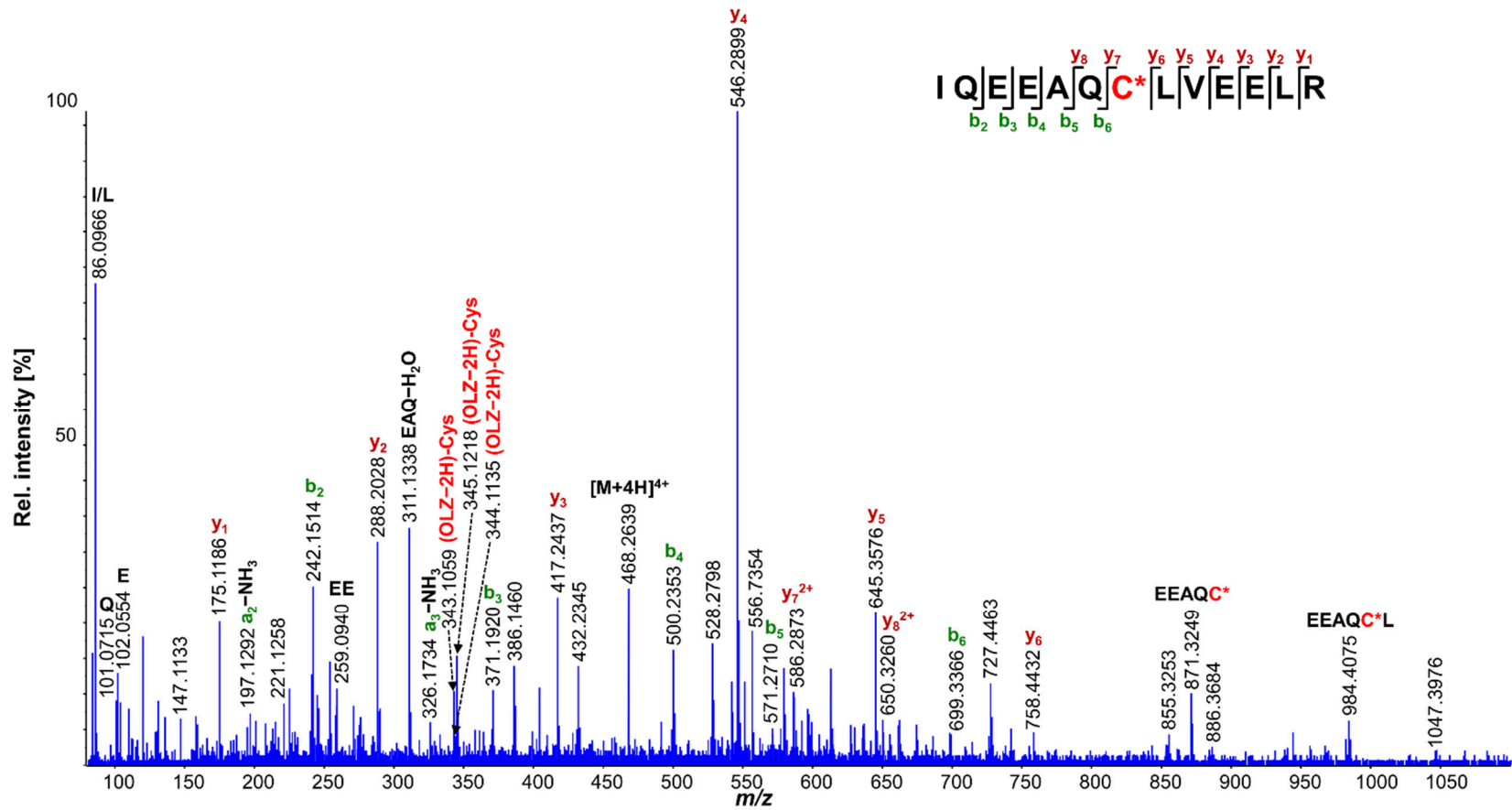


Figure S13 Identified (OLZ-2H)-rCYP2B1/2B2/2C11 peptide IQEEAQC*LVEELR (modified at Cys152/151; trypsin digest) MS/MS spectra. Targeted MS/MS was acquired for [M+4H]⁴⁺ at m/z 468.2.

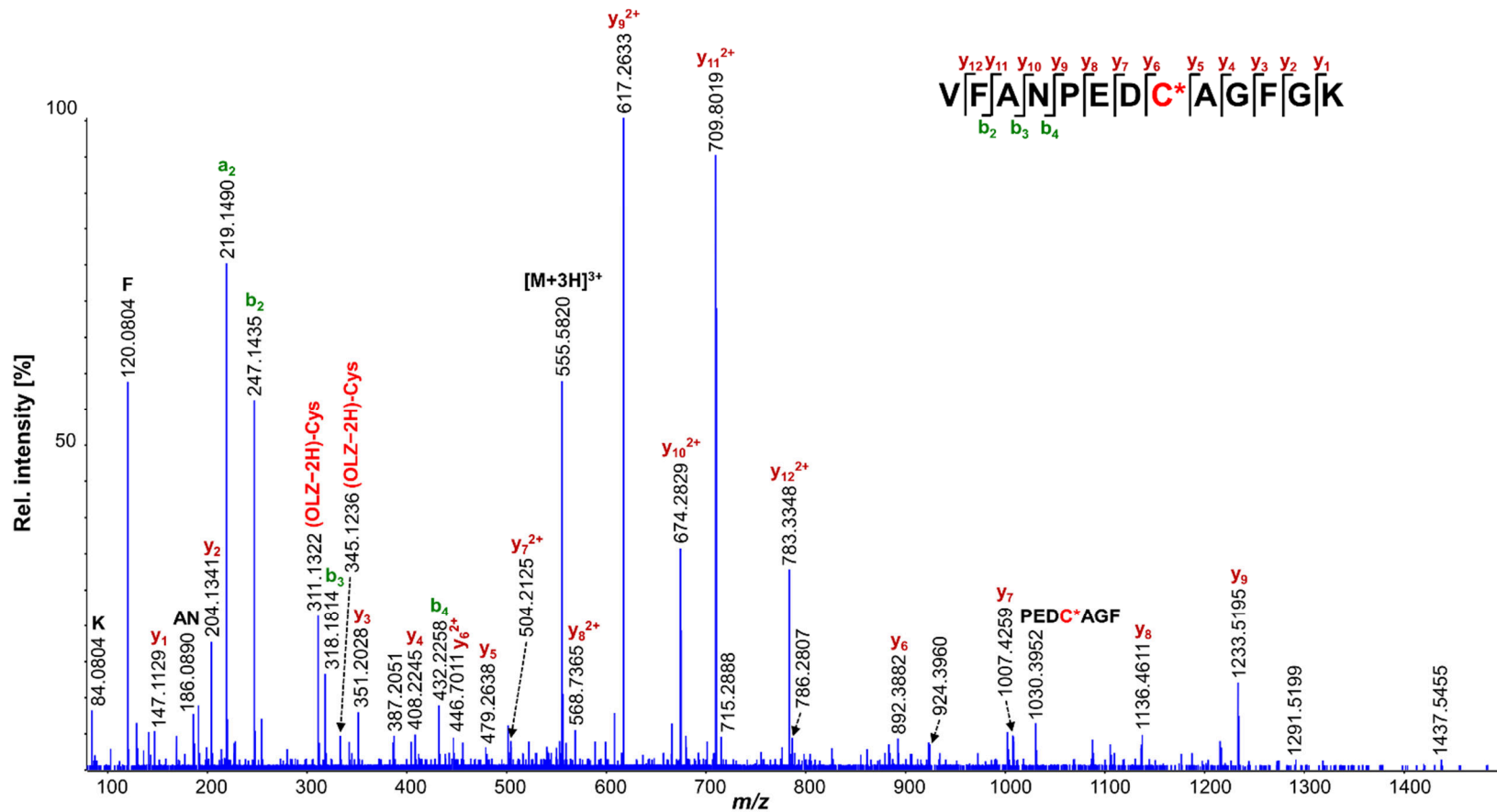


Figure S15 Identified (OLZ-2H)-rMGST1 peptide VFANPEDC*AGFGK (modified at Cys50, trypsin digestion) MS/MS spectra. Targeted MS/MS acquired for $[M+3H]^{3+}$ at m/z 555.6.

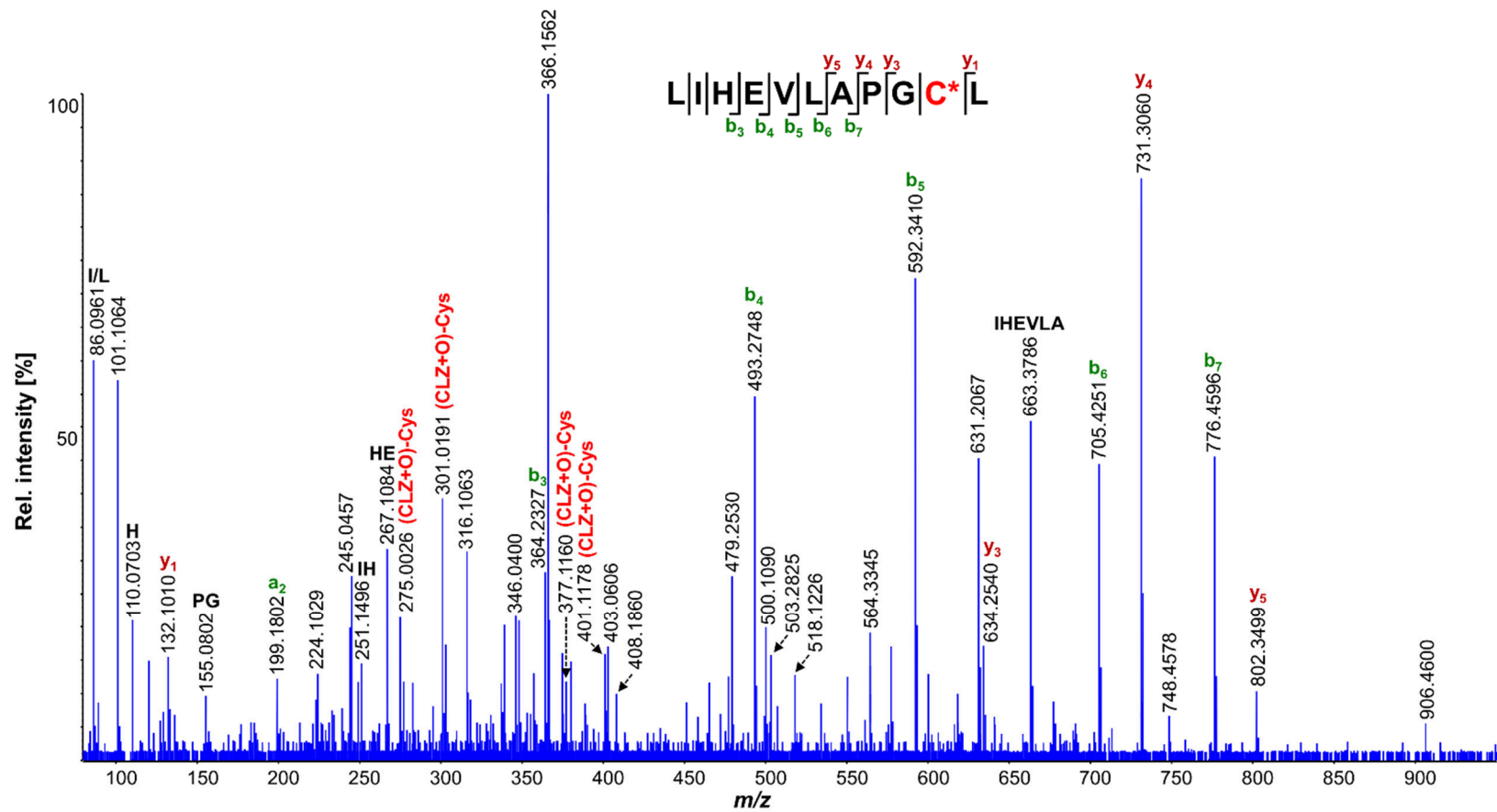


Figure S16 Identified (CLZ+O)-hGSP1 peptide LIHEVLAPGC*L (modified at Cys170, pepsin digestion) MS/MS spectra. Targeted MS/MS was acquired for $[M+3H]^{3+}$ at m/z 502.9.

Supporting tables

Table S1 Identified CLZ metabolites in RLM incubations^a

Transformation	Isomeric features									
	Met. ID	RT [min]	Met. ID	RT [min]	Met. ID	RT [min]	Met. ID	RT [min]	Met. ID	RT [min]
-CH ₂ -Cl+OH	M1 ^c	1.4	M2 ^c	1.5						
-Cl+OH	M3	1.5	M4	1.8						
+O-Cl+OH	M5 ^b	2.4	M7 ^b	3.0						
+O-HCl+GSH	M6 ^b	2.8								
-CH ₂ +O	M8 ^{b,c}	4.8	M33 ^c	11.3						
-HCl+GSH	M9 ^b	5.8								
+O	M21	8.7	M10	5.9	M23	9.1	M34	11.8	M35 ^b	12.1
-CH ₂ -C ₂ H ₂	M11 ^c	6.0								
-CH ₂ +O+GSH	M12 ^c	6.1	M14 ^c	6.4	M26 ^c	9.4				
+O+GSH	M13	6.2	M15	6.4	M27	9.5				
-C ₂ H ₂	M16	6.5								
+2O+GSH	M17 ^b	6.6								
-Cl+OH+GSH	M18	6.9								
+2O	M19 ^b	7.5								

Table S1 Continued

Transformation	Isomeric features									
	Met. ID	RT [min]	Met. ID	RT [min]	Met. ID	RT [min]	Met. ID	RT [min]	Met. ID	RT [min]
-CH ₂ -2H+GSH	M20	8.5	M22	8.9	M29	9.8				
-2H+GSH	M24 ^b	9.1	M25 ^b	9.3	M31 ^b	10.3				
-CH ₂	M28 ^{b,c}	9.7								
+O-2H+GSH	M30 ^b	9.8	M32 ^b	11.0						
	Parent^b	10.8								
+2O+2H	M36	12.8								
-C ₅ H ₁₀ N ₂ +O-2H+GSH	M37 ^c	13.5								

^aAll metabolites identified with mass accuracies within 10 ppm and isotope ratio difference <20%.

^bAlso found in CLZ-NO incubations.

^cAlso found in DCLZ incubations.

Table S2 Identified OLZ metabolites in RLM incubations^a

Transformation	Isomeric features									
	Met. ID	RT [min]	Met. ID	RT [min]	Met. ID	RT [min]	Met. ID	RT [min]	Met. ID	RT [min]
-CH ₂ +O	M1	1.3	M6	1.8						
+O	M2	1.4	M7	2.0	M24	5.3				
+O-2H+GSH	M3	1.5	M4	1.7	M18	4.4	M15	3.4		
+2O	M5	1.8	M11	3.1	M12	3.2	M20	4.7	M31	7.0
-CH ₂ -2H+GSH	M8	2.5	M9	2.7	M22	5.1				
-2H+GSH	M10	2.9	M25	5.3	M28	5.8	M35	9.0		
-CH ₂	M13	3.3								
-CH ₂ +O+GSH	M14	3.4	M19	4.6	M21	5.0				
	Parent	3.6								
-CH ₂ -C ₂ H ₂	M16	4.2								
-C ₂ H ₂	M17	4.3								
+O+GSH	M23	5.1	M26	5.5	M33	7.5	M34	8.5		
-C ₅ H ₁₀ N ₂ +2O+GSH	M27	5.7	M32	7.2						
+2O+GSH	M29	6.6	M30	6.9						

^aAll metabolites identified with mass accuracies within 10 ppm and isotope ratio difference <20%.

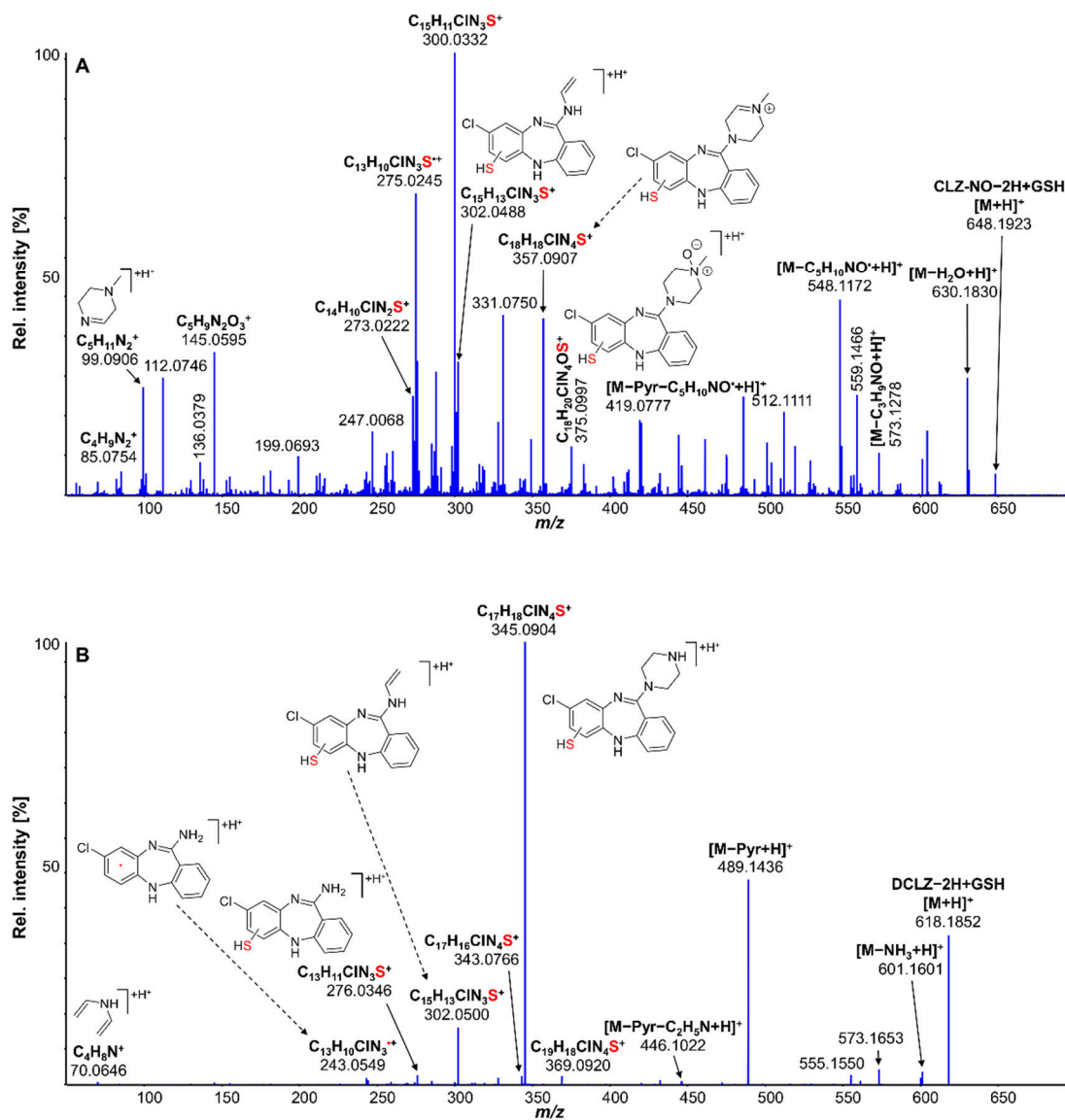
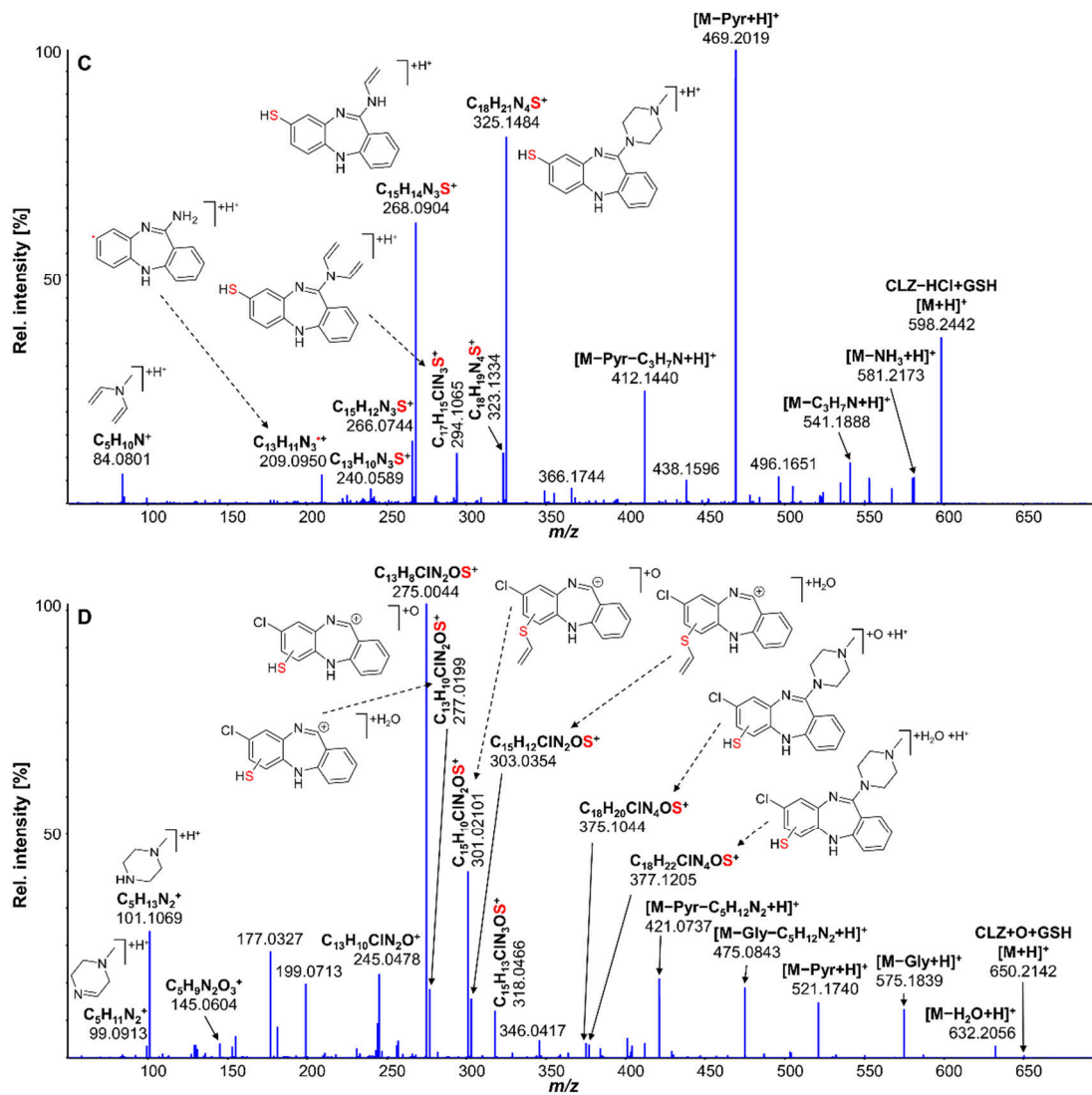


Figure S2 MS/MS spectra of (A) CLZ-NO-2H+GSH, (B) DCLZ-2H+GSH, (C) CLZ-HCl+GSH and (D) CLZ +O+GSH.



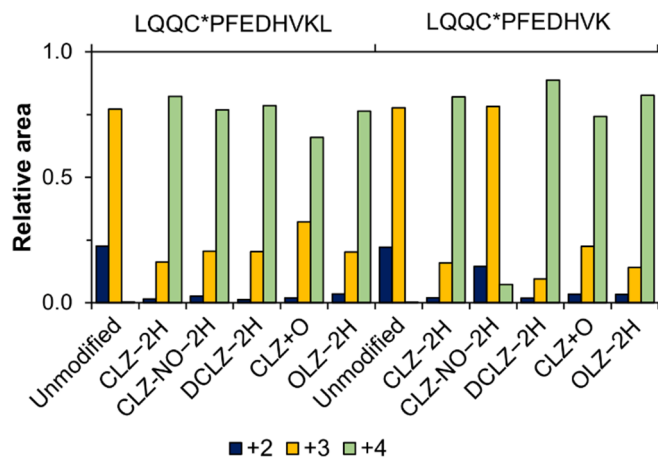


Figure S3 Peptide precursor ion charge distribution (+2 to +4) of standard peptides LQQCPFEDHVK and LQQCPFEDHVKL, and corresponding nitrogen ion-peptide adducts.

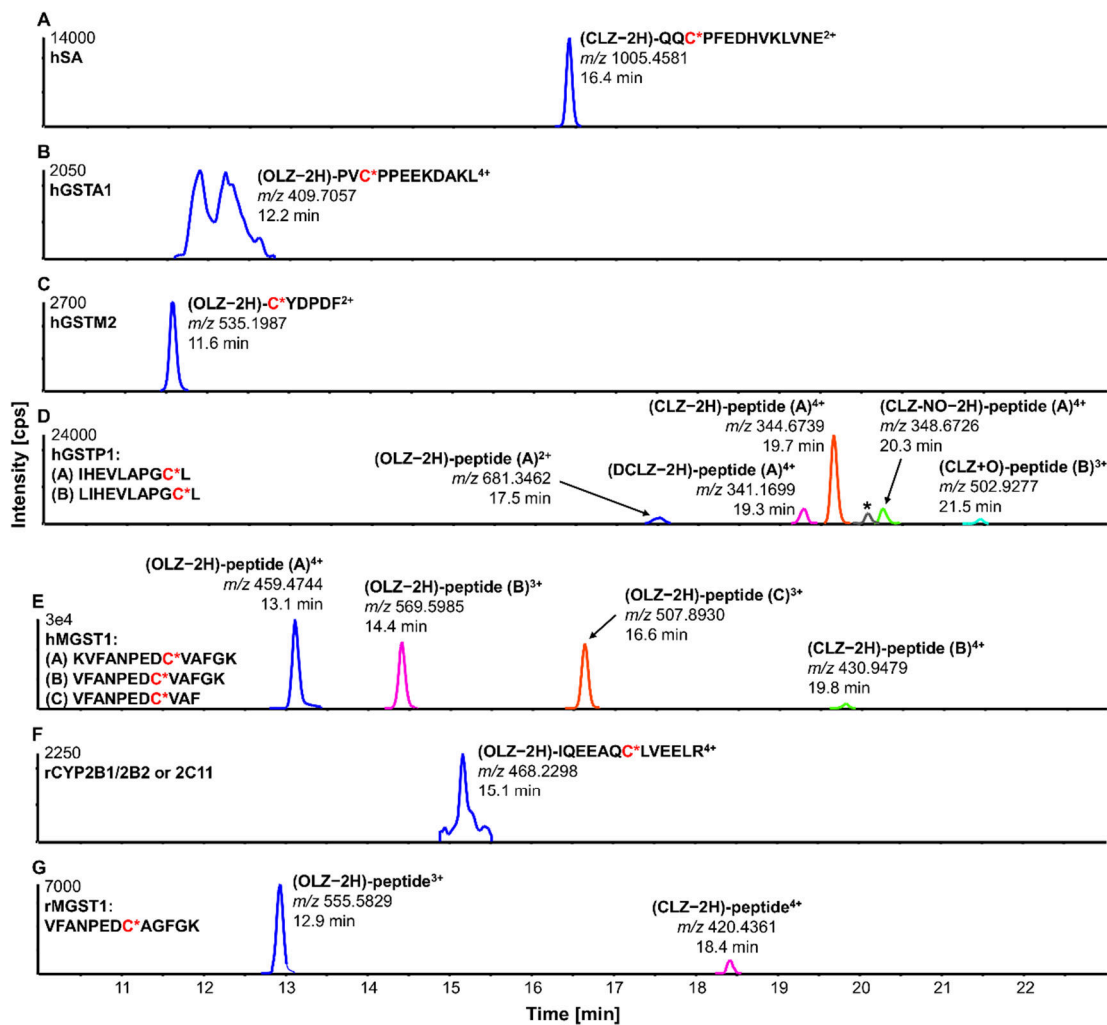


Figure S17 Overlaid extracted ion chromatograms (± 0.01 u) of all identified modified peptides from CLZ and OLZ incubations with (A) hSA, (B) hGSTA1, (C) hGSTM2, (D) hGSTP1 and (E) hMGST1, as well as (F) rCYP2B1/2B2/2C11 and (G) rMGST1 from RLM background. Not confidently identified peptide (CLZ+O)-IHEVLAPGC*L⁴⁺ (*m/z* 349.1765 at 20.0 min) was also highlighted (*).

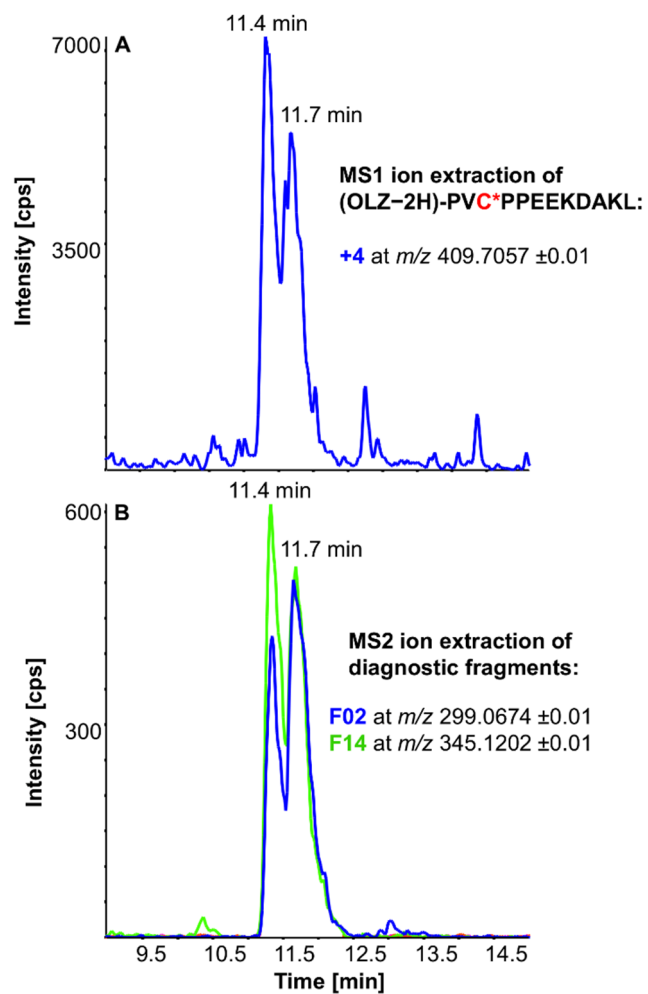


Figure S18 Comparison of (A) MS1 and (B) MS2 ion extractions of (OLZ-2H)-modified hGSTA1 peptide PVC¹¹²PPEEKDAKL to identify two partly co-eluting peaks at 11.4 and 11.7 min in target MS/MS experiments. MS2 ion extraction was based on MS/MS of [M+4H]⁴⁺.

REFERENCES

- Achour, B., Barber, J. and Rostami-Hodjegan, A. (2014). Expression of hepatic drug-metabolizing cytochrome P450 enzymes and their intercorrelations: a meta-analysis. *Drug Metabolism and Disposition*, 42(8), 1349–1356. doi: 10.1124/dmd.114.058834
- Aebersold, R. and Mann, M. (2003). Mass spectrometry-based proteomics. *Nature*, 422(6928), 198–207. doi: 10.1038/nature01511
- Aebersold, R. and Mann, M. (2016). Mass-spectrometric exploration of proteome structure and function. *Nature*, 537(7620), 347–355. doi: 10.1038/nature19949
- Ahlborg, U. G., Hanberg, A. and Kenne, K. (1992). *Risk assessment of polychlorinated biphenyls (PCBs)*. Nordic Council of Ministers. Stockholm, Sweden. Retrieved from <http://ki.se/sites/default/files/nordpcb-92.pdf>
- Ahmad, S., Niegowski, D., Wetterholm, A., Haeggström, J. Z., Morgenstern, R. and Rinaldo-Matthis, A. (2013). Catalytic characterization of human microsomal glutathione S -transferase 2: identification of rate-limiting steps. *Biochemistry*, 52(10), 1755–1764. doi: 10.1021/bi3014104
- Ahmadi, S. and Winter, D. (2019). Identification of unexpected protein modifications by mass spectrometry-based proteomics. In X. Wang and M. Kuruc (eds.), *Functional Proteomics. Methods in Molecular Biology* (1st ed., vol. 1871, 15, pp. 225–251). New York, NY : Humana Press. doi: 10.1007/978-1-4939-8814-3_15
- Akamine, Y., Sugawara-Kikuchi, Y., Uno, T., Shimizu, T. and Miura, M. (2017). Quantification of the steady-state plasma concentrations of clozapine and N-desmethylclozapine in Japanese patients with schizophrenia using a novel HPLC method and the effects of CYPs and ABC transporters polymorphisms. *Annals of Clinical Biochemistry*, 54(6), 677–685. doi: 10.1177/0004563216686377
- Al-Shakliah, N. S., Attwa, M. W., Kadi, A. A. and Alrabiah, H. (2020). Identification and characterization of in silico, in vivo, in vitro, and reactive metabolites of infigratinib using LC-ITMS: bioactivation pathway elucidation and in silico toxicity studies of its metabolites. *RSC Advances*, 10(28), 16231–16244. doi: 10.1039/c9ra10871h

- Almazroo, O. A., Miah, M. K. and Venkataramanan, R. (2017). Drug metabolism in the liver. *Clinics in Liver Disease*, 21(1), 1–20. doi: 10.1016/j.cld.2016.08.001
- Altman, R., Asch, E., Bloch, D., Bole, G., Borenstein, D., Brandt, K., ... Wolfe, F. (1986). Development of criteria for the classification and reporting of osteoarthritis: classification of osteoarthritis of the knee. *Arthritis and Rheumatism*, 29(8), 1039–1049. doi: 10.1002/art.1780290816
- Alzolibani, A. A., Al Robaee, A. A., Al-Shobaili, H. A. and Rasheed, Z. (2013). 4-Hydroxy-2-nonenal modified histone-H2A: a possible antigenic stimulus for systemic lupus erythematosus autoantibodies. *Cellular Immunology*, 284(1–2), 154–162. doi: 10.1016/j.cellimm.2013.07.011
- Ames, B. N., Durston, W. E., Yamasaki, E. and Lee, F. D. (1973). Carcinogens are mutagens: a simple test combining liver homogenates for activation and bacteria for detection. *Proceedings of the National Academy of Sciences of the United States of America*, 70(8), 2281–2285. doi: 10.1073/pnas.70.8.2281
- Andersohn, F., Konzen, C. and Edeltraut, G. (2007). Systematic review: agranulocytosis induced by nonchemotherapy. *Annals of Internal Medicine*, 146(9), 657–666. doi: 10.7326/0003-4819-146-7-200704030-00006
- Ang, W. H., Parker, L. J., De Luca, A., Juillerat-Jeanneret, L., Morton, C. J., Lo Bello, M., ... Dyson, P. J. (2009). Rational design of an organometallic glutathione transferase inhibitor. *Angewandte Chemie International Edition*, 48(21), 3854–3857. doi: 10.1002/anie.200900185
- Aniya, Y. and Imaizumi, N. (2011). Mitochondrial glutathione transferases involving a new function for membrane permeability transition pore regulation. *Drug Metabolism Reviews*, 43(2), 292–299. doi: 10.3109/03602532.2011.552913
- Annesley, T. M. (2003). Ion suppression in mass spectrometry. *Clinical Chemistry*, 49(7), 1041–1044. doi: 10.1373/49.7.1041
- Arakawa, S., Maejima, T., Fujimoto, K., Yamaguchi, T., Yagi, M., Sugiura, T., ... Yamazoe, Y. (2012). Resistance to acetaminophen-induced hepatotoxicity in glutathione S-transferase Mu 1-null mice. *The Journal of Toxicological Sciences*, 37(3), 595–605. doi: 10.2131/jts.37.595
- Argüelles, S., Machado, A. and Ayala, A. (2009). Adduct formation of 4-hydroxynonenal and malondialdehyde with elongation factor-2 in vitro and in vivo. *Free Radical Biology & Medicine*, 47(3), 324–330. doi: 10.1016/j.freeradbiomed.2009.05.010

- Atterbury, C. E., Maddrey, W. C. and Conn, H. O. (1978). Neomycin-sorbitol and lactulose in the treatment of acute portal-systemic encephalopathy. A controlled, double-blind clinical trial. *The American Journal of Digestive Diseases*, 23(5), 398–406. doi: 10.1007/BF01072921
- Attia, E., Steinglass, J. E., Timothy Walsh, B., Wang, Y., Wu, P., Schreyer, C., ... Marcus, M. D. (2019). Olanzapine versus placebo in adult outpatients with anorexia nervosa: a randomized clinical trial. *The American Journal of Psychiatry*, 176(6), 449–456. doi: 10.1176/appi.ajp.2018.18101125
- Attia, S. M. (2010). Deleterious effects of reactive metabolites. *Oxidative Medicine and Cellular Longevity*, 3(4), 238–253. doi: 10.4161/oxim.3.4.13246
- Ayala, A., Muñoz, M. F. and Argüelles, S. (2014). Lipid peroxidation: production, metabolism, and signaling mechanisms of malondialdehyde and 4-hydroxy-2-nonenal. *Oxidative Medicine and Cellular Longevity*, 360438. doi: 10.1155/2014/360438
- Bag, A., Pant, N. K., Jeena, L. M., Bag, N. and Jyala, N. S. (2013). GSTT1 null and MPO -463G>a polymorphisms and carboplatin toxicity in an Indian population. *Asian Pacific Journal of Cancer Prevention*, 14(8), 4739–4742. doi: 10.7314/apjcp.2013.14.8.4739
- Baillie, T. A. (2009). Approaches to the assessment of stable and chemically reactive drug metabolites in early clinical trials. *Chemical Research in Toxicology*, 22(2), 263–266. doi: 10.1021/tx800439k
- Baillie, T. A. and Davis, M. R. (1993). Mass spectrometry in the analysis of glutathione conjugates. *Biological Mass Spectrometry*, 22(6), 319–325. doi: 10.1002/bms.1200220602
- Baldessarini, R. J. and Frankenburg, F. R. (1991). Clozapine. A novel antipsychotic agent. *The New England Journal of Medicine*, 324(11), 746–754. doi: 10.1056/NEJM199103143241107
- Balogh, L. M. and Atkins, W. M. (2011). Interactions of glutathione transferases with 4-hydroxynonenal. *Drug Metabolism Reviews*, 43(2), 165–178. doi: 10.1016/j.physbeh.2017.03.040
- Balogh, L. M., Le Trong, I., Kripps, K. A., Tars, K., Stenkamp, R. E., Mannervik, B. and Atkins, W. M. (2009). Structural analysis of a glutathione transferase A1-1 mutant tailored for high catalytic efficiency with toxic alkenals. *Biochemistry*, 48(32), 7698–7704. doi: 10.1021/bi900895b

- Bannister, A. J. and Kouzarides, T. (2011). Regulation of chromatin by histone modifications. *Cell Research*, 21(3), 381–395. doi: 10.1038/cr.2011.22
- Barańczyk-Kuźma, A., Kuźma, M., Gutowicz, M., Kaźmierczak, B. and Sawicki, J. (2004). Glutathione S-transferase pi as a target for tricyclic antidepressants in human brain. *Acta Biochimica Polonica*, 51(1), 207–212. doi: 10.18388/abp.2004_3612
- Baron, J. M., Höller, D., Schiffer, R., Frankenberg, S., Neis, M., Merk, H. F. and Jugert, F. K. (2001). Expression of multiple cytochrome P450 enzymes and multidrug resistance-associated transport proteins in human skin keratinocytes. *Journal of Investigative Dermatology*, 116(4), 541–548. doi: 10.1046/j.1523-1747.2001.01298.x
- Barrera, G., Pizzimenti, S., Ciamporcerio, E., Daga, M., Ullio, C., Arcaro, A., ... Gentile, F. (2015). Role of 4-hydroxynonenal-protein adducts in human diseases. *Antioxidant & Redox Signaling*, 11(18), 1681–1702. doi: 10.1089/ars.2014.6166
- Barter, M. J., Bui, C. and Young, D. A. (2012). Epigenetic mechanisms in cartilage and osteoarthritis: DNA methylation, histone modifications and microRNAs. *Osteoarthritis and Cartilage*, 20(5), 339–349. doi: 10.1016/j.joca.2011.12.012
- Batth, T. S., Francavilla, C. and Olsen, J. V. (2014). Off-line high-pH reversed-phase fractionation for in-depth phosphoproteomics. *Journal of Proteome Research*, 13(12), 6176–6186. doi: 10.1021/pr500893m
- Beckett, G. J., Chapman, B. J., Dyson, E. H. and Hayes, J. D. (1985). Plasma glutathione S-transferase measurements after paracetamol overdose: evidence for early hepatocellular damage. *Gut*, 26(1), 26–31. doi: 10.1136/gut.26.1.26
- Benedetti, A., Comporti, M., Fulceri, R. and Esterbauer, H. (1984). Cytotoxic aldehydes originating from the peroxidation of liver microsomal lipids. Identification of 4,5-dihydroxydecenal. *Biochimica et Biophysica Acta (BBA)/Lipids and Lipid Metabolism*, 792(2), 172–181. doi: 10.1016/0005-2760(84)90219-4
- Benedetti, M. S., Whomsley, R., Poggesi, I., Cawello, W., Mathy, F.-X., Delporte, M.-L., ... Watelet, J.-B. (2009). Drug metabolism and pharmacokinetics. *Drug Metabolism Reviews*, 41(3), 344–390. doi: 10.1080/10837450902891295
- Benjamini, Y. and Hochberg, Y. (1995). Controlling the false discovery rate: a practical and powerful approach to multiple testing. *Journal of the Royal Statistical Society. Series B (Methodological)*, 57(1), 289–300. doi: 10.2307/2346101

- Bentz, M., Zaouter, C., Shi, Q., Fahmi, H., Moldovan, F., Fernandes, J. C. and Benderdour, M. (2012). Inhibition of inducible nitric oxide synthase prevents lipid peroxidation in osteoarthritic chondrocytes. *Journal of Cellular Biochemistry*, 113(7), 2256–2267. doi: 10.1002/jcb.24096
- Betteridge, D. J. (2000). What is oxidative stress? *Metabolism: Clinical and Experimental*, 49(2 SUPPL. 1), 3–8. doi: 10.1016/S0026-0495(00)80077-3
- Biemann, K. (1990). Appendix 5. Nomenclature for peptide fragment ions (positive ions). *Methods in Enzymology*, 193, 886–887. doi: 10.1016/0076-6879(90)93460-3
- Boerma, J. S., Dragovic, S., Vermeulen, N. P. E. and Commandeur, J. N. M. (2012). Mass spectrometric characterization of protein adducts of multiple P450-dependent reactive intermediates of diclofenac to human glutathione-S-transferase P1-1. *Chemical Research in Toxicology*, 25(11), 2532–2541. doi: 10.1021/tx300334w
- Boerma, J. S., Vermeulen, N. P. E. and Commandeur, J. N. M. (2011). Application of CYP102A1M11H as a tool for the generation of protein adducts of reactive drug metabolites. *Chemical Research in Toxicology*, 24(8), 1263–1274. doi: 10.1021/tx2001515
- Bolton, J. L. (2014). Quinone methide bioactivation pathway: contribution to toxicity and/or cytoprotection? *Current Organic Chemistry*, 18(1), 61–69. doi: 10.2174/138527281801140121123046
- Borlak, J. and Thum, T. (2001). Induction of nuclear transcription factors, cytochrome P450 monooxygenases, and glutathione S-transferase alpha gene expression in Aroclor 1254-treated rat hepatocyte cultures. *Biochemical Pharmacology*, 61(2), 145–153. doi: 10.1016/S0006-2952(00)00537-2
- Brennan, R. G. and Matthews, B. W. (1989). The helix-turn-helix DNA binding motif. *The Journal of Biological Chemistry*, 264(4), 22–25. Retrieved from <http://www.jbc.org/content/264/4/1903.long>
- Breuer, W., Shvartsman, M. and Cabantchik, Z. I. (2008). Intracellular labile iron. *The International Journal of Biochemistry and Cell Biology*, 40(3), 350–354. doi: 10.1016/j.biocel.2007.03.010
- Brodbelt, J. S. and Wilson, J. J. (2009). Infrared multiphoton dissociation in quadrupole ion traps. *Mass Spectrometry Reviews*, 28(3i), 390–424. doi: 10.1002/mas.20216

- Bruderer, R., Bernhardt, O. M., Gandhi, T., Miladinović, S. M., Cheng, L.-Y., Messner, S., ... Reiter, L. (2015). Extending the limits of quantitative proteome profiling with data-independent acquisition and application to acetaminophen-treated three-dimensional liver microtissues. *Molecular & Cellular Proteomics*, 14(5), 1400–1410. doi: 10.1074/mcp.M114.044305
- Bruenner, B. A., Jones, A. D. and German, J. B. (1995). Direct characterization of protein adducts of the lipid peroxidation product 4-hydroxy-2-nonenal using electrospray mass spectrometry. *Chemical Research in Toxicology*, 8(4), 552–559. doi: 10.1021/tx00046a009
- Buchard, A., Eefsen, M., Semb, S., Andersen, S. E., Morling, N., Bendtsen, F., ... Dalhoff, K. (2012). The role of the glutathione S-transferase genes GSTT1, GSTM1, and GSTP1 in acetaminophen-poisoned patients. *Clinical Toxicology (Philadelphia, Pa.)*, 50(1), 27–33. doi: 10.3109/15563650.2011.639713
- Burnette, W. N. (1981). “Western blotting”: electrophoretic transfer of proteins from sodium dodecyl sulfate-polyacrylamide gels to unmodified nitrocellulose and radiographic detection with antibody and radioiodinated protein A. *Analytical Biochemistry*, 112(2), 195–203. doi: 10.1016/0003-2697(81)90281-5
- Busenlehner, L. S., Codreanu, S. G., Holm, P. J., Bhakat, P., Hebert, H., Morgenstern, R. and Armstrong, R. N. (2004). Stress sensor triggers conformational response of the integral membrane protein microsomal glutathione transferase 1. *Biochemistry*, 43(35), 11145–11152. doi: 10.1021/bi048716k
- Cairney, D. G., Beckwith, H. K. S., Al-Hourani, K., Eddleston, M., Bateman, D. N. and Dear, J. W. (2016). Plasma paracetamol concentration at hospital presentation has a dose-dependent relationship with liver injury despite prompt treatment with intravenous acetylcysteine. *Clinical Toxicology (Philadelphia, Pa.)*, 54(5), 405–410. doi: 10.3109/15563650.2016.1159309
- Caldwell, G., Yan, Z., Tang, W., Dasgupta, M. and Hasting, B. (2009). ADME optimization and toxicity assessment in early- and late-phase drug discovery. *Current Topics in Medicinal Chemistry*, 9(11), 965–980. doi: 10.2174/156802609789630929
- Cameron, H. A. and Ramsay, L. E. (1984). The lupus syndrome induced by hydralazine: a common complication with low dose treatment. *British Medical Journal (Clinical Research Ed.)*, 289(6442), 410–412. doi: 10.1136/bmj.289.6442.410
- Cao, Z., Mou, R., Cao, Z., Lin, X., Ma, Y., Zhu, Z. and Chen, M. (2017). Quantitation of glutathione S-transferases in rice (*Oryza sativa* L.) roots exposed to cadmium

by liquid chromatography-tandem mass spectrometry using isotope-labeled wing peptides as an internal standard. *Plant Methods*, 13, 64. doi: 10.1186/s13007-017-0214-2

- Carbone, D. L., Doorn, J. A., Kiebler, Z., Ickes, B. R. and Petersen, D. R. (2005). Modification of heat shock protein 90 by 4-hydroxynonenal in a rat model of chronic alcoholic liver disease. *Journal of Pharmacology and Experimental Therapeutics*, 315(1), 8–15. doi: 10.1124/jpet.105.088088
- Carbone, D. L., Doorn, J. A., Kiebler, Z., Sampey, B. P. and Petersen, D. R. (2004). Inhibition of Hsp72-mediated protein refolding by 4-hydroxy-2-nonenal. *Chemical Research in Toxicology*, 17(11), 1459–1467. doi: 10.1021/tx049838g
- Carlsson, H. and Törnqvist, M. (2017). An adductomic approach to identify electrophiles in vivo. *Basic & Clinical Pharmacology and Toxicology*, 121, 44–54. doi: 10.1111/bcpt.12715
- Chalkley, R. J., Bandeira, N., Chambers, M. C., Clauser, K. R., Cottrell, J. S., Deutsch, E. W., ... Sun, R. X. (2014). Proteome informatics research group (iPRG)_2012: a study on detecting modified peptides in a complex mixture. *Molecular and Cellular Proteomics*, 13(1), 360–371. doi: 10.1074/mcp.M113.032813
- Chang, M., Shin, Y. G., van Breemen, R. B., Blond, S. Y. and Bolton, J. L. (2001). Structural and functional consequences of inactivation of human glutathione S-transferase P1-1 mediated by the catechol metabolite of equine estrogens, 4-hydroxyequilenin. *Biochemistry*, 40(15), 4811–4820. doi: 10.1021/bi002513o
- Chang, W.-H., Lin, S.-K., Lane, H.-Y., Wei, F.-C., Hu, W.-H., Lam, Y. W. F. and Jann, M. W. (1998). Reversible metabolism of clozapine and clozapine N-oxide in schizophrenic patients. *Progress in Neuro-Psychopharmacology and Biological Psychiatry*, 22(5), 723–739. doi: 10.1016/S0278-5846(98)00035-9
- Chaudhary, P., Sharma, R., Sahu, M., Vishwanatha, J. K., Awasthi, S. and Awasthi, Y. C. (2013). 4-Hydroxynonenal induces G2/M phase cell cycle arrest by activation of the ataxia telangiectasia mutated and Rad3-related protein (ATR)/checkpoint kinase 1 (Chk1) signaling pathway. *Journal of Biological Chemistry*, 288(28), 20532–20546. doi: 10.1074/jbc.M113.467662
- Chavez, J., Chung, W.-G., Miranda, C. L., Singhal, M., Stevens, J. F. and Maier, C. S. (2010). Site-specific protein adducts of 4-hydroxy-2(E)-nonenal in human THP-1 monocytic cells: protein carbonylation is diminished by ascorbic acid. *Chemical Research in Toxicology*, 23(1), 37–47. doi: 10.1021/tx9002462

- Chen, C.-H., Budas, G. R., Churchill, E. N., Disatnik, M.-H., Hurley, T. D. and Mochly-Rosen, D. (2008). Activation of aldehyde dehydrogenase-2 reduces ischemic damage to the heart. *Science*, 321(5895), 1493–1495. doi: 10.1126/science.1158554
- Cheng, J.-Z., Singhal, S. S., Sharma, A., Saini, M., Yang, Y., Awasthi, S., ... Awasthi, Y. C. (2001). Transfection of mGSTA4 in HL-60 cells protects against 4-hydroxynonenal-induced apoptosis by inhibiting JNK-mediated signaling. *Archives of Biochemistry and Biophysics*, 392(2), 197–207. doi: 10.1006/abbi.2001.2452
- Ciudad, A., Gutiérrez, M., Cañas, F., Gibert, J., Gascón, J., Carrasco, J.-L., ... Alvarez, E. (2005). Safety and effectiveness of olanzapine in monotherapy: a multivariate analysis of a naturalistic study. *Progress in Neuro-Psychopharmacology and Biological Psychiatry*, 29(6), 944–951. doi: 10.1016/j.pnpbp.2005.04.037
- Claas, F. H. J. (1989). Drug-induced agranulocytosis: review of possible mechanisms, and prospects for clozapine studies. *Psychopharmacology*, 99 Suppl, S113–S117. doi: 10.1007/BF00442574
- Clarke, N. J., Rindgen, D., Korfmacher, W. A. and Cox, K. A. (2001). Systematic LC/MS metabolite identification in drug discovery. *Analytical Chemistry*, 73(15), 430A-439A. doi: 10.1021/ac012480y
- Codreanu, S. G., Ullery, J. C., Zhu, J., Tallman, K. A., Beavers, W. N., Porter, N. A., ... Liebler, D. C. (2014). Alkylation damage by lipid electrophiles targets functional protein systems. *Molecular & Cellular Proteomics*, 13(3), 849–859. doi: 10.1074/mcp.M113.032953
- Codreanu, S. G., Zhang, B., Sobocki, S. M., Billheimer, D. D. and Liebler, D. C. (2009). Global analysis of protein damage by the lipid electrophile 4-hydroxy-2-nonenal. *Molecular & Cellular Proteomics*, 8(4), 670–680. doi: 10.1074/mcp.M800070-MCP200
- Cody, R. B., Burnler, R. C., Cassady, C. J. and Freiser, B. S. (1982). Consecutive collision-induced dissociations in Fourier transform mass spectrometry. *Analytical Chemistry*, 54(13), 2225–2228. doi: 10.1021/ac00250a021
- Cohen, S. D., Pumford, N. R., Khairallah, E. A., Boekelheide, K., Pohl, L. R., Amouzadeh, H. R. and Hinson, J. A. (1997). Selective protein covalent binding and target organ toxicity. *Toxicology and Applied Pharmacology*, 143(1), 1–12. doi: 10.1006/taap.1996.8074

- Coles, B., Wilson, I., Wardman, P., Hinson, J. A., Nelson, S. D. and Ketterer, B. (1988). The spontaneous and enzymatic reaction of N-acetyl-p-benzoquinonimine with glutathione: a stopped-flow kinetic study. *Archives of Biochemistry and Biophysics*, 264(1), 253–260. doi: 10.1016/0003-9861(88)90592-9
- Committee on Herbal Medicinal Products. (2013). *Assessment report on Curcuma xanthorrhiza Roxb. (C. xanthorrhiza D. Dietrich), rhizoma*. London, United Kingdom. Retrieved from http://www.ema.europa.eu/docs/en_GB/document_library/Herbal_-_HMPC_assessment_report/2013/06/WC500144564.pdf
- Conn, H. O. and Lieberthal, M. M. (1979). *The hepatic coma syndromes and lactulose*. Baltimore, MD: Williams & Wilkins. Retrieved from [http://www.gastrojournal.org/article/0016-5085\(79\)90191-4/abstract](http://www.gastrojournal.org/article/0016-5085(79)90191-4/abstract)
- Connor, R. E., Marnett, L. J. and Liebler, D. C. (2011). Protein-selective capture to analyze electrophile adduction of Hsp90 by 4-hydroxynonenal. *Chemical Research in Toxicology*, 24(8), 1275–1282. doi: 10.1021/tx200157t
- Cook, S. F., King, A. D., Chang, Y., Murray, G. J., Norris, H.-R. K., Dart, R. C., ... Wilkins, D. G. (2015). Quantification of a biomarker of acetaminophen protein adducts in human serum by high-performance liquid chromatography-electrospray ionization-tandem mass spectrometry: clinical and animal model applications. *Journal of Chromatography B. Analytical Technologies in the Biomedical and Life Sciences*, 985, 131–141. doi: 10.1016/j.jchromb.2015.01.028
- Copple, I. M., Goldring, C. E., Jenkins, R. E., Chia, A. J. L., Randle, L. E., Hayes, J. D., ... Park, B. K. (2008). The hepatotoxic metabolite of acetaminophen directly activates the Keap1-Nrf2 cell defense system. *Hepatology*, 48(4), 1292–1301. doi: 10.1002/hep.22472
- Croom, E. (2012). Metabolism of xenobiotics of human environments. In *Progress in Molecular Biology and Translational Science* (1st ed., vol. 112, 3, pp. 31–88). Elsevier Inc. doi: 10.1016/B978-0-12-415813-9.00003-9
- Curto, M., Comparelli, A., Ciavarella, G. M., Gasperoni, C., Lionetto, L., Corigliano, V., ... Baldessarini, R. J. (2015). Impairment of left ventricular function early in treatment with clozapine: a preliminary study. *International Clinical Psychopharmacology*, 30(5), 282–289. doi: 10.1097/YIC.0000000000000085
- Czerwinski, M., Gibbs, J. P. and Slattery, J. T. (1996). Busulfan conjugation by glutathione S-transferases alpha, mu, and pi. *Drug Metabolism and Disposition*, 24(9), 1015–1019. Retrieved from

<http://dmd.aspetjournals.org/content/24/9/1015>

- Dahlin, D. C., Miwa, G. T., Lu, A. Y. H. and Nelson, S. D. (1984). N-acetyl-p-benzoquinone imine: a cytochrome P-450-mediated oxidation product of acetaminophen. *Proceedings of the National Academy of Sciences of the United States of America*, 81(5), 1327–1331. doi: 10.1073/pnas.81.5.1327
- Dalvie, D., Kalgutkar, A. S. and Chen, W. (2015). Practical approaches to resolving reactive metabolite liabilities in early discovery. *Drug Metabolism Reviews*, 47(1), 56–70. doi: 10.3109/03602532.2014.984813
- Damsten, M. C., Commandeur, J. N. M., Fidler, A., Hulst, A. G., Touw, D., Noort, D. and Vermeulen, N. P. E. (2007). Liquid chromatography/tandem mass spectrometry detection of covalent binding of acetaminophen to human serum albumin. *Drug Metabolism & Disposition*, 35(8), 1408–1417. doi: 10.1124/dmd.106.014233
- Darweesh, S. K., Ibrahim, M. F. and El-Tahawy, M. A. (2017). Effect of N-acetylcysteine on mortality and liver transplantation rate in non-acetaminophen-induced acute liver failure: a multicenter study. *Clinical Drug Investigation*, 37(5), 473–482. doi: 10.1007/s40261-017-0505-4
- Datta, A., Kamthan, A. and Kamthan, M. (2015). *A simple protocol to detect interacting proteins by GST pull down assay coupled with MALDI or LC-MS/MS analysis*. doi: 10.1038/protex.2015.093
- Davis, D. C., Potter, W. Z., Jollow, D. J. and Mitchell, J. R. (1974). Species differences in hepatic glutathione depletion, covalent binding and hepatic necrosis after acetaminophen. *Life Sciences*, 14(11), 2099–2109. doi: 10.1016/0024-3205(74)90092-7
- de Graaf, E. L., Altelaar, A. F. M., van Breukelen, B., Mohammed, S. and Heck, A. J. R. (2011). Improving SRM assay development: a global comparison between triple quadrupole, ion trap, and higher energy CID peptide fragmentation spectra. *Journal of Proteome Research*, 10(9), 4334–4341. doi: 10.1021/pr200156b
- Di Palma, S., Hennrich, M. L., Heck, A. J. R. and Mohammed, S. (2012). Recent advances in peptide separation by multidimensional liquid chromatography for proteome analysis. *Journal of Proteomics*, 75(13), 3791–3813. doi: 10.1016/j.jprot.2012.04.033
- Dieckhaus, C. M., Fernández-Metzler, C. L., King, R., Krolikowski, P. H. and Baillie, T. A. (2005). Negative ion tandem mass spectrometry for the detection of

- glutathione conjugates. *Chemical Research in Toxicology*, 18(4), 630–638. doi: 10.1021/tx049741u
- Dong, H., Haining, R. L., Thummel, K. E., Rettie, A. E. and Nelson, S. D. (2000). Involvement of human cytochrome P450 2D6 in the bioactivation of acetaminophen. *Drug Metabolism & Disposition*, 28(12), 1397–1400. Retrieved from <http://dmd.aspetjournals.org/content/28/12/1397.long>
- Doorn, J. A. and Petersen, D. R. (2002). Covalent modification of amino acid nucleophiles by the lipid peroxidation products 4-hydroxy-2-nonenal and 4-oxo-2-nonenal. *Chemical Research in Toxicology*, 15(11), 1445–1450. doi: 10.1021/tx025590o
- Dorta, G., Siebenmann, R., Fröhli, P., Freytag, P. and Koelz, H. R. (1989). Clozapine-induced cholestatic jaundice: a case report. *Zeitschrift für Gastroenterologie*, 27(7), 388–390.
- Dragovic, S., Boerma, J. S., van Bergen, L., Vermeulen, N. P. E. and Commandeur, J. N. M. (2010). Role of human glutathione S-transferases in the inactivation of reactive metabolites of clozapine. *Chemical Research in Toxicology*, 23(9), 1467–1476. doi: 10.1021/tx100131f
- Dragovic, S., Venkataraman, H., Begheijn, S., Vermeulen, N. P. E. and Commandeur, J. N. M. (2014). Effect of human glutathione S-transferase hGSTP1-1 polymorphism on the detoxification of reactive metabolites of clozapine, diclofenac and acetaminophen. *Toxicology Letters*, 224(2), 272–281. doi: 10.1016/j.toxlet.2013.10.023
- Drake, J., Petroze, R., Castegna, A., Ding, Q., Keller, J. N., Markesbery, W. R., ... Butterfield, D. A. (2004). 4-Hydroxynonenal oxidatively modifies histones: implications for Alzheimer's disease. *Neuroscience Letters*, 356(3), 155–158. doi: 10.1016/j.neulet.2003.11.047
- Druckova, A., Mernaugh, R. L., Ham, A.-J. L. and Marnett, L. J. (2007). Identification of the protein targets of the reactive metabolite of teucrin A in vivo in the rat. *Chemical Research in Toxicology*, 20(10), 1393–1408. doi: 10.1021/tx7001405
- Du, F., Ruan, Q., Zhu, M. and Xing, J. (2013). Detection and characterization of ticlopidine conjugates in rat bile using high-resolution mass spectrometry: applications of various data acquisition and processing tools. *Journal of Mass Spectrometry*, 48(3), 413–422. doi: 10.1002/jms.3170
- Dubois, M., De Wuziers, I., Thome, J. P. and Kremers, P. (1996). P450 induction by

- rochlor 1254 and 3,3',4,4'-tetrachlorobiphenyl in cultured hepatocytes from rat, quail and man: interspecies comparison. *Comparative Biochemistry and Physiology Part C: Pharmacology, Toxicology and Endocrinology*, 113(1), 51–59. doi: 8665401
- Dunn, W. B., Broadhurst, D. I., Atherton, H. J., Goodacre, R. and Griffin, J. L. (2011). Systems level studies of mammalian metabolomes: the roles of mass spectrometry and nuclear magnetic resonance spectroscopy. *Chemical Society Reviews*, 40(1), 387–426. doi: 10.1039/b906712b
- Easterbrook, J., Fackett, D. and Li, A. P. (2001). A comparison of arochlor 1254-induced and uninduced rat liver microsomes to human liver microsomes in phenytoin O-deethylation, coumarin 7-hydroxylation, tolbutamide 4-hydroxylation, S-mephenytoin 4'-hydroxylation, chloroxazone 6-hydroxylation and testoste. *Chemico-Biological Interactions*, 134(3), 243–249. doi: 10.1016/S0009-2797(01)00159-4
- Eaton, D. L. and Bammler, T. K. (1999). Concise review of the glutathione S-transferases and their significance to toxicology. *Toxicological Sciences*, 49(2), 156–164. doi: 10.1093/toxsci/49.2.156
- Ejiri, N., Katayama, K. and Doi, K. (2005). Induction of cytochrome P450 isozymes by phenobarbital in pregnant rat and fetal livers and placenta. *Experimental and Molecular Pathology*, 78(2), 150–155. doi: 10.1016/j.yexmp.2004.07.002
- El-Bikai, R., Welman, M., Margaron, Y., Côté, J.-F., Macqueen, L., Buschmann, M. D., ... Benderdour, M. (2010). Perturbation of adhesion molecule-mediated chondrocyte-matrix interactions by 4-hydroxynonenal binding: implication in osteoarthritis pathogenesis. *Arthritis Research & Therapy*, 12(5), 1–14. doi: 10.1186/ar3173
- El Mansouri, F. E., Chabane, N., Zayed, N., Kapoor, M., Benderdour, M., Martel-Pelletier, J., ... Fahmi, H. (2011). Contribution of H3K4 methylation by SET-1A to interleukin-1-induced cyclooxygenase 2 and inducible nitric oxide synthase expression in human osteoarthritis chondrocytes. *Arthritis & Rheumatism*, 63(1), 168–179. doi: 10.1002/art.27762
- El Mansouri, F. E., Nebbaki, S.-S., Kapoor, M., Afif, H., Martel-Pelletier, J., Pelletier, J.-P., ... Fahmi, H. (2014). Lysine-specific demethylase 1-mediated demethylation of histone H3 lysine 9 contributes to interleukin 1beta-induced microsomal prostaglandin E synthase 1 expression in human osteoarthritic chondrocytes. *Arthritis Research & Therapy*, 16(3), R113. doi: 10.1186/ar4564

- Elias, J. E. and Gygi, S. P. (2010). Target-decoy search strategy for mass spectrometry-based proteomics. *Methods in Molecular Biology*, 604(August), 55–71. doi: 10.1007/978-1-60761-444-9_5
- Emwas, A.-H. M. (2015). The strengths and weaknesses of NMR spectroscopy and mass spectrometry with particular focus on metabolomics research. In J. Bjerrum (ed.), *Metabonomics. Methods in Molecular Biology* (1st ed., vol. 1277, 13, pp. 161–193). New York, NY : Humana Press. doi: 10.1007/978-1-4939-2377-9_13
- Engvall, E. and Perlmann, P. (1972). Enzyme-linked immunosorbent assay, Elisa. 3. Quantitation of specific antibodies by enzyme-labeled anti-immunoglobulin in antigen-coated tubes. *The Journal of Immunology*, 109(1), 129–135. Retrieved from <https://www.jimmunol.org/content/109/1/129.long>
- Esterbauer, H., Schaur, R. J. and Zollner, H. (1991). Chemistry and biochemistry of 4-hydroxynonenal, malonaldehyde and related aldehydes. *Free Radical Biology & Medicine*, 11(1), 81–128. doi: 10.1016/0891-5849(91)90192-6
- Fagan, E. and Wannan, G. (1996). Reducing paracetamol overdoses. *The BMJ*, 313(7070), 1417–1418. Retrieved from <http://www.bmj.com/content/313/7070/1417.long>
- Fang, J., Coutts, R. T., McKenna, K. F. and Baker, G. B. (1998). Elucidation of individual cytochrome P450 enzymes involved in the metabolism of clozapine. *Naunyn-Schmiedeberg's Archives of Pharmacology*, 358(5), 592–599. doi: 10.1007/PL00005298
- Federici, L., Lo Sterzo, C., Pezzola, S., Di Matteo, A., Scaloni, F., Federici, G. and Caccuri, A. M. (2009). Structural basis for the binding of the anticancer compound 6-(7-nitro-2,1,3-benzoxadiazol-4-ylthio)hexanol to human glutathione S-transferases. *Cancer Research*, 69(20), 8025–8034. doi: 10.1158/0008-5472.CAN-09-1314
- Fehsel, K., Loeffler, S., Krieger, K., Henning, U., Agelink, M., Kolb-Bachofen, V. and Klimke, A. (2005). Clozapine induces oxidative stress and proapoptotic gene expression in neutrophils of schizophrenic patients. *Journal of Clinical Psychopharmacology*, 25(5), 419–426. doi: 10.1097/01.jcp.0000177668.42640.fe
- Feist, P. and Hummon, A. B. (2015). Proteomic challenges: sample preparation techniques for microgram-quantity protein analysis from biological samples. *International Journal of Molecular Sciences*, 16(2), 3537–3563. doi: 10.3390/ijms16023537

- Fenn, J. B., Mann, M., Meng, C. K., Wong, S. F. and Whitehouse, C. M. (1989). Electrospray ionization for mass spectrometry of large biomolecules. *Science*, 246(49266), 64–71. doi: 10.1126/science.2675315
- Fernandez, M. P., Young, M. F. and Sobel, M. E. (1985). Methylation of type II and type I collagen genes in differentiated and dedifferentiated chondrocytes. *Journal of Biological Chemistry*, 260(4), 2374–2378. Retrieved from <http://www.jbc.org/content/260/4/2374.long>
- Fulton, B. and Goa, K. L. (1997). Olanzapine. A review of its pharmacological properties and therapeutic efficacy in the management of schizophrenia and related psychoses. *Drugs*, 53(2), 281–298. doi: 10.2165/00003495-199753020-00007
- Furey, A., Moriarty, M., Bane, V., Kinsella, B. and Lehane, M. (2013). Ion suppression; a critical review on causes, evaluation, prevention and applications. *Talanta*, 115, 104–122. doi: 10.1016/j.talanta.2013.03.048
- Galligan, J. J., Rose, K. L., Beavers, W. N., Hill, S., Tallman, K. A., Tansey, W. P. and Marnett, L. J. (2014). Stable histone adduction by 4-oxo-2-nonenal: a potential link between oxidative stress and epigenetics. *Journal of the American Chemical Society*, 136(34), 11864–11866. doi: 10.1021/ja503604t
- Gan, J., Zhang, H. and Humphreys, W. G. (2016). Drug-protein adducts: chemistry, mechanisms of toxicity, and methods of characterization. *Chemical Research in Toxicology*, 29(12), 2040–2057. doi: 10.1021/acs.chemrestox.6b00274
- Gardner, I., Leeder, J. S., Chin, T., Zahid, N. and Uetrecht, J. P. (1998a). A comparison of the covalent binding of clozapine and olanzapine to human neutrophils in vitro and in vivo. *Molecular Pharmacology*, 53(6), 999–1008. Retrieved from <http://molpharm.aspetjournals.org/content/53/6/999>
- Gardner, I., Zahid, N., MacCrimmon, D. and Uetrecht, J. P. (1998b). A comparison of the oxidation of clozapine and olanzapine to reactive metabolites and the toxicity of these metabolites to human leukocytes. *Molecular Pharmacology*, 53(6), 991–998. Retrieved from <http://molpharm.aspetjournals.org/content/53/6/991.long>
- Geib, T., LeBlanc, A., Shiao, T. C., Roy, R., Leslie, E. M., Karvellas, C. J. and Sleno, L. (2018). Absolute quantitation of acetaminophen-modified human serum albumin in acute liver failure patients by liquid chromatography/tandem mass spectrometry. *Rapid Communications in Mass Spectrometry*, 32(17), 1573–1582. doi: 10.1002/rcm.8206

- Geib, T., Lento, C., Wilson, D. J. and Sleno, L. (2019). Liquid chromatography-tandem mass spectrometry analysis of acetaminophen covalent binding to glutathione S-transferases. *Frontiers in Chemistry*, 7, 558. doi: 10.3389/fchem.2019.00558
- Geib, T., Sleno, L., Hall, R. A., Stokes, C. S. and Volmer, D. A. (2016). Triple quadrupole versus high resolution quadrupole-time-of-flight mass spectrometry for quantitative LC-MS/MS analysis of 25-hydroxyvitamin D in human serum. *Journal of the American Society for Mass Spectrometry*, 27(8), 1404–1410. doi: 10.1007/s13361-016-1412-2
- Giansanti, P., Tsiatsiani, L., Low, T. Y. and Heck, A. J. R. (2016). Six alternative proteases for mass spectrometry-based proteomics beyond trypsin. *Nature Protocols*, 11(5), 993–1006. doi: 10.1038/nprot.2016.057
- Gibson, J. D., Pumford, N. R., Samokyszyn, V. M. and Hinson, J. A. (1996). Mechanism of acetaminophen-induced hepatotoxicity: covalent binding versus oxidative stress. *Chemical Research in Toxicology*, 9(3), 580–585. doi: 10.1021/tx950153d
- Gillette, M. A. and Carr, S. A. (2013). Quantitative analysis of peptides and proteins in biomedicine by targeted mass spectrometry. *Nature Methods*, 10(1), 28–34. doi: 10.1038/nmeth.2309
- Glover, M. S., Shi, L., Fuller, D. R., Arnold, R. J., Radivojac, P. and Clemmer, D. E. (2015). On the split personality of penultimate proline. *Journal of the American Society for Mass Spectrometry*, 26(3), 444–452. doi: 10.1007/s13361-014-1049-y
- Golizeh, M., Abusarah, J., Benderdour, M. and Sleno, L. (2014). Covalent binding of 4-hydroxynonenal to matrix metalloproteinase 13 studied by liquid chromatography-mass spectrometry. *Chemical Research in Toxicology*, 27(9), 1556–1565. doi: 10.1021/tx5002095
- Golizeh, M., Geib, T. and Sleno, L. (2016). Identification of 4-hydroxynonenal protein targets in rat, mouse and human liver microsomes by two-dimensional liquid chromatography/tandem mass spectrometry. *Rapid Communications in Mass Spectrometry*, 30(13), 1488–1494. doi: 10.1002/rcm.7577
- Golizeh, M., LeBlanc, A. and Sleno, L. (2015). Identification of acetaminophen adducts of rat liver microsomal proteins using 2D-LC-MS/MS. *Chemical Research in Toxicology*, 28(11), 2142–2150. doi: 10.1021/acs.chemrestox.5b00317

- Gómez-Lechón, M. J., Donato, T., Ponsoda, X. and Castell, J. V. (2003). Human hepatic cell cultures: in vitro and in vivo drug metabolism. *Alternatives to Laboratory Animals*, 31(3), 257–265. doi: 10.1177/026119290303100307
- Grillo, M. P. (2015). Detecting reactive drug metabolites for reducing the potential for drug toxicity. *Expert Opinion on Drug Metabolism and Toxicology*, 11(8), 1281–1302. doi: 10.1517/17425255.2015.1048222
- Grimm, F. A., Hu, D., Kania-Korwel, I., Lehmler, H.-J., Ludewig, G., Hornbuckle, K. C., ... Robertson, L. W. (2015). Metabolism and metabolites of polychlorinated biphenyls. *Critical Reviews in Toxicology*, 45(3), 245–272. doi: 10.3109/10408444.2014.999365
- Griss, J. (2016). Spectral library searching in proteomics. *Proteomics*, 16(5), 729–740. doi: 10.1002/pmic.201500296
- Grønberg, M., Kristiansen, T. Z., Stensballe, A., Andersen, J. S., Ohara, O., Mann, M., ... Pandey, A. (2002). A mass spectrometry-based proteomic approach for identification of serine/threonine-phosphorylated proteins by enrichment with phospho-specific antibodies: identification of a novel protein, Frigg, as a protein kinase A substrate. *Molecular & Cellular Proteomics*, 1(7), 517–527. doi: 10.1074/mcp.M200010-MCP200
- Groom, H., Lee, M., Patil, P. and Josephy, P. D. (2014). Inhibition of human glutathione transferases by dinitronaphthalene derivatives. *Archives of Biochemistry and Biophysics*, 555–556, 71–76. doi: 10.1016/j.abb.2014.06.002
- Gross, J. H. (2004). *Mass Spectrometry - A Textbook* (1st ed.). Heidelberg, Germany : Springer-Verlag. doi: 10.1007/978-3-642-10711-5
- Guengerich, F. P. (2005). Generation of reactive intermediates. *Journal of Biochemical and Molecular Toxicology*, 19(3), 173–174. doi: 10.1002/jbt.20072
- Guengerich, F. P. (2008). Cytochrome P450 and chemical toxicology. *Chemical Research in Toxicology*, 21(1), 70–83. doi: 10.1021/tx700079z
- Guillén, M. D. and Goicoechea, E. (2008). Toxic oxygenated α,β -unsaturated aldehydes and their study in foods: a review. *Critical Reviews in Food Science and Nutrition*, 48(2), 119–136. doi: 10.1080/10408390601177613
- Habig, W. H., Pabst, M. J. and Jakoby, W. B. (1974). Glutathione S-transferases. The first enzymatic step in mercapturic acid formation. *The Journal of Biological Chemistry*, 249(22), 7130–7139. Retrieved from

<http://www.jbc.org/content/249/22/7130.long>

- Hadi, M., Dragovic, S., van Swelm, R., Herpers, B., van de Water, B., Russel, F. G. M., ... Groothuis, G. M. M. (2013a). AMAP, the alleged non-toxic isomer of acetaminophen, is toxic in rat and human liver. *Archives of Toxicology*, 87(1), 155–165. doi: 10.1007/s00204-012-0924-1
- Hadi, M., Westra, I. M., Starokozhko, V., Dragovic, S., Merema, M. T. and Groothuis, G. M. M. (2013b). Human precision-cut liver slices as an ex vivo model to study idiosyncratic drug-induced liver injury. *Chemical Research in Toxicology*, 26(5), 710–720. doi: 10.1021/tx300519p
- Hägg, S., Jönsson, A. K. and Spigset, O. (2009). Risk of venous thromboembolism due to antipsychotic drug therapy. *Expert Opinion on Drug Safety*, 8(5), 537–547. doi: 10.1517/14740330903117271
- Hampton, M. B., Kettle, A. J. and Winterbourn, C. C. (1998). Inside the neutrophil phagosome: oxidants, myeloperoxidase, and bacterial killing. *Blood*, 92(9), 3007–3017. doi: 10.1182/blood.V92.9.3007
- Han, X., Aslanian, A. and Yates 3rd, J. R. (2008). Mass spectrometry for proteomics. *Current Opinion in Chemical Biology*, 12(5), 483–490. doi: 10.1016/j.cbpa.2008.07.024
- Hancock, J. T., Desikan, R. and Neill, S. J. (2001). Role of reactive oxygen species in cell signalling pathways. *Biochemical Society Transactions*, 29(Pt 2), 345–350. doi: 10.1042/0300-5127:0290345
- Haroldsen, P. E., Reilly, M. H., Hughes, H., Gaskell, S. J. and Porter, C. J. (1988). Characterization of glutathione conjugates by fast atom bombardment/tandem mass spectrometry. *Biomedical and Environmental Mass Spectrometry*, 15(11), 615–621. doi: 10.1002/bms.1200151107
- He, N., Bai, S., Huang, Y., Xing, Y., Chen, L., Yu, F. and Lv, C. (2019). Evaluation of glutathione S-transferase inhibition effects on idiopathic pulmonary fibrosis therapy with a near-infrared fluorescent probe in cell and mice models. *Analytical Chemistry*, 91(8), 5424–5432. doi: 10.1021/acs.analchem.9b00713
- Heard, K., Anderson, V., Dart, R. C., Kile, D., Lavonas, E. J. and Green, J. L. (2017). Serum acetaminophen protein adduct concentrations in pediatric emergency department patients. *Journal of Pediatric Gastroenterology and Nutrition*, 64(4), 533–535. doi: 10.1097/MPG.0000000000001459

- Heazlewood, J. L. (2011). The green proteome: challenges in plant proteomics. *Frontiers in Plant Science*, 2, 6. doi: 10.3389/fpls.2011.00006
- Hebert, H., Schmidt-Krey, I. and Morgenstern, R. (1995). The projection structure of microsomal glutathione transferase. *The EMBO Journal*, 14(16), 3864–3869. doi: 10.1002/j.1460-2075.1995.tb00058.x
- Hebert, H., Schmidt-Krey, I., Morgenstern, R., Murata, K., Hirai, T., Mitsuoka, K. and Fujiyoshi, Y. (1997). The 3.0 Å projection structure of microsomal glutathione transferase as determined by electron crystallography of p21212 two-dimensional crystals. *Journal of Molecular Biology*, 271(5), 751–758. doi: 10.1006/jmbi.1997.1216
- Hellberg, K., Grimsrud, P. A., Kruse, A. C., Banaszak, L. J., Ohlendorf, D. H. and Bernlohr, D. A. (2010). X-ray crystallographic analysis of adipocyte fatty acid binding protein (aP2) modified with 4-hydroxy-2-nonenal. *Protein Science*, 19(8), 1480–1489. doi: 10.1002/pro.427
- Hinchman, C. A. and Ballatori, N. (1994). Glutathione conjugation and conversion to mercapturic acids can occur as an intrahepatic process. *Journal of Toxicology and Environmental Health*, 41(4), 387–409. doi: 10.1080/15287399409531852
- Hodgman, M. J. and Garrard, A. R. (2012). A review of acetaminophen poisoning. *Critical Care Clinics*, 28(4), 499–516. doi: 10.1016/j.ccc.2012.07.006
- Hopfgartner, G., Husser, C. and Zell, M. (2003). Rapid screening and characterization of drug metabolites using a new quadrupole–linear ion trap mass spectrometer. *Journal of Mass Spectrometry*, 38(2), 138–150. doi: 10.1002/jms.420
- Hopfgartner, G., Varesio, E., Tschäppät, V., Grivet, C., Bourgoigne, E. and Leuthold, L. A. (2004). Triple quadrupole linear ion trap mass spectrometer for the analysis of small molecules and macromolecules. *Journal of Mass Spectrometry*, 39(8), 845–855. doi: 10.1002/jms.659
- Houen, G. (2015). Peptide antibodies: past, present, and future. In J. M. Walker (ed.), *Methods in Molecular Biology* (1st ed., vol. 1348, 1, pp. 1–6). New York, NY : Humana Press. doi: 10.1007/978-1-4939-2999-3_1
- Huijbers, M. M. E., Montersino, S., Westphal, A. H., Tischler, D. and van Berkel, W. J. H. (2014). Flavin dependent monooxygenases. *Archives of Biochemistry and Biophysics*, 544, 2–17. doi: 10.1016/j.abb.2013.12.005
- Hummer, M., Kurz, M., Kurzthaler, I., Oberbauer, H., Miller, C. and Fleischhacker, W.

- W. (1997). Hepatotoxicity of clozapine. *Journal of Clinical Psychopharmacology*, 17(4), 314–317. doi: 10.1097/00004714-199708000-00012
- Illi, B., Colussi, C., Grasselli, A., Farsetti, A., Capogrossi, M. C. and Gaetano, C. (2009). NO sparks off chromatin: tales of a multifaceted epigenetic regulator. *Pharmacology & Therapeutics*, 123(3), 344–352. doi: 10.1016/j.pharmthera.2009.05.003
- Ingimarsson, O., MacCabe, J. H., Haraldsson, M., Jónsdóttir, H. and Sigurdsson, E. (2016). Neutropenia and agranulocytosis during treatment of schizophrenia with clozapine versus other antipsychotics: an observational study in Iceland. *BMC Psychiatry*, 16(1), 441. doi: 10.1186/s12888-016-1167-0
- Ishii, T., Tatsuda, E., Kumazawa, S., Nakayama, T. and Uchida, K. (2003). Molecular basis of enzyme inactivation by an endogenous electrophile 4-hydroxy-2-nonenal: identification of modification sites in glyceraldehyde-3-phosphate dehydrogenase. *Biochemistry*, 42(12), 3474–3480. doi: 10.1021/bi027172o
- Jakobsson, P.-J., Morgenstern, R., Mancini, J., Ford-Hutchinson, A. and Persson, B. (2008). Common structural features of MAPEG - A widespread superfamily of membrane associated proteins with highly divergent functions in eicosanoid and glutathione metabolism. *Protein Science*, 8(3), 689–692. doi: 10.1110/ps.8.3.689
- Jaladanki, C. K., Shaikh, A. and Bharatam, P. V. (2017). Biotransformation of isoniazid by cytochromes P450: analyzing the molecular mechanism using density functional theory. *Chemical Research in Toxicology*, 30(11), 2060–2073. doi: 10.1021/acs.chemrestox.7b00129
- James, L. P., Chiew, A., Abdel-Rahman, S. M., Letzig, L., Graudins, A., Day, P. and Roberts, D. (2013). Acetaminophen protein adduct formation following low-dose acetaminophen exposure: comparison of immediate-release vs. extended-release formulations. *European Journal of Clinical Pharmacology*, 69(4), 851–857. doi: 10.1007/s00228-012-1410-7
- James, L. P., Letzig, L., Simpson, P. M., Capparelli, E., Roberts, D. W., Hinson, J. A., ... Lee, W. M. (2009). Pharmacokinetics of acetaminophen-protein adducts in adults with acetaminophen overdose and acute liver failure. *Drug Metabolism & Disposition*, 37(8), 1779–1784. doi: 10.1124/dmd.108.026195
- James, L. P., Mayeux, P. R. and Hinson, J. A. (2003). Acetaminophen-induced hepatotoxicity. *Drug Metabolism & Disposition*, 31(12), 1499–1506. doi: 10.1124/dmd.31.12.1499

- James, L. P., Wells, E., Beard, R. H. and Farrar, H. C. (2002). Predictors of outcome after acetaminophen poisoning in children and adolescents. *The Journal of Pediatrics*, 140(5), 522–526. doi: 10.1067/mpd.2002.122936
- Jan, Y.-H., Heck, D. E., Dragomir, A.-C., Gardner, C. R., Laskin, D. L. and Laskin, J. D. (2014). Acetaminophen reactive intermediates target hepatic thioredoxin reductase. *Chemical Research in Toxicology*, 27(5), 882–894. doi: 10.1021/tx5000443
- Jancova, P., Anzenbacher, P. and Anzenbacherova, E. (2010). Phase II drug metabolizing enzymes. *Biomedical Papers*, 154(2), 103–116. doi: 10.5507/bp.2010.017
- Jemal, M. and Ouyang, Z. (2000). The need for chromatographic and mass resolution in liquid chromatography/tandem mass spectrometric methods used for quantitation of lactones and corresponding hydroxy acids in biological samples. *Rapid Communications in Mass Spectrometry*, 14(19), 1757–1765. doi: 10.1002/1097-0231(20001015)14:19<1757::AID-RCM90>3.0.CO;2-C
- Jenkins, R. E., Kitteringham, N. R., Goldring, C. E. P., Dowdall, S. M. J., Hamlett, J., Lane, C. S., ... Park, B. K. (2008). Glutathione-S-transferase pi as a model protein for the characterisation of chemically reactive metabolites. *Proteomics*, 8(2), 301–315. doi: 10.1002/pmic.200700843
- Ji, X., Johnson, W. W., Sesay, M. A., Dickert, L., Prasad, S. M., Ammon, H. L., ... Gilliland, G. L. (1994). Structure and function of the xenobiotic substrate binding site of a glutathione S-transferase as revealed by X-ray crystallographic analysis of product complexes with the diastereomers of 9-(S-glutathionyl)-10-hydroxy-9,10-dihydrophenanthrene. *Biochemistry*, 33(5), 1043–1052. doi: 10.1021/bi00171a002
- Ji, X., Tordova, M., O'Donnell, R., Parsons, J. F., Hayden, J. B., Gilliland, G. L. and Zimniak, P. (1997). Structure and function of the xenobiotic substrate-binding site and location of a potential non-substrate-binding site in a class π glutathione S-transferase. *Biochemistry*, 36(32), 9690–9702. doi: 10.1021/bi970805s
- Ji, Y., Neverova, I., Eyk, J. E. Van and Bennett, B. M. (2006). Nitration of tyrosine 92 mediates the activation of rat microsomal glutathione S-transferase by peroxynitrite. *Journal of Biological Chemistry*, 281(4), 1986–1991. doi: 10.1074/jbc.M509480200
- Jian, W., Liu, H.-F., Zhao, W., Jones, E. and Zhu, M. (2012). Simultaneous screening of glutathione and cyanide adducts using precursor ion and neutral loss scans-

- dependent product ion spectral acquisition and data mining tools. *Journal of the American Society for Mass Spectrometry*, 23(5), 964–976. doi: 10.1007/s13361-012-0354-6
- Jiang, X., Shamshurin, D., Spicer, V. and Krokhin, O. V. (2013). The effect of various S-alkylating agents on the chromatographic behavior of cysteine-containing peptides in reversed-phase chromatography. *Journal of Chromatography B: Analytical Technologies in the Biomedical and Life Sciences*, 915–916, 57–63. doi: 10.1016/j.jchromb.2012.12.010
- Johnson, W. W., Liu, S., Ji, X., Gilliland, G. L. and Armstrong, R. N. (1993). Tyrosine 115 participates both in chemical and physical steps of the catalytic mechanism of a glutathione S-transferase. *Journal of Biological Chemistry*, 268(16), 11508–11511. Retrieved from <http://www.jbc.org/content/268/16/11508.abstract?sid=2a882a46-6483-47f4-83d5-b8f64cae8b08>
- Jollow, D. J., Mitchell, J. R., Potter, W. Z., Davis, D. C., Gillette, J. R. and Brodie, B. B. (1973). Acetaminophen-induced hepatic necrosis. II. Role of covalent binding in vivo. *The Journal of Pharmacology and Experimental Therapeutics*, 187(1), 195–202. Retrieved from <http://jpet.aspetjournals.org/content/187/1/195.long>
- Kalgutkar, A. S., Dalvie, D., Obach, R. S. and Smith, D. A. (2012). Role of reactive metabolites in drug-induced toxicity – the tale of acetaminophen, halothane, hydralazine, and tienilic Acid. In R. Mannhold, H. Kubinyi and G. Folkers (eds.), *Reactive Drug Metabolites* (1st ed., 4, pp. 71–92). Weinheim, Germany : Wiley-VCH Verlag GmbH & Co. KGaA. doi: 10.1002/9783527655748.ch4
- Kalsi, S. S., Dargan, P. I., Waring, W. S. and Wood, D. M. (2011). A review of the evidence concerning hepatic glutathione depletion and susceptibility to hepatotoxicity after paracetamol overdose. *Open Access Emergency Medicine*, 3, 87–96. doi: 10.2147/OAEM.S24963
- Kane, J., Honigfeld, G., Singer, J. and Meltzer, H. (1988). Clozapine for the treatment-resistant schizophrenic. A double-blind comparison with chlorpromazine. *Archives of General Psychiatry*, 45(9), 789–796. doi: 10.1001/archpsyc.1988.01800330013001
- Kap, E. J., Richter, S., Rudolph, A., Jansen, L., Ulrich, A., Hoffmeister, M., ... Chang-Claude, J. (2014). Genetic variants in the glutathione S-transferase genes and survival in colorectal cancer patients after chemotherapy and differences according to treatment with oxaliplatin. *Pharmacogenetics and Genomics*, 24(7), 340–347. doi: 10.1097/FPC.0000000000000059

- Karas, M. and Hillenkamp, F. (1988). Laser Desorption Ionization of Proteins with Molecular Masses Exceeding 10 000 Daltons. *Analytical Chemistry*, 60(20), 2299–2301. doi: 10.1021/ac00171a028
- Kenna, J. G. (2013). A new twist to an old tale: Novel insights into the differential toxicities of acetaminophen and its regioisomer N-acetyl-meta-aminophenol (AMAP). *Archives of Toxicology*, 87(1), 15–18. doi: 10.1007/s00204-012-0945-9
- Kevin Park, B., Coleman, J. W. and Kitteringham, N. R. (1987). Drug disposition and drug hypersensitivity. *Biochemical Pharmacology*, 36(5), 581–590. doi: 10.1016/0006-2952(87)90706-4
- Kilian, J. G., Kerr, K., Lawrence, C. and Celemajer, D. S. (1999). Myocarditis and cardiomyopathy associated with clozapine. *The Lancet*, 354(9193), 1841–1845. doi: 10.1016/S0140-6736(99)10385-4
- King, R., Bonfiglio, R., Fernandez-Metzler, C., Miller-Stein, C. and Olah, T. (2000). Mechanistic investigation of ionization suppression in electrospray ionization. *Journal of the American Society for Mass Spectrometry*, 11(11), 942–950. doi: 10.1016/S1044-0305(00)00163-X
- Klopčič, I. and Dolenc, M. S. (2019). Chemicals and Drugs Forming Reactive Quinone and Quinone Imine Metabolites. *Chemical Research in Toxicology*, 32(1), 1–34. doi: 10.1021/acs.chemrestox.8b00213
- Koen, Y. M., Yue, W., Galeva, N. A., Williams, T. D. and Hanzlik, R. P. (2006). Site-specific arylation of rat glutathione S-transferase A1 and A2 by bromobenzene metabolites in vivo. *Chemical Research in Toxicology*, 19(11), 1426–1434. doi: 10.1021/tx060142s
- Kokubo, J., Nagatani, N., Hiroki, K., Kuroiwa, K., Watanabe, N. and Arai, T. (2008). Mechanism of destruction of microtubule structures by 4-hydroxy-2-nonenal. *Cell Structure and Function*, 33(1), 51–59. doi: 10.1247/csf.07038
- Kon, K., Kim, J.-S., Jaeschke, H. and Lemasters, J. J. (2004). Mitochondrial permeability transition in acetaminophen-induced necrosis and apoptosis of cultured mouse hepatocytes. *Hepatology*, 40(5), 1170–1179. doi: 10.1002/hep.20437
- Korprasertthaworn, P., Polasek, T. M., Sorich, M. J., McLachlan, A. J., Miners, J. O., Tucker, G. T. and Rowland, A. (2015). In vitro characterization of the human liver microsomal kinetics and reaction phenotyping of olanzapine metabolism. *Drug*

Metabolism and Disposition, 43(11), 1806–1814. doi: 10.1124/dmd.115.064790

- Kuiper, H. C., Langsdorf, B. L., Miranda, C. L., Joss, J., Jubert, C., Mata, J. E. and Stevens, J. F. (2010). Quantitation of mercapturic acid conjugates of 4-hydroxy-2-nonenal and 4-oxo-2-nonenal metabolites in a smoking cessation study. *Free Radical Biology & Medicine*, 48(1), 65–72. doi: 10.1016/j.freeradbiomed.2009.10.025
- Kulkarni, A. (1984). The metabolism of insecticides: the role of monooxygenase enzymes. *Annual Review of Pharmacology and Toxicology*, 24(1), 19–42. doi: 10.1146/annurev.pharmtox.24.1.19
- Kusama, M., Kubota, T., Matsukura, Y., Matsuno, K., Ogawa, S., Kanda, Y. and Iga, T. (2006). Influence of glutathione S-transferase A1 polymorphism on the pharmacokinetics of busulfan. *Clinica Chimica Acta*, 368(1–2), 93–98. doi: 10.1016/j.cca.2005.12.011
- Kweekel, D. M., Gelderblom, H., Antonini, N. F., Van der Straaten, T., Nortier, J. W. R., Punt, C. J. A. and Guchelaar, H.-J. (2009). Glutathione-S-transferase pi (GSTP1) codon 105 polymorphism is not associated with oxaliplatin efficacy or toxicity in advanced colorectal cancer patients. *European Journal of Cancer*, 45(4), 572–578. doi: 10.1016/j.ejca.2008.10.015
- Laine, J. E., Auriola, S., Pasanen, M. and Juvonen, R. O. (2009). Acetaminophen bioactivation by human cytochrome P450 enzymes and animal microsomes. *Xenobiotica*, 39(1), 11–21. doi: 10.1080/00498250802512830
- Lam, B. K., Penrose, J. F., Xu, K., Baldasaro, M. H. and Austen, K. F. (1997). Site-directed mutagenesis of human leukotriene C4 synthase. *Journal of Biological Chemistry*, 272(21), 13923–13928. Retrieved from <https://www.jbc.org/content/272/21/13923>
- Lameh, J., Burstein, E. S., Taylor, E., Weiner, D. M., Vanover, K. E. and Bonhaus, D. W. (2007). Pharmacology of N-desmethylozapine. *Pharmacology & Therapeutics*, 115(2), 223–231. doi: 10.1016/j.pharmthera.2007.05.004
- Landsteiner, K. and Jacobs, J. (1935). Studies on the sensitization of animals with simple chemical compounds. *Journal of Experimental Medicine*, 61(5), 643–656. doi: 10.1084/jem.61.5.643
- Lange, V., Picotti, P., Domon, B. and Aebersold, R. (2008). Selected reaction monitoring for quantitative proteomics: a tutorial. *Molecular Systems Biology*, 4(1), 222–235. doi: 10.1038/msb.2008.61

- Langman, R. E. and Cohn, M. (2000). Self-nonsel self discrimination revisited. Introduction. *Seminars in Immunology*, 12(3), 159–162. doi: 10.1006/smim.2000.0227
- Larsen, M. R., Trelle, M. B., Thingholm, T. E. and Jensen, O. N. (2006). Analysis of posttranslational modifications of proteins by tandem mass spectrometry. *BioTechniques*, 40(6), 790–798. doi: 10.2144/000112201
- Larson, A. M., Polson, J., Fontana, R. J., Davern, T. J., Lalani, E., Hynan, L. S., ... the Acute Liver Failure Study Group. (2005). Acetaminophen-induced acute liver failure: results of a United States multicenter, prospective study. *Hepatology*, 42(6), 1364–1372. doi: 10.1002/hep.20948
- LeBlanc, A., Shiao, T. C., Roy, R. and Sleno, L. (2014). Absolute quantitation of NAPQI-modified rat serum albumin by LC-MS/MS: monitoring acetaminophen covalent binding in vivo. *Chemical Research in Toxicology*, 27(9), 1632–1639. doi: 10.1021/tx500284g
- Ledent, P., Duez, C., Vanhove, M., Lejeune, A., Fonzé, E., Charlier, P., ... Frère, J.-M. (1997). Unexpected influence of a C-terminal-fused His-tag on the processing of an enzyme and on the kinetic and folding parameters. *FEBS Letters*, 413(2), 194–196. doi: 10.1016/S0014-5793(97)00908-3
- Lee, S. J., Kim, C. E., Seo, K. W. and Kim, C. D. (2010). HNE-induced 5-LO expression is regulated by NF-kappaB/ERK and Sp1/p38 MAPK pathways via EGF receptor in murine macrophages. *Cardiovascular Research*, 88(2), 352–359. doi: 10.1093/cvr/cvq194
- Lee, S. J., Seo, K. W., Yun, M. R., Bae, S. S., Lee, W. S., Hong, K. W. and Kim, C. D. (2008a). 4-Hydroxynonenal enhances MMP-2 production in vascular smooth muscle cells via mitochondrial ROS-mediated activation of the Akt/NF-kappaB signaling pathways. *Free Radical Biology & Medicine*, 45(10), 1487–1492. doi: 10.1016/j.freeradbiomed.2008.08.022
- Lee, W. M. (2004). Acetaminophen and the U.S. Acute Liver Failure Study Group: lowering the risks of hepatic failure. *Hepatology*, 40(1), 6–9. doi: 10.1002/hep.20293
- Lee, W. M., Squires Jr, R. H., Nyberg, S. L., Doo, E. and Hoofnagle, J. H. (2008b). Acute liver failure: summary of a workshop. *Hepatology*, 47(4), 1401–1415. doi: 10.1002/hep.22177
- Leeming, M. G., Donald, W. A. and O’Hair, R. A. J. (2017). Nontargeted identification

- of reactive metabolite protein adducts. *Analytical Chemistry*, 89(11), 5748–5756. doi: 10.1021/acs.analchem.6b04604
- Lemercier, J.-N., Meier, B. W., Gomez, J. D. and Thompson, J. A. (2004). Inhibition of glutathione S-transferase P1-1 in mouse lung epithelial cells by the tumor promoter 2,6-di-tert-butyl-4-methylene-2,5-cyclohexadienone (BHT-quinone methide): protein adducts investigated by electrospray mass spectrometry. *Chemical Research in Toxicology*, 17(12), 1675–1683. doi: 10.1021/tx049811x
- Leonardo, Q.-F., Juliana, G.-R. and Fernando, C.-A. J. (2017). Atypical neuroleptic malignant syndrome associated with use of clozapine. *Case Reports in Emergency Medicine*, 2017, 2174379. doi: 10.1155/2017/2174379
- Levin, D. E., Hollstein, M., Christman, M. F. and Ames, B. N. (1984). Detection of oxidative mutagens with a new salmonella tester strain (TA102). *Methods in Enzymology*, 105, 249–254. doi: 10.1016/s0076-6879(84)05032-1
- Levsen, K., Schiebel, H.-M., Behnke, B., Dötzer, R., Dreher, W., Elend, M. and Thiele, H. (2005). Structure elucidation of phase II metabolites by tandem mass spectrometry: an overview. *Journal of Chromatography A*, 1067(1–2), 55–72. doi: 10.1016/j.chroma.2004.08.165
- Lewis, D. F. V., Ioannides, C. and Parke, D. V. (1998). Cytochromes P450 and species differences in xenobiotic metabolism and activation of carcinogen. *Environmental Health Perspectives*, 106(10), 633–641. doi: 10.1289/ehp.98106633
- Li, X. (2009). Glutathione and glutathione-S-transferase in detoxification mechanisms. In D. A. Casciano, S. C. Sahu, B. Ballantyne, T. Marrs and T. Syversen (eds.), *General, Applied and Systems Toxicology* (2). Chichester : John Wiley & Sons, Ltd. doi: 10.1002/9780470744307.gat166
- Liebler, D. C. (2008). Protein damage by reactive electrophiles: targets and consequences. *Chemical Research in Toxicology*, 21(1), 117–128. doi: 10.1021/tx700235t
- Liebler, D. C. and Zimmerman, L. J. (2013). Targeted quantitation of proteins by mass spectrometry. *Biochemistry*, 52(22), 3797–3806. doi: 10.1021/bi400110b
- Lin, G., McKay, G. and Midha, K. K. (1996). Characterization of metabolites of clozapine N-oxide in the rat by micro-column high performance liquid chromatography/mass spectrometry with electrospray interface. *Journal of Pharmaceutical and Biomedical Analysis*, 14(11), 1561–1577. doi: 10.1016/0731-7085(96)01738-4

- Liu, T., Du, F., Zhu, F. and Xing, J. (2011). Metabolite identification of artemether by data-dependent accurate mass spectrometric analysis using an LTQ-Orbitrap hybrid mass spectrometer in combination with the online hydrogen/deuterium exchange technique. *Rapid Communications in Mass Spectrometry*, 25(21), 3303–3313. doi: 10.1002/rcm.5214
- Liu, Z. C. and Uetrecht, J. P. (1995). Clozapine is oxidized by activated human neutrophils to a reactive nitrenium ion that irreversibly binds to the cells. *The Journal of Pharmacology and Experimental Therapeutics*, 275(3), 1476–1483. Retrieved from <http://jpet.aspetjournals.org/content/275/3/1476.long>
- Lobach, A. R. and Uetrecht, J. (2014). Involvement of myeloperoxidase and NADPH oxidase in the covalent binding of amodiaquine and clozapine to neutrophils: implications for drug-induced agranulocytosis. *Chemical Research in Toxicology*, 27(4), 699–709. doi: 10.1021/tx500019u
- Loeb, L. A. and Harris, C. C. (2008). Advances in chemical carcinogenesis: a historical review and prospective. *Cancer Research*, 68(17), 6863–6872. doi: 10.1158/0008-5472.CAN-08-2852
- Lohmann, W., Hayen, H. and Karst, U. (2008). Covalent protein modification by reactive drug metabolites using online electrochemistry/liquid chromatography/mass spectrometry. *Analytical Chemistry*, 80(24), 9714–9719. doi: 10.1021/ac801699g
- Loziuk, P. L., Sederoff, R. R., Chiang, V. L. and Muddiman, D. C. (2014). Establishing ion ratio thresholds based on absolute peak area for absolute protein quantification using protein cleavage isotope dilution mass spectrometry. *Analyst*, 139(21), 5439–5450. doi: 10.1039/c4an00567h
- Lu, M.-L., Wu, Y.-X., Chen, C.-H., Kuo, P.-T., Chen, Y.-H., Lin, C.-H. and Wu, T.-H. (2016). Application of plasma levels of olanzapine and N-desmethyl-olanzapine to monitor clinical efficacy in patients with schizophrenia. *PLoS ONE*, 11(2), e0148539. doi: 10.1371/journal.pone.0148539
- Lu, Y., Meng, Q., Zhang, G. and Bei, X. (2008). Clozapine-induced hepatotoxicity in rat hepatocytes by gel entrapment and monolayer culture. *Toxicology in Vitro*, 22(7), 1754–1760. doi: 10.1016/j.tiv.2008.08.002
- Luan, S., Wan, H., Wang, S., Li, H. and Zhang, B. (2017). Efficacy and safety of olanzapine/fluoxetine combination in the treatment of treatment-resistant depression: a meta-analysis of randomized controlled trials. *Neuropsychiatric Disease and Treatment*, 13, 609–620. doi: 10.2147/NDT.S127453

- Ludwig, C., Amon, S., Gillet, L., Collins, B. C., Rosenberger, G. and Aebersold, R. (2018). Data-independent acquisition-based SWATH-MS for quantitative proteomics: a tutorial. *Molecular Systems Biology*, 14(8), e8126. doi: 10.15252/msb.20178126
- Ly, T. and Julian, R. R. (2009). Ultraviolet photodissociation: developments towards applications for mass-spectrometry-based proteomics. *Angewandte Chemie International Edition*, 48(39), 7130–7137. doi: 10.1002/anie.200900613
- Ma, L., Wen, B., Ruan, Q. and Zhu, M. (2008a). Rapid screening of glutathione-trapped reactive metabolites by linear ion trap mass spectrometry with isotope pattern-dependent scanning and postacquisition data mining. *Chemical Research in Toxicology*, 21(7), 1477–1483. doi: 10.1021/tx8001115
- Ma, X., Chen, C., Krausz, K. W., Idle, J. R. and Gonzalez, F. J. (2008b). A metabolomic perspective of melatonin metabolism in the mouse. *Endocrinology*, 149(4), 1869–1879. doi: 10.1210/en.2007-1412
- Maggs, J. L., Naisbitt, D. J., Tetley, J. N. A., Pirmohamed, M. and Park, B. K. (2000). Metabolism of lamotrigine to a reactive arene oxide intermediate. *Chemical Research in Toxicology*, 13(11), 1075–1081. doi: 10.1021/tx0000825
- Maggs, J. L., Williams, D., Pirmohamed, M. and Park, B. K. (1995). The metabolic formation of reactive intermediates from clozapine, a drug associated with agranulocytosis in man. *Journal of Pharmacology and Experimental Therapeutics*, 275(3), 1463–1475. Retrieved from <http://jpet.aspetjournals.org/content/275/3/1463.long>
- Mahmood, T. and Yang, P.-C. (2012). Western blot: technique, theory, and trouble shooting. *North American Journal of Medical Sciences*, 4(9), 429–434. doi: 10.4103/1947-2714.100998
- Mahr, S., Burmester, G.-R., Hilke, D., Göbel, U., Grützkau, A., Häupl, T., ... Müller, B. (2006). Cis- and trans-acting gene regulation is associated with osteoarthritis. *The American Journal of Human Genetics*, 78(5), 793–803. doi: 10.1086/503849
- Maleki, L. A., Majidi, J., Baradaran, B., Abdolalizadeh, J. and Akbari, A. M. (2013). Production and characterization of murine monoclonal antibody against synthetic peptide of CD34. *Human Antibodies*, 22(1–2), 1–8. doi: 10.3233/HAB-130265
- Mamyryn, B. A. (2001). Time-of-flight mass spectrometry (concepts, achievements, and prospects). *International Journal of Mass Spectrometry*, 206(3), 251–266. doi: 10.1016/S1387-3806(00)00392-4

- Mann, M., Hendrickson, R. C. and Pandey, A. (2001). Analysis of proteins and proteomes by mass spectrometry. *Annual Review of Biochemistry*, 70, 437–473. doi: 10.1146/annurev.biochem.70.1.437
- Manning, L. R. and Manning, J. M. (2018). Contributions to nucleosome dynamics in chromatin from interactive propagation of phosphorylation/acetylation and inducible histone lysine basicities. *Protein Science*, 27(3), 662–671. doi: 10.1002/pro.3359
- Mans, D. R. A., Lafleur, M. V. M., Westmijze, E. J., Horn, I. R., Bets, D., Schuurhuis, G. J., ... Retèl, J. (1992). Reactions of glutathione with the catechol, the ortho-quinone and the semi-quinone free radical of etoposide Consequences for DNA inactivation. *Biochemical Pharmacology*, 43(8), 1761–1768. doi: 10.1016/0006-2952(92)90708-q
- Manvich, D. F., Webster, K. A., Foster, S. L., Farrell, M. S., Ritchie, J. C., Porter, J. H. and Weinshenker, D. (2018). The DREADD agonist clozapine N-oxide (CNO) is reverse-metabolized to clozapine and produces clozapine-like interoceptive stimulus effects in rats and mice. *Scientific Reports*, 8(1), 3840. doi: 10.1038/s41598-018-22116-z
- Manyike, P. T., Kharasch, E. D., Kalthorn, T. F. and Slattery, J. T. (2000). Contribution of CYP2E1 and CYP3A to acetaminophen reactive metabolite formation. *Clinical Pharmacology & Therapeutics*, 67(3), 275–282. doi: 10.1067/mcp.2000.104736
- March, R. E. and Todd, J. F. J. (2015). Radio frequency quadrupole technology: evolution and contributions to mass spectrometry. *International Journal of Mass Spectrometry*, 377(1), 316–328. doi: 10.1016/j.ijms.2014.07.030
- Martignoni, M., de Kanter, R., Grossi, P., Mahnke, A., Saturno, G. and Monshouwer, M. (2004). An in vivo and in vitro comparison of CYP induction in rat liver and intestine using slices and quantitative RT-PCR. *Chemico-Biological Interactions*, 151(1), 1–11. doi: 10.1016/j.cbi.2004.10.002
- Martignoni, M., Groothuis, G. M. M. and de Kanter, R. (2006). Species differences between mouse, rat, dog, monkey and human CYP-mediated drug metabolism, inhibition and induction. *Expert Opinion on Drug Metabolism & Toxicology*, 2(6), 875–894. doi: 10.1517/17425255.2.6.875
- Matzinger, P. (1994). Tolerance, danger, and the extended family. *Annual Review of Immunology*, 12, 991–1045. doi: 10.1146/annurev.iy.12.040194.005015
- Mauriala, T., Chauret, N., Oballa, R., Nicoll-Griffith, D. A. and Bateman, K. P. (2005).

- A strategy for identification of drug metabolites from dried blood spots using triple-quadrupole/linear ion trap hybrid mass spectrometry. *Rapid Communications in Mass Spectrometry*, 19(14), 1984–1992. doi: 10.1002/rcm.2013
- Mazaleuskaya, L. L., Sangkuhl, K., Thorn, C. F., FitzGerald, G. A., Altman, R. B. and Klein, T. E. (2015). PharmGKB summary: pathways of acetaminophen metabolism at the therapeutic versus toxic doses. *Pharmacogenetics and Genomics*, 25(8), 416–426. doi: 10.1097/FPC.0000000000000150
- McCarthy, M. M. and Nugent, B. M. (2013). Epigenetic contributions to hormonally-mediated sexual differentiation of the brain. *Journal of Neuroendocrinology*, 25(11), 1133–1140. doi: 10.1111/jne.12072
- McGill, M. R., Lebofsky, M., Norris, H. R. K., Slawson, M. H., Bajt, M. L., Xie, Y., ... Jaeschke, H. (2013). Plasma and liver acetaminophen-protein adduct levels in mice after acetaminophen treatment: dose-response, mechanisms, and clinical implications. *Toxicology and Applied Pharmacology*, 269(3), 240–249. doi: 10.1016/j.taap.2013.03.026
- Megger, D. A., Bracht, T., Meyer, H. E. and Sitek, B. (2013). Label-free quantification in clinical proteomics. *Biochimica et Biophysica Acta (BBA) - Proteins and Proteomics*, 1834(8), 1581–1590. doi: 10.1016/j.bbapap.2013.04.001
- Mehmood, S., Allison, T. M. and Robinson, C. V. (2015). Mass spectrometry of protein complexes: from origins to applications. *Annual Review of Physical Chemistry*, 66, 453–474. doi: 10.1146/annurev-physchem-040214-121732
- Michalski, A., Cox, J. and Mann, M. (2011). More than 100,000 detectable peptide species elute in single shotgun proteomics runs but the majority is inaccessible to data-dependent LC-MS/MS. *Journal of Proteome Research*, 10(4), 1785–1793. doi: 10.1021/pr101060v
- Miller, E. C. and Miller, J. A. (1947). The presence and significance of bound aminoazo dyes in the livers of rats fed p-dimethylaminoazobenzene. *Cancer Research*, 7(7), 468–480. Retrieved from <https://cancerres.aacrjournals.org/content/7/7/468>
- Miller, E. C. and Miller, J. A. (1952). In vivo combinations between carcinogens and tissue constituents and their possible role in carcinogenesis. *Cancer Research*, 12(8), 547–556.
- Mitchell, J. R., Jollow, D. J., Potter, W. Z., Davis, D. C., Gillette, J. R. and Brodie, B. B. (1973a). Acetaminophen-induced hepatic necrosis. I. Role of drug metabolism.

- The Journal of Pharmacology and Experimental Therapeutics*, 187(1), 185–194. Retrieved from <http://jpet.aspetjournals.org/content/187/1/185.long>
- Mitchell, J. R., Jollow, D. J., Potter, W. Z., Gillette, J. R. and Brodie, B. B. (1973b). Acetaminophen-induced hepatic necrosis. IV. Protective role of glutathione. *The Journal of Pharmacology and Experimental Therapeutics*, 187(1), 211–217. Retrieved from <http://jpet.aspetjournals.org/content/187/1/211.long>
- Mittal, B., Tulsyan, S., Kumar, S., Mittal, R. D. and Agarwal, G. (2015). Cytochrome P450 in cancer susceptibility and treatment. *Advances in Clinical Chemistry*, 71, 77–139. doi: 10.1016/bs.acc.2015.06.003
- Moldogazieva, N. T., Mokhosoev, I. M., Feldman, N. B. and Lutsenko, S. V. (2018). ROS and RNS signalling: adaptive redox switches through oxidative/nitrosative protein modifications. *Free Radical Research*, 52(5), 507–543. doi: 10.1080/10715762.2018.1457217
- Moldovan, L. and Moldovan, N. I. (2004). Oxygen free radicals and redox biology of organelles. *Histochemistry and Cell Biology*, 122(4), 395–412. doi: 10.1007/s00418-004-0676-y
- Morales, V. and Richard-Foy, H. (2000). Role of histone N-terminal tails and their acetylation in nucleosome dynamics. *Molecular and Cellular Biology*, 20(19), 7230–7237. doi: 10.1128/MCB.20.19.7230-7237.2000
- Morgenstern, R., Zhang, J. and Johansson, K. (2011). Microsomal glutathione transferase 1: mechanism and functional roles. *Drug Metabolism Reviews*, 43(2), 300–306. doi: 10.3109/03602532.2011.558511
- Morquette, B., Shi, Q., Lavigne, P., Ranger, P., Fernandes, J. C. and Benderdour, M. (2006). Production of lipid peroxidation products in osteoarthritic tissues: new evidence linking 4-hydroxynonenal to cartilage degradation. *Arthritis & Rheumatism*, 54(1), 271–281. doi: 10.1002/art.21559
- Mukanganyama, S., Masimirembwa, C. M., Naik, Y. S. and Hasler, J. A. (1997). Phenotyping of the glutathione S-transferase M1 polymorphism in Zimbabweans and the effects of chloroquine on blood glutathione S-transferases M1 and A. *Clinica Chimica Acta*, 265(2), 145–155. doi: 10.1016/S0009-8981(97)00104-6
- Mukanganyama, S., Widersten, M., Naik, Y. S., Mannervik, B. and Hasler, J. A. (2002). Inhibition of glutathione S-transferases by antimalarial drugs possible implications for circumventing anticancer drug resistance. *International Journal of Cancer*, 97(5), 700–705. doi: 10.1002/ijc.10054

- Muldrew, K. L., James, L. P., Coop, L., McCullough, S. S., Hendrickson, H. P., Hinson, J. A. and Mayeux, P. R. (2002). Determination of acetaminophen-protein adducts in mouse liver and serum and human serum after hepatotoxic doses of acetaminophen using high-performance liquid chromatography with electrochemical detection. *Drug Metabolism & Disposition*, 30(4), 446–451. doi: 10.1124/dmd.30.4.446
- Münzel, T., Steven, S. and Daiber, A. (2014). Organic nitrates: update on mechanisms underlying vasodilation, tolerance and endothelial dysfunction. *Vascular Pharmacology*, 63(3), 105–113. doi: 10.1016/j.vph.2014.09.002
- Murata, M. and Kawanishi, S. (2011). Mechanisms of oxidative DNA damage induced by carcinogenic arylamines. *Frontiers in Bioscience*, 16, 1132–1143. doi: 10.2741/3739
- Murray, M. (2006). Role of CYP pharmacogenetics and drug-drug interactions in the efficacy and safety of atypical and other antipsychotic agents. *Journal of Pharmacy and Pharmacology*, 58(7), 871–885. doi: 10.1211/jpp.58.7.0001
- Mutlib, A. E., Dickenson, P., Chen, S.-Y., Espina, R. J., Daniels, J. S. and Gan, L.-S. (2002). Bioactivation of benzylamine to reactive intermediates in rodents: formation of glutathione, glutamate, and peptide conjugates. *Chemical Research in Toxicology*, 15(9), 1190–1207. doi: 10.1021/tx020063q
- Nägele, E., Vollmer, M., Hörth, P. and Vad, C. (2004). 2D-LC/MS techniques for the identification of proteins in highly complex mixtures. *Expert Review of Proteomics*, 1(1), 37–46. doi: 10.1586/14789450.1.1.37
- National Center for Biotechnology Information. (2020). *PubMed*. Retrieved from <https://pubmed.ncbi.nlm.nih.gov/>
- Navari, R. M., Qin, R., Ruddy, K. J., Liu, H., Powell, S. F., Bajaj, M., ... Loprinzi, C. L. (2016). Olanzapine for the prevention of chemotherapy-induced nausea and vomiting. *The New England Journal of Medicine*, 375(2), 134–142. doi: 10.1056/NEJMoal515725
- Nerland, D. E., Cai, J., Pierce, W. M. and Benz, F. W. (2001). Covalent binding of acrylonitrile to specific rat liver glutathione S-transferases in vivo. *Chemical Research in Toxicology*, 14(7), 799–806. doi: 10.1021/tx010002c
- Ng, W., Kennar, R. and Uetrecht, J. (2014). Effect of clozapine and olanzapine on neutrophil kinetics: implications for drug-induced agranulocytosis. *Chemical Research in Toxicology*, 27(7), 1104–1108. doi: 10.1021/tx500183x

- Nicholson, D. W., Ali, A., Vaillancourt, J. P., Calaycay, J. R., Mumford, R. A., Zamboni, R. J. and Ford-Hutchinson, A. W. (1993). Purification to homogeneity and the N-terminal sequence of human leukotriene C4 synthase: a homodimeric glutathione S-transferase composed of 18-kDa subunits. *Proceedings of the National Academy of Sciences of the United States of America*, 90(5), 2015–2019. doi: 10.1073/pnas.90.5.2015
- Nielsen, J., Young, C., Ifteni, P., Kishimoto, T., Xiang, Y.-T., Schulte, P. F. J., ... Taylor, D. (2016). Worldwide differences in regulations of clozapine use. *CNS Drugs*, 30(2), 149–161. doi: 10.1007/s40263-016-0311-1
- Nightingale, K. P., Wellinger, R. E., Sogo, J. M. and Becker, P. B. (1998). Histone acetylation facilitates RNA polymerase II transcription of the *Drosophila* hsp26 gene in chromatin. *The EMBO Journal*, 17(10), 2865–2876. doi: 10.1093/emboj/17.10.2865
- Nobuoka, A., Takayama, T., Miyanishi, K., Sato, T., Takanashi, K., Hayashi, T., ... Niitsu, Y. (2004). Glutathione-S-transferase P1-1 protects aberrant crypt foci from apoptosis induced by deoxycholic acid. *Gastroenterology*, 124(2), 428–443. doi: 10.1053/j.gastro.2004.05.021
- Norrgård, M. A., Hellman, U. and Mannervik, B. (2011). Cys-X scanning for expansion of active-site residues and modulation of catalytic functions in a glutathione transferase. *Journal of Biological Chemistry*, 286(19), 16871–16878. doi: 10.1074/jbc.M111.230078
- Nott, A., Nitarska, J., Veenliet, J. V., Schacke, S., Derijck, A. A. H. A., Sirko, P., ... Riccio, A. (2013). S-nitrosylation of HDAC2 regulates the expression of the chromatin-remodeling factor Brm during radial neuron migration. *Proceedings of the National Academy of Sciences of the United States of America*, 110(8), 3113–3118. doi: 10.1073/pnas.1218126110
- O’Grady, J. G., Schalm, S. W. and Williams, R. (1993). Acute liver failure: redefining the syndromes. *The Lancet*, 342(8866), 273–275. doi: 10.1016/0140-6736(93)91818-7
- O’Neal, K. D., Chari, M. V., McDonald, C. H., Cook, R. G., Yu-Lee, L., Morrisett, J. D. and Shearer, W. T. (1996). Multiple cis-trans conformers of the prolactin receptor proline-rich motif (PRM) peptide detected by reverse-phase HPLC, CD and NMR spectroscopy. *Biochemical Journal*, 315(Pt 3), 833–844. doi: 10.1042/bj3150833
- Oakley, A. J., Bello, M. Lo, Battistoni, A., Ricci, G., Rossjohn, J., Villar, H. O. and

- Parker, M. W. (1997a). The structures of human glutathione transferase P1-1 in complex with glutathione and various inhibitors at high resolution. *Journal of Molecular Biology*, 274(1), 84–100. doi: 10.1006/jmbi.1997.1364
- Oakley, A. J., Rossjohn, J., Lo Bello, M., Caccuri, A. M., Federici, G. and Parker, M. W. (1997b). The three-dimensional structure of the human Pi class glutathione transferase P1-1 in complex with the inhibitor ethacrynic acid and its glutathione conjugate. *Biochemistry*, 36(3), 576–585. doi: 10.1021/bi962316i
- Obach, R. S. and Dobo, K. L. (2008). Comparison of metabolite profiles generated in Aroclor-induced rat liver and human liver subcellular fractions: Considerations for in vitro genotoxicity hazard assessment. *Environmental and Molecular Mutagenesis*, 49(8), 631–641. doi: 10.1002/em
- Oesch, F., Fabian, E., Oesch-Bartlomowicz, B., Werner, C. and Landsiedel, R. (2007). Drug-metabolizing enzymes in the skin of man, rat, and pig. *Drug Metabolism Reviews*, 39(4), 659–698. doi: 10.1080/03602530701690366
- Ogorzaiek Loo, R. R., Dales, N. and Andrews, P. C. (1996). The effect of detergents on proteins analyzed by electrospray ionization. In J. R. Chapman (ed.), *Protein and peptide analysis by mass spectrometry. Methods in molecular biology* (1st ed., vol. 61, pp. 141–160). Totowa, NJ : Humana Press. doi: 10.1385/0-89603-345-7:141
- Okubo, M., Narita, M., Murayama, N., Akimoto, Y., Goto, A. and Yamazaki, H. (2016). Individual differences in in vitro and in vivo metabolic clearances of the antipsychotic drug olanzapine from non-smoking and smoking Japanese subjects genotyped for cytochrome P4502D6 and flavincontaining monooxygenase 3. *Human Psychopharmacology*, 31(2), 83–92. doi: 10.1002/hup.2515
- Olsen, J. V., Macek, B., Lange, O., Makarov, A., Horning, S. and Mann, M. (2007). Higher-energy C-trap dissociation for peptide modification analysis. *Nature Methods*, 4(9), 709–712. doi: 10.1038/nmeth1060
- Orton, C. R. and Liebler, D. C. (2007). Analysis of protein adduction kinetics by quantitative mass spectrometry: competing adduction reactions of glutathione-S-transferase P1-1 with electrophiles. *Chemico-Biological Interactions*, 168(2), 117–127. doi: 10.1002/ana.22528
- Pan, Y., Cao, M., You, D., Qin, G. and Liu, Z. (2019). Research progress on the animal models of drug-induced liver injury: current status and further perspectives. *BioMed Research International*, 2019, 1283824. doi: 10.1155/2019/1283824

- Papakonstanti, E. A. and Stournaras, C. (2008). Cell responses regulated by early reorganization of actin cytoskeleton. *FEBS Letters*, 582(14), 2120–2127. doi: 10.1016/j.febslet.2008.02.064
- Park, B. K., Kitteringham, N. R., Maggs, J. L., Pirmohamed, M. and Williams, D. P. (2005). The role of metabolic activation in drug-induced hepatotoxicity. *Annual Review of Pharmacology and Toxicology*, 45, 177–202. doi: 10.1146/annurev.pharmtox.45.120403.100058
- Parker, L. J., Ciccone, S., Italiano, L. C., Primavera, A., Oakley, A. J., Morton, C. J., ... Parker, M. W. (2008). The anti-cancer drug chlorambucil as a substrate for the human polymorphic enzyme glutathione transferase P1-1: kinetic properties and crystallographic characterisation of allelic variants. *Journal of Molecular Biology*, 380(1), 131–144. doi: 10.1016/j.jmb.2008.04.066
- Patskovsky, Y., Patskovska, L., Almo, S. C. and Listowsky, I. (2006). Transition state model and mechanism of nucleophilic aromatic substitution reactions catalyzed by human glutathione S-transferase M1a-1a. *Biochemistry*, 45(12), 3852–3862. doi: 10.1021/bi051823+
- Patten, C. J., Thomas, P. E., Guy, R. L., Lee, M., Gonzalez, F. J., Guengerich, F. P. and Yang, C. S. (1993). Cytochrome P450 enzymes involved in acetaminophen activation by rat and human liver microsomes and their kinetics. *Chemical Research in Toxicology*, 6(4), 511–518. doi: 10.1021/tx00034a019
- Pearson, P. G., Howald, W. N. and Nelson, S. D. (1990). Screening strategy for the detection of derivatized glutathione conjugates by tandem mass spectrometry. *Analytical Chemistry*, 62(17), 1827–1836. doi: 10.1021/ac00216a019
- Pereira, A. and Dean, B. (2006). Clozapine bioactivation induces dose-dependent, drug-specific toxicity of human bone marrow stromal cells: a potential in vitro system for the study of agranulocytosis. *Biochemical Pharmacology*, 72(6), 783–793. doi: 10.1016/j.bcp.2006.06.006
- Peterman, S. M., Duczak, N., Kalgutkar, A. S., Lame, M. E. and Soglia, J. R. (2006). Application of a linear ion trap/Orbitrap mass spectrometer in metabolite characterization studies: examination of the human liver microsomal metabolism of the non-tricyclic anti-depressant nefazodone using data-dependent accurate mass measurements. *Journal of the American Society for Mass Spectrometry*, 17(3), 363–375. doi: 10.1016/j.jasms.2005.11.014
- Peters Jr., T. (1985). Serum albumin. *Advances in Protein Chemistry*, 37, 161–245. doi: 10.1016/S0065-3233(08)60065-0

- Peters, U., Preisler-Adams, S., Hebeisen, A., Hahn, M., Seifert, E., Lanvers, C., ... Lamprecht-Dinnesen, A. (2000). Glutathione S-transferase genetic polymorphisms and individual sensitivity to the ototoxic effect of cisplatin. *Anti-Cancer Drugs*, 11(8), 639–643. doi: 10.1097/00001813-200009000-00007
- Peterson, L. A. (2013). Reactive metabolites in the biotransformation of molecules containing a furan ring. *Chemical Research in Toxicology*, 26(1), 6–25. doi: 10.1021/tx3003824
- Picotti, P. and Aebersold, R. (2012). Selected reaction monitoring-based proteomics: workflows, potential, pitfalls and future directions. *Nature Methods*, 9(6), 555–566. doi: 10.1038/nmeth.2015
- Pimviriyakul, P., Thotsaporn, K., Sucharitakul, J. and Chaiyen, P. (2017). Kinetic mechanism of the dechlorinating flavin-dependent monooxygenase HadA. *Journal of Biological Chemistry*, 292(12), 4818–4832. doi: 10.1074/jbc.M116.774448
- Pirmohamed, M., Naisbitt, D. J., Gordon, F. and Park, B. K. (2002). The danger hypothesis - potential role in idiosyncratic drug reactions. *Toxicology*, 181–182, 55–63. doi: 10.1016/S0300-483X(02)00255-X
- Pirmohamed, M. and Park, K. (1997). Mechanism of clozapine-induced agranulocytosis: current status of research and implications for drug development. *CNS Drugs*, 7(2), 139–158. doi: 10.2165/00023210-199707020-00005
- Pirmohamed, M., Williams, D., Madden, S., Templeton, E. and Park, B. K. (1995). Metabolism and bioactivation of clozapine by human liver in vitro. *Journal of Pharmacology and Experimental Therapeutics*, 272(3), 984–990. Retrieved from <http://jpet.aspetjournals.org/content/272/3/984.long>
- Pittenauer, E. and Allmaier, G. (2009). High-energy collision induced dissociation of biomolecules: MALDI-TOF/RTOF mass spectrometry in comparison to tandem sector mass spectrometry. *Combinatorial Chemistry & High Throughput Screening*, 12(2), 137–155. doi: 10.2174/138620709787315436
- Poli, G., Schaur, R. J., Siems, W. G. and Leonarduzzi, G. (2008). 4-Hydroxynonenal: a membrane lipid oxidation product of medicinal interest. *Medicinal Research Reviews*, 28(4), 569–631. doi: 10.1002/med.20117
- Poloyac, S. M., Tortorici, M. A., Przychodzin, D. I., Reynolds, R. B., Xie, W., Frye, R. F. and Zemaitis, M. A. (2004). The effect of isoniazid on CYP2E1- and CYP4A-mediated hydroxylation of arachidonic acid in the rat liver and kidney. *Drug*

Metabolism and Disposition, 32(7), 727–733. doi: 10.1124/dmd.32.7.727

- Pond, S. M. and Tozer, T. N. (1984). First-pass elimination basic concepts and clinical consequences. *Clinical Pharmacokinetics*, 9(1), 1–25. doi: 10.2165/00003088-198409010-00001
- Poole, C. F. and Lenca, N. (2017). Reversed-phase liquid chromatography. In *Liquid Chromatography: Fundamentals and Instrumentation* (2nd ed., vol. 1, 4, pp. 91–123). Elsevier Inc. doi: 10.1016/B978-0-12-805393-5.00004-X
- Potter, W. Z., Davis, D. C., Mitchell, J. R., Jollow, D. J., Gillette, J. R. and Brodie, B. B. (1973). Acetaminophen-induced hepatic necrosis. 3. Cytochrome P-450-mediated covalent binding in vitro. *The Journal of Pharmacology and Experimental Therapeutics*, 187(1), 203–210. Retrieved from <http://jpet.aspetjournals.org/content/187/1/203.long>
- Prade, L., Huber, R., Manoharan, T. H., Fahl, W. E. and Reuter, W. (1997). Structures of class pi glutathione S-transferase from human placenta in complex with substrate, transition-state analogue and inhibitor. *Structure*, 5(10), 1287–1295. doi: 10.1016/S0969-2126(97)00281-5
- Preissner, S., Kroll, K., Dunkel, M., Senger, C., Goldsobel, G., Kuzman, D., ... Preissner, R. (2010). SuperCYP: a comprehensive database on Cytochrome P450 enzymes including a tool for analysis of CYP-drug interactions. *Nucleic Acids Research*, 38(Database issue), D237–D243. doi: 10.1093/nar/gkp970
- Prescott, L. F. (2000). Paracetamol, alcohol and the liver. *British Journal of Clinical Pharmacology*, 49(4), 291–301. doi: 10.1046/j.1365-2125.2000.00167.x
- Pumford, N. R., Hinson, J. A., Potter, D. W., Rowland, K. L., Benson, R. W. and Roberts, D. W. (1989). Immunochemical quantitation of 3-(cystein-S-yl)acetaminophen adducts in serum and liver proteins of acetaminophen-treated mice. *The Journal of Pharmacology and Experimental Therapeutics*, 248(1), 190–196. Retrieved from <http://jpet.aspetjournals.org/content/248/1/190>
- Qi, Y., Geib, T., Schorr, P., Meier, F. and Volmer, D. A. (2015a). On the isobaric space of 25-hydroxyvitamin D in human serum: potential for interferences in liquid chromatography/tandem mass spectrometry, systematic errors and accuracy issues. *Rapid Communications in Mass Spectrometry*, 29(1), 1–9. doi: 10.1002/rcm.7075
- Qi, Y., Geib, T. and Volmer, D. A. (2015b). Determining the binding sites of β -cyclodextrin and peptides by electron-capture dissociation high resolution tandem

- mass spectrometry. *Journal of the American Society for Mass Spectrometry*, 26(7), 1143–1149. doi: 10.1007/s13361-015-1118-x
- Qiu, Y., Benet, L. Z. and Burlingame, A. L. (1998). Identification of the hepatic protein targets of reactive metabolites of acetaminophen in vivo in mice using two-dimensional gel electrophoresis and mass spectrometry. *The Journal of Biological Chemistry*, 273(28), 17940–17953. doi: 10.1074/jbc.273.28.17940
- Quinete, N., Esser, A., Kraus, T. and Schettgen, T. (2017). PCB 28 metabolites elimination kinetics in human plasma on a real case scenario: Study of hydroxylated polychlorinated biphenyl (OH-PCB) metabolites of PCB 28 in a highly exposed German Cohort. *Toxicology Letters*, 276, 100–107. doi: 10.1016/j.toxlet.2017.05.025
- Rademacher, P. M., Woods, C. M., Huang, Q., Szklarz, G. D. and Nelson, S. D. (2012). Differential oxidation of two thiophene-containing regioisomers to reactive metabolites by cytochrome P450 2C9. *Chemical Research in Toxicology*, 25(4), 895–903. doi: 10.1021/tx200519d
- Ralat, L. A. and Colman, R. F. (2006). Identification of tyrosine 79 in the tocopherol binding site of glutathione S-transferase pi. *Biochemistry*, 45(41), 12491–12499. doi: 10.1021/bi061330k
- Raucy, J. L., Lasker, J. M., Lieber, C. S. and Black, M. (1989). Acetaminophen activation by human liver cytochromes P450IIE1 and P450IA2. *Archives of Biochemistry and Biophysics*, 271(1), 270–283. doi: 10.1016/0003-9861(89)90278-6
- Rautio, J., Meanwell, N. A., Di, L. and Hageman, M. J. (2018). The expanding role of prodrugs in contemporary drug design and development. *Nature Reviews Drug Discovery*, 17(8), 559–587. doi: 10.1038/nrd.2018.46
- Rebecchi, K. R., Go, E. P., Xu, L., Woodin, C. L., Mure, M. and Desaire, H. (2011). A general protease digestion procedure for optimal protein sequence coverage and PTM analysis of recombinant glycoproteins: application to the characterization of hLOXL2 glycosylation. *Analytical Chemistry*, 83(22), 8484–8491. doi: 10.1021/ac2017037.A
- Reddy, V. B. G., Doss, G. A., Creighton, M., Kochansky, C. J., Vincent, S. H., Franklin, R. B. and Karanam, B. V. (2004). Identification and metabolism of a novel dihydrohydroxy-S-glutathionyl conjugate of a peroxisome proliferator-activated receptor agonist, MK-0767 [(±)-5-[(2,4-dioxothiazolidin-5-yl)methyl]-2-methoxy-n-[[4-trifluoromethyl]phenyl]methyl]benzamide], in ra. *Drug*

Metabolism and Disposition, 32(10), 1154–1161. doi: 10.1124/dmd.104.000240

- Reed, T., Perluigi, M., Sultana, R., Pierce, W. M., Klein, J. B., Turner, D. M., ... Butterfield, D. A. (2008). Redox proteomic identification of 4-hydroxy-2-nonenal-modified brain proteins in amnesic mild cognitive impairment: insight into the role of lipid peroxidation in the progression and pathogenesis of Alzheimer's disease. *Neurobiology of Disease*, 30(1), 107–120. doi: 10.1016/j.nbd.2007.12.007
- Reed, T. T., Pierce, W. M., Markesbery, W. R. and Butterfield, D. A. (2009). Proteomic identification of HNE-bound proteins in early Alzheimer disease: insights into the role of lipid peroxidation in the progression of AD. *Brain Research*, 1274, 66–76. doi: 10.1016/j.brainres.2009.04.009
- Reilly, T. P., Lash, L. H., Doll, M. A., Hein, D. W., Woster, P. M. and Svensson, C. K. (2000). A role for bioactivation and covalent binding within epidermal keratinocytes in sulfonamide-induced cutaneous drug reactions. *Journal of Investigative Dermatology*, 114(6), 1164–1173. doi: 10.1046/j.1523-1747.2000.00985.x
- Reinemer, P., Dirr, H. W., Ladenstein, R., Schäffer, J., Gallay, O. and Huber, R. (1991). The three-dimensional structure of class pi glutathione S-transferase in complex with glutathione sulfonate at 2.3 Å resolution. *The EMBO Journal*, 10(8), 1997–2005. doi: 10.1016/0022-2836(92)90692-d
- Riahi, Y., Cohen, G., Shamni, O. and Sasson, S. (2010). Signaling and cytotoxic functions of 4-hydroxyalkenals. *American Journal of Physiology-Endocrinology and Metabolism*, 299(6), E879–886. doi: 10.1152/ajpendo.00508.2010
- Riley, N. M. and Coon, J. J. (2018). The role of electron transfer dissociation in modern proteomics. *Analytical Chemistry*, 90(1), 40–64. doi: 10.1021/acs.analchem.7b04810
- Roberts, D. W., Lee, W. M., Hinson, J. A., Bai, S., Swearingen, C. J., Stravitz, R. T., ... James, L. P. (2017). An immunoassay to rapidly measure acetaminophen protein adducts accurately identifies patients with acute liver injury or failure. *Clinical Gastroenterology and Hepatology*, 15(4), 555–562.e3. doi: 10.1016/j.cgh.2016.09.007
- Roe, M. R., Xie, H., Bandhakavi, S. and Griffin, T. J. (2007). Proteomic mapping of 4-hydroxynonenal protein modification sites by solid-phase hydrazide chemistry and mass spectrometry. *Analytical Chemistry*, 79(10), 3747–3756. doi: 10.1021/ac0617971

- Ruan, Q., Peterman, S., Szewc, M. A., Ma, L., Cui, D., Humphreys, W. G. and Zhu, M. (2008). An integrated method for metabolite detection and identification using a linear ion trap/Orbitrap mass spectrometer and multiple data processing techniques: application to indinavir metabolite detection. *Journal of mass spectrometry*, 43(2), 251–261. doi: 10.1002/jms.1311
- Ruan, Q. and Zhu, M. (2010). Investigation of bioactivation of ticlopidine using linear ion trap/Orbitrap mass spectrometry and an improved mass defect. *Chemical Research in Toxicology*, 23(5), 909–917. doi: 10.1021/tx1000046
- Ruef, J., Moser, M., Bode, C., Kübler, W. and Runge, M. S. (2001). 4-hydroxynonenal induces apoptosis, NF-kappaB-activation and formation of 8-isoprostane in vascular smooth muscle cells. *Basic Research in Cardiology*, 96(2), 143–150. doi: 10.1007/s003950170064
- Rumack, B. H., Peterson, R. C., Koch, G. G. and Amara, I. A. (1981). Acetaminophen overdose. 662 cases with evaluation of oral acetylcysteine treatment. *Archives of Internal Medicine*, 141(3), 380–385. doi: 10.1001/archinte.1981.00340030112020
- Ryder, S. D. and Beckingham, I. J. (2001). ABC of diseases of liver, pancreas, and biliary system. Other causes of parenchymal liver disease. *BMJ*, 322(7281), 290–292. doi: 10.1136/bmj.322.7281.290
- Sabbioni, G. and Turesky, R. J. (2017). Biomonitoring human albumin adducts: the past, the present, and the future. *Chemical Research in Toxicology*, 30(1), 332–366. doi: 10.1021/acs.chemrestox.6b00366
- Saeki, M., Saito, Y., Nagano, M., Teshima, R., Ozawa, S. and Sawada, J. (2002). mRNA expression of multiple cytochrome P450 isozymes in four types of cultured skin cells. *International Archives of Allergy and Immunology*, 127(4), 333–336. doi: 10.1159/000057751
- Saha, S., Chant, D., Welham, J. and McGrath, J. (2005). A systematic review of the prevalence of schizophrenia. *PLoS Medicine*, 2(5), e141. doi: 10.1371/journal.pmed.0020141
- Samara, M. T., Goldberg, Y., Levine, S. Z., Furukawa, T. A., Geddes, J. R., Cipriani, A., ... Leucht, S. (2017). Initial symptom severity of bipolar I disorder and the efficacy of olanzapine: a meta-analysis of individual participant data from five placebo-controlled studies. *The Lancet Psychiatry*, 4(11), 859–867. doi: 10.1016/S2215-0366(17)30331-0

- Sawers, L., Ferguson, M. J., Ihrig, B. R., Young, H. C., Chakravarty, P., Wolf, C. R. and Smith, G. (2014). Glutathione S-transferase P1 (GSTP1) directly influences platinum drug chemosensitivity in ovarian tumour cell lines. *British Journal of Cancer*, *111*(6), 1150–1158. doi: 10.1038/bjc.2014.386
- Schaur, R. J. (2003). Basic aspects of the biochemical reactivity of 4-hydroxynonenal. *Molecular Aspects of Medicine*, *24*(4–5), 149–159. doi: 10.1016/S0098-2997(03)00009-8
- Schiødt, F. V., Rochling, F. A., Casey, D. L. and Lee, W. M. (1997). Acetaminophen toxicity in an urban county hospital. *New England Journal of Medicine*, *337*(16), 1112–1117. doi: 10.1056/NEJM199802193380810
- Schlisser, A. E., Yan, J. and Hales, B. F. (2010). Teratogen-induced oxidative stress targets glyceraldehyde-3-phosphate dehydrogenase in the organogenesis stage mouse embryo. *Toxicological Sciences*, *118*(2), 686–695. doi: 10.1093/toxsci/kfq287
- Schmidt, G., Börsch, G., Müller, K.-M. and Ricken, D. (1987). Clozapine-induced cholestatic liver lesions. A case study. *Deutsche Medizinische Wochenschrift*, *112*(21), 844–846. doi: 10.1055/s-2008-1068152
- Schwenger, E., Dumontet, J. and Ensom, M. H. H. (2011). Does olanzapine warrant clinical pharmacokinetic monitoring in schizophrenia? *Clinical Pharmacokinetics*, *50*(7), 415–428. doi: 10.2165/11587240-000000000-00000
- Schwöbel, J. A. H., Wondrousch, D., Koleva, Y. K., Madden, J. C., Cronin, M. T. D. and Schüürmann, G. (2010). Prediction of michael-type acceptor reactivity toward glutathione. *Chemical Research in Toxicology*, *23*(10), 1576–1585. doi: 10.1021/tx100172x
- Scott Obach, R. and Kalgutkar, A. S. (2010). Reactive electrophiles and metabolic activation. In C. A. McQueen (ed.), *Comprehensive Toxicology* (2nd ed., vol. 1, 15, pp. 309–347). Elsevier Ltd. doi: 10.1016/B978-0-08-046884-6.00115-9
- Séguin, B. and Uetrecht, J. (2003). The danger hypothesis applied to idiosyncratic drug reactions. *Current Opinion in Allergy and Clinical Immunology*, *3*(4), 235–242. doi: 10.1097/01.all.0000083953.99396.a2
- Sen, N. (2015). Epigenetic regulation of memory by acetylation and methylation of chromatin: implications in neurological disorders, aging, and addiction. *NeuroMolecular Medicine*, *17*(2), 97–110. doi: 10.1007/s12017-014-8306-x

- Shah, K. and Maghsoudlou, P. (2016). Enzyme-linked immunosorbent assay (ELISA): the basics. *British Journal of Hospital Medicine*, 77(7), C98–C101. doi: 10.12968/hmed.2016.77.7.C98
- Sharma, A. M., Novalen, M., Tanino, T. and Uetrecht, J. P. (2013). 12-OH-nevirapine sulfate, formed in the skin, is responsible for nevirapine-induced skin rash. *Chemical Research in Toxicology*, 26(5), 817–827. doi: 10.1021/tx400098z
- Sheehan, D., Meade, G., Foley, V. M. and Dowd, C. A. (2001). Structure, function and evolution of glutathione transferases: implications for classification of non-mammalian members of an ancient enzyme superfamily. *Biochemical Journal*, 360(Pt 1), 1–16. doi: 10.1042/bj3600001
- Shen, J., Abu-Amer, Y., O’Keefe, R. J. and McAlinden, A. (2017). Inflammation and epigenetic regulation in osteoarthritis. *Connective Tissue Research*, 58(1), 49–63. doi: 10.1080/03008207.2016.1208655
- Shen, S., Hargus, S. J., Martin, B. M. and Pohl, L. R. (1997). Cytochrome P4502C11 is a target of diclofenac covalent binding in rats. *Chemical Research in Toxicology*, 10(4), 420–423. doi: 10.1021/tx960167z
- Shi, Q., Abusarah, J., Zaouter, C., Moldovan, F., Fernandes, J. C., Fahmi, H. and Benderdour, M. (2014). New evidence implicating 4-hydroxynonenal in the pathogenesis of osteoarthritis in vivo. *Arthritis & Rheumatology*, 66(9), 2461–2471. doi: 10.1002/art.38704
- Shilov, I. V., Seymour, S. L., Patel, A. A., Loboda, A., Tang, W. H., Keating, S. P., ... Schaeffer, D. A. (2007). The Paragon Algorithm, a next generation search engine that uses sequence temperature values and feature probabilities to identify peptides from tandem mass spectra. *Molecular and Cellular Proteomics*, 6(9), 1638–1655. doi: 10.1074/mcp.T600050-MCP200
- Shin, N.-Y., Liu, Q., Stamer, S. L. and Liebler, D. C. (2007). Protein targets of reactive electrophiles in human liver microsomes. *Chemical Research in Toxicology*, 20(6), 859–867. doi: 10.1021/tx700031r
- Siems, W. G., Hapner, S. and van Kuijk, F. J. G. M. (1989). 4-hydroxynonenal inhibits Na(+)-K(+)-ATPase. *Free Radical Biology & Medicine*, 20(2), 215–223. Retrieved from <https://www.sciencedirect.com/science/article/pii/0891584995020411?via%3Dihub>
- Siems, W. and Grune, T. (2003). Intracellular metabolism of 4-hydroxynonenal.

- Molecular Aspects of Medicine*, 24(4–5), 167–175. doi: 10.1016/S0098-2997(03)00011-6
- Sies, H., Berndt, C. and Jones, D. P. (2017). Oxidative stress. *Annual Review of Biochemistry*, 86, 715–748. doi: 10.1146/annurev-biochem-061516-045037
- Silkworth, J. B., Koganti, A., Illouz, K., Possolo, A., Zhao, M. and Hamilton, S. B. (2005). Comparison of TCDD and PCB CYP1A induction sensitivities in fresh hepatocytes from human donors, Sprague-Dawley rats, and rhesus monkeys and HepG2 cells. *Toxicological Sciences*, 87(2), 508–519. doi: 10.1093/toxsci/kfi261
- Sivilotti, M. L. A., Yarema, M. C., Juurlink, D. N., Good, A. M. and Johnson, D. W. (2005). A risk quantification instrument for acute acetaminophen overdose patients treated with N-acetylcysteine. *Annals of Emergency Medicine*, 46(3), 263–271. doi: 10.1016/j.annemergmed.2005.04.004
- Sleno, L., Varesio, E. and Hopfgartner, G. (2007). Determining protein adducts of fipexide: mass spectrometry based assay for confirming the involvement of its reactive metabolite in covalent binding. *Rapid Communications in Mass Spectrometry*, 21(24), 4149–4157. doi: 10.1002/rcm.3329
- Smith, D. B. and Johnson, K. S. (1988). Single-step purification of polypeptides expressed in *Escherichia coli* as fusions with glutathione S-transferase. *Gene*, 67(1), 31–40. doi: 10.1016/0378-1119(88)90005-4
- Sobott, F., Watt, S. J., Smith, J., Edelman, M. J., Kramer, H. B. and Kessler, B. M. (2009). Comparison of CID versus ETD based MS/MS fragmentation for the analysis of protein ubiquitination. *Journal of the American Society for Mass Spectrometry*, 20(9), 1652–1659. doi: 10.1016/j.jasms.2009.04.023
- Splawiński, J., Kuźniar, J., Filipiak, K. and Zieliński, W. (2006). Evaluation of drug toxicity in clinical trials. *Science and Engineering Ethics*, 12(1), 139–145. doi: 10.1007/s11948-006-0014-y
- Stelzer, G., Rosen, N., Plaschkes, I., Zimmerman, S., Twik, M., Fishilevich, S., ... Lancet, D. (2016). The GeneCards suite: from gene data mining to disease genome sequence analyses. *Current Protocols in Bioinformatics*, 54(1), 1.30.1-1.30.33. doi: 10.1002/cpbi.5
- Stocco, G., Pelin, M., Franca, R., De Iudicibus, S., Cuzzoni, E., Favretto, D., ... Decorti, G. (2014). Pharmacogenetics of azathioprine in inflammatory bowel disease: a role for glutathione-S-transferase? *World Journal of Gastroenterology*, 20(13), 3534–3541. doi: 10.3748/wjg.v20.i13.3534

- Stoehlmacher, J., Park, D. J., Zhang, W., Groshen, S., Tsao-Wei, D. D. and Lenz, H.-J. (2002). Association between glutathione S-transferase P1, T1, and M1 genetic polymorphism and survival of patients with metastatic colorectal cancer. *Journal of the National Cancer Institute*, 94(12), 936–942. doi: 10.1093/jnci/94.12.936
- Strange, R. C., Jones, P. W. and Fryer, A. A. (2000). Glutathione S-transferase: genetics and role in toxicology. *Toxicology Letters*, 112–113, 357–363. doi: 10.1016/S0378-4274(99)00230-1
- Subramaniam, R., Roediger, F., Jordan, B., Mattson, M. P., Keller, J. N., Waeg, G. and Butterfield, D. A. (1997). The lipid peroxidation product, 4-hydroxy-2-trans-nonenal, alters the conformation of cortical synaptosomal membrane proteins. *Journal of Neurochemistry*, 69(3), 1161–1169. doi: 10.1046/j.1471-4159.1997.69031161.x
- Sutherland, A., Naessens, K., Plugge, E., Ware, L., Head, K., Burton, M. J. and Wee, B. (2018). Olanzapine for the prevention and treatment of cancer-related nausea and vomiting in adults. *Cochrane Database of Systematic Reviews*, 9(9), CD012555. doi: 10.1002/14651858.CD012555.pub2
- Svensson, R., Rinaldi, R., Swedmark, S. and Morgenstern, R. (2000). Reactivity of cysteine-49 and its influence on the activation of microsomal glutathione transferase 1: evidence for subunit interaction. *Biochemistry*, 39(49), 15144–15149. doi: 10.1021/bi001764u
- Tabb, D. L., Vega-Montoto, L., Rudnick, P. A., Mulayath, A., Ham, A.-J. L., Bunk, D. M., ... Spiegelman, C. (2010). Repeatability and reproducibility in proteomic identifications by liquid chromatography-tandem mass spectrometry. *Journal of Proteome Research*, 9(2), 761–766. doi: 10.1021/pr9006365
- Taylor, A., Waddington, J. C., Meng, X. and Park, B. K. (2016). Mass spectrometric and functional aspects of drug-protein conjugation. *Chemical Research in Toxicology*, 29(12), 1912–1935. doi: 10.1021/acs.chemrestox.6b00147
- Takeshita, T. and Kanaly, R. A. (2019). In vitro DNA/RNA adductomics to confirm DNA damage caused by benzo[a]pyrene in the Hep G2 cell line. *Frontiers in Chemistry*, 7, 491. doi: 10.3389/fchem.2019.00491
- Tanaka, K., Waki, H., Ido, Y., Akita, S., Yoshida, Y., Yoshida, T. and Matsuo, T. (1988). Protein and polymer analyses up to m/z 100 000 by laser ionization time-of-flight mass spectrometry. *Rapid Communications in Mass Spectrometry*, 2(8), 151–153. doi: 10.1002/rcm.1290020802

- Tang, W. H., Shilov, I. V. and Seymour, S. L. (2008). Nonlinear fitting method for determining local false discovery rates from decoy database searches. *Journal of Proteome Research*, 7(9), 3661–3667. doi: 10.1021/pr070492f
- Terada, T. and Hira, D. (2015). Intestinal and hepatic drug transporters: pharmacokinetic, pathophysiological, and pharmacogenetic roles. *Journal of Gastroenterology*, 50(5), 508–519. doi: 10.1007/s00535-015-1061-4
- Tesfa, D., Keisu, M. and Palmblad, J. (2009). Idiosyncratic drug-induced agranulocytosis: possible mechanisms and management. *American Journal of Hematology*, 84(7), 428–434. doi: 10.1002/ajh.21433
- Thompson, R. A., Isin, E. M., Ogebe, M. O., Mettetal, J. T. and Williams, D. P. (2016). Reactive metabolites: current and emerging risk and hazard assessments. *Chemical Research in Toxicology*, 29(4), 505–533. doi: 10.1021/acs.chemrestox.5b00410
- Thomson, J. J. (1913). *Rays of positive electricity and their application to chemical analyses*. London : Longmans, Green and Company.
- Tirmenstein, M. A. and Nelson, S. D. (1989). Subcellular binding and effects on calcium homeostasis produced by acetaminophen and a nonhepatotoxic regioisomer, 3'-hydroxyacetanilide, in mouse liver. *Journal of Biological Chemistry*, 264(17), 9814–9819. Retrieved from <http://www.jbc.org/content/264/17/9814>
- Towbin, H., Staehelin, T. and Gordon, J. (1979). Electrophoretic transfer of proteins from polyacrylamide gels to nitrocellulose sheets: procedure and some applications. *Proceedings of the National Academy of Sciences of the United States of America*, 76(9), 4350–4354. doi: 10.1073/pnas.76.9.4350
- Tsolis, K. C., Bei, E. S., Papathanasiou, I., Kostopoulou, F., Gkretsi, V., Kalantzaki, K., ... Economou, A. (2015). Comparative proteomic analysis of hypertrophic chondrocytes in osteoarthritis. *Clinical Proteomics*, 12(1), 12. doi: 10.1186/s12014-015-9085-6
- Tucker, P. (2013). Liver toxicity with clozapine. *Australian and New Zealand Journal of Psychiatry*, 47(10), 975–976. doi: 10.1177/0004867413488224
- Uchida, K. and Stadtman, E. R. (1992). Modification of histidine residues in proteins by reaction with 4-hydroxynonenal. *Proceedings of the National Academy of Sciences of the United States of America*, 89(10), 4544–4548. doi: 10.1073/pnas.89.10.4544

- Uchida, K. and Stadtman, E. R. (1993). Covalent attachment of 4-hydroxynonenal to glyceraldehyde-3-phosphate dehydrogenase. A possible involvement of intra- and intermolecular cross-linking reaction. *The Journal of Biological Chemistry*, 268(9), 6388–6393. Retrieved from <http://www.jbc.org/content/268/9/6388.long>
- Uetrecht, J. (2007). Idiosyncratic drug reactions: current understanding. *Annual Review of Pharmacology and Toxicology*, 47, 513–539. doi: 10.1146/annurev.pharmtox.47.120505.105150
- Uetrecht, J. (2008). Idiosyncratic drug reactions: past, present, and future. *Chemical Research in Toxicology*, 21(1), 84–92. doi: 10.1021/tx700186p
- Uetrecht, J. and Naisbitt, D. J. (2013). Idiosyncratic adverse drug reactions: current concepts. *Pharmacological Reviews*, 65(2), 779–808. doi: 10.1016/B978-0-12-801238-3.64242-3
- Uetrecht, J. P. (1992). Metabolism of clozapine by neutrophils. Possible implications for clozapine-induced agranulocytosis. *Drug Safety*, 7(Supplement 1), 51–56. doi: 10.2165/00002018-199200071-00011
- Uetrecht, J. P. (1996). Reactive metabolites and agranulocytosis. *European Journal of Haematology*, 57(S60), 83–88. doi: 10.1111/j.1600-0609.1996.tb01651.x
- Vaillancourt, F., Fahmi, H., Shi, Q., Lavigne, P., Ranger, P., Fernandes, J. C. and Benderdour, M. (2008). 4-Hydroxynonenal induces apoptosis in human osteoarthritic chondrocytes: the protective role of glutathione-S-transferase. *Arthritis Research and Therapy*, 10(5), R107. doi: 10.1186/ar2503
- Vaillancourt, F., Morquette, B., Shi, Q., Fahmi, H., Lavigne, P., Di Battista, J. A., ... Benderdour, M. (2007). Differential regulation of cyclooxygenase-2 and inducible nitric oxide synthase by 4-hydroxynonenal in human osteoarthritic chondrocytes through ATF-2/CREB-1 transactivation and concomitant inhibition of NF-kappaB signaling cascade. *Journal of Cellular Biochemistry*, 100(5), 1217–1231. doi: 10.1002/jcb.21110
- Vaitukaitis, J. L. (2004). Development of the home pregnancy test. *Annals of the New York Academy of Sciences*, 1038(1), 220–222. doi: 10.1196/annals.1315.030
- van Iersel, M. L. P. S., Ploemen, J.-P. H. T. M., Lo Bello, M., Federici, G. and van Bladeren, P. J. (1997). Interactions of alpha, beta-unsaturated aldehydes and ketones with human glutathione S-transferase P1-1. *Chemico-Biological Interactions*, 108(1–2), 67–78. Retrieved from <https://www.sciencedirect.com/science/article/abs/pii/S0009279797000963?via>

%3Dihub

- Van Weemen, B. K. and Schuurs, A. H. W. M. (1971). Immunoassay using antigen-enzyme conjugates. *FEBS Letters*, 15(3), 232–236. doi: 10.1016/0014-5793(71)80319-8
- Vargo, M. A., Nguyen, L. and Colman, R. F. (2004). Subunit interface residues of glutathione S-transferase A1-1 that are important in the monomer-dimer equilibrium. *Biochemistry*, 43(12), 3327–3335. doi: 10.1021/bi030245z
- Vega, M. C., Walsh, S. B., Mantle, T. J. and Coll, M. (1998). The three-dimensional structure of Cys-47-modified mouse liver glutathione S-transferase P1-1. Carboxymethylation dramatically decreases the affinity for glutathione and is associated with a loss of electron density in the alphaB-310B region. *Journal of Biological Chemistry*, 273(5), 2844–2850. doi: 10.1074/jbc.273.5.2844
- Vredenburg, G., Vassell, K. P. T., Commandeur, J. N. M., Vermeulen, N. P. E. and Vos, J. C. (2013). Reconstitution of the interplay between cytochrome P450 and human glutathione S-transferases in clozapine metabolism in yeast. *Toxicology Letters*, 222(3), 247–256. doi: 10.1016/j.toxlet.2013.07.023
- Vuk, A., Kuzman, M. R., Baretic, M. and Osvatic, M. M. (2017). Diabetic ketoacidosis associated with antipsychotic drugs: case reports and a review of literature. *Psychiatria Danubina*, 29(2), 121–135. doi: 10.24869/psyd.2017.121
- Wagmann, L., Meyer, M. R. and Maurer, H. H. (2016). What is the contribution of human FMO3 in the N-oxygenation of selected therapeutic drugs and drugs of abuse? *Toxicology Letters*, 258, 55–70. doi: 10.1016/j.toxlet.2016.06.013
- Walgren, J. L., Mitchell, M. D. and Thompson, D. C. (2005). Role of metabolism in drug-induced idiosyncratic hepatotoxicity. *Critical Reviews in Toxicology*, 35(4), 325–361. doi: 10.1080/10408440590935620
- Wallin, H. and Morgenstern, R. (1990). Activation of microsomal glutathione transferase activity by reactive intermediates formed during the metabolism of phenol. *Chemico-Biological Interactions*, 75(2), 185–199. doi: 10.1016/0009-2797(90)90117-6
- Walton, K., Coombs, M. M., Catterall, F. S., Walker, R. and Ioannides, C. (1997). Bioactivation of the mushroom hydrazine, agaritine, to intermediates that bind covalently to proteins and induce mutations in the Ames test. *Carcinogenesis*, 18(8), 1603–1608. doi: 10.1093/carcin/18.8.1603

- Wang, L. and Marcus, R. K. (2018). Overload effects in reversed phase protein separations using capillary-channeled polymer fiber columns. *Biotechnology Progress*, 34(5), 1221–1233. doi: 10.1002/btpr.2688
- Wang, Y., Yang, F., Gritsenko, M. A., Wang, Y., Clauss, T., Liu, T., ... Smith, R. D. (2011). Reversed-phase chromatography with multiple fraction concatenation strategy for proteome profiling of human MCF10A cells. *Proteomics*, 11(10), 2019–2026. doi: 10.1002/pmic.201000722
- Wei, X. and Yin, H. (2015). Covalent modification of DNA by α , β -unsaturated aldehydes derived from lipid peroxidation: recent progress and challenges. *Free Radical Research*, 49(7), 905–917. doi: 10.3109/10715762.2015.1040009
- Wen, B. and Nelson, S. D. (2011). Common biotransformation reactions. In M. S. Lee and M. Zhu (eds.), *Mass Spectrometry in Drug Metabolism and Disposition: Basic Principles and Applications* (1st ed., 2, pp. 13–41). Hoboken, NJ: John Wiley & Sons, Inc. doi: 10.1002/9780470929278.ch2
- Wendel, A. and Cikryt, P. (1981). Binding of paracetamol metabolites to mouse liver glutathione S-transferases. *Research Communications in Chemical Pathology and Pharmacology*, 33(3), 463–473. Retrieved from <http://europepmc.org/abstract/med/7330451>
- Wiciński, M. and Węciewicz, M. M. (2018). Clozapine-induced agranulocytosis/granulocytopenia: mechanisms and monitoring. *Current Opinion in Hematology*, 25(1), 22–28. doi: 10.1097/MOH.0000000000000391
- Williams, D. P., Pirmohamed, M., Naisbitt, D. J., Maggs, J. L. and Park, B. K. (1997). Neutrophil cytotoxicity of the chemically reactive metabolite(s) of clozapine: possible role in agranulocytosis. *The Journal of Pharmacology and Experimental Therapeutics*, 283(3), 1375–1382. Retrieved from <http://jpet.aspetjournals.org/content/283/3/1375.long>
- Williams, D. P., Pirmohamed, M., Naisbitt, D. J., Uetrecht, J. P. and Park, B. K. (2000). Induction of metabolism-dependent and -independent neutrophil apoptosis by clozapine. *Molecular Pharmacology*, 58(1), 207–216. doi: 10.1124/mol.58.1.207
- Wishart, D. S., Knox, C., Guo, A. C., Shrivastava, S., Hassanali, M., Stothard, P., ... Woolsey, J. (2006). DrugBank: a comprehensive resource for in silico drug discovery and exploration. *Nucleic Acids Research*, 34(Database issue), D668–D672. doi: 10.1093/nar/gkj067
- Wu Chou, A. I., Lu, M.-L. and Shen, W. W. (2014). Hepatotoxicity induced by

- clozapine: a case report and review of literature. *Neuropsychiatric Disease and Treatment*, 10, 1585–1587. doi: 10.2147/NDT.S67654
- Wu, Q., Yuan, H., Zhang, L. and Zhang, Y. (2012). Recent advances on multidimensional liquid chromatography-mass spectrometry for proteomics: from qualitative to quantitative analysis--a review. *Analytica Chimica Acta*, 731, 1–10. doi: 10.1016/j.aca.2012.04.010
- Wysocki, V. H., Joyce, K. E., Jones, C. M. and Beardsley, R. L. (2008). Surface-induced dissociation of small molecules, peptides, and non-covalent protein complexes. *Journal of the American Society for Mass Spectrometry*, 19(2), 190–208. doi: 10.1016/j.jasms.2007.11.005
- Xia, Y.-Q., Miller, J. D., Bakhtiar, R., Franklin, R. B. and Liu, D. Q. (2003). Use of a quadrupole linear ion trap mass spectrometer in metabolite identification and bioanalysis. *Rapid Communications in Mass Spectrometry*, 17(11), 1137–1145. doi: 10.1002/rcm.1037
- Xie, Y., McGill, M. R., Cook, S. F., Sharpe, M. R., Winefield, R. D., Wilkins, D. G., ... Jaeschke, H. (2015). Time course of acetaminophen-protein adducts and acetaminophen metabolites in circulation of overdose patients and in HepaRG cells. *Xenobiotica*, 45(10), 921–929. doi: 10.1097/OGX.000000000000256.Prenatal
- Yan, Z. and Caldwell, G. W. (2004). Stable-isotope trapping and high-throughput screenings of reactive metabolites using the isotope MS signature. *Analytical Chemistry*, 76(23), 6835–6847. doi: 10.1021/ac040159k
- Yang, F., Shen, Y., Camp, D. G. and Smith, R. D. (2012). High-pH reversed-phase chromatography with fraction concatenation for 2D proteomic analysis. *Expert Review of Proteomics*, 9(2), 129–134. doi: 10.1586/epr.12.15
- Yang, J., Tallman, K. A., Porter, N. A. and Liebler, D. C. (2015). Quantitative chemoproteomics for site-specific analysis of protein alkylation by 4-hydroxy-2-nonenal in cells. *Analytical Chemistry*, 87(5), 2535–2541. doi: 10.1021/ac504685y
- Yao, M., Ma, L., Humphreys, W. G. and Zhu, M. (2008). Rapid screening and characterization of drug metabolites using a multiple ion monitoring-dependent MS/MS acquisition method on a hybrid triple quadrupole-linear ion trap mass spectrometer. *Journal of Mass Spectrometry*, 43(10), 1364–1375. doi: 10.1002/jms

- Yarmush, M. L. and Jayaraman, A. (2002). Advances in proteomic technologies. *Annual Review of Biomedical Engineering*, 4, 349–373. doi: 10.1146/annurev.bioeng.4.020702.153443
- Yates, J. R., Ruse, C. I. and Nakorchevsky, A. (2009). Proteomics by mass spectrometry: approaches, advances, and applications. *Annual Review of Biomedical Engineering*, 11, 49–79. doi: 10.1146/annurev-bioeng-061008-124934
- Yeung, Y.-G., Nieves, E., Angeletti, R. H. and Stanley, E. R. (2008). Removal of detergents from protein digests for mass spectrometry analysis. *Analytical Biochemistry*, 382(2), 135–137. doi: 10.1016/j.ab.2008.07.034
- Yukinaga, H., Iwabuchi, H., Okazaki, O. and Izumi, T. (2012). Glutathione S-transferase pi trapping method for generation and characterization of drug-protein adducts in human liver microsomes using liquid chromatography-tandem mass spectrometry. *Journal of Pharmaceutical and Biomedical Analysis*, 67–68, 186–192. doi: 10.1016/j.jpba.2012.04.035
- Zanger, U. M. and Schwab, M. (2013). Cytochrome P450 enzymes in drug metabolism: regulation of gene expression, enzyme activities, and impact of genetic variation. *Pharmacology and Therapeutics*, 138(1), 103–141. doi: 10.1016/j.pharmthera.2012.12.007
- Zhai, X.-H., Huang, J., Wu, F.-X., Zhu, D.-Y. and Wang, A.-C. (2016). Impact of XRCC1, GSTP1, and GSTM1 polymorphisms on the survival of ovarian carcinoma patients treated with chemotherapy. *Oncology Research and Treatment*, 39(7–8), 440–446. doi: 10.1159/000447337
- Zhang, B., Kirov, S. and Snoddy, J. (2005). WebGestalt: an integrated system for exploring gene sets in various biological contexts. *Nucleic Acids Research*, 33(Web Server issue), W741–W748. doi: 10.1093/nar/gki475
- Zhang, H., Ma, L., He, K. and Zhu, M. (2008). An algorithm for thorough background subtraction from high-resolution LC/MS data: application to the detection of troglitazone metabolites in rat plasma, bile, and urine. *Journal of Mass Spectrometry*, 43(9), 1191–1200. doi: 10.1002/jms.1432
- Zhang, H. and Yang, Y. (2008). An algorithm for thorough background subtraction from high-resolution LC/MS data: application for detection of glutathione-trapped reactive metabolites. *Journal of Mass Spectrometry*, 43(9), 1181–1190. doi: 10.1002/jms

- Zhang, H., Zhang, D. and Ray, K. (2003). A software filter to remove interference ions from drug metabolites in accurate mass liquid chromatography/mass spectrometric analyses. *Journal of Mass Spectrometry*, 38(10), 1110–1112. doi: 10.1002/jms.521
- Zhang, W., Yin, K., Li, B. and Chen, L. (2013). A glutathione S-transferase from *Proteus mirabilis* involved in heavy metal resistance and its potential application in removal of Hg²⁺. *Journal of Hazardous Materials*, 261, 646–652. doi: 10.1016/j.jhazmat.2013.08.023
- Zhou, S. (2003). Separation and detection methods for covalent drug-protein adducts. *Journal of Chromatography B. Analytical Technologies in the Biomedical and Life Sciences*, 797(1–2), 63–90. doi: 10.1016/S1570-0232(03)00399-4
- Zhou, S., Chan, E., Duan, W., Huang, M. and Chen, Y.-Z. (2005). Drug bioactivation, covalent binding to target proteins and toxicity relevance. *Drug Metabolism Reviews*, 37(1), 41–213. doi: 10.1081/DMR-200028812
- Zhu, M., Zhang, D., Zhang, H. and Shyu, W. C. (2009a). Integrated strategies for assessment of metabolite exposure in humans during drug development: analytical challenges and clinical development considerations. *Biopharmaceutics & Drug Disposition*, 184(4), 163–184. doi: 10.1002/bdd.659
- Zhu, P., Ding, W., Tong, W., Ghosal, A., Alton, K. and Chowdhury, S. (2009b). A retention-time-shift-tolerant background subtraction and noise reduction algorithm (BgS-NoRA) for extraction of drug metabolites in liquid chromatography/mass spectrometry data from biological matrices. *Rapid Communications in Mass Spectrometry*, 23(11), 1563–1572. doi: 10.1002/rcm.4041
- Zlatković, J., Todorović, N., Tomanović, N., Bošković, M., Djordjević, S., Lazarević-Pašti, T., ... Filipović, D. (2014). Chronic administration of fluoxetine or clozapine induces oxidative stress in rat liver: a histopathological study. *European Journal of Pharmaceutical Sciences*, 59, 20–30. doi: 10.1016/j.ejps.2014.04.010
- Zubarev, R. A. (2004). Electron-capture dissociation tandem mass spectrometry. *Current Opinion in Biotechnology*, 15(1), 12–16. doi: 10.1016/j.copbio.2003.12.002